

DD8200876-DD8200895

ZfK-459

Proceedings

**of the X-th International Symposium on Selected Topics
of the Interaction of Fast Neutrons and Heavy Ions
with Atomic Nuclei**

organized by

**the Technical University of Dresden
November 17 – 21, 1980 in Gaussig (GDR)**

edited by

G. Musiol, W. Wagner, M. Josch

September 1981

Diese Publikation wurde in der Abteilung Literatur und Information des Zentralinstitutes für Kernforschung hergestellt

AKADEMIE DER WISSENSCHAFTEN DER DDR
ZENTRALINSTITUT FÜR KERNFORSCHUNG
ROSSENDORF BEI DRESDEN

ZfK - 459

PROCEEDINGS

of the X-th International Symposium on Selected
Topics of the Interaction of Fast Neutrons and
Heavy Ions with Atomic Nuclei

organized by

the Technical University of Dresden
November 17 - 21, 1980 in Gaussig (GDR)

edited by

G. Musiol, W. Wagner, M. Josch

September 1981

Organizing Committee

A. Barthel
G. Musiol
W. Wagner

Technical University Dresden

Section of Physics, Applied Nuclear Physics Group

Materials of the previous symposiums have been published in:

- 1971: Wiss. Zeitschrift TU Dresden 21 (1972) 691
1972: ZfK - 261 (1973)
1973: ZfK - 271 (1974)
1974: Wiss. Zeitschrift TU Dresden 24 (1975) i351
1975: ZfK - 324 (1976)
1976: not published
1977: ZfK - 376 (1978)
1978: ZfK - 382 (1979)
1979: ZfK - 410 (1980)

Preface

This report contains the contributions presented at the "X-th International Symposium on Selected Topics of the Interaction of Fast Neutrons and Heavy Ions with Atomic Nuclei" organized by the Applied Nuclear Physics Group of the Technical University Dresden.

The Symposium was devoted to current problems in experimental and theoretical investigations of nuclear reactions, covering a broad range of aspects. The main effort was made to the nuclear fission process and the heavy ion reactions.

At this X-th symposium participated scientists from nine countrys and two international scientific organisations which presented results obtained in more than twenty instituts.

We would like to thank all participants, especially the lecturers, chairmens and summary-talkers for their effort and active work during the sessions and all subsequent informal discussions. Further we want to thank the International Department of the Technical University Dresden for the valuable support in organizing this symposium. A special thank is due to the stoff of the rest home in Gaussig. Moreover, we would like to thank the Central Instituts of Nuclear Research of the Academy of Science of GDR for making possible the publication of this report. We are much indepted for technical assistance and preparing this proceedings to A. Barthel, K. Lenzendorf and S. Woitek.

G. Musiol
W. Wagner

<u>CONTENTS</u>	<u>Page</u>
PREFACE	3
SCIENTIFIC PROGRAMME	5
LIST OF PARTICIPANTS	9
 <u>SESSION I "FISSION"</u>	
I. 1. Chairman: G. Musiol	
Absolute Methods of Fission Cross-Section Measurements (rus.)	11
V. I. Shpakov et. al.	
Accuracy of the TCAPM in Fission Cross-Section Measurement	
R. Arlt	
Determination of Fission Cross-Sections Relative to the	
(n,p)-Standard	
S. Cierjacks	
I. 2. Chairman: V. I. Shpakov	
Accuracy Requirements for Fission Cross-Sections Relevant	27
to Reactor Technology	
H. D. Lemmel	
Absolute Fission Cross-Section Measurement on 235-U at	35
8.4 MeV Using the TCAPM	
R. Arlt, W. Wagner et. al.	
I. 3. Chairman: S. Cierjacks	
Absolute Fission Cross-Section Measurement on 236-U with	40
2.6. MeV Neutrons (rus.)	
I. D. Alkhazov, A. V. Fomitshev et. al.	
Absolute Fission Cross-Section Measurement on 235-U at	44
2.6. MeV using the TCAPM (rus.)	
R. Arlt, M. Josch et. al.	
Determination of the Nonefficiency of a Pulse Fission	48
Chamber (rus.)	
R. Arlt, K. Herbach et. al.	
Alpha-Counting on Thin Fission Foils (rus.)	
R. Arlt, K. Merla, F.-G. Ortlepp	
Electronic Equipment used in Fission Cross-Section Measurements	
at the TU Dresden	
H.-G. Ortlepp	

	Page
Measurement of Fission Cross-Section Ratios using Track-Etched Detectors <u>M. Varnagy et. al.</u>	51
I. 4. Chairman: H. D. Lemmel	
Dynamics of Nuclear Fission <u>K. Dietrich</u>	54
Fine Structure Observation and Analysis in the Near Fission Threshold of Th-Isotopes <u>J. Blons, D. Paya et. al.</u>	68
Status of the 235-U (n,f)-Cross-Section Standard (rus.) (Included in the Paper at Page 9) <u>V. I. Shpakov</u>	
Features of the Energy Dependence of $\bar{\nu}$ in Fission (rus.) <u>B. D. Kuzminov</u>	72
I. 5. Chairman: R. Arlt	
Reactor Calculation Methods <u>C. Reiche</u>	73
Economy of Nuclear Power Plants (germ.) <u>G. Buhl</u>	81
High-Energetic Neutron Emission in Fission <u>H. Märten, D. Seeliger</u>	98
On-Line Experiment for the Determination of Neutron Emission Spectra by the Two-Dimensional Measurement of the Neutron Time-Of-Flight and the Scintillator Proton Recoil Energy <u>W. Grimm, H. Märten et. al.</u>	102
Summary of Session I: <u>S. Cierjacks</u>	
<u>SESSION II "HEAVY-ION-INDUCED REACTIONS"</u>	
II. 1. Chairman: R. Reif	
Application of Wigner-Transformations in Heavy-Ion Reactions <u>H. Esbensen</u>	106
Models and Theories for Heavy-Ion Collisions <u>G. Wolschin</u>	112

	Page
Investigation of the Neutron Spectra in Li-Ion-Induced Reactions (rus.) <u>L. V. Tschulkov</u>	
The Role of Deep Inelastic Transfers in Production of "Direct" Alpha Particles in Nuclear Reaction Induced by Heavy-Ions <u>L. Pomarski et.al.</u>	118
II. 2. Chairman: K. Dietrich	
Resonance Phenomena in Heavy-Ion Reactions <u>I. Rotter</u>	122
Dynamical Potentials and Charge Equilibration in Deep-Inelastic HI-Collisions <u>E. F. Hefter, K. A. Gridnev</u>	128
II. 3. Chairman: L. Münchow	
Energy Dissipation in HI-Reactions <u>R. Schmidt</u>	141
Angular Momentum Dissipation in Deep-Inelastic Heavy-Ion Collisions <u>G. Saupe</u>	134
Shell Effects in the Element Distribution of the $^{238}\text{U} + ^{238}\text{U}$ Reaction <u>P. Mädler et. al.</u>	137
Summary of Session II: <u>G. Wolschin</u>	
<u>SESSION III "NEUTRON-INDUCED REACTIONS"</u>	
III. 1. Chairman: L. Pomarski	
Model Calculations of Fast-Neutron-Induced Reaction Cross-Sections <u>M. Herman et. al.</u>	144
(n,Alpha)-Reaction Cross-Section Measurement at 3 MeV (rus.) <u>G. Helfer et. al.</u>	150
Gamma-Ray Multiplicities from ^{56}Fe (n,xn Gamma)-Reactions at 14.6 MeV <u>R. Antalik, P. Oblozinsky et. al.</u>	153
III. 2. Chairman: D. Seeliger	
Investigation of ^{28}Si (n,Alpha) ^{25}Mg in Terms of Statistical and Direct Reaction Mechanism <u>D. Hermsdorf</u>	158

	Page
Excitation of the Ground State Band and the 3^+ Non-Normal Parity State in ^{28}Si by Neutron Inelastic Scattering at Incident Energies between 6.8 and 14.8 MeV <u>D. Schmidt, T. Streil et. al.</u>	164
Evaluation of Gamma-Production Cross-Sections of Neutron-Induced Reactions in Si <u>D. Hermsdorf, E. Paffrath</u>	169
The Neutron Resonance Shift at ^{238}UF <u>K. Seidel, W. Pilz et. al.</u>	172
<u>SESSION IV "MISCELLANEOUS"</u>	
Chairman: P. Oblozinsky	
Rotating Target Intense Neutron Generators <u>T. Sztarizskai</u>	176
Rotating Target for a 300 KeV Neutron source: Design <u>J. Pivarzs et. al.</u>	185
Biomedical Research in the JINR Dubna Using Muonic Atoms <u>B. M. Sabirov</u>	189
Methodical Aspects of Muonic X-Ray Measurements <u>B. M. Sabirov et. al.</u>	194
X-Ray Diagnostics of Ion-Loaded Electron Rings at the Prototype of a Collective Accelerator in the JINR Dubna <u>G. Zschornack et. al.</u>	199
Symmetrical Effects in Bent Crystal X-Ray Spectrometers <u>G. Zschornack et. al.</u>	202
Sum-Rule for Inelastic scattering of Electrons and Nucleons <u>A. I. Blochin et. al.</u>	205
Evaluation of $(n,2n)$ - and $(n,3n)$ -Cross Sections for Fissionable Nuclei <u>V. M. Bitchkov et. al.</u>	208
Summary of Session III and IV: <u>D. Seeliger</u>	

List of Participants

Ärlt, R.	TU Dresden	GDR
Berces, J.	Univ. Debrecen	Hungaria
Buhl, G.	Kraftwerksanl.-Bau, Berlin	GDR
Chojnacki, S.	Univ. Warsaw	Poland
Cierjacks, S.	KFZ Karlsruhe	PRG
Dietrich, K.	TU München	PRG
Eckstein, P.	VIK Dubna	USSR
Esbensen, H.	Nordita, Kobenhaven	Denmark
Förtsch, H.	TU Dresden	GDR
Pomitshew, A.V.	RI Leningrad	USSR
Geßner, Th.	TU Dresden	GDR
Hefter, E.	Univ. Hannover	PRG
Helfer, H.	TU Dresden	GDR
Herbach, K.-W.	TU Dresden	GDR
Hermann, K.	IINR Swierk	Poland
Hermsdorf, D.	TU Dresden	GDR
Hoffmann, D.	SAAS Lohmen	GDR
Jahn, U.	TU Dresden	GDR
Josch, K.	TU Dresden	GDR
Kugler, A.	CSAV Rez	CSSR
Kusch, W.	IINR Swierk	Poland
Lemmel, H.D.	IIDS IAE, Vienna	Austria
Mädler, P.	TU Dresden	GDR
Märten, H.	TU Dresden	GDR
Merla, K.	TU Dresden	GDR
Münchow, L.	ZfK Rossendorf	GDR
Musiol, G.	TU Dresden	GDR
Oblozinsky, P.	SAS Bratislava	CSSR
Ortlepp, H.-G.	TU Dresden	GDR
Paffrath, E.	TU Dresden	GDR
Pausch, G.	TU Dresden	GDR
Paya, D.	CEN Saclay	France
Pfitzner, A.	ZfK Rossendorf	GDR
Pilz, W.	TU Dresden	GDR
Piverre, J.	SAS Bratislava	CSSR
Pomorski, L.	VIK Dubna	USSR
Reiche, C.	ZfK Rossendorf	GDR
Reif, R.	TU Dresden	GDR
Richter, U.	TU Dresden	GDR
Rotter, I.	ZfK Rossendorf	GDR
Sabirov, B. M.	VIK Dubna	USSR

Saupe, G.	TU Dresden	GDR
Schmidt, D.	TU Dresden	GDR
Schmidt, R.	TU Dresden	GDR
Schwengner,	TU Dresden	GDR
Schulz, H.	ZfK Rossendorf	GDR
Seeliger, D.	TU Dresden	GDR
Seidel, K.	TU Dresden	GDR
Shpakov, V. I.	RI Leningrad	USSR
Stobinski, B.	TU Dresden	GDR
Streil, T.	TU Dresden	GDR
Sztarizskai, T.	Univ. Debrecen	Hungary
Teichert, J.	TU Dresden	GDR
Theilig, B.	TU Dresden	GDR
Tschammer, H.	VIK Dubna	GDR
Tschulkov, L.V.	IAE Moskov	USSR
Unholzer, S.	TU Dresden	GDR
Varnagy, M.	Univ. Debrecen	Hungary
Wagner, W.	TU Dresden	GDR
Wolschin, G.	Univ. Heidelberg	FRG
Zschornack, G.	VIK Dubna	USSR

Лекция на Международный симпозиум
по взаимодействию быстрых нейтронов с ядрами, Гауссии, ГДР, 1980 г.

МЕТОДЫ АБСОЛЮТНЫХ ИЗМЕРЕНИЙ СЕЧЕНИЙ
ДЕЛЕНИЯ

Шаков В.И., Алхазов И.Д., Коваленко С.С.,
Фомичев А.В.

Введение

Данные по сечениям деления тяжелых ядер являются важнейшими ядерно-физическими константами для атомной энергетики и техники. В особенной степени это относится к сечению деления $^{235}_{\text{U}}$, которое в диапазоне энергий 100 кэВ - 20 МэВ является признанным международным стандартом. Измерениям и оценкам сечений деления посвящено большое число работ, проводившихся в целом ряде ведущих центров мира. Однако точность и достоверность имеющихся в настоящее время данных не удовлетворяют современным потребностям.

Подавляющее большинство результатов по сечениям деления получено в относительных измерениях с использованием в качестве опорной величины сечения деления $^{235}_{\text{U}}$. Эти измерения являются наиболее простыми, но содержат в себе в качестве систематической ошибки погрешность стандарта, а также чувствительны к эффектам рассеяния нейtronов, т.к. $^{235}_{\text{U}}$ - недороговой изотоп.

Для измерений сечения деления $^{235}_{\text{U}}$ также ряда наиболее важных нуклидов - $^{238}_{\text{U}}$, $^{237}_{\text{Np}}$, $^{139}_{\text{Pu}}$, используются методы абсолютные или подобные абсолютным, в которых измеряются нейтронный поток и число делений в мишени с известной массой делящегося вещества. Эти измерения можно разделить на 3 группы: I. Абсолютные измерения, 2. Измерения форм, 3. Низкоэнергетические измерения с нормировкой при тепловой энергии нейtronов.

В I-ой группе в измерениях определяется абсолютная величина нейтронного потока и соответственно абсолютная величина сечения. В остальных группах, исходя из известной энергетической зависимости эффективности нейтронного монитора, определяется форма зависимости сечения от энергии, которая затем нормируется к абсолютным величинам сечений деления (тепловому в 3-ем случае). Эти группы целесообразно объединить при рассмотрении, т.к. в методическом отношении они похожи и, как правило, проводятся на одиних и тех же установках.

Измерения в большинстве случаев проводятся в широком диапазоне энергий нейtronов на источниках нейtronов моноэнергетических или с "белым" спектром, причем последние являются наиболее эффективными, т.к. позволяют одновременно получать сечения во всем диапазоне энергий. При измерениях формы используются нейтронные детекторы с гладкой и плоской зависимостью

эффективности от энергии. При измерениях с нормировкой при тепловых энергиях используются детекторы с зависимостью от энергии $\frac{1}{\sqrt{E}}$ (n,α) или 10^{-8} (n,α) - реакции). Измерения с нормировкой при тепловой энергии проводятся в диапазоне энергий нейтронов, в которой сечение деления ^{235}U из-за сложности структуры не используется в качестве стандарта, поэтому из-за недостатка места в докладе рассматриваться не будут.

Наряду с этим проводились измерения и при фиксированных энергиях нейтронов 1 , 2 , которые хотя и дают отдельные значения сечений, однако используемый в них метод коррелированных по времени сопутствующих частиц позволяет исключить значительное число систематических ошибок, а результаты их могут с успехом служить для проверки и нормирования измерений формы.

Если методы регистрации числа делений во всех работах практически одинаковы - ионизационные камеры или газовые сцинтилляционные камеры с телесным углом 2π (исключение составляет лишь работа 3 , где применялся поверхностно-барьерный детектор), то методы измерения нейтронных протонов - конструкция и принцип работы мониторов - представляют некоторое разнообразие.

В данном докладе будут изложены наиболее употребимые методы абсолютных измерений и измерений формы, выполненных за последние 10 лет.

Измерения с черным детектором

Измерения сечения деления ^{235}U проводились в Аргонской национальной лаборатории 4 , 5 и Национальном бюро стандартов 6 . В качестве абсолютного монитора нейтрочного потока использовался так называемый "черный счетчик", предложенный Пенитцем 7 . Счетчик представляет собой цилиндр из водорода содержащего пластического или жидкого сцинтиллятора с осевым входным каналом, доходящим приблизительно до середины цилиндра. Счетчик может работать только с хорошо коллимированным пучком нейтронов, полностью укладывающимся в пределах входного канала. Нейтроны регистрируются по протонам отдачи. При этом нейtron, претерпевший соударение на дне входного канала и отразившийся в заднюю полусферу, практически со 100%-ной вероятностью вновь попадает в сцинтиллятор. В результате счетчик имеет эффективность, близкую к 100% в достаточно широком диапазоне энергий. Этот диапазон зависит от размеров счетчика, однако при увеличении счетчика существенно возрастает его собственный фон, что является особенно трагичным при измерении нейтронов с малой энергией. Поэтому черный счетчик не является универсальным прибором в широком диапазоне энергии, и требуется создание ряда счетчиков специфических размеров для отдельных энергетических интервалов.

Однако практическая пригодность таких счетчиков в области энергии нейтронов выше 8-10 МэВ остается сомнительной. Зависимость эффективности счетчика от энергии для счетчика длиной 40 см и диаметром 13 см приведена на рис.1.

Эффективность счетчика с хорошей точностью может быть рассчитана по программе, предложенной Пенитцем, и основанной на методе Монте-Карло⁸. Проверка расчета прямым измерением на основе метода сопутствующих частиц⁹ показала согласие в пределах 1,5%.

Амплитудный спектр импульсов черного счетчика (рис.2) имеет низкоэнергетическую часть до нулевых энергий. Поэтому при определении абсолютного интеграла по спектру процедура экстраполяции к нулевой энергии, необходимая из-за дискриминации шумов, является весьма критичной.

Измерения в Аргоннской национальной лаборатории проводились на ускорителе Ван-де-Граафа в диапазоне энергий нейтронов 35 кэВ - 3,5 МэВ (измерения формы)⁴ и 200 кэВ - 6,0 МэВ (абсолютные измерения)⁵. Измерения в Национальном бюро стандартов - также на ускорителе Ван-де-Граафа в диапазоне энергии 200 кэВ - 1,2 МэВ (абсолютные измерения). В качестве монозергетического источника нейтронов с энергией выше 4,5 МэВ использовалась реакция $D(d,n)^3He$ и $^{7}Li(p,n)^7Be$ при

$$E_n < 4,5 \text{ МэВ.}$$

В обоих случаях использовался импульсный режим работы ускорителя с длительностью импульса несколько наносекунд. Для уменьшения фонов в детекторах использовался отбор событий по времени пролета и по амплитуде.

Деления регистрировались многослойными плоскопараллельными ионизационными камерами. Мишени ^{235}U толщиной 100-150 мкг/см были нанесены на подложки из железа или молибдена толщиной 0,15 мм. Масса ^{235}U в мишениях в работах^{4,5} определялась по α -счету в малой геометрии. Примеси других нуклидов - масс-спектрометрией и колориметрическим массовым анализом. В работе⁶ масса ^{235}U определялась относительно стандартного слоя в тепловом потоке нейтронов.

Схемы экспериментальных установок приведены на рис.3.

При одинаковом нейтронном потоке скорость счета в черном детекторе приблизительно в 10^6 раз больше чем в камере делений. Поэтому для получения удовлетворительной счетности в камере делений оба детектора должны располагаться на существенно разном расстоянии от источника нейтронов. Более того, в работах^{4,5} камера делений находилась в условиях "открытой геометрии", т.е. облучалась неколлимированным пучком нейтронов. Все это приводит к возрастанию эффектов рассеяния нейтронов, в частности на массивных стенах камеры, увеличению влияния анизотропии нейтронного пучка и увеличению ошибок в определении геометрии облучения обоих детекторов. В работе⁶ использовалась специаль-

ная сборка из Li_2CO_3 и полиметилема, установленная на ми-
шениной части ускорителя, которая формировалась пучок в пределах
плоского угла $\pm 4^\circ$ с однородностью, по измерениям авторов, луч-
ше 1%. Нейтронный монитор во всех случаях помещался в массивную
защиту из борированного полиметилема и свинца, на входе защиты
устанавливался прецизионный коллиматор, определяющий телесный
угол на детектор.

Ниже следуют перечисления эффектов, искажающих результат
измерений и способы определения поправок.

1. Фон нейтронного монитора складывается из постоянного
"комнатного" фона и фона, связанного с пучком нейтронов. Фон
нейтронов с уменьшенной энергией, а также нейтроны 2-ой группы
отделялись по времени пролета. χ -фон, связанный с пучком,
определялся путем перекрытия входного коллиматора пробкой и
составлял величину от 0,2 до 1% в зависимости от энергии ней-
тронов.

2. Фон в камере деления из-за наложения α -импульсов и
нейтронов с низкой энергией также подавлялся по времени про-
лета. Однако эффект от 2-ой группы нейтронов из-за малой про-
летной базы не мог быть отделен и вклад делений, вызванных эти-
ми нейтронами, определялся из соотношений соответствующих пиков
во временном спектре нейтронного детектора. Фон от дейтонов,
попадающих на части ионопровода, а также фон от стенок камеры
проверялись как удалением мишени ускорителя, так и урановых
мишеней. Обе составляющие фона оказались пренебрежимо малыми.

3. Искажение нейтронного потока может происходить из-за
взаимодействия с входной частью коллиматора, рассеяния от внут-
ренней поверхности коллиматора в счетчик нейтронов, рассеяния и
поглощения нейтронов при прохождении камеры делений, рассеяния и
поглощения в воздухе и, в случай открытой геометрии, в рабо-
тах^{4,5}, из-за рассеяния на материалах и воздухе вблизи мишени
делящегося вещества. Последний эффект может приводить к увели-
чению счета в камере из-за возрастания эффективной длины пробега
нейтронов в слое. Кроме того, следует отметить эффект обратного
рассеяния от защиты в счетчик нейтронов, вышедших из него без
взаимодействия. Все перечисленные поправки рассчитывались с ис-
пользованием данных по сечениям взаимодействия из библиотеки
ENDF/B-IV. Поправка на взаимодействие нейтронов с входной
частью коллиматора определялась в работе экспериментально, пу-
тем измерений с коллиматорами 4-х разных диаметров. Было найдено,
что это взаимодействие эквивалентно увеличению эффективного диа-
метра коллиматора на 1,5%. В работах^{5,6} эта поправка вообще не
вводилась.

4. Определение интеграла амплитудного спектра нейтронного счетчика производилось с помощью фильтрования по методу Монте-Карло этого спектра распределением Пауссона (рис.2). Параметры фильтрования были энергией нейtronов, постоянные распределения Пауссона, которое характеризует эмиссию фотоэлектронов на аномале fotoумножителя. Процедура определения интеграла в работах^{4,5} не описывается.

5. Эффективность регистрации делений рассчитывалась в работах^{5,6} из величины потерь в счете из-за дискриминации шумов и поглощения осколков в слое вещества с учетом углового распределения осколков. В работе⁶ поправка на эффективность не вводилась, так как масса урана определялась относительно образца в той же камере. По-видимому, пренебрежение угловым распределением осколков при энергии нейtronов 1 МэВ может приводить к некоторой ошибке.

6. Геометрический фактор определялся из отношений и длиметров мишени и входного отверстия коллиматора нейтронного детектора. Однако представляется, что неблагоприятные условия эксперимента — недостаточная коллимация пучков, большое расстояние между детекторами, "открытая" геометрия (в работах^{4,5}) могут служить источником дополнительных ошибок и приводить к более сложной зависимости фактора от геометрии установки.

7. Эффективность нейтронных детекторов рассчитывалась по методу Монте-Карло, исходя из геометрии счетчика, сечения и углового распределения (π, ρ)-рассеяния, светового выхода сцинтилятора и т.д. с учетом взаимодействия нейtronов с ядрами углерода и пуассоновского распределения при эмиссии фотоэлектронов. Существенное влияние последнего фактора, приводящего к заметному расширению амплитудного спектра протонов, было обнаружено в работе¹⁰.

Результаты измерений формы, проведенные в работе⁴, нормировались по четырем величинам сечений, полученных авторами в абсолютных измерениях.

Как видно из сказанного, используемый метод содержит большое число поправок и, соответственно, источников систематических ошибок. Следует отметить, что измерения в работе⁵ представляют собой повторение измерений в работе⁴ по существу в тех же условиях. Результаты этих измерений заметно отличаются, причем причина этих измерений авторами не указывается и в общем остается неясной.

Типичные величины поправок и систематических погрешностей приведены в таблице I.

Таблица I

Типичные величины поправок и погрешностей при измерениях
с "черным" счетчиком

Эффект	Поправка (%)	Погрешность (%)
I. Фон нейтронного детектора	0,2-I	0,1
2. Фон в камере делений	0,I	0,I
3. Эффект от 2-ой группы нейронов и "хвоста" нейтронного пика	3-13	0,2-I
4. Рассеяние нейронов на коллиматоре счетчика	I,5	0,2
5. Рассеяние от стенок коллиматора внутрь	0,I-I,5	0,05-0,3
6. Рассеяние нейронов в ионизационной камере	I-2	0,2-0,5
7. Поглощение нейронов в ионизационной камере	I-2,5	0,2-0,3
8. Рассеяние нейронов в воздухе	5-I2	0,5-I,2
9. Обратное рассеяние от защиты в счетчик	0,I-I,5	0,2-0,5
I0. Рассеяние нейронов в окрестности мишени и вызванное этим увеличение счета		0,7
II. Определение интеграла протонного пика		0,I
I2. Эффективность камеры делений	0,I-0,5	0,I-0,2
I3. Мертвое время		0,2
I4. Геометрический фактор		0,5
I5. Эффективность нейтронного счетчика	3,5-II,5	I - 2

Измерения относительно (n, p)-рассеяния

Нейтронный поток определяется путем счета протонов, испущенных при взаимодействии его с тонким водородосодержащим радиатором. Такой метод, строго говоря, является относительным. Однако в связи с высокой точностью стандарта-сечения ($n-p$)-рассеяния, измерения, выполненные этим методом, принято относить к абсолютным. В силу ряда преимуществ простота, хорошее быстродействие, эффективность в широком интервале энергий нейтронов, низкая чувствительность к γ -фону — он является наиболее употребимым и, в частности, для измерений на источниках с "белым" спектром (10-16). Эти измерения являются темой отдельного доклада, поэтому здесь, для сопоставления с измерениями, с помощью черного счетчика целесообразно только перечислить основные источники систематических ошибок.

1. Фон нейтронного детектора состоит из временинезависимого "комнатного" фона, фона от $C(n,\alpha)$ реакции на углероде радиатора и, в случае использования для регистрации протонов

$Si(Li)$ — детектора — реакции на кремний с образованием заряженных частиц. Величина фона в этом случае меньше, чем у счетчика черного.

2. Фон в камере делений при измерениях на источнике с белым спектром в основном связан с частичным замедлением нейтронов, приводящим к увеличению времени пролета.

3. Искажения нейтронного пучка связаны с рассеянием его на мишнях делящегося вещества и окнах на камере, а также на свинцовой защите перед нейтронным детектором. Оно меньше по величине, чем в случае черного счетчика, что связано с хорошей коллимацией пучка, большими пролетными расстояниями и близким взаимным расположением детекторов.

4. В ряде работ^{3,II,I2,I3} протоны отдачи коллимировались при регистрации, амплитудный спектр их не достигал нуля и экстраполяции к нулевой энергии для определения интеграла не требовалось. В других работах^{I4,I5,I6} экстраполяция к нулевой энергии была необходима, причем величина поправки имеет заметную величину.

5. Эффективность регистрации делений такая же как и в случае черного счетчика.

6. Геометрический фактор не водится, так как из-за хорошей коллимации пучка, больших пролетных расстояний, можно считать, что оба детектора находятся в одном и том же пучке нейтронов.

7. Эффективность нейтронного монитора определяется из эффективности регистрации протонов массы водорода в реакторе и сечения (n,p)-рассеяния. При этом должны быть учтены однородность толщины радиатора и угловое распределение протонов отдачи (известное с точностью не лучше 2%).

Таблица 2

Типичные величины поправок и погрешностей при измерениях
относительно (n, ρ) - рассеяния

Эффект	Поправка (%)	Погрешность (%)
1. Фон нейтронного детектора	1-5	0,2-0,5
2. Фон детектора делений	0,1	0,1
3. Искажение нейтронного пучка	1	0,1
4. Определение интеграла протон- ного пика	0,5-5,0	0,2-1,0
5. Эффективность регистрации делений	0,1-0,5	0,1-0,2
6. Угловое распределение протонов отдачи	2,5	0,2
7. Зависимость времени срабатывания нейтронного детектора от энергии		0,4
8. Относительная энергетическая калибровка 2-х детекторов		0,5
9. Мертвое время	1,7	0,1

8. Зависимость времени срабатывания дискриминатора нейтронного монитора от амплитуды протонного импульса и т.с. от энергии нейтронов, что приводит к временному сдвигу и ошибке в энергетической калибровке.

В таблице 2 приводятся технические величины поправок и погрешностей измерений.

9. Точность энергетической калибровки в обоих детекторах, которая определяет не только точность абсолютной энергетической шкалы, но при измерениях на источниках с белым спектром, может приводить к ошибке в величине самого сечения.

Измерения с использованием сопутствующей активности

Эти измерения можно разбить на 2 группы:

- с использованием сопутствующих частиц,
- с использованием сопутствующей наведенной активности.

a) Измерения с использованием сопутствующих частиц

В этом случае источником нейтронов служат реакции

$T(d,n)^4\text{He}$ и $D(d,\gamma)^3\text{He}$. Сопутствующие нейtronам -частицы и гелионы служат для абсолютного измерения нейтронного потока. Измерения проводятся методами коррелированных и некоррелированных по времени сопутствующих частиц. В первом случае регистрируются совпадения между делениями и сопутствующими частицами, а величина сечения определялась из отношения числа совпадений и сопутствующих частиц^{1,2}. Этот метод является темой отдельного доклада и здесь можно только отметить, что по сравнению с предыдущими методами число источников систематических ошибок сведено к минимуму. В экспериментальные данные вводятся 3 поправки:

1. Фон в канале сопутствующих частиц (0,1-3%).

2. Искажение нейтронного потока (0,5-2,5%).

3. Эффективность регистрации делений (1-2%).

Основной вклад в погрешность измерений (1-2,5%) вносит статистика.

Метод некоррелированных по времени сопутствующих частиц был использован в работе¹⁸ для измерения сечения деления ^{235}U нейтронами с энергией 2,5 МэВ. В этой работе сопутствующие гелионы с энергией 700 кэВ регистрировались проточным пропорциональным счетчиком, а деления - ионизационной камерой. При обработке результатов измерений рассчитывался геометрический фактор и вводились поправки на угловое распределение реакции, искажение нейтронного пучка, эффективность регистрации гелионов и делений.

Основная трудность заключалась в определении интеграла по пику низкоэнергетических гелионов, полученных в детекторе с плохим энергетическим разрешением, на фоне тритонов и протонов из сопутствующей реакции $D(d,\rho)\text{H}$. Погрешность

величины этого интеграла была порядка 5% и превышала все остальные погрешности.

б) Измерения с использованием сопутствующей наведенной активности.

Измерения сечения деления ^{235}U нейтронами с энергией 0,6 МэВ таким же образом проводились в работе⁴. В качестве источника нейтронов использовалась реакция $^{51}\text{V}(\text{p},\text{n})^{51}\text{Cr}$. Источник нейтронов входил внутрь ионизационной камеры, состоящей из 2-х концентрических сфер. На поверхности внутренней сферы был нанесен слой ^{235}U с неоднородностью, не превышающей 5%. После облучения нейtronный поток определялся по γ -активности от распада ^{51}Cr , которая измерялась $\text{NaI}(\text{Te})$ -спектрометром, откалиброванным по образцовому источнику ^{51}Cr . Точность измерения была плохой из-за значительного нейтронного фона. Фоновые нейтроны возникали из-за бомбардировки диафрагмы и ионопровода ускорителя (1-2%), а также из-за рассеяния от стен и окружающих предметов (1-5%). Кроме того большой вклад в погрешность вносило рассеяние нейтронов на деталях камеры, которое приводило к удалению пробега в слое урана на 2,5-4,2%. Полная погрешность результата составила 4,9-6,9%.

Измерения на нейтронных источниках

В работах¹⁹⁻²¹ проводились абсолютные измерения сечений деления ^{235}U при 5-х фиксированных энергиях нейтронов с использованием фотонейтронных источников $^{24}\text{Na}-\text{Be}$ (964 кэВ), $^{140}\text{La}-\text{Be}$ (770 кэВ), $^{24}\text{Mg}-\text{D}$ (265 кэВ), $^{72}\text{Ga}-\text{D}$ (140 кэВ) и $^{124}\text{Sf}-\text{Be}$ (23 кэВ).

Спектр нейтронов от этих источников представляет собой мосснергетическую линию, расширенную за счет кинематических эффектов с низкоэнергетическим хвостом, возникающим за счет рассеяния нейтронов внутри источника. Энергия нейтронов от таких источников м.б. рассчитана по ~~известным~~ данным по энергиям связи и энергии γ -излучения.

Источники представляли собой сферический γ -эмиттер, окруженный сферической разборной оболочкой диаметром 35 мм. Интенсивность источников определялась измерением с высокой точностью методом марганцевой звезды. Схема эксперимента представлена на рис.4. Источник помещался между двумя урановыми мишенями, деления в которых регистрировались тремяными детекторами. Такая геометрия эксперимента делает это относительно нечувствительным к точному расположению источника в центре, для расчета телесного угла от источника на мишени достаточно только измерить расстояние ~~мишени~~, что особенно важно, принимая во внимание высокую γ -активность источников (порядка сотен кюри). Малые размеры источников при вычислении телесных позволяют считать их точечными.

Основную ошибку в измерения вносит эффект термализации нейтронов на окружающих предметах. Хотя стены и потолок помещения, в котором проводился эксперимент, были покрыты бором, эффект от рассеянных нейтронов оказывался. Поэтому измерения велись при различных расстояниях от источников до мишени с последующей экстраполяцией его к 0. Из-за короткого времени жизни γ -источников (15 часов - 50 дней) в результаты измерений вводились поправки на распад. Трековые детекторы располагались на некотором расстоянии от мишени, поэтому определялась эффективность регистрации осколков.

Погрешность полученных данных оценивается авторами величиной порядка 3%.

Результаты измерений и состояние стандарта -
сечения деления ^{235}U

На рис.5 представлены результаты, полученные в цитированных работах в сравнении с оцененными величинами из библиотек ENDF/B-IV и ENDF/B-V . При сопоставлении этих данных обращает на себя внимание ряд обстоятельств.

Данные, полученные разными авторами, существенно различаются, особенно в диапазонах энергий нейтронов 2-5 МэВ и 14-18 МэВ, где величина расхождения достигает 7-10%. При этом отличаются не только величины сечений, но и форма, что наглядно видно из сопоставления оцененных данных.

Анализ результатов разных авторов показывает существование определенных тенденций, так данные Ширьякова^I систематически выше других, а данные Карлсона^{II} систематически ниже.

Данные, полученные с использованием "черного" детектора, в большинстве случаев ниже и, во всяком случае, не выше, чем данные, полученные с использованием (p, p')-рассеяния. Это говорит о возможности существования систематических ошибок измерений.

При этом такие ошибки не являются присущими определенному методу, т.к. измерения Ширьякова и Карлсона выполнены аналогичными методами. На основе сопоставления данных, так же как на основе анализа погрешностей измерений невозможно сделать заключение о преимуществах того или другого метода. Очевидно, что чем большее разнообразие экспериментальных методик будет использовано, тем меньше будет влияние специфических систематических ошибок. Кроме того, очевидна необходимость прецизионных абсолютных измерений методами, содержащими минимальное количество источников систематических ошибок при отдельных значениях энергий нейтронов, результаты которых могут служить критерием оценки данных и осуществлять нормировку и контроль измерений формы.

Примером может служить энергетическая точка 14,5-15 МэВ, где наблюдается максимальный разброс данных.

Великолепное согласие результатов 4-х последних измерений Арльта и др.¹, Кансса² (методом коррелированных сопутствующих частиц) Цирра¹² и Карисона¹¹ (относительно (π, ρ)-рассеяния) позволяет считать полученное значение $2,07-2,09 \cdot 10^{24} \text{ см}^2$ достоверным. Это же значение рекомендует библиотека ENDF/B-V

Измерение Арльта²², выполненное методом коррелированных сопутствующих частиц на нейтронах с энергией 2,5 МэВ дало величину 2,15 бари, заметно более низкую, чем рекомендуемая обеими библиотеками, но прекрасно согласующуюся с данными работы Пенитца⁵, выполненной с использованием "черного" счетчика и работы Бартона³, выполненной с использованием (π, ρ)-рассеяния²³. Следует отметить, что измерения Кансса¹⁸ в данном случае дали более высокое значение. Измерения Кукса¹⁸ методом некоррелированных сопутствующих частиц дали очень высокое значение, которое, по-видимому, нельзя считать достоверным.

Обращает на себя внимание то обстоятельство, что подавляющее большинство данных, полученных в последних работах, за исключением измерений Цирьякса^{14,15} лежит ниже рекомендованных значений, т.е. по мере усовершенствования экспериментальной методики и увеличения точности измерений имеется тенденция к снижению величин сечений деления. Нужно сказать, что при измерениях сечений деления на других нуклидах - ^{238}U , ^{237}Np , ^{239}Pu - результаты последних измерений, как правило, ниже результатов более ранних работ.

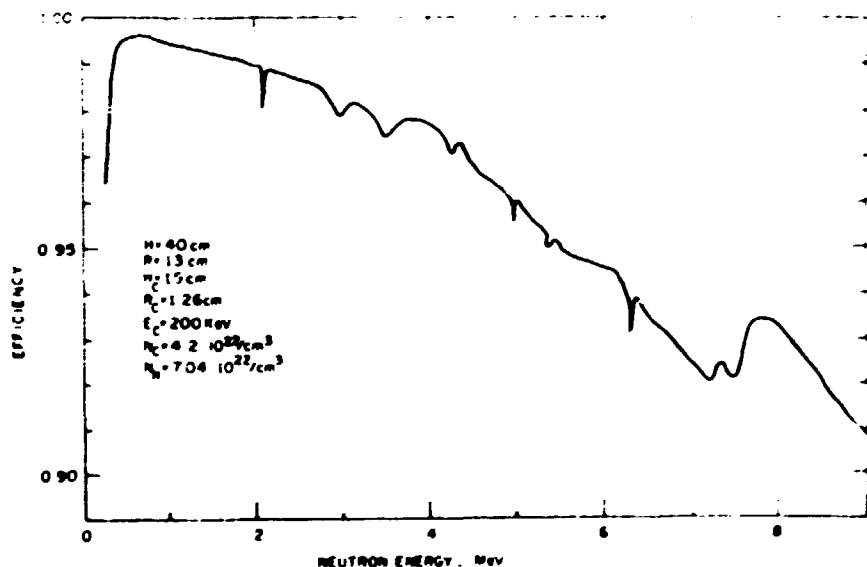


Рис ... Зависимость эффективности регистрации черного счетчика от энергии нейтронов.

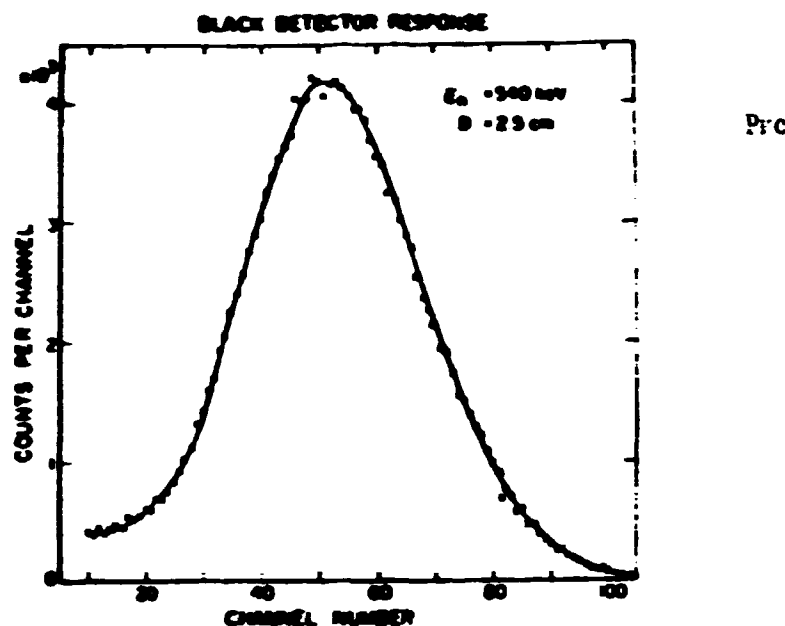


Рис. 2. Амплитудный спектр импульсов черного счетчика.

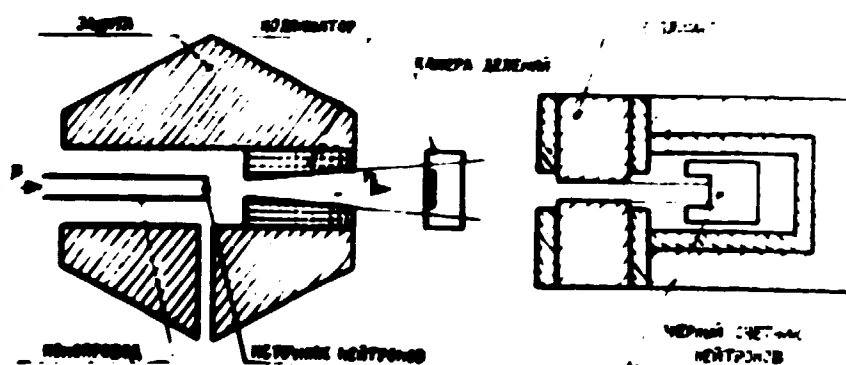
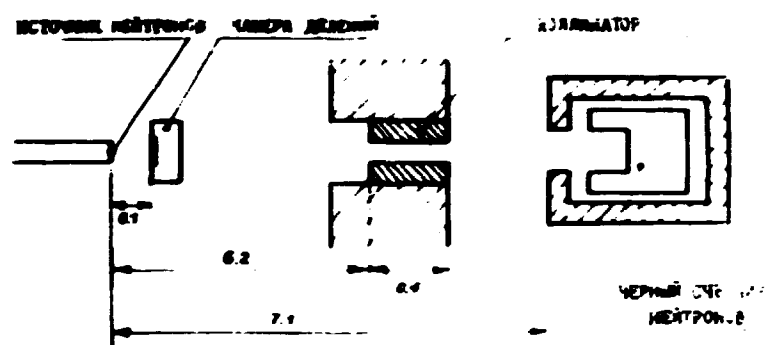


Рис.3. Схемы измерительных установок
а) из работ Пёнитца^{4,5}
б) из работ Воссена⁶

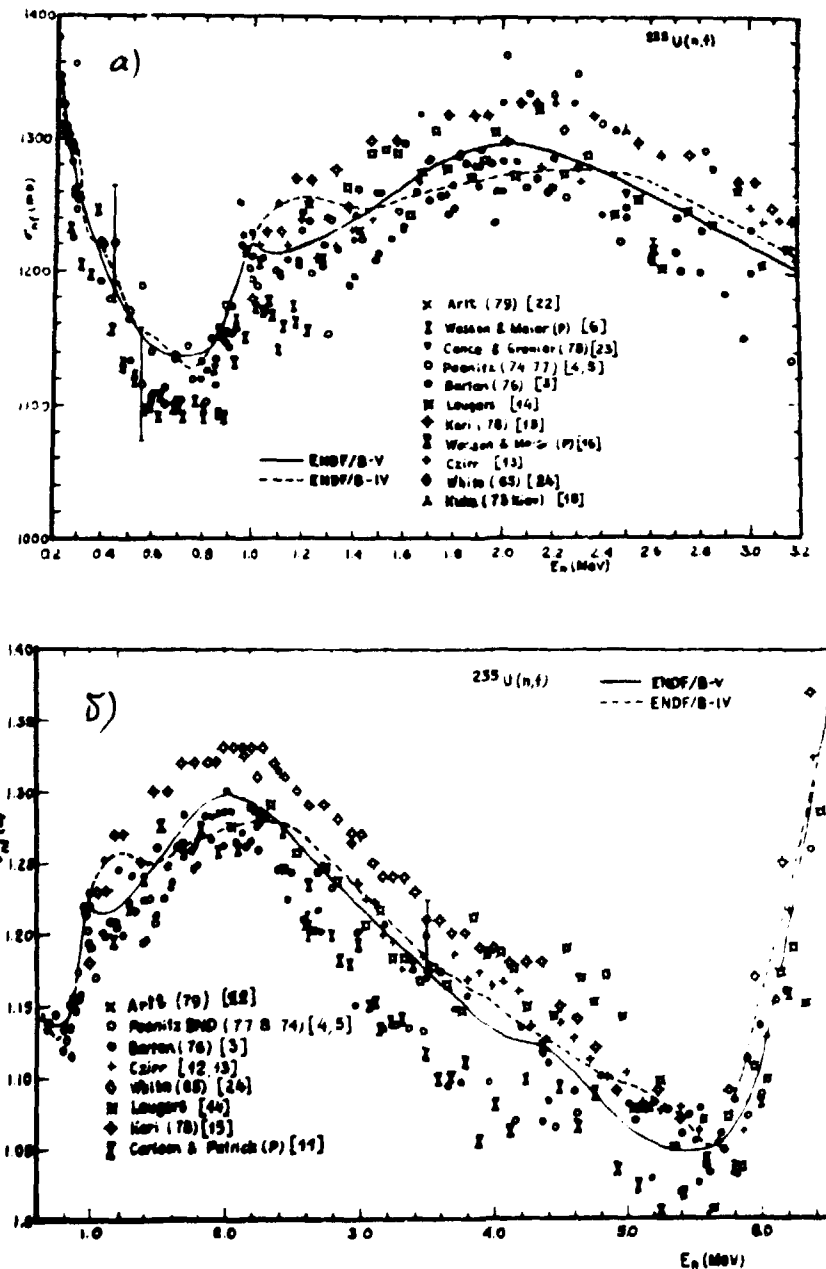


Рис.5а,б. Результаты измерений сечений деления ^{235}U и
оценки библиотек ENDF/ B-IV и ENDF/ B-V
в диапазоне энергий нейтронов

а) 0,2 – 3,2 МэВ

б) 0,6 – 6,6 МэВ

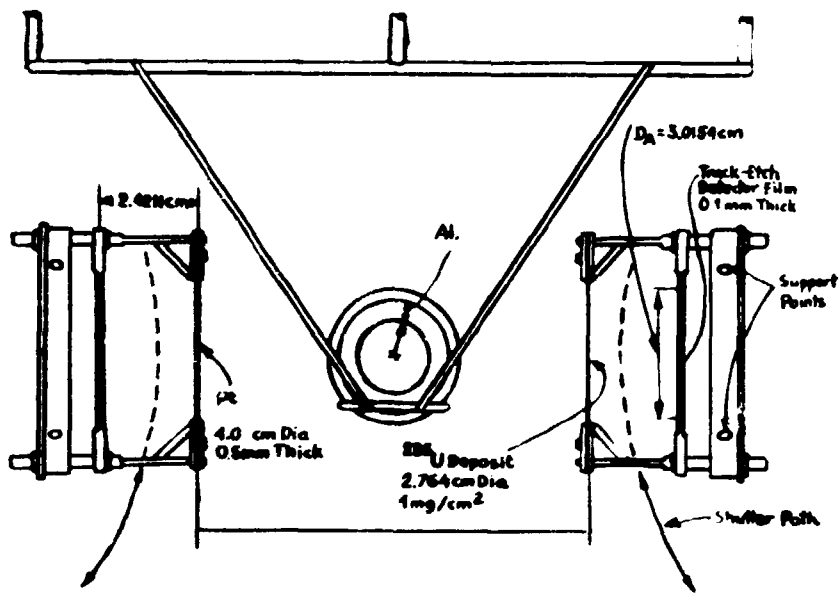


Рис.4. Схема измерений на фотонейтроник источниках

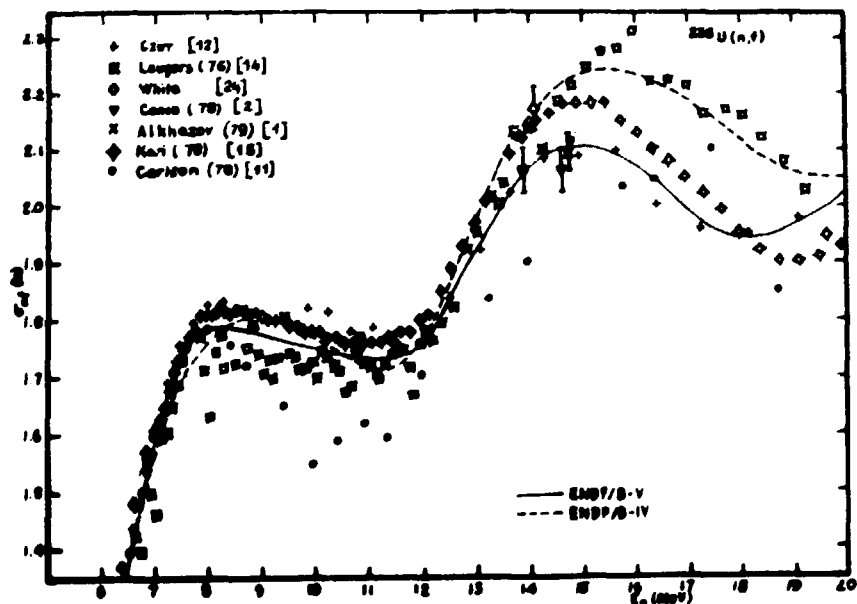


Рис.5в. Результаты измерений сечений деления ^{235}U и
оценки библиотек ENDF/B-IV и ENDF/B-V
в диапазоне энергий нейтронов 6-20 МэВ

Литература

1. Алхазов И.Д., Душин В.Н., Коваленко С.С. и др. - Атомная энергия, 1979, т.47, с.416
2. Cance M., Grenier G., In Proc. of NEANDC/NEACRP Spec. Meeting on Fast Neutron Sect. of U-233, U-235, U-238 and Pu-239, Argonne, USA, 1976 (ANL - 76 - 90, 1976), p.237
3. Barton D.M. et al. - Nucl. Sci. and Engineering, 1976, v.60, p.369
4. Poenitz W.P. et al.- Nucl. Sci. and Engineering, 1976, v.53, p.370
5. Poenitz W.P. et al.- Nucl. Sci and Engineering, 1977, v.64, p.894
6. Meier M.M., Wasson O.A., Duvall K.C. - Bull. Am. Phys. Soc., 1979, v.24, p.888
7. Poenitz W.P. - Nucl. Instr. and Methods, 1973, v.109, p.413
8. Poenitz W.P. - ANL-7915, Argonne, USA, 1972
9. Meier M.M. et al. In proc. of Conf. on Nuclear Cross Sect. and Technology, Washington D.C., USA, 1975 (NBS Special Publication 425, 1975), v.1, p.75
10. Lamaze G.P. et al.Ref.9, p.73
11. Carlson A.D., Patrick B.H. In proc. of Internat. Conf. on Neutr. Phys. and Nucl. Data for Reactors, Harwell, UK, 1978, p.881
12. Czirr J.B., Sidhu G.S. - Nucl. Sci. and Engineering, 1975, v.57, p.18
13. Czirr J.B., Sidhu G.S. - Nucl. Sci. and Engineering, 1975, v.58, p.371
14. Leugers B., Cierjacks S., Brots P. et al., Ref.2, p.246
15. Kari K., Cierjacks S., Ref.11, p.905
16. Wasson O.A., Ref.2, p.281
17. Hopkins J.C., Breit G. - Nuclear Data Tables, 1971, v.A9, p.137
18. Кукс И.М., Разумовский Л.А., Селицкий Ю.А. идр. - Ядерно-физические исследования в СССР, 1974, вып.17, с.33
19. Gilliam D.M., Knoll G.F. - Ann. of Nucl. Energy, 1975, v.2, p.637
20. Robertson J.C.,et al., Trans. of Am. Nucl. Soc., 1975, v.21, p.503
21. Davis M.C. et al., Trans. of Am. Nucl. Soc., 1975, v.21, p.663
22. Arlt R. et al., Bull. of Am. Phys. Soc., 1979, v.24, p.889
23. Cance M., Grenier G., Ref.11, p.864
24. White P.H. - Nucl. Energy, 1965, v.A/B 19, p.325

Accuracy Requirements for Fission Cross-Sections Relevant
to Reactor Technology

H. D. Lemmel
IAEA Nuclear Data Section
P.O. Box 100, A-1400 Wien

The economics of a nuclear power station are determined by a large variety of parameters from a wide range of science and technology as well as social and environment aspects. The uncertainty of nuclear data is a non-negligible facet within the problems encountered in the design and operation of a nuclear power station. A thumb-rule says that a 1000 MW nuclear power station costs 1 billion US\$ and the electrical output is worth 100 million \$ per year [2]. In view of such enormous figures, the consideration of the accuracy requirements of nuclear data becomes important even though it represents only one facet of the problem. Having in mind that many boundary conditions, in particular increasing safety requirements, will raise the nuclear power costs even further, one must realize that nuclear data is one of the few facets of the nuclear power problem where a reduction of costs can be achieved by more accurate nuclear data. Consequently, considerable efforts are justified to determine the accuracy requirements of nuclear data and to request experimental nuclear physicists and their funding authorities to meet the requirements determined [see references 1 to 14].

Generally, more accurate nuclear data are required to improve the understanding of fundamental physics underlying the processes that take place

- a.) within the fuel itself, and
- b.) within the structural materials and reactor components.

My topic is to consider the accuracy requirements for the fission cross-sections which, besides the capture cross-sections and the fission neutron yields, are the most important data for the nuclear fuel. More accurate knowledge of nuclear data

- may allow to reduce the required fuel enrichment,
- may allow extended burnup of the fuel,
- may allow better predictions of the performance of highly irradiated fuel during storage and reprocessing,
- and may, in particular, allow more flexibility in the design of alternate reactor types with different fuel compositions and with different neutron spectra.

Compare in particular ref. [8].

Having realized that more accurate nuclear data may bring savings for the design of more economic nuclear power reactors, one must realize at the same time that the measurement of nuclear data for the transactinium isotopes with the precision required is not a trivial matter either and requires significant investments. It is therefore essential to analyze which data are needed to which accuracy and with which priority. Since many years various national and international nuclear data committees therefore review their nuclear data requirements, and the IAEA Nuclear Data Section compiles these requirements in the World Request List WRENDA [1].

Investments for measuring precise nuclear data are not only needed in the form of accelerators and laboratory equipment but probably even more in the education of nuclear physicists. The experimental difficulties of modern precision measurements of nuclear data are such that only a limited number of laboratories in the world can fulfill the requirements. Many of these laboratories continue to find adequate support. Several new ones are reaching a state which enables them to significant contributions. But in some other laboratories one finds that the importance of nuclear data measurements and evaluations is not always sufficiently recognized so that experienced nuclear data physicists are forced into other subjects of research.

Data uncertainties in the fission cross-sections of actinide isotopes may have different reasons:

1. There are no accurate measurements: this is usually the case in inconvenient ranges of neutron energies and for certain isotopes where target materials are difficult to obtain.
2. There is only a single accurate measurement: this needs confirmation by another experiment possibly using a different method.
3. There are several accurate measurements which are discrepant. This is the most interest-

ing case as this may give the key for detecting unknown systematic errors and lead to improved experiments.

In June 1980 the International Nuclear Data Committee (INDC) had its 11th Meeting in Vienna. There is a standing subcommittee reviewing particularly disturbing data discrepancies, in cooperation with a similar subcommittee of the NEANDC (OECD Nuclear Energy Agency Nuclear Data Committee). I will refer to their findings later on. A most useful summary was given by M.G. Sowerby in May 1980 [9] which indicates that out of the 16 most serious data discrepancies considered, 12 concern the transactinium nuclides, and 6 out of these 12 concern discrepancies in important fission cross-sections.

Let us now have a more detailed look at WRENDA. The current issue is WRENDA 79/80 [1]. At present, national committees review their requests to be included in the 1981 issue, but these are not yet available.

WRENDA 79/80 includes requirements from 15 countries. Requests are included only if they were reviewed and confirmed by official bodies such as national nuclear data committees, and if it was found that existing experimental data do not have the required accuracy.

WRENDA 79/80 contains a total of 1780 requests, of which 60% are new or modified since the 1976/77 edition. 40% are continuing requests from the previous edition. 455 requests from the old edition were deleted because the request was either considered as fulfilled or withdrawn for other reasons. Three quarters of the requests relate to fission reactor technology, including nuclear material safeguards. The remaining quarter relates to nuclear fusion, where the number of requests increased from 328 in the 1976 edition to 449 in the 1979 edition.

Häfele et al [13] recently summarized the data requirements included in WRENDA for fast reactor technology. Within this category about 45% relate to structural materials and fission products. About 35% relate to the transactinium isotopes, mostly to their capture cross-sections, fission cross-sections, and the fission neutron yield \bar{v} .

U-235

The fission cross-section of U-235, this being not only the most important fissile isotope but also a standard reference material basic to other measurements, has been a top-priority request ever since 1966 when the first international nuclear data request list was published [14]. Already at that time, an accuracy of 1% has been requested for wide energy ranges. In retrospective, this was at that time a wishful thinking rather than a justified request. When formulating an accuracy requirement, one has to find a compromise between what is desirable and what is possible. Consequently, there is some element of personal judgement involved, and it is not surprising if the one requestor asks for 2% accuracy while the other is satisfied with 3% for the same purpose.

The requests compiled in the current issue of WRENDA have been formulated after careful consideration by various specialists. If one takes all these carefully justified requests together, the "wishful thinking" from 1966 is more or less confirmed. The U-235 fission cross-section is needed, with priority 1, from 0 milli-eV to 20 MeV, in large energy ranges with an accuracy of 1%; in other energy ranges 2 or 3% are considered sufficient. However, contrary to the past, the challenge of the 1% accuracy of fission cross-sections appears no longer to be unrealistic, as will be demonstrated in the present Gaussia Symposium.

The history of the 2200 m/s value of the U-235 fission cross-section illustrates the problem involved. In 1966 [15] this value was believed to be as accurate as $\pm 0.4\%$; yet the presently assumed value is 1.4% higher. It was only in 1974 that the 2200 m/s value of the U-235 fission cross-section was raised by about 1% because the U-234 half-life was reduced by 2% and due to more accurate sample-thickness corrections. But still today there exists a disturbing 1.5% discrepancy [16] for the thermal U-235 fission cross-section when measured either with monoenergetic neutrons or in a well-defined thermal Maxwellian spectrum. Thus the requested accuracy of 1% was not yet reached even for a value as basic as the thermal U-235 fission cross-section.

Considerable progress has been made in the resolved resonance region, but the more accurate data require increased accuracy in the interpretation of the available data. A month ago there was a evaluation workshop at the Brookhaven National Laboratory, where significant discrepancies were found between various different methods of deducing various resonance parameters and level spacings from the resolved resonance data available [17]. At present a review is going on under the guidance of J. G. Ulrich to shed some light on this topic. A set of resonance parameter data was sent to me on a magnetic tape to various interested laboratories with the request to determine average level spacings. The different results will be compared and evaluated by J. G. Ulrich so that it is hoped that a comparison will give significant information about the uncertainties introduced by different models of data interpretation.

In the present paper I tried to summarize the state of affairs in the field of fission cross-sections. I hope that the reader will find the paper especially useful for his work in the field of nuclear data compilation.

WRENDA 79/80

Summary of requests for fission cross-section measurements

For details see WRENDA itself [1]

Isotope	Energy Range	Required Accuracy	Comments
Th-232	1 MeV - 5 MeV	5%	fast reactors
	1.5 MeV - 7.2 MeV	5%	for neutron dosimetry using spectrum unfolding; 10% discrepancies between integral and differential data
	11 MeV - 14 MeV	10%	hybrid system design
	14.2 MeV	15%	neutron multipliers
Pa-233 Pa-234	500 eV - 3 MeV	5-15%	
U-232	1 keV - 3 MeV	50%	
U-233	0 eV - 100 eV	1%	
	100 eV - 20 MeV	5%	absolute
	1 keV - 10 MeV	1%	relative to U-235
U-234	1 keV - 3 MeV	50%	
U-235			reference standard, priority 1
	0 eV - 1 eV	1%	shape of low energy range for thermal reactors standard for other data
	7.5 eV - 11.5 eV	1%	for normalization at higher energies
	up to 1 keV	3%	
	1 keV - 15 MeV	1-3%	above 200 keV standard for other data; needed: 1. excitation function with calibration at several energies 2. measurements with overlapping energy ranges 3. new evaluation
	fiss. spec. average	2%	as integral test
U-236	1 keV - 3 MeV	10-50%	
	100 keV - 10 MeV	5%	relative to U-235
U-237	1 keV - 3 MeV	50%	
U-238			priority 1, may become a reference standard, also used for dosimetry
	500 keV - 1.3 MeV	4-5%	problem: data near threshold
	1.3 MeV - 15 MeV	1-2%	relative to U-235
		3%	absolute
	fiss. spec. average	2%	as integral test
U-239			new priority 1 request
	1 - 2 MeV	15%	
	50 keV - 7 MeV	2%	
	up to 15 MeV	1%	relative to U-235

Isotope	Energy Range	Required Accuracy	Comments
Np-238	1 keV - 2 MeV	50%	
Np-239	0 eV - 10 MeV	30%	
Np-240	1 keV - 2 MeV	50%	
Pu-236	1 keV - 2 MeV	10%	priority 1
Pu-237	1 keV - 2 MeV	50%	
Pu-238	1 keV - 15 MeV	15%	priority 1
Pu-239			highest priority request for fast reactor calculations
	0 eV - 1 eV	1%	
	1 eV - 3 MeV	2%	
	3 MeV - 20 MeV	2-5%	
Pu-240	0 eV - 15 MeV	3-10%	
Pu-241			priority 1
	0 eV - 10 eV	1-3%	
	10 eV - 15 MeV	5-10%	
Pu-242			priority 1
	1 keV - 3 MeV	10%	
	20 keV - 400 keV	3%	
Pu-243	1 keV - 3 MeV	50%	
Am-241			new priority 1 requests
	0 eV - 15 MeV	20%	
	1 keV - 3 MeV	10%	
	10 keV - 1.5 MeV	5-10%	
Am-242			
Am-242m			
Am-243			
	0 eV - 15 MeV	15%	new priority 1 requests
Cm-242			
Cm-243			
Cm-244			
Cm-245			
	0 eV - 15 MeV	30%	partly new priority 1 requests, possibly 10% for Cm-244 and Cm-245
Cm-246			
Cm-247			
Cm-248			
Bk-249			
	1 keV - 3 MeV	50%	lower priority
Cf-250			
Cf-251			
Ea-253			
	0 eV - 10 keV	10%	old priority 1 requests

I would like to mention a work that has been performed by Musgrave, Boldeman et al [18]. They measured the angular distribution of fission fragments from the U-235(n,f) and U-233(n,f) reactions, using monoenergetic neutrons of energies between 50 keV and 1.85 MeV at 100 keV intervals. Such measurements have been done earlier. Musgrave et al then undertook a channel analysis to seek simultaneous fits to the fission cross-sections and to the angular fragment distribution data, using transition state spectra and barrier parameters from Just et al (1979). It appears that their channel analysis was quite successful for the 100 keV range fission of U-233 and U-235, and preferable to the usual statistical approach. The statistical behaviour of the U-235 s-wave fission widths has presented a problem for nearly a decade. A suitable set of fission channels could be found by Musgrave et al, indicating that the contribution through the 2⁻ band may be the largest component in low-energy s-wave fission. Up to a few hundred keV good agreement with the experimental cross-sections can be achieved using only a few channels. Thus, this method could possibly be useful in predicting unmeasured fission cross-sections of other transactinides.

It is noteworthy that the accuracy of data in the resonance region may be limited by computer economics. The best representation of resonance parameters seems to be provided by the Reich-Moore formalism. However, in the processing of evaluated data files, the high computer costs required for this formalism make it at present economically unfeasible. Consequently, the Reich-Moore formalism, which was provided in the ENDF/B-IV format, is no longer used in ENDF/B-V [22].

The unsatisfactory situation of U-235 fission cross-sections in the 14 MeV range was illustrated by Arlt et al [19] and confirmed by the Discrepancy Subcommittee of the INDC, which concluded that the recent measurements in the MeV range can be divided into a group with higher fission cross-sections and another one with lower data, and the discrepancy remains unresolved.

The work done at Dresden and Leningrad, that will be reported today in the subsequent papers, will contribute to solve this disturbing discrepancy. Updatings of the existing U-235 evaluations may then become necessary.

To achieve the required accuracies for the full energy range will be very difficult. M.G. Sowerby [9] formulates:

In view of the large number of existing data, new measurements should be made

- (a) if the accuracy is likely to be significantly better than previously, or
- (b) if a new technique is used, or
- (c) if errors in earlier work can be identified.

For more accurate data two main problems require attention:

- to improve techniques for neutron flux measurements,
- and to improve the determination of fission foil masses.

In both cases inter-laboratory comparisons are considered and should be supported.

Th, U, Pa isotopes

New requirements for data of Th-232, U-233 and other U and Pa isotopes arose from the interest in Th-U reactors in order to avoid the risks involved in the accumulation of Pu-239.

Here again it is amazing that one of the oldest requests has not yet been fulfilled: For U-233 there exists not a single accurate and absolute fission cross-section measurement with monoenergetic neutrons in the thermal energy range. Only measurements of the curve shape exist, and measurements in a thermal Maxwellian spectrum or relative to U-235, which all is not quite sufficient.

For the higher energy range the NEANDC/INDC Subcommittee on Discrepancies concluded, that there are many recent data of good quality. But in the essential energy range

- between 100 keV and 1 MeV there are significant discrepancies in the fission cross-section, amounting to more than 5%;
- the accuracy above 1.2 MeV is certainly not better than 3% to 4%;
- an accuracy of 1% as requested is out of reach;
- more absolute measurements are needed.

For Th-232 the situation is not bad, as there exist several new measurements covering the full energy range of interest. The Discrepancy Subcommittee concluded

- that there is a small energy-scale problem near threshold;
- some discrepancies in the 8-10 MeV range are encountered;
- more accurate 14 MeV values are needed, as several data sets are normalized to this point;
- the new measurements available partly supersede the ENDF/B-5 evaluation, and therefore a new evaluation is required.

The requirements for U-238 have been increased as the INDC considers to include U-238 among the recommended reference standard materials. It is also essential for reactor dosimetry. The problems with U-238 concern more the capture cross-sections and resonance parameters.

Higher actinides

The requirements for the higher actinides result from the fact that their concentration in fast breeder fuels is in some cases 100 or 1000 times as high than in conventional thermal reactors (compare J. Bouchard [7]). Some of these appear in a concentration of kilograms per ton of fuel, so that their fission cross-sections need to be known with high accuracy. Others, that appear in lower concentrations, need to be known only with accuracies of 30 to 50%. In these cases nuclear theory supported by experiments at some energies may be sufficient.

For Am-241, which is one of the more important actinides, the fission cross-section requirements seem to be fulfilled below 100 keV. The INDC Discrepancy Subcommittee noted however a factor-2 discrepancy between the measured resonance integral and that deduced from the resonance parameters.

Pu-239

Let me now consider the data situation using the example of Pu-239, to examine whether the accuracy requirements are fulfilled. Quite recently a new fission cross-section measurement for Pu-239 was published by Magemans et al [20]. In the eV and keV range we have now 12 experiments. Some of them are discrepant, others agree quite well. The discrepancies in the different energy ranges are illustrated in the following table. It is statistically legitimate to ignore extreme values, as the "standard deviation" is defined such that about one third of the data lies outside.

Experiments of (Pu-239) up to 30 keV

Energy range				Requested Accuracy
0.03 - 0.1 eV	4	experiments agree within	0.6%	
0.1 - 0.5 eV	4		3.0%	1%
10 - 20 eV	7	of 9 experiments agree within	1.0%	
20 - 30	8	10	5.4%	
30 - 40	6	10	17. %	
40 - 50	7	9	7. %	
50 - 100	6	9	3. %	
0.1 - 0.2 keV	7	10	5. %	
0.2 - 0.3	5	8	1.7%	2%
0.3 - 1	7	10	7.5%	
1 - 5	9	11	5. %	
5 - 6	7	10	7. %	
6 - 10	6	10	2.5%	
10 - 20	5	8	6. %	
20 - 30	4	5	2.5%	

How can we decide whether the requested accuracy has been achieved? L.N. Usachev formulates [1]: A request can be considered as fulfilled when at least 3 measurements with different methods agree within the requested accuracy.

Thus, the thermal range, where 4 experiments agree within 0.6% looks very satisfactory. However, one must be very careful. It is possible that these 4 experiments are all correlated by using the same standard reference values [$B-10(n,\alpha)$, $T_{1/2}(\text{Pu-239})$] and by using at least partly similar techniques. The next energy range up to 0.5 eV, which is far away from the 0.0253 eV reference point, shows that there are still problems to solve. In the other energy ranges listed in the table between 10 eV and 30 keV the situation is partly already very satisfactory. The 17% discrepancy in the 30-40 eV range is not serious because the cross-section is here quite small. The requested accuracy of 2% seems to be reached in limited energy ranges. The existing 5% discrepancy in other energy ranges can likely be reduced by a careful evaluation of the different experiments and their error sources and uncertainties.

In the keV/MeV energy range, accuracies required are 1% to 2%, with increased requirements in the range below 1 MeV. The accuracy of experimental data is certainly still insufficient. Also the capture-to-fission cross-section ratio α requires new precise determination.

In the 14 MeV range I can again quote the work performed at Dresden where an accuracy of $\pm 1\%$

was achieved, which is better than requested. But the Usachev-requirement that at least 3 independent measurements must agree within the required accuracy has not yet been fulfilled. The spread of data is $\pm 4\%$.

In this survey I had to restrict myself to the more important nuclides. I would like to add a concluding remark.

Error correlations

Precision measurements in the 1% accuracy range require utmost care in the documentation of corrections and uncertainties. Let me demonstrate this using the example of the Pu-239 data in the keV range.

Approximately, there are 9 experiments with a 3% accuracy each. Calculating a weighted average of the 9 experiments, the error will be reduced to the required 1% - provided the experiments are independent. Of course, they are not independent, and the true uncertainty lies somewhere in between of 1% and 3%. The correct uncertainty can be estimated only by a careful error correlation analysis. For the main fissile isotopes U-235 and Pu-239 such a correlation analysis exists, for example, by Kon'shin [21]. The new rules for the ENDF/B format [22] permit the inclusion of error correlations. There are also various problems involved when comparing experimental data that have different energy resolutions. Related problems were discussed at the Nuclear Data Evaluation Workshop in Brookhaven, September 1980 [12]. I would like to forward a recommendation of this Workshop which was seconded by the IAEA Meeting of Nuclear Reaction Data Centers (Sept/Oct 1980).

When reporting precision measurements of nuclear data, the authors should be as specific as possible in quoting the size of all corrections performed together with their estimated uncertainties, also quoting standard cross-sections, half-lives and other reference values together with their assumed uncertainties. Possibly this should be done not only in the text but in tabular form. If the measurement is a function of energy, such tabulations of corrections and uncertainties are required for different energy ranges and possible correlations between the data at different energies should be discussed.

This will then enable the data evaluator to consider the data with the weight they deserve. Many good experiments are known which must be down-weighted or ignored, because the publication includes insufficient information about corrections and error analysis, either because the author did not take it important or the journal editor did not want to include too many details. In any case, detailed information about corrections and error analysis should be submitted together with the data to the nuclear data center, so that sufficient detail can be included in the EXFOR data file [23] which has developed to a significant information system supplementing conventional publications.

Literature on accuracy requirements for fission cross-sections

- [1] D. W. Mair, editor, WRENDA 79/80, INDC(SEC)-73, Oct. 1971
- [2] J. L. Rowlands, Nuclear data for reactor design, operation and safety, 1978 Harwell Conference on Neutron Physics and Nuclear Data for Reactors and other Applications, Proceedings by OECD, 1978
- [3] B. H. Patrick, Fast fission cross-sections of the major transactinium isotopes, 1978 Harwell Conference, as above
- [4] O. Ozer, Nuclear data needs for LWR applications, 1979 Knoxville Conference on Nuclear Data, Proceedings being published
- [5] Ph. Hammer, Nuclear data needs for plutonium breeders, 1979 Knoxville Conference, as above
- [6] H. Kisters, Nuclear data needs for the analysis of generation and burn-up of actinide isotopes in nuclear reactors, 1979 Knoxville Conference, as above
- [7] J. Bouchard, Comprehensive review of TND requirements for U and U-Pu fuelled thermal and fast reactors, and their associated fuel cycles, 1979 Cadarache Meeting on Transactinium Isotope Nuclear Data, IAEA-TECDOC-232, IAEA 1980
- [8] H. Kouts, TND requirements for alternate fuel cycles, 1979 Cadarache Meeting, as above
- [9] M. G. Sowerby, Review of Important Nuclear Data Discrepancies, NEANDC-124 = INDC(UK)-33, May 1980
- [10] B. H. Patrick and M. G. Sowerby, An Assessment of the accuracy requirements on higher actinide nuclear data for fast reactors, NEANDC(UK)-174 = INDC(UK)-34, June 1980

- [14] Z.H. Fröhner et al., Report of the Inconsistency Subcommittee to the 11th INEC-Meeting, June 1980. Not yet published
- [15] J.J. Scheidt, Summary Review on the Nuclear Data Evaluation Workshop, Brookhaven National Laboratory, 22-25 Sept. 1980
- [16] S. Răpeanu, P. Ilie, G. Vasiliu, C. Popescu, St. Boeriu, O. Constantinescu, S. Mateescu, Report ISNE-148-1980 (in Romanian)
- [17] European-American Nuclear Data Committee, RENAK, EANDC-10 (March 1986)

Other references

- [18] G.H. Westcott, K. Ekberg, G.C. Hanna, N.J. Laiender, S. Senatani, P.M. Attree, A survey of values of the 2200 m/s constants for four fissile nuclides, At. En. Review 2, No. 2 (1965) p.3
- [19] H.D. Lemmel, Remarks on the 2200 m/s and 20°C Maxwellian neutron data for U-233, U-235, Pu-239 and Pu-241, Int. Symp. on Neutron Standards and Appl., (March 1977) NBS Special Publ. 493 p.17
- [20] P. Raboy, report IFANDC(P)-213 (1980)
- [21] J.W. Bildman, private communication 1980, to be published
- [22] S. Arlt et al., progress report ZFK-350 (1978)
- [23] C. Wagemans, G. Joliers, H. Willems, H. Barthélémy, Measurement of the μ -232(n,f) cross-section from thermal up to 10 keV neutron energy. Annals of Nucl. En., 2 (1960) 435
- [24] T.A. Kon'shin, B.I. Sukharevski, V.B. Sharov, Determination of the errors in evaluated data with allowances for correlations: emulsion of μ -232, α -232, α -231 and of μ -231 for the Evaluated Nuclear Data Library ENDF-B. English translation by TANP, I (DOE/DP)-132 (April 1979)
- [25] P. Raboy, Data formats and procedures for the evaluated nuclear data file ENDL, ENDF-4, ENDF-5, ENDF-6, ENDF-7 = ENDF-10P, Brookhaven Natl. Lab. Rep.
- [26] M.J. Rodriguez, private communication, Nuclear Data Department

AN ABSOLUTE FISSION CROSS SECTION MEASUREMENT ON ^{235}U AT 8.4 MeV NEUTRON ENERGY

R. Ditt, M. Josch, G. Martel, H.-C. Oehlert, C. Thausch, L. Richter, M. Reichenbacher, M. Rauher
Technische Universität Dresden, Department of Physics, D-0100 - 01027 Dresden

I.B. Alkhakov, N.V. Kapchinsky, I.I. Kharlamov, A.S. Novikov, V.I. Shpakov
Khlopin - Radiuminstitute Leningrad, USSR

Abstract

The fission cross section (f.c.s.) of ^{235}U was measured absolutely applying the time correlated associated particles method (TCAPM) for the determination of the 8.4 MeV monoenergetic neutron flux. Corrections and errors are given.

Introduction

The precise determination of the ^{235}U f.c.s. has been a topic of extensive investigation during the recent ten years. The reason is its general use as a neutron reaction cross section standard which should be known with an accuracy of 1 % /1/.

After the Specialists Meeting on Fission Neutron Cross Sections held in Argonne in 1976 /2/ it could be stated that the reached accuracy of the ^{235}U f.c.s. over an energy range up to about 14 MeV is at the order of 1 %. Taking into consideration the possible influence of any new source effects a further enhancement of the precision of fission cross sections by an additional uncertainty of $\sim 2 \%$ is required /3/.

Since 1975 cooperative efforts of the Tandem and the Teploj-atomkern-institut in Leningrad have been directed on the application of the TCAPM for absolute f.c.s. measurement at selected spot-points of neutron energy /4/. In this way a new unified and precise base for the realization of f.c.s.-shape measurements in the energy region from 1 MeV up to 20 MeV should be created.

At a neutron energy of about 14.7 MeV the TCAPM in connexion with the source reaction $\text{T}(\text{d},\text{n})^3\text{He}$ is well established now. The results of our recent measurements on ^{235}U , ^{238}U , ^{232}Th and ^{239}Pu were published earlier /5/. Due to careful investigations of possible sources of systematic errors typical uncertainties between 1.1 % and 1.8 % could be achieved /6/.

Experimental equipments for f.c.s. measurements at 2.6 MeV and about 8 MeV using the $\text{D}(\text{d},\text{n})^3\text{He}$ reaction for the production of monoenergetic neutrons were described also recently /7/.

The TCAPM for absolute fission cross section measurement at 8.4 MeV

Preliminary experimental data of a first f.c.s. measurement on ^{235}U using the TCAPM in this energy region have been reported in ref. /4,7/.

Monoenergetic neutrons were produced applying the $\text{D}(\text{d},\text{n})^3\text{He}$ reaction at the 5 MV - Tandemgenerator of the ZfK Rossendorf. As source targets thin $(\text{CD}_2)^n$ -foils were used. To separate the associated ^3He -particles from the intense background of charged particles a silicon surface-barrier-detector telescope was employed. A special fast particle discriminator has been developed to rea-

lize the TCAPM.

Further measurements of the ^{235}U f.c.s. had been provided at a neutron energy of (8.46 ± 0.25) MeV to reduce the unacceptable large statistical error of the first experiment. For this purpose the neutron production rate at a deuteron energy of 9.5 MeV had to be enhanced by a factor $5 - 10$. This could be obtained

- by use of a new rotating target mechanism with an increased effective diameter to diminish thermal damage of the target foils
- by use of a larger entrance diaphragma of the associated particle counting system.

A neutron flux within the cone of $(1.5 - 2) \cdot 10^3$ per second and msrad has been realized.

The associated ^3He -particles were identified applying the dE/dx -particle identification method in some modification for use in a small dynamic range /6/. A new fast particle identifier was developed which generates a particle spectrum within a defined energy window. This particle spectrum (fig. 1) was summed over the whole measurement time. The amount of alpha-background events within the ^3He -window could be determined effectively by change of the $(\text{CD}_2)^n$ -target foil with a $(\text{CH}_2)^n$ -foil of comparable thickness.

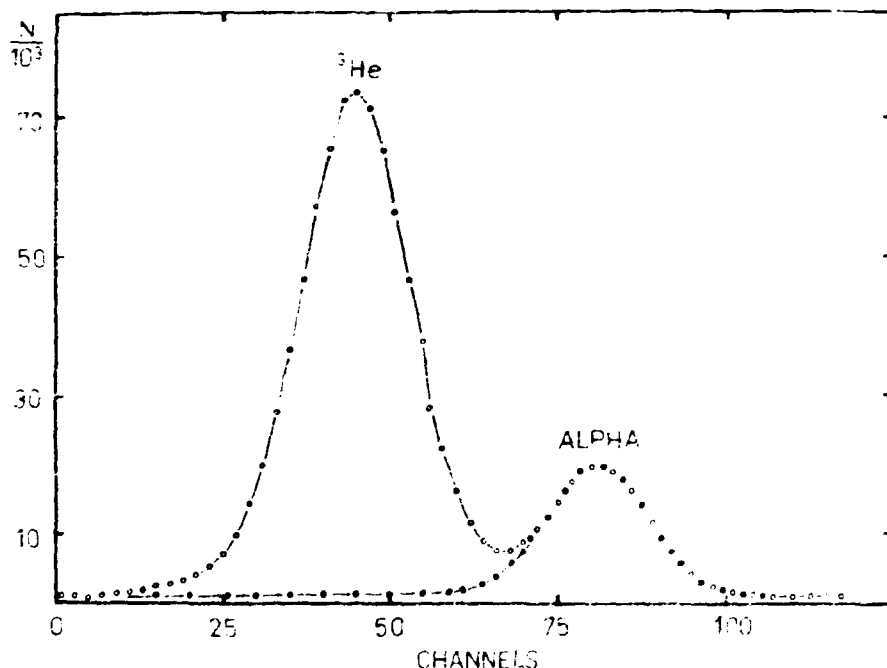


Fig. 1 Particle spectrum of the particle identifier. The alpha-peak arises from the reaction $^{12}\text{C}(\text{d},\alpha)^{10}\text{B}$.

Optimizing the particle separation a typical amount of alpha-background of 2 - 3 % could be obtained.

To consider the main condition of the TCAPM, that all neutrons of the cone have to be able to induce some fission event in the sample, the profile of the neutron cone was scanned again. In this geometry a FWHM = 4.5° of the neutron intensity distribution was measured which is in agreement with appropriate kinematical calculations/8/ (fig. 2).

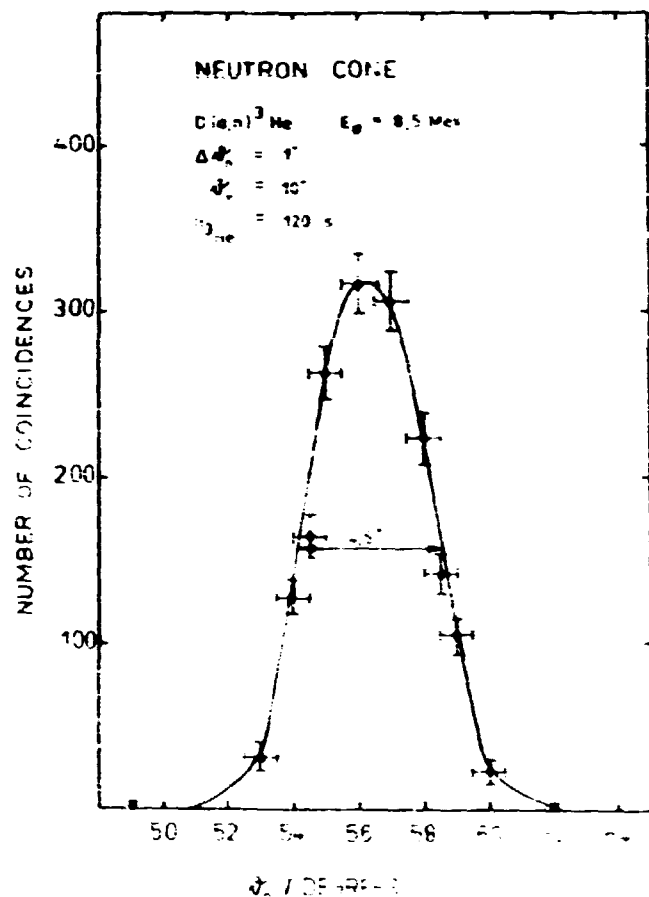


Fig. 2 Neutron cone profile in the case of
a 6 mm telescope diaphragma.

Tab. 1 Experimental conditions of the
 ^{235}U f.c.s. measurement

E_n	(8.46 ± 0.25) MeV
E_d	9.5 MeV
$(\text{CD}_2)^n$ - foil	(0.9 ± 0.1) mg/cm ²
beam current	~ 500 nA
focus	63 mm
target ring	630 mm
rotation	2 s ⁻¹
target angle	75°
telesc.-diaphr.	6 mm
^3He angle	(41.5 ± 1.5) °
solid angle	~ 1.25 sterad
^3He count.-rate	$(1.5 - 2) \cdot 10^3$ s ⁻¹
ΔE-detector	14 μm / 140 keV
E_p -detector	43 μm / 13 keV
time resolution	~ 2 ns

The mean fission rate could be increased by optimization of the areal densities of the five ^{235}U - targets which were arranged inside a multiplate pulse-fission-chamber.

The experimental conditions of the f.c.s. measurement of ^{235}U are given in table 1.

The applied corrections to the measured f.c.s. value and its partial uncertainties to the standard deviation of the cross section are quoted in table 2. It can be seen that the uncertainty of the absolute determination of the neutron flux due to the application of the TQIM is of the same order as the uncertainties due to the determination of target parameters.

Providing a careful optimization of all experimental conditions uncertainties of absolute f.c.s. measurements at about 8.5 MeV neutron energy of $\sim 2\%$ could be expected. The accuracy of 1 %, however, seems to be somewhat unrealistic at present.

Result

In table 3 our result is compared with f.c.s. values measured by other authors. Measurements applying three independent and in principle different methods are available. Excellent agreement within the given standard deviations is observed between

fission chamber	5 targets
gas pressure	1.9 kPa H_2
total ^{235}U	
areal density	(1.042 ± 0.007) mg/cm ²
neutron cone	$\theta_{\text{cone}} = 4.5^\circ$
	total width $\sim 10^\circ$
max. target dist.	6 cm / 18.5°

Tab. 2 Corrections and uncertainties
of the ^{235}U f.c.s. measurement

weighting	$\pm 1.0 \%$
inhomogeneity	$\pm 0.9 \%$
cone geometry	$+ 0.15 \pm 0.05 \%$
 counting of TCAFM coincidences:	
statistics	$\pm 1.52 \%$
random coincidences	$+ 7.46 \pm 0.59 \%$
efficiency of the fission chamber:	
extrapolation to zero pulse height	$+ 2.25 \pm 0.67 \%$
absorption of fragments in the fissile layers	
	$+ 1.45 \pm 0.30 \%$
 counting of ass. particles:	
statistics	$< \pm 40^{-4} \%$
alpha-background	$+ 2.82 \pm 1.23 \%$
neutron scattering	$+ 0.25 \pm 0.40 \%$
 standard deviation	
	± 2.4

Tab. 3 Measured fission cross sections of ^{235}U at $8 + 14.7 \text{ MeV}$

Institute	Method	Energy MeV	$\bar{\sigma}_f$ barn	$\frac{\sigma_f}{\bar{\sigma}_f}$
ANL (1974) /9/	(n,p)	8.27	1.83	2.1 statistical uncertainty
KFK (1976) /10/	(n,p)	8.44	1.750	2.24 statistical uncertainty
(1978) /11/		8.4	1.81 ± 0.16	3.33 standard deviation
ANL (1977) /12/	black neutron detect.	8.27	1.793 ± 0.062	3.5% standard deviation
NBS (1973) /13/	(n,p)	8.4	1.75	2 - 3 % stat. uncertainty
TU (1979) /14/	TCAFM	8.0	1.74 ± 0.11	6.3% standard deviation
(1980) /6/		8.46	1.801 ± 0.043	2.4% standard deviation

Figure 3 shows our 14.7 MeV and 8.4 MeV results for the f.c.s. of ^{235}U in comparison with experimental data of recent f.c.s. shape measurements and with data files of f.c.s. evaluations. /14/. Discrepancies with KFK /10/ are obvious at both energies. The point at 8.4 MeV confirms most of compiled files while some data revision at 14.7 MeV has been provided last time.

the KFK /11/, the ANL /12/ and the TU /6/ measurement results obtained at a neutron energy of 8.4 MeV. Possible reasons for the slight discrepancies between KFK /11/ and KFK /10/ results are discussed in ref. /6/. From the agreement between KFK /10/ and NBS /13/ it could be supposed, that the same $^3\text{He}(\text{n},\text{n})^3\text{He}$ reaction reference data has been applied for the calculation of the absolute counting efficiency of the recoil proton detection systems used. As it has been stated in ref. /13/, the measured f.c.s. shapes of ^{235}U and ^{238}U agree but a 5% discrepancy between the determined absolute values is observed.

Compiling the available measurement data for the ^{235}U f.c.s. at 8.4 MeV it can be supposed that the accuracy is of the order of 2%. Therefore the mean value of recent f.c.s. measurement results could be suitable as a normalization cross section in low energy region of the second fission stage at 8 on plateau.

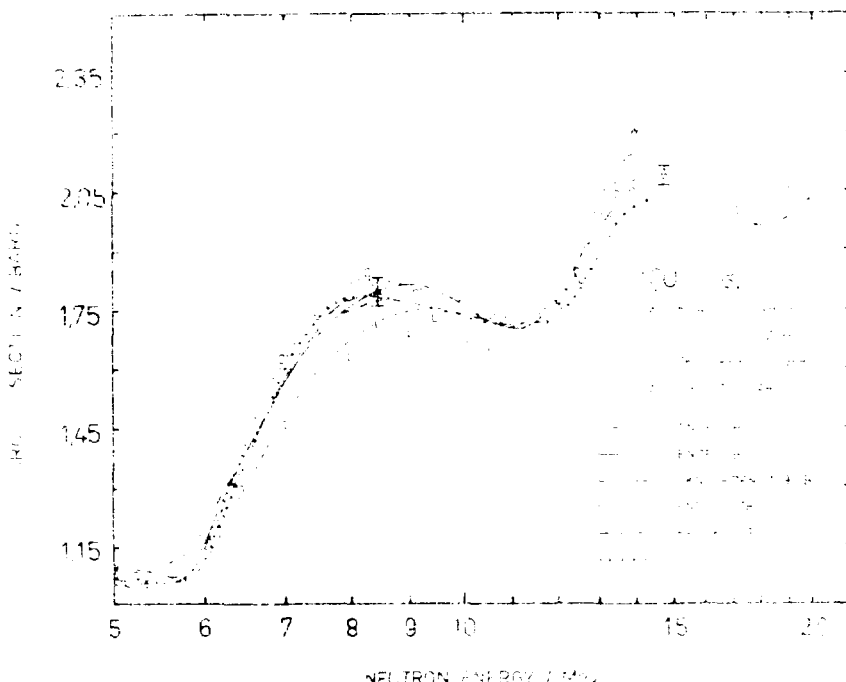


Fig. 3 Comparison of the results obtained at the TU Dresden (x) with shape measurement data and evaluated data files of the ^{255}U fission cross section

References

- /1/ D.W. Morrison ed., NEAND 7/79, INDC(SWD) - 75, Inst. Vienna 1979
- /2/ W.P. Poenitz, A.B. Smith ed., Proc. of the NEUTRON 78 Conf. Neutron Fast Fission Cross Sections, Arcoeur 1978, IAEA - No. - 78 - 177
- /3/ W.P. Poenitz, Proc. Internat. Spec. Symp. on Neutron Sources and Applications, Wallernau 1977, KRC Washington Spec. Issl. No. 1, p.261
- /4/ R. Arlt et al., Proc. Conf. on Nucl. Cross Sections and Parameters, Novosibirsk 1979, Bull. Am. Phys. Soc. 24 (73) 780
- /5/ R. Arlt et al., Kernenergie 24 (81) 48 , TU - 65 - 79 (1979)
- /6/ W. Wagner, Dissertation 1971, TU Dresden, Sektion Physik
- /7/ R. Arlt et al., Proc. IX. Intern. Symp. on the Interact. of Fast Neutrons with Nuclei, Gaussig 1972, ZfK - 410 (1880), p. 108 and p.122
- /8/ L. Raics, Dissertation 1978, Kossuth-University Debrecen
- /9/ J.R. Cairr et al., Nucl. Sci. Eng. 52 (1975) 18
- /10/ B. Leughers et al., loc. cit. /2/, p. 240
- /11/ K. Kari, Dissertation 1978, KFK - 2673, Karlsruhe 1978
- /12/ W.P. Poenitz, Nucl. Sci. Eng. 64 (1977) 894
- /13/ A.D. Carlson et al., Proc. Conf. on Neutron Phys. and Nucl. Data for Reactors and other Applic., Harwell 1978, p. 880
- /14/ Swedish Nuclear Data Committee, "Compilation of Actinide Neutron Nuclear Data", NEAND(OR) - 153/L, INDC(SWD) - 13/L, Stockholm 1979

Доклад на Международный симпозиум
по взаимодействию быстрых нейтронов
с ядрами, Гауссик, ГДР, 1980 г.

АБСОЛЮТНЫЕ ИЗМЕРЕНИЯ СЕЧЕНИЯ ДЕЛЕНИЯ ^{236}U НЕЙТРОНАМИ
С ЭНЕРГИЕЙ 2,6 МЭВ

Алказов И.Д., Витенко В.А., Душин В.Н., Косточкин О.И.,
Петржак К.А., Фомичев А.В., Шлаков В.И., Малкин Л.З.

Радиевый институт им. В.Г.Хлопина,
СССР

Арльт Р., Вагнер В., Музоль Г., Ортлеши Х.-Г., Тайхнер Р.
Технический университет Дрезден,
ГДР

Настоящая работа - очередная из серии проводимых с 1972 г. в Радиевом институте им. В.Г.Хлопина абсолютных измерений сечений деления. Цель этих измерений - получение данных для реакторной техники. Известно, что при работе реактора на быстрых нейтронах, накапливается широкий набор нуклидов от урана до кюрия, которые хотя и не являются основными реакторными изотопами, могут оказать заметное влияние на топливный цикл реактора. Для количественной оценки этого влияния необходимы данные по нейтронным сечениям большинства активидных нуклидов.

В настоящей работе представлены результаты абсолютных измерений сечения деления ^{236}U нейtronами с энергией 2,6 МэВ. Ряд авторов I-3 измерял ранее сечение деления ^{236}U , используя разнообразные источники нейтронов - моноэнергетические I,2 и с белым спектром³. Во всех работах использовалась методика измерений относительно сечения деления ^{235}U . Настоящая работа единственная, которая дает величину сечения деления ^{236}U , измеренную абсолютным методом.

Применяемый в работе метод коррелированных по времени сопутствующих частиц является модификацией ранее использовавшегося в измерениях на нейтронах с энергией 14,7 МэВ⁴. Схема эксперимента приведена на рис. I. Для получения нейтронов использовалась реакция $\text{D}(\text{d},\text{n})^3\text{He}$. Источником нейтронов служила мишень, состоящая из стальной подложки толщиной 0,3 мм с нанесенными на нее слоем титана, в котором растворен дейтерий (атомное отношение 0,8). Мишень облучалась пучком дейтонов, ускоренных до энергии 120 кэВ. Пучок коллимировался диафрагмами диаметром 0,3 мм. Ток на мишень составлял 200 мкА, что давало плотность потока нейтронов в районе делительной камеры $10^4 \text{ I}/\text{см}^2 \cdot \text{сек}$. Детектор сопутствующих частиц регистрировал все заряженные частицы в телесном угле $\Delta\Omega$. Использовался поверхностью-барьерный кремниевый детектор площадью 1 см² с собственным разрешением 20 кэВ.

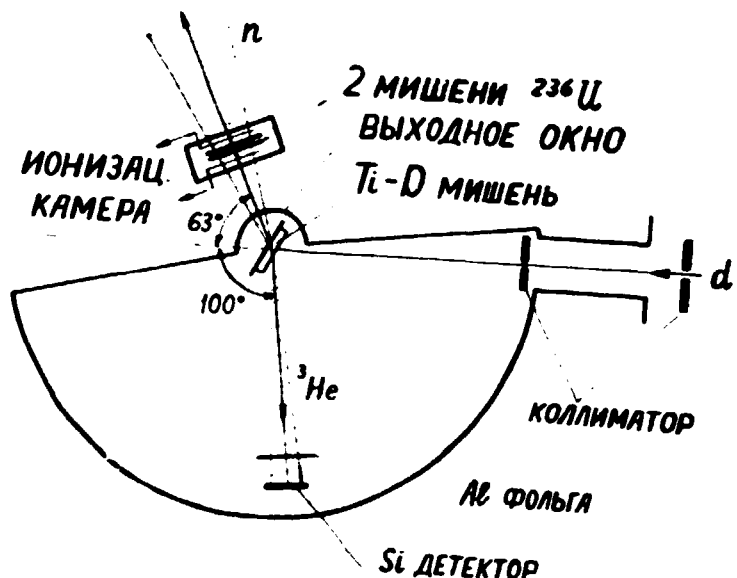


Рис.1.
Схема эксперимента

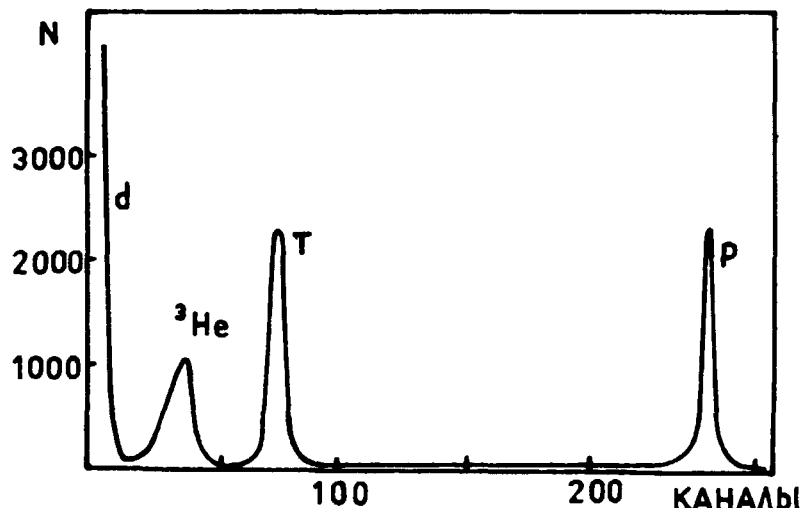


Рис. 2.
Амплитудний
спектр в каналі
сопутствуючих
частич

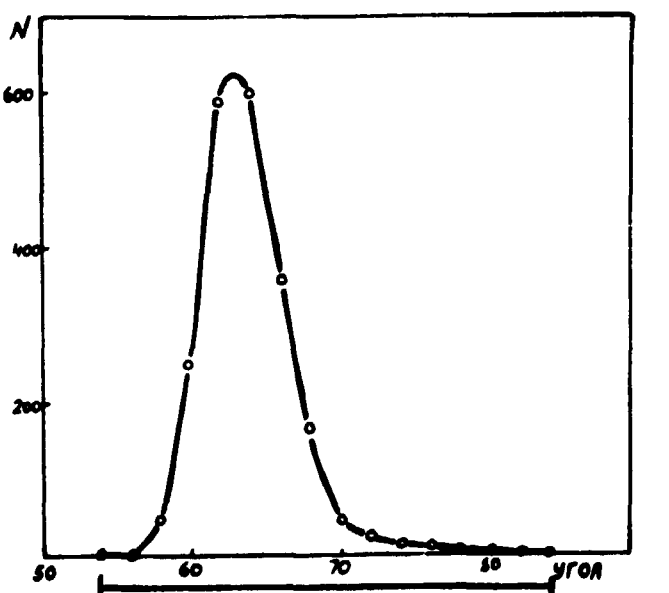


Рис. 3.
Профіль нейтрон-
ного конуса.
В нижній частині
рисунка зображені
угловий розмір
мишень деля-
щогося вещества.

От потока рассеянных дейtronов детектор защищался алюминиевой фольгой толщиной 240 мкг/см². С детектора предусилитель формировал 2 сигнала: временной для схемы совпадения (Фронт импульса меньше 10 нс) и амплитудный, необходимый для выделения гелионов из спектра заряженных частиц. Собственное разрешение амплитудного канала, измеренное по α -линии ^{239}Pu составило 3% и позволяло достаточно четко разделять пика ^3He (0,7 МэВ), ^3H (1,1 МэВ) и ^1H (3 МэВ).

Фон протонов и тритонов под пиком ^3He невелик и определялся линейной экстраполяцией. Фон рассеянных дейtronов существенно зависит от качества и толщины алюминиевого фильтра перед детектором. В эксперименте обеспечивалась пренебрежимо малая его величина. Качество спектра заряженных частиц (рис.3) контролировалось во время измерений непрерывно.

Телесный угол заряженных частиц задает конус нейтронов, в который помещается исследуемый образец ^{236}U . Обязательным условием метода коррелированных по времени сопутствующих частиц является то, чтобы конус нейтронов полностью попадал на мишень делящегося вещества. Профиль нейтронного конуса рассчитывался из кинематики реакции $D(d,n)^3\text{He}$. Для учета козмического расширения нейтронного конуса, вызванного кулоновским рассеянием ^3He в титановой мишени его профиль определялся экспериментально. Из рис.3 видно, что весь конус нейтронов хорошо укладывается в пределах мишени ^{236}U .

Энергия нейтронов определялась методом времени пролета. Было получено значение средней энергии спектра нейтронов в конусе, равное 2,594 МэВ, что согласуется с величиной, известной из кинематики реакции 4 . Ширина спектра на половине высоты составляла 120 кэВ. Оценивались возможные искажения спектра при взаимодействии дейtronов с элементами конструкции. Сделан вывод о том, что хотя спектр нейтронов и не является моноэнергетическим, искажения его невелики и в данном опыте могут не учитываться.

Для регистрации делительных событий использовалась плоско-параллельная ионизационная камера, содержащая 2 мишени делящегося вещества. Для определения эффективности камеры рассчитывались потери осколков в активных слоях мишеней с учетом углового распределения осколков 5 . Потери событий из-за дискриминации шумов определялись линейной экстраполяцией амплитудного спектра осколков к нулевой энергии.

Мишени делящегося вещества изготавливались в Радиевом институте методом термораспыления. Толщина подложек из сплава никеля с хромом составляла 0,13 мм. Однородность слоев контролировалась по α -счету детектором с малой диафрагмой, масса ^{236}U определялась по известному периоду полураспада ^{236}U . Для изготовления мишеней использовался ^{236}U высокой чистоты. Содержание примесей других изотопов не превышало 0,1%.

Полученная в результате измерений величина сечения деления ^{236}Li нейтронами с энергией 2,6 MeV составляет
 $(0,890 \pm 0,037) \cdot 10^{-24} \text{ см}^2$

В работе² для этого сечения приводится значение
 $(0,885 \pm 0,053) \cdot 10^{-24} \text{ см}^2$. Нормировка относительных данных из
работ I, 3 на величину сечения деления ^{235}U , рекомендованную
библиотекой ENDF/B-IV⁷, дает величины сечения деления
 ^{236}Li , равные соответственно 0,86 и $0,874 \cdot 10^{-24} \text{ см}^2$.

Основной составляющей результата наших измерений является
статистическая ошибка. Величины вводимых поправок и составляющие
погрешности результата приведены в таблице I.

Таблица I
Поправки и составляющие погрешности измерения

Эффект	Поправка (в %)	Погрешность (в %)
Неоднородность слоя минерал и поглощение осколков в мишени	2,0	0,2
Экстраполяция к нулевой энергии	1,2	0,5
Фон в канале гелиевов	3,1	0,5
Рассеяние нейтронов в конусе	1,9	0,3
Статистика		4
Полная погрешность		4,2

Литература

1. Meadows J.W. - Nuclear Sci. and Engineering, 1978, v.65, p.171
2. Lamphere R.W. - Phys. Rev., 1955, v.100, p.763
3. Behrens J.W., Carlson G.A. - Nuclear Sci. and Engineering, 1977, v.63, p.250.
4. Алказов И.Д. и др. - Атомная энергия, 1979, т.47, стр.416
5. Arlt R. et al. Informationen Technische Universität Dresden 05 - 5 - 79, Dresden, GDR, 1979
6. Schmarek W.R. - Nuclear Data Sheets, 1977, v.20, p.192

Абсолютное измерение сечения деления ^{235}U при $E_n = 2.6 \text{ МэВ}$ по методу коррелированных по времени сопутствующих частиц

Р. Арлт , В. Вагнер , М. Йом , Г. Музоль , Х.Г. Ортлелл , Р. Тайхнер
Технический университет г. Дрездена , ГДР

И.Д. Алхазов , Л.В. Драгчинский , В.Н. Душин , О.И. Косточкин , С.С. Коваленко , К.А. Петрак , В.И. Шпаков
Радиевый институт им. В.Г. Хлопина , г. Ленинград

В экспериментах на 150-киловольтном каскадном генераторе Технического Университета г. Дрездена впервые был применен метод коррелированных по времени сопутствующих частиц для абсолютного измерения сечения деления /1/ при энергии налетающих нейтронов 2.6 МэВ. Чтобы достичь требуемую точность 1-2% нужно добывать статистическую погрешность меньше одного процента в счете событий деления. Для этого необходимо несколько недель времени измерения. Для сбора и предварительной обработки множества в это время появляющихся данных служит связь эксперимента с малой ЭВМ типа **KRS 4200** через КАМАК /2/.

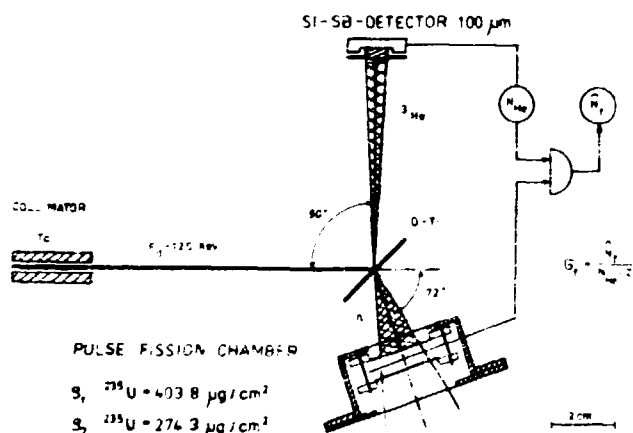


Рис. I. Принцип измерения

Моноэнергетические нейтроны энергии 2.6 МэВ производятся реакцией $\text{D}(\text{d}, \gamma)^3\text{He}$ (рис. I). Коллиматором исключается сдвиг фокуса пучка по дейтериевой мишени, так как стабильные геометрические условия являются неотъемлемым предусловием для метода сопутствующих частиц. Для выбранного угла регистрации гелий-онов -90° - зависимость энергии нейтронов от энергии налетающих дейтонов достаточно мала. Кроме того, этот угол является оптимумом для одновременного получения большой энергии гелионов и малого числа рассеянных дейтонов.

Статистические величины от гелионов и протонов из конкурирующей реакции $\text{D}(\text{d}, \rho)\text{T}$ удаляются путем выборки по энергии в сомножитель орбитального дейтона (рис. I). Для разработки быстрый односторонний сцинтиллятор, в котором получать соответствующую информацию. Для отключения гелионов от большого числа рассеянных дейтонов предложен метод симметрической фольги, толщина которой необходима точно подбирать, так как энергия гелиона не выше 200 кэВ.

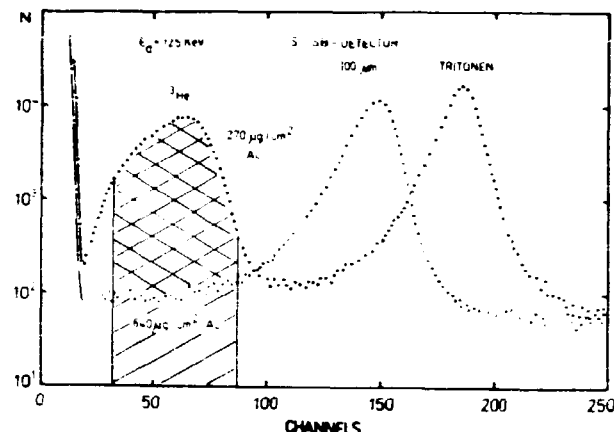


Рис.2. Определение фона под пиком сопутствующих гелионов в спектре заряженных частиц.

Для точного определения фона тритонов под пиком гелионов было проведено измерение спектра фольгой, толщину которой подбирали таким образом, чтобы гелионы были поглощены при минимальной потери энергии тритонов (рис.2 открытые кружки).

Для проверки топографии нейтронного конуса был применен "спиральнообразный" пластмассовый спинтиллятор, с помощью которого было определено число соударений $n - ^3\text{He}$ как функция угла относительно направления налетающих дейтонов (рис.3, сплошная линия).

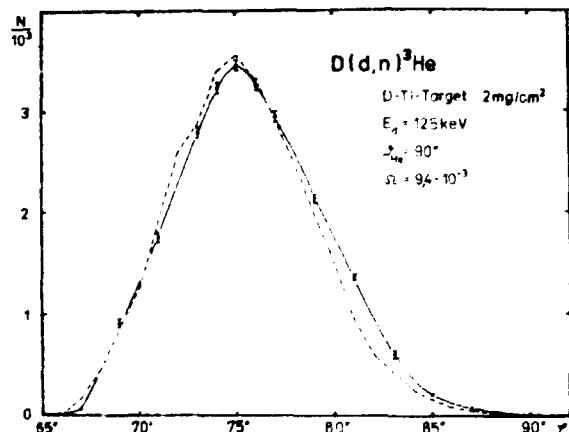


Рис.3. Угловое распределение нейтронов конуса по горизонтали.

Распределение нейтронов, определяемое размером ядра и лейтениевой массой и торможением дейтонов также было рассчитано программой (рис.3, штриховые линии). Этой же программой было рассчитано распределение по энергиям нейтронов. В данных условиях средняя энергия равна (2.46 ± 0.16) МэВ, полуширина 11.2 кэВ.

Детектором симметрии деления однажды быстрая двухиллюминационная исходящая линия камеры заполненная металиком. Достигнутое временное разрешение в районе $\tau = 4$ не позволяло в достаточной мере подавлять случайные события. Частоты неэффективности канала регистрации деления и выпада расхождения неизучены описаны работы /1, 2, 4/.

Число ядер на единицу площадки было определено из измерения α - активности в "матовой геометрии". При расчете числа ядер использовался период полураспада ^{235}U - $(7.038 \pm 0.048) \cdot 10^9$ лет полученный в работе /7/. Коррекция толщины была сделана для нейтронов в рамках распределения, налетавших неперпендикулярно. С учетом этих коррекций сечение деления ^{235}U нейтронами энергии 3.0 МэВ было определено с погрешностью в полтора процента.

Наш результат:

$$(1.415 \pm 0.012) \text{ барн}$$

Величины отдельных коррекций приведены в таблице. Число значение находится в районе самых низких сечений (рис.4).

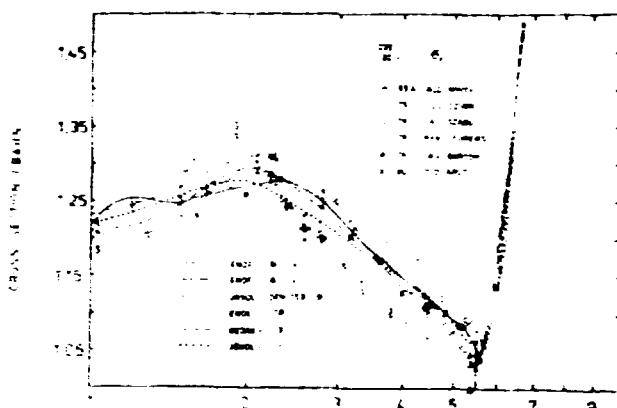


Рис.4. Сравнение нашего результата с сечениями деления.

Это наверно указывает на то, что более старые слегка заниженные значения еще учитываются со слишком высоким весом.

Таблица

Величины поправок, их погрешности и их вклад в суммарную ошибку

	k	$\Delta k/k$	$\Delta G/G$
Статистическая погрешность	-	-	0.90%
Случайные совпадения	-0.47%	5%	0.45%
Изотропизация к нулевой энергии осколков	+7.08%	25%	0.35%
Поглощение в мишени осколков деления	+0.11%	14%	0.30%
Фон тритонов	+0.37%	20%	0.50%
Рассеяние нейтронов	+0.27%	25%	0.25%
Число ядер в мишени	-	-	0.90%
Неоднородность	-	-	0.40%
Нейтроны налетающие неперпендикулярно	+0.25%	30%	0.05%

I n t e p a t y p a

- /1/ Arlt , R. et. al. , Proc. of the IX. Internat. Symp. on the Interact. of Fast Neutrons with Nuclei , Gaussig 1979 , ZfK - 410 (1980) 108
- /2/ Arlt , R. et. al. , Nucl. Instr. and Meth. 169 (1980) 381
- /3/ Arlt , R. et. al. , Preprint TU Dresden 05-05-79
- /4/ Dushin , V.N. , Proc. of the VIII. Internat. Symp. on the Interact. of Fast Neutrons with Nuclei , Gaussig 1978 , ZfK - 382 (1979) 153
- /5/ Jaffey , A.H. et. al. , Phys. Rev. C4 (1971) 1889

Определение абсолютной эффективности быстрой камеры деления

Р. Арльт, К. Гербах, Р. Тейхнер, В. Вагнер
Технический Университет Дрезден, Секция физики

Для точного определения абсолютного сечения деления по методу коррелированных по времени сопутствующих частиц с погрешностью в 1 - 2% требуется знание абсолютной эффективности регистрации осколков деления ε_f в камере деления с точностью около 0.2% /1, 2/.

Эффективность камеры деления ограничивается:

1. поглощением осколков в делящемся слое мишени
2. дискриминацией низкоэнергетических импульсов деления порогом временного дискриминатора в цепи камеры

Влияние этих эффектов учитывается в измерениях сечения деления соответствующими коррекциями /3/.

Целью этой работы является непосредственное измерение неэффективности камеры деления, которая с учетом выше названных коррекций обычно считается равным нулю. Проведенные измерения таким образом должны служить доказательством того, что других ограничивающих эффективности факторов, связанных с конструкцией или режимом камеры деления нет.

Использованная плоскопараллельная камера деления имела следующие параметры:

рабочий газ:	CH_4
высокое напряжение:	400 В
давление:	$1.1 \cdot 10^5$ Паскаля
межэлектродное расстояние:	3 мм
временное разрешение:	2 нс
диаметр мишени:	21 мм

Мишенью служил тонкий слой ^{252}Cf ($1 \text{ мкг}/\text{см}^2$) с активностью по делению в 400 Беккерелл. Этим исключается коррекция на поглощение осколков. Режим камеры оптимизировался по наилучшему разделению осколков деления от альфа-частиц натуральной активности ^{252}Cf и по временному разрешению /4/.

Настоящие измерения проводились по принципу регистрации осколков деления в совпадении с нейтронами деления /5/. Принципиальная схема дана на рис. I.

Временный спектр совпадений (рис. 2) характеризуется мгновенным пиком коррелированных событий и постоянным линейным фоном. Неэффективность камеры деления определяется следующим выражением /6/:

$$1 - \varepsilon_f = \frac{N_1}{N_1 + N_p \cdot N_f \cdot \Delta t}$$

где N_1 - число фоновых событий на канал,
 N_p - число событий в мгновенном пике,
 N_f - число зарегистрированных делений,

Таблица I
Результаты измерений

Величина	Символ	Измеренное значение	Погрешность ξ_f
		14.22 ± 0.33	0.06%
см. текст		1356124 ± 1665	0.004%
		422.72 ± 0.06	0.0004%
		0.8784 ± 0.0087	0.029%
число делений выше порога		$(357.4 \pm 1) \cdot 10^5$	0.001%
число событий полученных экстраполяцией		$(0.61 \pm 0.13) \cdot 10^5$	0.036%
фон нейтронного детектора		17.4 ± 1.65	0.027%
число зарегистрированных нейтронов (мин $^{-1}$)		652.7 ± 6.9	0.244%
коррекция на задержанные нейтроны		$(2.8 \pm 2.4) \cdot 10^{-4}$	0.025%
эффективность камеры деления		$(100.04 \pm 0.43) \%$	

Δt - временная единица канала.

Во время измерения считались числа делений N_f и нейтронов N_n и регистрировались временный и амплитудный спектры камеры. На рис.3 изображены амплитудные спектры с порогом дискриминации и без порога в области плато, разделяющего альфа-частицы и осколки деления.

До и после измерения анализировался фон в нейтронном детекторе. При определении неэффективности учитывались:

1. влияние порога линейной экстраполяции плато к нулевой энергии
2. фон в нейтронном детекторе
3. влияние γ -активности мишени ^{252}Cf на отношение подавления блока дискриминации, которое составляло $(8 \pm 2) \cdot 10^{-5}$
4. влияние задержанных нейтронов деления при энергетическом пороге нейтронного детектора в (0.9 ± 0.1) МэВ.

В табл.I собраны результаты измерений. Можно заключить, что эффективность камеры деления во всяком случае больше 99.6%.

На достигнутом уровне погрешности измерений не наблюдалось дополнительные источники неэффективности.

Ученые коррекции на измеренной величине неэффективности не превышали 3%, но определяли уже 75% ошибки результата. Основной вклад в погрешность вносили фон в нейтронном детекторе.

L i t e r a t u r e:

- (1) Arlt,R. u.a.: TU Dresden- Information 05-5-79 (1979)
- (2) Alkhanov,Id. et. al.: Preprint TU Dresden 05-37-78 (1978)
- (3) Arlt,R. u.a.: TU Dresden- Information 05-36-79 (1979)
- (4) Adolph,L.: Dipl. - Arbeit TU Dresden (1979)
- (5) Момен В.К.: "Определение эффективного периода полураспада ^{252}Cf ".
Атомная энергия Т.40 вып.2, февраль 1976 г.
- (6) Bergelt,H.: Dipl. - Arbeit TU Dresden (1980)

MEASUREMENT OF FISSION CROSS-SECTION RATIOS USING
TRACK-ETCHED DETECTORS

M. Várnagy, S. Juhász, J. Csikai, M.A.B. Siddique⁺
and P. Raics

Institute of Experimental Physics, Kossuth University,
H-4001 Debrecen 1, PF. 105, Hungary

Fission cross-section ratios of $^{238}\text{U}/^{235}\text{U}$, $^{238}\text{U}/^{237}\text{Np}$, $^{235}\text{U}/^{237}\text{Np}$ and
 $^{239}\text{Pu}/^{235}\text{U}$ were determined in the range of 13.5-14.8 MeV neutron energy. The
fission fragments were detected by a polycarbonate solid state nuclear track
detector /SSNTD/.

1. Introduction

Fast neutron cross sections for ^{235}U , ^{238}U and ^{239}Pu have been reviewed in detail by Poenitz and Guenther¹ Lapenes² and Patrick³. The deviations in $\sigma_{n,f}$ values measured by different authors around 14 MeV are related to the energy dependence of the fission cross sections near the /n,2nf/ threshold as the bombarding energy is not always well defined. At 14 MeV the change in $\sigma_{n,f}$ is especially significant for ^{235}U , while for ^{239}Pu it can be neglected.

The aim of this work was to study the applicability of SSNTD for /n,f/ cross-section ratio measurements and to determine the $\sigma_{n,f}$ cross-section curves for ^{235}U , ^{238}U , ^{237}Np and ^{239}Pu around 14 MeV.

2. Experimental technique

The details of this experiments and some preliminary results were published in an our earlier paper⁴.

Neutrons were produced by a 180 KeV Cockcroft - Walton generator using the T/d,n/ ^4He reaction. Tritium target of 150 $\mu\text{g}/\text{cm}^2$ on a 0.3 mm thick aluminium backing was bombarded with an analysed D⁺ beam of 100 μA . The neutron energies were changed by the emission angle to the beam.

The fission events from samples were detected with Makrofol KG SSNTD /12 μm in thickness and 30 mm in diameter/. Two detector foils and two fissile samples /e.g. ^{238}U and ^{235}U / were stacked in 2T geometry in such a way that the fission fragments emitted in forward direction were detected.

The fissile samples were prepared by the Hlopin Institute in Leningrad /USSR/ as well as in the CEA /France/ / ^{239}Pu /. The samples of 19 mm diameter were deposited onto an Al-holder /0.2 mm thick and 40 mm in diameter/. The isotopic composition and thickness of the deposits /summarized in Table I./ have been determined at the Hlopin Institute and CEA and were checked by an α -spectrometric method at our Institute.

Relative fission cross-sections were determined at six angles /0°, 30°, 60°, 90°, 120°, and 150°/ in such a way that the detector stacks were placed on the front window of a fission chamber. At each angle the measurements were repeated five times. Etching of the detector foils was carried out in 20 % KOH solution at a temperature of 60° C. The etched foils were evaluated by a Jumping Spark Counter⁵.

3. Results and discussion

Results obtained in this experiments compared to the previous data are presented in Fig 1. The ranges of correction factors and the errors are given in Table II.

+ On leave from Atomic Energy Centre, Dacca, SAEC, Bangladesh

Table I.
Isotopic composition and areal density of fissile samples

Sample	Isotopic composition %			Areal density μg/cm ²	relative to ²³⁵ U
	²³⁴ U	²³⁵ U	²³⁶ U		
²³⁵ U	0.0010	99.9955	0.0035	170	1
²³⁷ Np	239Pu	241Am		148	0.85
²³⁷ Np	99.9917	0.0078	0.0005		
²³⁹ Pu	-	99.9964	0.0036	670	3.85
²³⁸ U	depleted by a factor of 230			190	1.13

Table II.
Range of correction factors and errors

Effect	Range of corrections %	Range of errors %
Statistical	-	1.1-1.5
Mass ratio		2.6-4.3
Detector efficiency	1.2-17.5	3.2-4.5
Spark-counting efficiency	1 - 3.8	0.2
Neutron-flux variation	0.9	0.1
Forward-backward anisotropy	negligible	-
Fission due to other isotopes	negligible	-
Thermal neutrons	negligible	-
Total	3.8-23.4	4.5-6.0

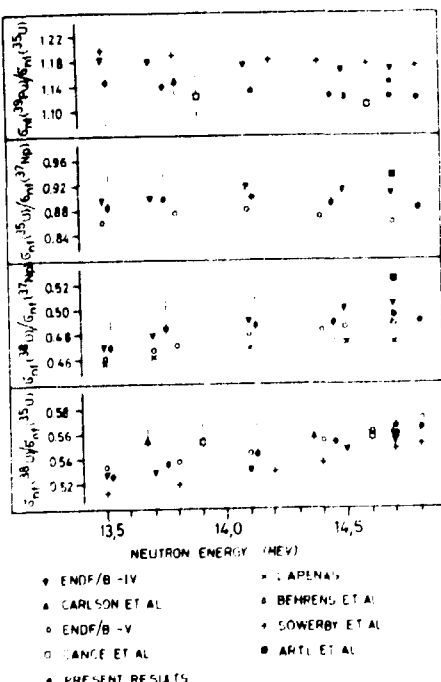


Fig. 1. Comparison of various relative cross sections

There are three effects which can cause variation in the detector efficiency, namely the fission-track-range variation in target material, detector thickness and anisotropy in the angular distribution. The range of fission fragments has been determined from empirical formulas⁶⁻⁷ while the fission fragment angular distribution was taken into account by using the data of Blumberg and Leachman⁸⁻⁹.

The possible presence of the thermal neutron background was controlled by the measurements of the fission cross-section ratio for $^{238}\text{U}/^{235}\text{U}$ as a function of distance from the neutron source. No change was observed in the cross-section ratio indicating negligible amount of slow neutrons in this experiment.

As it can be seen in Fig 1 the trends of the relative cross sections within the limits of errors are in good agreement with those given by other authors^{2,10-11}, however, the errors of our measurements are relatively high compared to other investigations. This is mainly due to the uncertainty in the determination of the sample thickness as well as in the detector efficiency. The error caused by the detector foil can be decreased by choosing thin foils with the same thickness.

The results prove the possible use of track-etched detectors in combination with the J.S.C. for the fission cross section measurements.

The authors are grateful to Dr. Cs. M. Buczkó and Mr. L. Vas for their assistance in the alpha spectrometry and in the operation of electronic systems, respectively.

References

1. W.P. Poenitz, P.T. Guenther, Proc. NEADC/NEARCRP Specialist Meeting on Fast Fission Cross Sections, ANL-76-90 /1976/.
2. A.A. Lapenas, Izmerenie Spektrov neitronov aktivatsionnym metodom, Izdatel'stvo "Zinatne", Riga /1975/.
3. B.H. Patrick, Proc. of Intern. Conf. on Neutron Physics and Nuclear Data for Reactors and Other Applied Purposes, Härwell, United Kingdom; September 1978, OECD/NEA / 1978 /.
4. M.Várnagy, S. Juhász and J.Csikai, 5. Vsesoyuznoi konferentsii po neitronnoi fizike, Kiev, 15-19 Sept. 1980.
5. M.Várnagy et al, Nuclear Instr. and Meth. 141 /1977/. 489
6. A. I. Nazarov, V.V.F. Frunze, Voprosy Atomnoy Nauki i Techniki /Yadernye Konstanty/, 25 /1977/ 3.
7. J. Tripier et al, Nucl. Instr. and Methods. 115 /1974/ 29.
8. L. Blumberg and R.B. Leachman, Phys. Rev. 116 /1959/ 102.
9. R.B. Leachman and L. Blumberg, Phys. Rev. 137 /1965/. B 814.
10. J. Behrens and G.W. Carlson, Nuclear Science and Engineering 63 /1977/ 250.
11. M.G. Sowerby et al. Annals of Nucl. Sci and Eng. Vol 1. /Pergamon Press, 1974/ 409.
12. ENDF/B-IV Dosimetry File /Ed. by B.A. Magurno, April /1975/, BNL-NCS-50446.
13. ENDF/D-V for $^{232}\text{Th}/n,f/$, $^{235}\text{U}/n,f/$, $^{238}\text{U}/n,f/$ and $^{237}\text{Np}/n,f/$ from magnetic tape of IAEA/.
14. M.Cance and G.Grenier, Nucl. Sci. and Eng. 68/1978/ 197.
15. R.Arlt et al, 5. Vsesoyuznoi konferentsii po neitronnoi fizike, Kiev, 15-19 Sept., 1980.
16. G.W. Carlson, J.W. Behrens, Nucl. Sci and Eng. 66 /1978/ 205.

"Dynamics of nuclear fission"

by K. Dietrich

Physik-Department der Technischen Universität München
8046 Garching, James Franck Str. BRD

In this talk I want to start with a short historical survey of the theory of fission. I then shall discuss in some detail recent attempts to describe the fission process in analogy to Brownian motion. Finally, I shall shortly comment on alternative recent approaches, especially the time-dependent Hartree Fock- (or BCS-) method.

§1, Historical Survey

Shortly after the experimental discovery of the fission process by Hahn and Straßmann, N. Bohr and J.A.Wheeler¹ succeeded to understand the main features of the process on the basis of two basic assumptions: (i) The nuclear fission proceeds by the formation of a "compound nucleus" the lifetime of which is sufficiently long such that a thermal equilibrium of all the degrees of freedom of the system is reached. The system hereby "forgets" the way it was formed except for conserved quantities and decays independently of the way it was formed.

(ii) The dependence of the (potential) energy of the nucleus on its shape can be described by the (static) "liquid drop model" (LDM). As a result of the competition between surface- and Coulomb-energy, a barrier develops which the nucleus has to overcome in order to undergo fission.

The (static) LDM did not lead to an understanding of asymmetric fission - the lowest saddle point of the potential landscape calculated within the LDM turned out to be reflexion-symmetric with respect to a central plane perpendicular to the axis of rotational symmetry. I may remind you that calculations

within the dynamical LDM (especially incompressible, irrotational, non-viscous flow) also did not lead to an understanding of the mass asymmetry.

Only after Strutinski's discovery of the shell-correction method², the change from symmetric to asymmetric division as a function of the mass number of the fissioning system could be related to shell effects. At the same time, this method led to an interpretation of the observed intermediate structure of the fission yield in terms of a "second valley" of the deformation potential. Quite recently, Blons et al³ proved even the existence of a "3rd valley" for fission of ^{231}Th and ^{233}Th which had been postulated by P. Möller and J.R. Nix⁴ on the basis of calculations within Strutinski's method.

The second "branch" of theoretical studies emerged from the picture of the fission process as a compound nuclear reaction in combination with the LDM: Complete thermal equilibrium suggests that the excess ($E^{\infty} - E_f$) of excitation energy E^{∞} above the higher of the two barriers is statistically distributed among all the degrees of freedom of the system. As a consequence of the additional hypothesis of a conserved K-quantum number on the passage from saddle to scission^{5,6} the angular distribution of fission fragments must be determined by the square $|D_{MK}^I|^2$ of one symmetric top wavefunction if only one "transition state" is populated^{5,6} ($E^{\infty} \geq E_f$) or by a statistically weighted sum of $|D_{MK}^I|^2$, if many of them contribute⁷.

Once the system has passed the fission barrier, the fact that the fission mode is unstable leads to a redistribution of the energy (E_f) stored in deformation onto the other degrees of freedom. It is the details of this dynamical process which are still unraveled. In particular we would like to know the state of the system at the moment of final rupture between the nascent fragments ("scission point"), since the

masses, charges, angular momenta of the fragments). In order to obtain further relevant experimental information we must thus study in more detail the fine structure of the mass and charge distribution for given kinetic energy of the fragments (especially odd-even effects) and the angular momenta of fission fragments. If the mechanism for producing the angular momenta of the fragments is the bending mode, these angular momenta depend sensitively on the deformation of the fragments at scission¹¹.

Of great interest is, of course, also further experimental and theoretical work on the emission of light particles (α , p, d, t, etc) close to scission.

Beside this mainstream of theoretical studies a most interesting paper was published by Kramers¹² already 1946, but stayed quite unnoticed in nuclear physics. In this work Kramers studied the decay of a system, which at time $t=0$ is given by a certain initial distribution (see fig.1). Subsequent time evolution is essentially a thermalization within each fragment.

Rather different assumptions on the state of the system at scission have been made (complete thermal equilibrium⁸, partial thermal equilibrium⁹, collective excitations only¹⁰) in the course of time. Why is it so difficult to decide experimentally between these pictures? The reason is that we observe the fragments at large times after the scission stage. At these times the system has "forgotten" the state it went through at scission apart from "conserved quantities" (i.e.

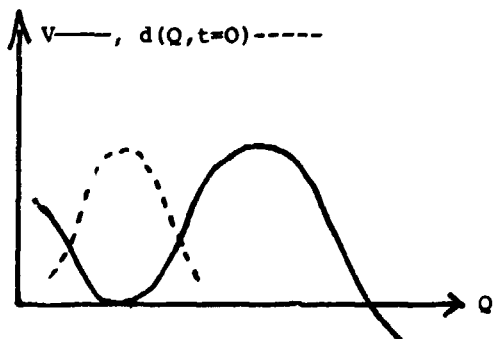


Fig. 1 : Schematic plot of collective potential V , initial distribution $d(Q; t=0)$

The collective degree Q interacts with a "reservoir" of randomly distributed degrees of freedom. Due to certain statistical assumptions one may derive what is called a "Kramers--Chandrasekhar-equation" for the time-evolution of this distribution. This is precisely the problem of nuclear fission if we are willing to accept the statistical assumptions which underly the derivation of this equation. But the same problem arises in other fields of physics: For instance an impurity which is trapped at $t=0$ in some valley of the lattice potential and which can escape by coupling to the lattice ions would satisfy a similar equation of motion. Indeed, Kramer's paper became very famous in solid state physics. Let us now discuss the basic physical ideas of Kramer's approach in some detail.

§2, The Fission Process as a Problem of Brownian Motion

The fission process represents a large scale collective motion which is coupled to the intrinsic degrees of freedom of the system. The collective and intrinsic degrees play a similar rôle as the degrees of freedom of the pollen particles and the molecules of the liquid, resp. of the classical case of Brownian motion.

The natural starting point of a theory of such a system is a Hamiltonian which is composed of a collective part $H_{\text{coll}}(\hat{Q}, \hat{P})$ depending on the collective variables \hat{Q} and their conjugate momenta \hat{P} only, an intrinsic part $H_{\text{intr}}(\hat{x}, \hat{p})$ dependent on the intrinsic variables \hat{x} and their conjugate momenta \hat{p} and a coupling H_{cplg} which we assume to depend on the intrinsic and collective variables only:

$$\hat{H} = H_{\text{coll}}(\hat{Q}, \hat{P}) + H_{\text{intr}}(\hat{x}, \hat{p}) + H_{\text{crys}}(\hat{x}, \hat{Q}) \quad (1)$$

$$H_{\text{coll}}(\hat{Q}, \hat{P}) = \frac{\hat{P}^2}{2m} + U(\hat{Q}) \quad (1')$$

We should realize that the derivation of such a Hamiltonian for a system of fermions represents already a problem on its own merit. We may assume that we have derived the form (1) of the Hamiltonian within the cranking theory which implies that the collective motion is slow compared to the intrinsic one. Let us now assume that there are many intrinsic degrees of freedom and that the intrinsic motion is in a state of great complexity. Then a perturbation of the intrinsic motion at a given time $t=0$ is expected to "decay" more rapidly than a perturbation of the collective motion. A measure of this loss of memory are the relaxation times. Let us thus assume that the collective variables Q are distinguished from the intrinsic variables x by larger relaxation times:

$$\tau_{\text{rel}}(Q) \gg \tau_{\text{rel}}(x) \quad (2)$$

The validity of the inequality (2) for shape degrees Q can be deduced from the analysis of deep inelastic heavy ion reactions (HIR)¹³. If we assume the validity of the somewhat stronger statement, that the average collective variables $\langle Q(t) \rangle$ change only by negligible amounts within the relaxation time $\tau_{\text{rel}}(x)$ of the intrinsic degrees, the intrinsic degrees will always remain close to a thermal equilibrium if they started to be in a thermal equilibrium at some initial time. This then suggests to treat the intrinsic (microscopic) degrees as a heat bath coupled to the ("macroscopic") collective shape degrees and to assume that the deviation of the reservoir distribution from the canonical form can be treated as a small perturbation. On the other hand, the dynamics of the collective macroscopic degrees is to be treated explicitly. Hofmann and Siemens formulated this "linear response theory", which is

widely used in the theory of condensed matter, for the description of heavy ion reactions¹⁴. Let me note in passing that another way to introduce statistical features is to treat the matrix-elements of the coupling Hamiltonian as random numbers.

This method has been applied to the description of heavy ion reactions and recently also of fission by Weidenmüller et al.¹⁵ and by Nörenberg et al¹⁶. The resulting equations for the macroscopic distribution function $d(Q, P; t)$ look very similar to the ones of the linear response theory but differ by the microscopic expressions obtained for the friction and dissipation tensor. Let me describe in a short way how one proceeds in principle in order to obtain an equation of motion for a macroscopic distribution function $d(Q, P, t)$:

We start from the equation of motion for the complete density operator $\hat{\rho}(t)$ of the system ($\hbar=1$)

$$i\dot{\rho} = [\hat{H}, \hat{\rho}] \quad (3)$$

(i) With a projection technique due to Nakajima and Zwanzig¹⁷ we may rewrite equ.(3) in terms of an equation of motion for the "reduced density matrix" defined by

$$\langle Q' | \hat{\rho} | Q \rangle = T_{\hat{Q}x} \langle Q' x | \hat{\rho}(t) | Q x \rangle \quad (4)$$

or, equivalently, for its Wigner transform. The Wigner function is defined by introducing "relative" an "centre of mass" coordinates

$$q = Q' - Q \quad ; \quad \tilde{Q} = \frac{Q + Q'}{2}$$

in $\langle Q' | \hat{\rho} | Q \rangle$ and taking the Fourier transform with respect to the relative coordinate q

$$d(\tilde{Q}, P; t) := \int dq e^{iPq} \tilde{\rho}(q, \tilde{Q}; t) \quad (5)$$

$$\tilde{\rho}(q, \tilde{Q}; t) := \langle \tilde{Q} + \frac{q}{2} | \hat{\rho}(t) | \tilde{Q} - \frac{q}{2} \rangle \quad (5')$$

The physical significance of the Wigner transform is that it represents a probability density in the phase space of the collective variables Q, P if we go to the classical limit. It is precisely this function which we need in order to calculate the average cross section for fission: Assuming that the macroscopic observables like mass, charge, angular momenta of the fragments a.s.o. are known functions $\Omega(Q, P)$ of our set of collective variables, the measured final distribution P(a) is given by

$$P(a) = \int dQ dP d(\tilde{Q}, P; t \rightarrow +\infty) \delta[\Omega(Q, P) - a] \quad (6)$$

where "a" are the measured values of the observables $\Omega(Q, P)$.

The Nakajima-Zwanzig equation which is obtained from (3) for the Wignerfunction (5) has the general form

$$\hat{d}(t) = \hat{I}(t) + \int_0^t \hat{K}(t-t') \hat{d}(t') dt' \quad (7)$$

Here $\hat{I}(t)$ is a term dependent on the initial conditions at time $t=0$, while \hat{K} describes the propagation of the system from time t' to time t . Due to condition (2) one can show that $\hat{I}(t) \rightarrow 0$ for $t > \tau_{\text{rel}}(x)$ and that $\hat{K}(t-t')$ is negligible for times t' preceding t by more than $\tau_{\text{rel}}(x)$:

$$K(t-t') \approx 0 \text{ for } t' < t - \tau_{\text{rel}}(x)$$

Assuming that the macroscopic distribution function $d(Q, P, t)$ changes very little within a time interval of length $\tau_{\text{rel}}(x)$, we may replace $d(Q, P, t')$ by $d(Q, P, t)$ in the integral of equ.(7) (Markov approximation):

$$\hat{d}(t) \approx \int_0^t dt' K(t-t') \cdot \hat{d}(t) \quad (8)$$

As a last step one simplifies the integral kernel, which is still a highly complicated functional, either by perturbation theory like in linear response theory¹⁴ or by introducing random matrix assumptions^{15,16}.

These approximations are of a statistical nature. They are thus not dependent on whether the collective degrees of freedom behave almost classically or quantum-mechanically. In the "locally harmonic approximation", the quantum mechanical equation and the classical equation for $d(Q, P, t)$ become equal. Quantum-effects in the equation of motion for the Wigner function are thus unimportant, if at any given time t the collective potential $U(Q)$ (see (1')) can be approximated with good accuracy by a quadratic expansion around the "average trajectory" $Q(t) = \langle Q \rangle$

$$U(Q) \approx U(\langle Q(t) \rangle) + (Q - \langle Q(t) \rangle) \frac{\partial U}{\partial \langle Q \rangle}$$

$$+ \frac{1}{2} (Q - \langle Q(t) \rangle)^2 \frac{\partial^2 U}{\partial Q^2} \quad (9)$$

in the whole domain where $d(Q, P; t)$ is substantially different from 0. If the collective inertia μ , the friction and the diffusion coefficients are approximately constant in this domain ($\mu = \mu(Q)$; $\gamma = \gamma(Q)$; $D = D(Q)$) one finds the following equation of motion for $d(Q; P, t)$:

$$\begin{aligned} \frac{\partial d(Q, P, t)}{\partial t} = & - \frac{P}{\mu} \frac{\partial d}{\partial Q} + \left(\frac{\partial U}{\partial Q} + (H - \langle Q \rangle) \frac{\partial^2 U}{\partial Q^2} \right) \frac{\partial d}{\partial P} \\ & + \gamma \frac{\partial^2}{\partial P^2} \left(\frac{P}{\mu} d \right) + D \frac{\partial^2 d}{\partial P^2} \end{aligned} \quad (10)$$

with

$$\langle Q(t) \rangle := \int dP Q d(Q, P, t) \quad (11)$$

which is referred to as a "Fokker-Planck equation" in recent publications of nuclear physics and as "Kramers-Chandrasekhar equation" in statistical mechanics. Let me note in passing that in the high temperature limit the friction and diffusion coefficients are related by the Einstein relation

$$D = \gamma \cdot T \quad (12)$$

where T is the temperature of the reservoir of intrinsic variables.

The linear response theory relates the coefficients D and γ to the microscopic Hamiltonian $H_{\text{cplg}}(x, Q)$. For the case that H_{cplg} is a sum of shape-dependent single particle potentials

$$H_{\text{cplg}}(x, Q) = \sum_{i=1}^A V(x_i; Q) \quad (13)$$

the form of γ and D was explicitly calculated in ref. 18. It is the widely discussed case of "one-body dissipation". More

recently, the effect of two-body interactions on γ and D was taken into account¹⁹. An extension to systems which are superfluid at temperature T=0 is in progress. I believe personally that an approach to the fission problem which is based on a Brownian theory is promising and represents a natural extension of the existing theories of nuclear fission, which incorporates the extreme statistical theory of Fong⁸ (maximalisation of phase space unter given constraints) as well as the theory of Nix and Swiatecki¹⁰ (obtained for $\gamma=D=0$) as special cases.

What has been done and what is being done on these lines? Several preliminary studies based on a K-C equation of type (10) were performed recently:

A. Jensen et al.¹⁸ Performed microscopic calculation for the friction tensor for fission of ^{238}U (deformations between 1st minimum and 2nd saddle) Grangé et al.²⁰ studied the time dependence of the fluctuation for an inverted oscillator potential starting with an initial distribution which was localized in the vicinity of the top of the barrier.

Pomorski et al.²¹ studied the time evolution due to equ.(10) in a somewhat more realistic case: The potential U(Q) depended on 3 deformation variables Q (elongation, mass asymmetry, neck diameter) but with one of them (neck diameter) being related to the other two by a constraint. The potential was calculated within Strutinski's method. The friction and inertial tensor were chosen phenomenologically (friction tensor $\rightarrow 0$ and inertia of mass asymmetry mode $\rightarrow \infty$ beyond the scission point) and the dissipation and friction tensor were related by the fluctuation dissipation theorem. The experimentally observed distributions of the mass and the kinetic energy of the fragments could be reproduced with reasonable choices of the inertia and the friction.

An undesirable feature which is common to all the simple appli-

cations of Fokker Planck equations is the strong dependence of the final distribution from the initial one. The reasons are probably that the number of degrees of freedom is too low and (more important) that the initial distribution is chosen at the saddle point or even slightly beyond the top of the barrier in order to avoid the problems connected with tunneling. As a consequence the time which elapses up to scission is too short for the system to lose the memory of its initial state.

In the last part of my talk I wish to mention some alternative theoretical approaches which also merit great interest.

§3. Alternative approaches to the fission dynamics

In a series of papers Ledergerber et al.²² and Schütte²³ studied a semi-classical model describing the passage from saddle to scission. The time-dependence of the collective variables was classically given and the time-dependent Schrödinger equation with a simple model Hamiltonian was solved in a limited space of internal excitations. All the authors came to the conclusion that a substantial amount of intrinsic excitations is generated on the way from saddle to scission. Schütte in particular showed that these intrinsic excitations are preferentially pairs of quasi-particles with time-reversed single particle quantum numbers. Let us note that - apart from the special case of symmetric fission - quasiparticles differing only by time reversal have the same distribution in space. If odd-even effects in the proton or neutron number distribution are observed this may thus either mean that Cooper pairs survive up to scission or that pairs of quasi-particles in time-reversed orbits play an important rôle. Very interesting experimental information on odd-even effects was recently obtained²⁴. The drawback of these model calculations is that they lack selfconsistency. This was overcome by some first calculations²⁵ based on a time dependent Hartree-Fock (TDHF) or time-dependent BCS method. The applicability of TDHF to

low energy fission is expected to be at least as justified as for heavy ion reactions. The large number of orbitals in a nucleus like ^{236}U makes it technically impossible to carry out a calculation without some undesirable simplifications such as axial symmetry and reflexion symmetry. Thus the results must be viewed as model studies. A feature which is likely to be realistic is the time of some 10^{-21} sec. required for passage from saddle to scission.

In conclusion I would like to emphasize that low-energy fission constitutes a valuable complement to deep inelastic heavy ion reactions in that the excitation energy is lower so that more details of nuclear structure such as shell effects survive the statistical averaging. Furthermore, the angular momentum of the fissioning system is very low for low energy fission while the average angular momentum of the "dinuclear system" is large for a typical deep inelastic reaction.

List of References

- 1 N. Bohr, J.A.Wheeler, Phys. Rev. 56, 426 (1939)
- 2 V.M.Strutinski, Nucl.Phys. A95 (1967) 420
- 3 J.Błons, C.Mazur, D.Paya, M.Ribrag, H.Weigmann, report to this conference by Dr. Paya
- 4 P.Möller and J.R.Nix, Conference on the Physics and Chemistry of Nuclear Fission, Rochester, Vol. I, p. 103 (IAEA, Vienna 1973)
- 5 A.Bohr, Proc. Interna. Conf. on the Peaceful Uses of Atomic Energy, Vol. 2, p. 151 (1956)
- 6 V.M.Strutinski, Sov. Phys. JETP 3, 638 (1956)

- 7 I.Halpern,V.M.Strutinski,Proc.Intern.Conf.on the Peaceful
Uses of Atomic Energy 15,408P/1513(1958)
- 8 P.Fong,Phys.Rev.102(1956)434
- 9 W.Nörenberg,Conf.on the Phys. and Chem.of Nucl.Fission,
Vienna, SM-126/IAEA,Vienna,1969)
- 10 J.R.Nix,W.J.Swiatecki,Nucl.Phys.71(1965)1;J.R.Nix,Nucl.Phys.
A130,(1969)241
- 11 M.Zielinska-Pfabé,K.Dietrich,Phys.Lett.49B(1974)123;preprint
TU-Munich, 1979

L.G.Moretto,R.P.Schmitt,Phys.Rev.C21(1980)204
- 12 H.A.Kramers,Physica VII,284(1940)
- 13 G.Wolschin,W.Nörenberg,Phys.Rev.Lett.41(10)691(1978)
G.Wolschin,Nucl.Phys.A316(1-2)(1979)146 (with references to
earlier work)
- 14 H.Hofmann,P.J.Siemens,Nucl.Phys.A257,165(1976);
ibid Nucl.Phys.A275,464(1977)
- 15 D.Agassi,C.M.Ko,H.A.Weidenmüller,Ann.Phys.107(1977)140,
ibid 117(1977)237
H.A.Weidenmüller,"Transport theories of heavy ion reactions",
Progr.in particle and nuclear physics, 1980
- 16 S.Ayik and W.Nörenberg,Z.Physik A 288,401(1978)

- 17 S.Nakajima,Progr.Theor.Phys.20,1338(1960)
R.W.Zwanzig in "Selected Topics in Statistical Mechanics XIX,
New York/London:Gordong and Breach 1967
R.W.Zwanzig,J.Chem.Phys.33(1960)1338
- 18 A.S.Jensen,K.Reese,H.Hofmann,P.J.Siemens,Conf.on Phys.and
Chem.of Nucl.Fission,Jülich 1979,IAEA SM/241-H4,Vienna

- 19 E.Werner,H.S.Wio,H.Hofmann,K.Pomorski,"Nucl.dissipation with residual interactions studied by means of the Mori formalism preprint (fall 1980)Phys.Dept.of the TUM,8046 Garching(FRG)
- 20 P.Grangé,H.C.Pauli,H.A.Weidenmüller:"The influence of thermal fluctuation on the kinetic energy distribution of fission fragments",preprint MPI H-1979-V8
- 21 K.Pomorski,H.Hofmann,"On the dynamics of fission as a dissipative process,preprint (summer 1980)Phys.Dept.TUM,8046 Garching (FRG)
- 22 T.Ledergerber,Z.Paltiel,H.C.Pauli,G.Schütte,Y.Yariv,Z.Fraenkel, Phys.Lett.56B,417(1975)
- 23 G.Schütte,Phys.Lett.89B(1979)11;Z.Phys.A288(1978)161
- 24 H.Nifenecker,C.Signarbieux,R.Babinet,J.Poitou,3rd IAEA Symp. on Phys.and Chem.of Fission,Rochester 1973,Vo.II,p.117 C.Signarbieux,preprint CEN-Saclay,B.P.No.2,91190 Gif-sur-Yvette P.Armbruster et al.priv.comm.
- 25 S.E.Koonin and J.R.Nix,Phys.Rev.C13(1976)209
J.Blocki and H.Flocard,Nucl.Phys.A273(1976)45
J.W.Negele,S.E.Koonin,P.Möller,J.R.Nix,A.J.Sierk,P.R.C17
(1978)1098
K.Dietrich,J.Nemeth,preprint of the Technische Universität München,8046 Garching, Jan.1981 (to be published in Zeitschrift für Physik).

FINE STRUCTURE OBSERVATION AND ANALYSIS IN THE
NEAR FISSION THRESHOLD OF Th ISOTOPES

J. Blons, C. Mazur, D. Paya and M. Ribrag
DPh-N/MF, CEN Saclay, BP 2, 91190 Gif-sur-Yvette, France

and

H. Weigman
CBNM, Geel, Belgium

Abstract

High resolution measurements reveal the presence of a fine structure in the gross resonances located near the fission threshold of ^{230}Th and $^{232}\text{Th} + \text{neutron}$. The properties of such a structure can be understood only in the framework of a third minimum in the fission barrier. As predicted by the calculations, the metastable states in this minimum have a stronger quadrupole deformation than in the second minimum and an octupole deformation.

The resonant structure in the near threshold fission cross section of the thorium isotopes has long been a challenge in understanding the fission barrier penetrability conditions. The explanations proposed in terms of a single or a double humped fission barrier failed to reproduce even the rough behaviour, when numerical calculations were performed. In hopes that a more detailed description of the fission cross section will help to solve the problem, we have undertaken a series of high resolution measurements.

Several experiments were performed during the past few years. We first used the neutron time of flight facility connected with the AL 60 Saclay linear accelerator to measure the fission cross section of ^{232}Th along with the fission fragment angular anisotropy [1]. The fission cross section measurement was repeated at the Geel linear accelerator GELINA which provided us with a better energy resolution. This last run was accompanied by a fission cross section measurement of ^{230}Th , also at GELINA [2]. In all these experiments the fission detector was a six-cell gas scintillator where the sixth cell was loaded with a neptunium deposit used to monitor the neutron flux. The anisotropy measurements were performed by setting against the Th-deposit, a grid which stopped the fragments emitted at an angle larger than 30° (in one experiment) or 45° (in a second experiment). The best energy resolution was achieved in the GELINA runs : 42 ps/m for the ^{232}Th cross section (i.e. 2.3 keV at a neutron energy of 1.6 MeV) and 84 ps/m for the ^{230}Th cross section (i.e. 1.7 keV at a neutron energy of 0.7 MeV). The results are displayed in Figs. 1 and 2.

Since we are mainly interested in the resonances let us concentrate on those located at 0.7 MeV in the ^{230}Th cross section and at 1.6 and 1.7 MeV in the ^{232}Th cross section. They are blown up in Figs. 3, 4 and 5. Each of them reveals a fine structure which was not observed earlier. Indeed, fine structure peaks with about the same width (10 keV) have been reported in the cross section of other actinides [3] and were interpreted as intermediate structure effects due to compound nucleus states in the second well of the fission barrier. However, these peaks have some typical properties which are not met in the thorium case : their spacings obey a statistical law (Wigner distribution) and the fission fragment angular distribution does not vary from peak to peak. We shall see later that the spacings of the Th peaks are connected by a relationship which is more strict than a simple probability distribution ; as for the fission fragment angular distribution, Figs. 3, 4 and 5 show that, even if no fine structure is apparent in the data due to a poorer energy resolution, the anisotropy is not constant. Rather, the fragments are more forward peaked on the high energy side of each gross structure, the spin increases on the average with energy. Such a behaviour is incompatible with the properties of compound nucleus states but strongly suggests the presence of simpler collective states. This conclusion is supported by the cal-

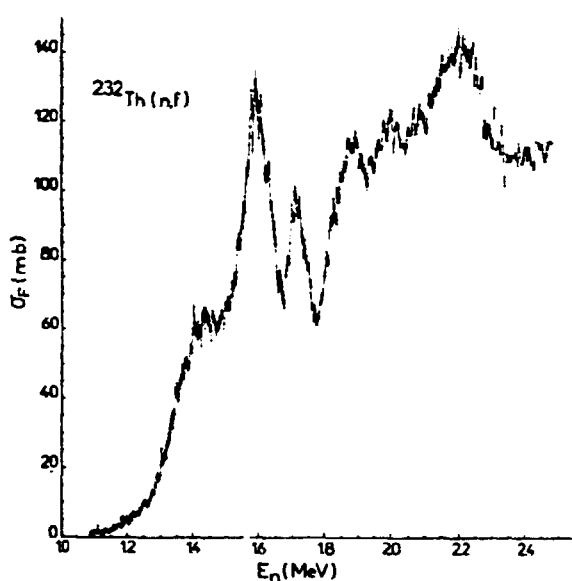


Fig. 1 - ^{232}Th fission cross section

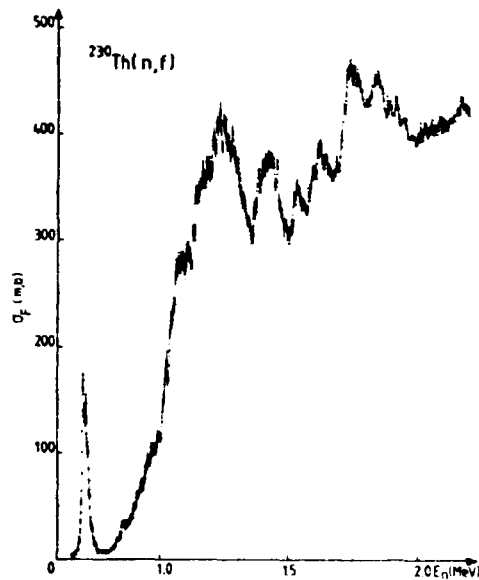


Fig. 2 - ^{230}Th fission cross section

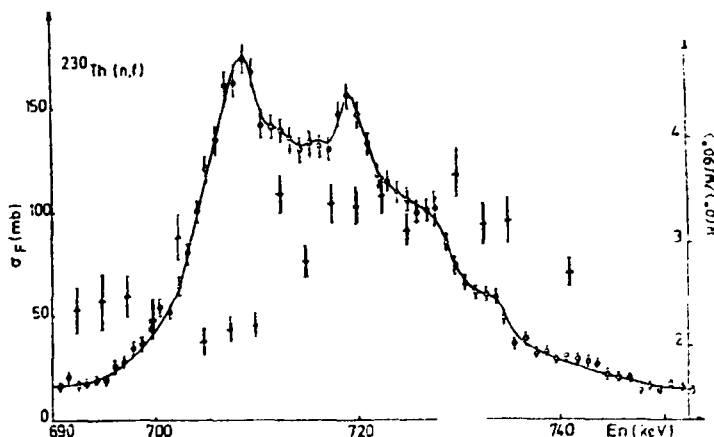


Fig. 3 - ^{230}Th fission cross section (\diamond) near 720 keV and anisotropy ratio (\dagger) [\square]

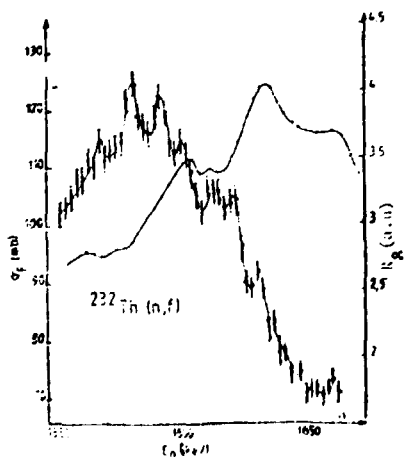


Fig. 4 - ^{232}Th fission cross section (\diamond) near 1600 keV and anisotropy ratio (\dagger)

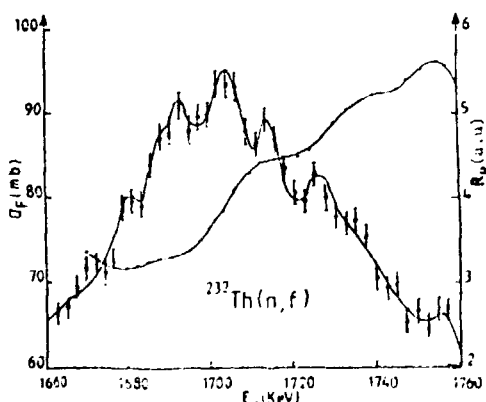


Fig. 5 - Some as Fig. 4 near 1700 keV

culations and the systematics of the fission barrier parameters which show that, in the thorium isotopes, the first maximum is much lower than the neutron binding energy. As a consequence, it is no longer possible to distinguish between class I and class II states in the first and the second well ; so, the usual intermediate structure, as it is found in heavier actinides, cannot develop. But the calculations provide an alternative explanation of the fine structure with the appearance of a third minimum in the fission barrier of light actinides when octupole deformations are permitted [4]. Since the minimum is very shallow only the first rotational states can lie below the top of the barrier and they should occur as pairs of states with different parities due to the space symmetry violation.

The data have been analysed in terms of the above considerations. The cross section is calculated as

$$\sigma_f(E) = \sum_{K,J,\pi} \sigma_{CN}^{J\pi}(E) \frac{T_f^{KJ\pi}(E)}{T_n^{J\pi}(E) + T_Y^{J\pi}(E) + T_f^{KJ\pi}(E)}$$

where the compound nucleus cross section σ_{CN} and the transmission coefficients T_n and T_Y in the neutron and γ -ray channels are given for each spin and parity $J\pi$ by an optical model code. The T_f 's are the transmission coefficients of suitable fission barriers ; for a given projection K , the parameters of the different barriers are set equal except for an energy shift which reflects the presence of a rotational band :

$$E_j = E_{K\pi} + \frac{\hbar^2}{2J} \left[J(J+1) - K(K+1) + \delta_{K,1/2} (-1)^{J+1/2} a_\tau (J+1/2) \right]$$

The 0.7 MeV resonance in ^{230}Th is a simple case since it is well isolated, without any pedestal and since a series of angular distribution measurements are now available which permit, with some confidence, to assign a spin value to the different components of the fine structure. For instance, in comparing the 55° and 80° data [5] one can assert that the 708 keV and 719 keV peaks must have a spin 3/2 whereas, in order to fit the 0° to 90° ratio [6], a value of 7/2 is needed near 730 keV together with values of 1/2 below 720 keV. A detailed discussion of the spin and parity assignment is given elsewhere [7]. Fig. 6 shows that a perfect fit can be achieved with two rotational bands with quantum numbers $K^\pi = 1/2^+$ and $K^\pi = 1/2^-$ and the following parameters :

$$\hbar^2/2J = (1.9 \pm 0.1)\text{keV} \quad a_+ = 0.2 \pm 0.1$$

$$E_{1/2^-} - E_{1/2^+} = (9 \pm 1)\text{keV} \quad a_- = -0.3 \pm 0.1$$

while the moment of inertia J , as measured in neighbouring nuclei, is two times larger in the second well than in the first well, our value is more than three times larger. This is an additional evidence of a third minimum with a stronger deformation.

The analysis of the ^{232}Th cross section is more complicated because the pedestal cross section on which the resonances sit disturbs somewhat the angular distributions. In order to describe correctly this pedestal which is presumably formed by already open fission channels one has to begin the analysis at lower energy, in the region where the cross section begins to rise ; this means fitting the cross section and the anisotropy from about 0.7 MeV up to 1.8 MeV or more and reproducing all the fine structure observed in this range. Of course it is easy to build a fine structure by adding more and more new fission channels ; but this procedure gives too high a cross section above 2.5 MeV when all fission channels are open and, on the other hand, one knows from calculations that the number of single particle levels in this energy range does not exceed 8. The analysis has been conducted along this direction and using the results of the ^{230}Th analysis. Although it is still in a preliminary stage, Fig. 7 shows that both the gross and the fine structures can be accounted for, provided that the third well may contain two vibrational resonances.

By way of conclusion I would like to say that although some of the experimental results have

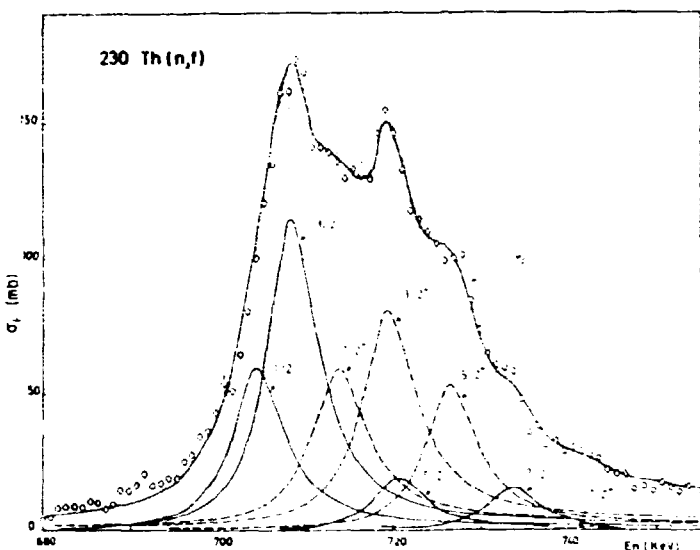
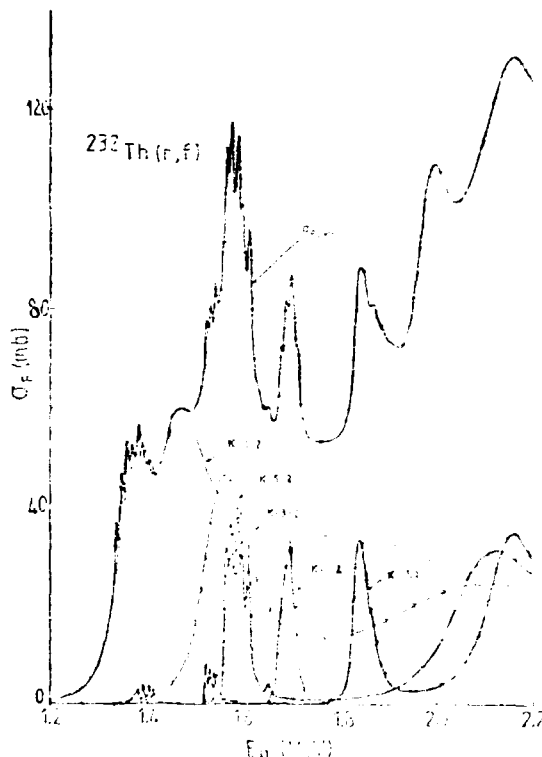


Fig. 6 - ^{230}Th cross section calculated as a superposition of two rotational bands with opposite parities and $K=1/2$.



been obtained several years ago, the analysis has to progress very cautiously because in the third minimum we are faced with states with unusual properties. There was a time when the very existence of the third minimum was questionned. To day, in view of the coherence of all the results, its appears as firmly established and no doubt more interesting consequences will be derived from a complete analysis of the data.

Fig. 7 - ^{232}Th cross section calculated in the same manner as in Fig. 6 when several K fission channels are involved.

- [1] J. Blons, C. Mazur and D. Paya, Phys. Rev. Lett. 35 (1975) 1749.
- [2] J. Blons, C. Mazur, D. Paya, M. Ribrag and H. Weigmann, Phys. Rev. Lett. 41 (1978) 1282.
- [3] P. Clässel, H. Rösler and H.J. Specht, Nucl. Phys. A256 (1976) 220.
G. Barreau, Thesis, University of Bordeaux, CEN BG 7706 (1977).
- [4] P. Möller and J.R. Nix, Physics and chemistry of fission, Rochester 1973 (IAEA, Vienna) vol. p.103.
- [5] L.R. Veeser and D.W. Muir, private communication.
- [6] B. Leroux, private communication.
P. Bruneau, Thesis, University Bordeaux, CEN BG 1567 (1980).
- [7] J. Blons, Thesis, University of Paris, to be published.

НЕКОТОРЫЕ ОСОБЕННОСТИ ЭНЕРГЕТИЧЕСКОЙ ЗАВИСИМОСТИ СРЕДНЕГО ЧИСЛА МГНОВЕННЫХ НЕЙТРОНОВ ДЕЛЕНИЯ

Б.Д.Кузьминов, В.В.Малиновский, В.М.Пиксайкин, И.Н.Семенова
Физико-энергетический институт, Обнинск, СССР

Аннотация

В работе обсуждаются особенности метода и результатов измерения энергетической зависимости среднего числа мгновенных нейтронов при делении ядер урана-236, урана-238, нептуния-237. Выполнен совместный анализ экспериментальных данных по $\bar{\nu}_p$ и кинетическим энергиям осколков при делении ряда ядер.

I. Введение

Исследование факторов, влияющих на энергетическую зависимость среднего числа мгновенных нейтронов деления, представляет не только практический интерес, но и позволяет более глубоко понять физический смысл явлений, происходящих на последней стадии процесса деления ядер. К ним следует отнести такие проблемы как перекачка энергии коллективного движения в энергию внутреннего возбуждения, механизм разрядки сильно возбужденных осколков деления и др.

Энергия, уносимая мгновенным излучением, - кинетическая энергия осколков деления и энергия затрачиваемая на испускание нейтронов и γ -квантов, - черпается из энергии деления и энергии возбуждения делящегося ядра.

$$\bar{E}_f + E^* = \bar{E}_k + \bar{\nu}_p \bar{E}_\nu + E_\gamma$$

где \bar{E}_f - энергия деления, усредненная по всем способам деления; E^* - энергия возбуждения делящегося ядра; \bar{E}_k - средняя кинетическая энергия осколков деления; $\bar{\nu}_p$ - среднее число мгновенных нейтронов, испускаемых осколками деления; \bar{E}_ν - средняя энергия, затрачиваемая на испускание одного нейтрона; E_γ - средняя суммарная энергия, уносимая мгновенными γ -квантами.

Изменение энергии возбуждения делящегося ядра может оказать влияние на все компоненты уравнения баланса энергии. В связи с этим не исключено отклонение энергетической зависимости $\bar{\nu}_p$ от линейной. Детальные исследования влияния энергии возбуждения на энергетическую энергию осколков при делении ряда ядер свидетельствуют о наличии двух особенностей: проявление локальных изменений и плавного уменьшения (для некоторых ядер - увеличения) \bar{E}_k по мере роста энергии возбуждения делящегося ядра. Такое поведение одного из членов уравнения баланса энергии не может не отразиться на величине других составляющих.

Результаты измерения $\bar{\nu}_p$ при делении ядер ^{236}U , ^{238}U и ^{237}Np нейtronами, полученные в настоящей работе, совместно с литературными данными по $\bar{\nu}_p$ и \bar{E}_k использованы для анализа особенностей их энергетических зависимостей.

2. Экспериментальный метод

Измерения $\bar{\nu}_p$ при делении исследуемых ядер нейtronами проводились относительно величины $\bar{\nu}_p$ при спонтанном делении ^{252}Cf . Ионизационные камеры со слоями исследуемых веществ и ^{252}Cf размещались внутри детектора вторичных нейтронов на пути сколлимированного пучка моноэнергетических нейтронов, вызывающих деления. Детектор нейтронов представлял сборку из 16 счетчиков, наполненных гелием-3 и расположенных в полиэтиленовом цилиндрическом блоке. В центре блока имелась полость для размещения камеры деления.

Измерение числа мгновенных нейтронов осуществлялось в режиме временного анализа.

Импульс с камеры деления запускал канал счета нейтронов в зависимости от времени. Время измерений значительное превышало среднее время жизни мгновенных нейтронов деления в детекторе, что позволяло зарегистрировать как эффект, так и фоновую подложку. Использование нескольких групп памяти допускало параллельные измерения числа нейтронов деления для исследуемого изотопа и для ^{252}Cf .

Измерения $\bar{\nu}_p$ при разных энергиях нейтронов, вызвавших деление, проводились на электростатическом ускорителе ФЭИ ЭГ-1. Для получения нейтронов использовались реакции $T(p, n)$ и $D(d, n)$. Энергетическое разрешение для нейтронов при работе на твердой тритиевой мишени составляло около 30 кэВ. Защита детектора нейтронов от первичного излучения осуществлялась бетонной стеной толщиной 2 м. Формирование пучка нейтронов производилось каналом с диаметром 40 мм, пробитом в бетонной стене. Пучок нейтронов после прохождения через измерительную систему попадал в ловушку, изготовленную из сорированного полистирина. Внутри ловушки располагался монитор нейтронного потока.

При обработке результатов измерений вносились поправки, учитывающие специфику детектора нейтронов, ионизационных камер и электронной аппаратуры. Плохо поддающийся расчетному определению является эффект, связанный с зависимостью числа регистрируемых нейтронов от эффективности регистрации осколков деления. Качественно эту зависимость можно объяснить несколькими эффектами: зависимостью числа испускаемых осколками нейтронов от кинетической энергии осколков; угловой зависимостью амплитудного распределения импульсов, создаваемых осколками в ионизационной камере, и зависимостью задержки временной отметки запуска счета нейтронов от формы этих импульсов. Исследования детектора показали малую чувствительность эффективности регистрации нейтронов к угловому распределению осколков деления. При использовании

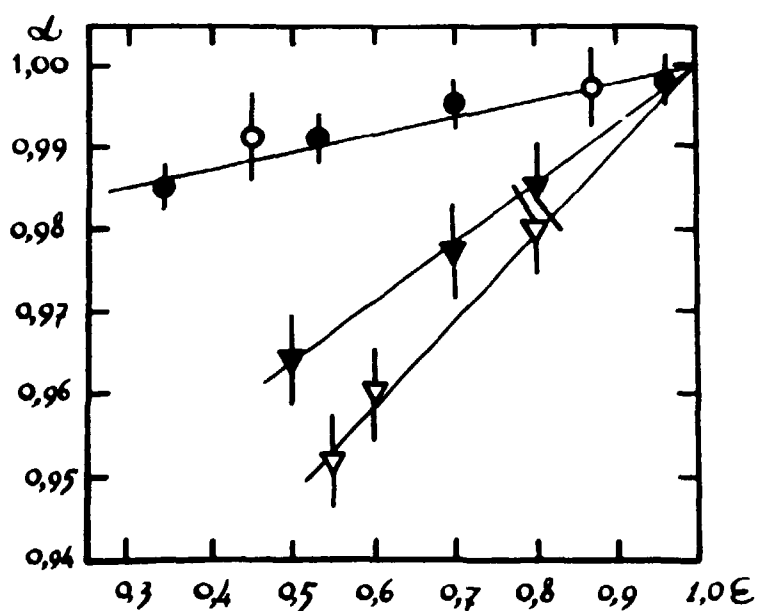


Рис. I. Доля регистрируемых нейтронов деления в зависимости от эффективности регистрации осколков деления. ● - ^{252}Cf ; ○ - ^{238}U ; ▼ - ^{236}U ; ▽ - ^{237}Np .

быстрой ионизационной камеры (длительность импульса около 40 нсек) временные задержки не могут оказать сколь-нибудь заметное влияние на эффективность регистрации нейтронов деления. По-видимому основной вклад в обсуждаемом эффекте принадлежит первому явлению – зависимости числа испускаемых нейтронов от кинетической энергии осколков деления. В настоящей работе влияние уровня порога регистрации импульсов в канале осколков деления на эффективность регистрации нейтронов деления изучалась экспериментально. На рис. I приведены результаты исследований.

В результате измерений вносились поправки, учитывающие следующие эффекты: δ_1 – различие энергетических спектров нейтронов деления; δ_2 – зависимость эффективности регистрации нейтронов от положения источника за осью детектора; δ_3 – различие

диаметров слоев исследуемого вещества и ^{252}Cf ; δ_4 - просчеты из-за совпадения в пределах мертвого времени импульсов от нейтронов деления; δ_5 - просчеты из-за совпадения в пределах мертвого времени импульса от нейтрона деления и фонового импульса; δ_6 - дискриминация в канале осколков деления; δ_7 - различные толщины слоев исследуемого вещества и ^{252}Cf ; δ_8 - спонтанные деления и счет наклонных импульсов от α -частиц; δ_9 - угловую анизотропию осколков деления; δ_{10} - примесь фоновых нейтронов при использовании реакции $\text{D}(\text{d}, \text{n})$.

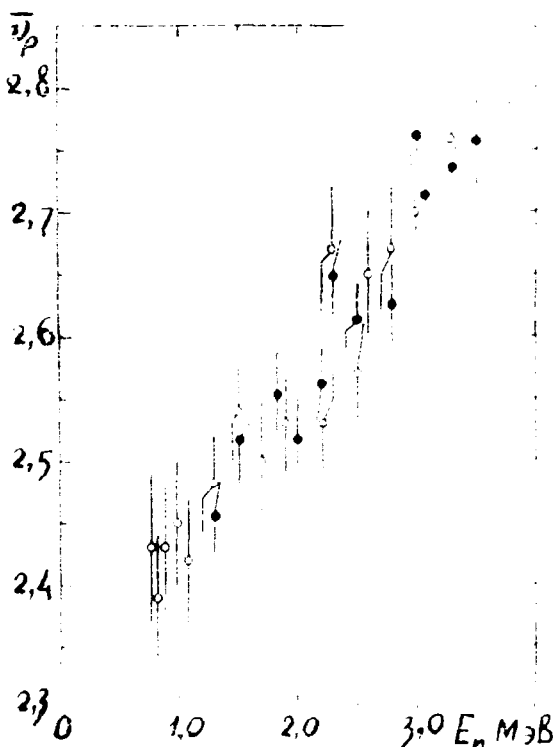
Величины поправок и их погрешности приведены в таблице 1.

Tachina 1.

Величина поправки (δ)	Погреш- ность (%)	Величина поправки (δ)	Погрешность (%)
δ_1 $-(0,7 \div 1,3)$	$\pm 0,3$	δ_2 236u	$\pm 1,5$
δ_2 $+ 0,5$	$\pm 0,2$	238u $+ 4,6$	$\pm 0,1$
238u $+ 4,6$	$\pm 0,3$	237Nr $+ 4,4$	$\pm 0,9$
237Nr $+ 4,4$	$\pm 0,3$	δ_3 $- 0,3$	$\pm 0,1$
δ_3 $- 0,3$	$\pm 0,2$	δ_4 $- (1,0 \div 1,6)$	$\pm 0,2 \div 0,9$
δ_4 $+ (0,1 \div 0,6)$	$\pm 0,06$	δ_5 $+ 1,0$	$\pm 0,1$

3. Основные результаты изучения

на рисунках 2-4 представлены результаты измерений, полученные в ходе данной работы и других работ. В первом приложении описаны методы определения $\tau_{\text{р}}$ в различных...
 ...модификациях квантовых корреляций ($\tau = 0$) для всех трех задач синтеза.



Число 2. Доказательство неравенства $\overline{v}_p \leq \overline{v}$ для
единичного вектора \overline{u} в \mathbb{R}^n .

$\sigma = \text{maximum value}; \quad 0 = [1]$

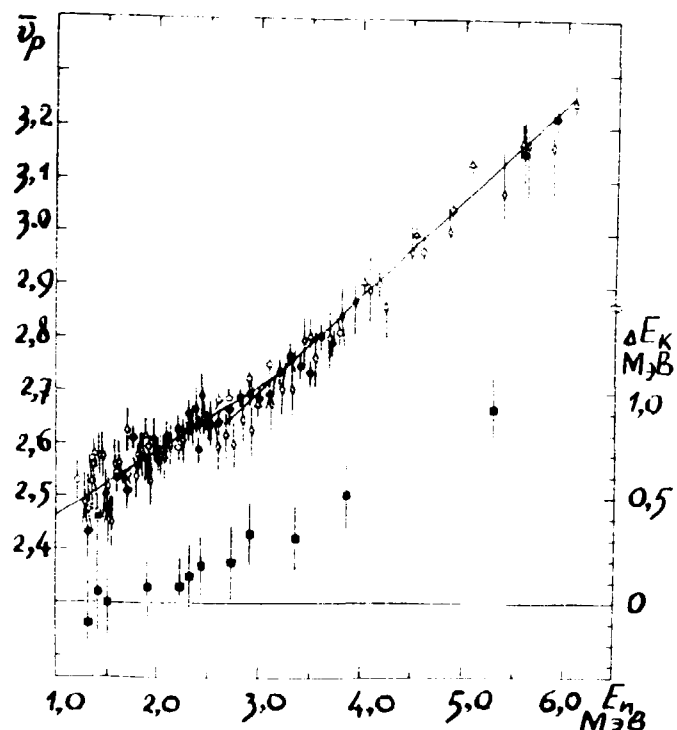


Рис.3. Результаты измерения \bar{v}_p при делении ядер ^{238}U нейтронами. Δ - [9]; \diamond - [10]; \circ - [11]; \bullet - настоящая работа.
 ■ - изменения кинетической энергии осколков при делении ядер ^{238}U нейтронами $\Delta\bar{E}_k = \bar{E}_k(1,6 \text{ мэв}) - \bar{E}_k(E_n)$ [4].

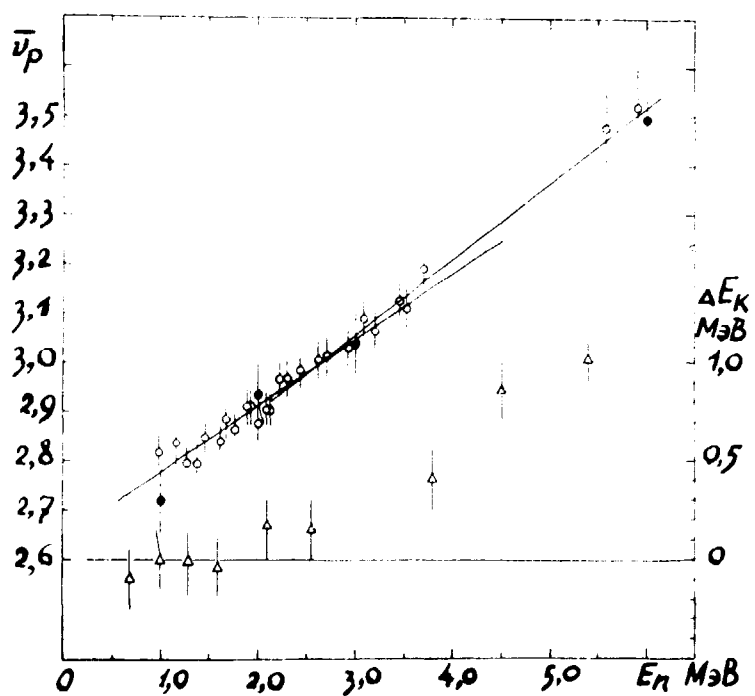


Рис.4. Зависимость среднего числа мгновенных нейтронов \bar{v}_p от энергии нейтронов, вызывающих деление ядер ^{237}Np .
 ● - [12]; ○ - настоящая работа. Δ - изменения средней кинетической энергии осколков $\Delta\bar{E}_k = \bar{E}_k(1\text{мэв}) - \bar{E}_k(E_n)$ [2].

Таблица 2

Ядро-мишень	E_n (МэВ)	$d\nu/dE_n$ (МэВ $^{-1}$)
^{238}U	I - 2,7	$0,121 \pm 0,009$
	2,7 - 6	$0,182 \pm 0,005$
^{277}Np	I - 3	$0,134 \pm 0,010$
	3 - 6	$0,154 \pm 0,009$

ядер были использованы для определения скорости роста (ν_p с учетом изменений E_k).

Результаты анализа приведены в таблице 3.

Таблица 3

Ядро - мишень	^{233}U	^{235}U	^{238}U	^{237}Np	^{239}Pu	^{240}Pu	^{241}Pu
$d\nu/dE^*$ (МэВ $^{-1}$)	0,107	0,125	0,130	0,125	0,104	0,111	0,120

Из таблицы 3 следует, что на испускание одного нейтрона затрачивается 8 - 10 МэВ. Одной из причин такого большого значения этой величины может служить зависимость E_γ от E^* . Существует специфическая особенность конкуренции испускания γ -квантов и нейтронов осколками [3, 4]. После вылета первого нейтрона ядро-осколок с малой энергией возбуждения и большим спином. Второму нейтрону трудно найти конечное состояние с малой энергией и большим спином, что, по-видимому, увеличивает время жизни ядра по отношению к испусканию нейтрона. В работе [4] получено, что в среднем $dE_\gamma/d\nu$ составляет около 1 МэВ.

Другая особенность энергетической зависимости ν_p состоит в локальных отклонениях от линейной функции. Этот эффект отчетливо проявляется при делении ^{232}Th [5] и ^{233}U [6] нейtronами.

Результаты измерения ν_p для ^{236}U , полученные в настоящей работе, совместно с результатами работы [7] свидетельствуют о ступенчатом росте ν_p по мере увеличения энергии нейтронов. Имеющиеся данные по кинетической энергии осколков для ^{236}U [8] не могут быть использованы для объяснения такой закономерности. Это интересное явление заслуживает дополнительного тщательного исследования.

Действительно в той области энергий нейтронов, где происходит уменьшение E_k , скорость роста ν_p увеличивается, т.е. по-видимому, происходит перераспределение энергии деления между кинетической энергией осколков и их энергией возбуждения. Литературные данные по ν_p и E_k для ряда ядер были использованы для определения скорости роста (ν_p с учетом изменений E_k).

Результаты анализа приведены в таблице 3.

Таблица 3

Ядро - мишень	^{233}U	^{235}U	^{238}U	^{237}Np	^{239}Pu	^{240}Pu	^{241}Pu
$d\nu/dE^*$ (МэВ $^{-1}$)	0,107	0,125	0,130	0,125	0,104	0,111	0,120

Из таблицы 3 следует, что на испускание одного нейтрона затрачивается 8 - 10 МэВ. Одной из причин такого большого значения этой величины может служить зависимость E_γ от E^* . Существует специфическая особенность конкуренции испускания γ -квантов и нейтронов осколками [3, 4]. После вылета первого нейтрона ядро-осколок с малой энергией возбуждения и большим спином. Второму нейтрону трудно найти конечное состояние с малой энергией и большим спином, что, по-видимому, увеличивает время жизни ядра по отношению к испусканию нейтрона. В работе [4] получено, что в среднем $dE_\gamma/d\nu$ составляет около 1 МэВ.

Другая особенность энергетической зависимости ν_p состоит в локальных отклонениях от линейной функции. Этот эффект отчетливо проявляется при делении ^{232}Th [5] и ^{233}U [6] нейtronами.

Результаты измерения ν_p для ^{236}U , полученные в настоящей работе, совместно с результатами работы [7] свидетельствуют о ступенчатом росте ν_p по мере увеличения энергии нейтронов. Имеющиеся данные по кинетической энергии осколков для ^{236}U [8] не могут быть использованы для объяснения такой закономерности. Это интересное явление заслуживает дополнительного тщательного исследования.

Л и т е р а т у р а

1. Воробьев В.Г., Кузьминов Б.Д., Сергачев А.И., Таракко М.Э., Ядерная физика, 1969, т.9, стр.296.
2. Кузьминов Б.Д., Сергачев А.И., Смиренина Л.Д. - Ядерная физика, 1970, т.II, стр.297.
3. Johansson S.A.E., Nucl.Phys., 1964, v.60, p.378.
4. Thomas T.G., Grover J.R., Phys.Rev., 1967, v.150, p.980.
5. Caruana J., Boldeman J.W., Walsh R.L., Nucl.Phys., 1977, A285, 217.
6. Boldeman J.W., Bertram W.K., Walsh R.L., Nucl.Phys., 1976, A265, 337.
7. Conde H., Holberg M.J., Nucl.Energy., 1971, 25, 331.
8. Дьяченко Н.П., Кузьминов Б.Д., Малиновский В.В. и др. Ядерная физика, 1979, т.30, стр.904.
9. Soleilhac M., Prebaut J., Cauchan I., J.Nucl.Energy, 1969, 23, 257.
10. Савин М.В., Хохлов Е.А., Парамонова И.Н., Чиркин В.А. Атомная энергия, 1972, т.32, стр.408.
11. Нурпесов Б., Володин К.Е., Нестеров В.Г., Прохорова Л.И., Смиренин Г.Н., Турчин Ю.М. - Атомная энергия, 1975, т.39, вып.3, стр.199.
12. Veeser L.R., Phys.Rev., 1978, C17, 385.

REACTOR CALCULATION METHODS

Christian Beiche

Zentralinstitut für Kernforschung, Rossendorf, DDR - 8051 Dresden

The fundamental problem in the field of reactor calculations consists in evaluating the neutron distribution in the reactor. From that, the interesting physical parameters can be derived directly, like in the case of power generation, or by means of additional physical relations, as e.g. in the case of phase and temperature distribution in the flowing coolant.

The basic relation of neutron kinetics is the transport equation

$$\frac{1}{v} \frac{\partial}{\partial t} \Phi(\vec{r}, \vec{\omega}, E, t) + \vec{\omega} \cdot \nabla \Phi(\vec{r}, \vec{\omega}, E, t) + \sum_i (\vec{r}, E) \Phi(\vec{r}, \vec{\omega}, E, t) = \int dE' \int d\vec{\omega}' \sum_j (\vec{r}, \vec{\omega}', E') \Phi(\vec{r}, \vec{\omega}', E', t) + \\ + \chi(E) \int dE' \int d\vec{\omega}' \nu(E') \sum_i (\vec{r}, E') \Phi(\vec{r}, \vec{\omega}', E', t) + S^{ext}(\vec{r}, \vec{\omega}, E, t)$$

[$\Phi(\vec{r}, \vec{\omega}, E, t)$ = angular neutron flux]
+ initial and boundary conditions.

This equation describes the statistical mean value of the angular flux.

Other statistical effects, which e.g. occur as zero power noise in reactors of very small power, are not included in this equation.

The dominating topic of reactor calculation doesn't consist in the solution of the initial value problem but in the solution of the boundary value problem, and here the calculation of the homogeneous eigenvalue problem is of special importance.

It is obvious, that the neutron transport equation is much too complicated for giving a simple solution. Solving practical tasks requires therefore the introduction of approximations. In the practice some groups of typical problems can be distinguished from series calculations, necessary to optimize construction and operation behaviour of power reactors, to precision calculations of experiments, for finding out uncertainties in data or calculation methods or for checking the accuracy of routine calculations.

Although the analytical solutions of the transport equation are very interesting from the mathematical point of view and contribute to the development of the theory of singular equations, they can be ignored in practical analysis of reactor problems because they are limited to the simplest exercises only.

Now we consider those approximations being important to practical calculations. The goal is to reduce the number of free variables. At first we want to separate from the energy variable. Due to the resonance structure of the cross-sections the energy dependence is very complex, but should not be treated in detail here. The expedient consists in the introduction of neutron groups with group averaged cross-sections. By it the energy problem is now shifted to the calculation of these group constants. The number of energy groups varies between 1 and 4 in thermal and 15 and 30 in fast reactor calculations. Spectra are calculated with group numbers between 30 and some thousands.

In treating the spatial problem several methods are in use. Monte-Carlo-methods allow to take into account the full complexity of geometry and neutron-nucleus interaction. They are favoured to calculate integral parameters instead of distribution functions. Very often the generation game is applied, where the histories of a number of neutrons are followed from their emission to their absorption or escape. During the history free flights alternate with collision processes and are determined by probability distributions. For decreasing the computer time a number of variance reducing tricks are introduced into the calculational procedures.

The S_n -methods form another group of approximations. For one- or two-dimensional geometries the angular dependence of flux is considered to be piecewise linear so that the transport equation is reduced to a set of differential equations for the supporting functions.

$$\Phi(x, \omega, E) = \frac{\omega - \omega_{j-1}}{\omega_j - \omega_{j-1}} \Phi(x, \omega_j, E) + \frac{\omega_j - \omega}{\omega_j - \omega_{j+1}} \Phi(x, \omega_{j+1}, E) \quad \omega = \bar{\omega}.$$

$$[\frac{1}{3}(2\omega_j + \omega_{j-1}) \frac{d}{dx} + \Sigma_t(x, E)] \Phi(x, \omega_j, E) + [\frac{1}{3}(\omega_j + 2\omega_{j+1}) \frac{d}{dx} + \Sigma_t(x, E)] \Phi(x, \omega_{j+1}, E) = \\ = 2 \frac{4}{\omega_j - \omega_{j+1}} \int_{\omega_{j+1}}^{\omega_j} d\omega S(x, \omega, E)$$

S_4 -approximation, coupled with the spherical harmonics expansion of the cross-sections, satisfies most accuracy requirements.

Spherical harmonics approximations have proved to be a powerful tool for solving reactor calculation problems. Assuming an isotropic and homogeneous medium the scattering process is azimuthally symmetric about the initial neutron direction. Expanding the scattering cross-section as well as the angular flux in terms of Legendre polynomials one gets by using the spherical harmonics addition theorems a first order set of differential equations for the expansion coefficients. The first two coefficients are identical with the total neutron flux, and the neutron current respectively.

$$\Sigma_s(x, \omega + \omega, E' - E) = \sum_{l=0}^{\infty} \frac{2l+1}{4\pi} \Sigma_{sl}(x, E' - E) P_l(\cos \theta) \quad \Phi(x, \omega, E) = \sum_{l=0}^{\infty} \frac{2l+1}{4\pi} \Phi_l(x, E) P_l(\omega) \\ \frac{1}{2l+1} \frac{d}{dx} \Phi_{l+1}(x, E) + \Sigma_{sl}(x, E) \Phi_l(x, E) + \frac{l+1}{2l+1} \frac{d}{dx} \Phi_{l+1}(x, E) = \int dE' \Sigma_{sl}(x, E' - E) \Phi_l(x, E) + \delta_{l0} \frac{\Sigma(E)}{K_{eff}} \int dE' \nu(E) \Sigma_{sl}(x, E) \Phi_l(x, E) \\ \Phi_0(x, E) = \int d\omega d\Omega \Phi(x, \omega, E) = \text{neutron flux } \Phi(x, E) \quad K_{eff} = \text{eigenvalue} = \\ \Phi_1(x, E) = \int d\omega d\Omega \Phi(x, \omega, E) = \text{neutron current} \quad = \text{effective multiplication factor}$$

Starting from the S_1 -approximation by eliminating the neutron current via a Pick's law the diffusion equation for the flux can be obtained. To attain to simple expressions the anisotropic scattering integral is neglected but its contribution is tried to be compensated by the introduction of a transport cross-section instead of the total one.

$$-\nabla \left(\frac{1}{3\Sigma_{tot}(\vec{r})} \nabla \Phi_g(\vec{r}) \right) + \Sigma_g(\vec{r}) \Phi_g(\vec{r}) = \sum_j \Sigma_{sgj}(\vec{r}) \Phi_j(\vec{r}) + \frac{\chi_g}{K_{eff}} \sum_j \nu_j \Sigma_{tj}(\vec{r}) \Phi_j(\vec{r})$$

g, j = energy group index

Σ_{sg} = transport cross-section

$$\text{fission source iteration: } -\nabla(D_g \nabla \Phi_g^{(0)}) + \Sigma_g \Phi_g^{(0)} = \sum_j \Sigma_{sgj}^{(0)} + \frac{\chi_g}{K_{eff}} \sum_j \nu_j \Sigma_{tj}^{(0)} \Phi_j^{(0)}$$

The simplicity of the diffusion equation promotes it to the top favourite in the practical reactor analysis. For that reason this approximation is sometimes applied to such cases also, which not correspond to the suppositions. The effects are partly checked by means of more accurate calculations and result often in fitting the parameters.

The development of calculation programmes received a big boom after the fission iteration has been proved to give always the unique nonnegative solution of the finite differences form of the diffusion equation.

In one-dimensional geometries the numerical solution is very simple. The calculation in two or three dimensions is more problematic because especially the number of mesh points rises up considerably. Since the size of the diffusion length is used as a directive for the distance of the mesh points, the number of energy-space points can amount to 100000 in two and many millions in three dimensions. Furthermore the convergence rate of the iteration process reduces with increasing number of mesh points.

In search of more powerful numerical procedures a number of techniques has been developed, which start from a coarse mesh and use simple polynomials or superpose special solutions. Often these coarse mesh methods are used in combination with fine mesh calculations for accelerating the latter. Presently the development of new methods is not finished. Of course, the use of more refined methods increases the difficulties of their handling. While the finite differences programmes can be operated by anybody, the advanced programmes require deeper insight into the physical and numerical processes.

Briefly it should be mentioned that the macro-distribution of the neutron flux in a reactor is usually superposed by a micro-distribution, caused by the heterogeneous structure of the fuel cell. A special group of codes fulfills the calculations of micro-distributions in cells or supercells and yields cell averaged multigroup cross-sections. The first collision probability method is used widely in these codes. The difficulties consist in the calculation of the probability matrix taking into consideration the resonance structure of the cross-sections.

There is a number of further subjects of reactor calculations like burn up, shielding or safety calculations with their specific methods which cannot be treated here.

The development of computer codes for all these special cases results necessarily in the generation of programme systems where the codes are linked together.

For solving many reactor calculation problems one can make use of codes from the international library managed by the IAEA. But the implementation and handling of an unknown programme is not unproblematic generally.

**Einschätzung der Wirtschaftlichkeit von
Kernkraftwerken unter besonderer Beach-
tung der Brennstoffökonomie**

Buhl,
VE Kombinat Kernkraftwerk "Bruno Leuschner", Greifswald,
Bereich Forschung, Berlin, DDR

1. Überblick

Die Wirtschaftlichkeit von Kernkraftwerken war in den 60er Jahren an eine Reihe von Bedingungen geknüpft. Neben den grundsätzlichen Voraussetzungen – wie Vorhandensein des "Knowhow" und einer industriellen Basis zur Errichtung von Kernkraftwerken – gehörten v. a. folgende Punkte dazu:

- kaum vorhandene eigene konventionelle Energieträger
- Bezahlung des Forschungsaufwandes aus dem Staatshaushalt und
- Einsatz der Kernkraftwerke im Grundlastbereich.

Im Ergebnis der 70er Jahre, insbesondere infolge der konzentrierten Nutzung von Wissenschaft und Technik in der Produktion und den Auswirkungen der Energiekrise, sind die Kernkraftwerke praktisch über Nacht absolut wirtschaftlich geworden.

Die in Tabelle 1 ausgewiesenen Stromerzeugungskosten westlicher Industrieländer sind keine illusionären Werte, es sind tatsächlich erreichte und bekanntgegebene Kosten der letzten Jahre.

Will man die Ursachen dieser Entwicklung ergründen, so muß man zunächst die wichtigsten Faktoren, die die internationalen Wirtschaftsbeziehungen erheblich beeinflusser, nennen: /8/

- Verschärfung des Krisenprozesses im Kapitalismus
- Aufschwung der nationalen und sozialen Befreiungsbewegungen
- Veränderungen der wirtschaftlichen Strukturen im Weltmaßstab in bisher unbekanntem Maße
- Relative Verknappung und damit Aufwandserhöhung bei Verfügbarkeit bzw. Aufschluß der Ressourcen
- Auswirkungen des Tempogewinns bei der Einführung neuer Erzeugnisse, Verfahren und Technologien aus Wissenschaft und Technik in die Produktion
- Vertiefung der wirtschaftlichen und wissenschaftlich-technischen Zusammenarbeit über Ländergrenzen hinweg.

Das Wechselspiel dieser Faktoren ist die Basis für die Preisentwicklung auf den Hauptwarenmarkten in den 70er Jahren. Es führte zu den hinlänglich bekannten qualitativen und quantitativen Änderungen in bisher unbekannten Ausmaßen, wie

- sprunghaften Preisanstieg auf den Hauptwarenmarkten
- Herausbildung eines höheren Niveaus der Weltmarktpreise und

- grundlegende Veränderungen der Weltmarktpreisrelationen, insbesondere zwischen Fertigerzeugnissen und Rohstoffen.

Für die Kernenergie bewirkt dieser Prozeß, daß die Kernkraftwerke infolge der angedeuteten Relationsveränderungen ihre Wirtschaftlichkeit im Verhältnis zu den anderen Kraftwerkstypen erheblich verbesserten. Begünstigt wurde dies von folgenden Faktoren:

- Enorme Steigerungsraten der Preise für konventionelle Energieträger
- Wirksamwerden großer Kernkraftwerks - Blockeinheiten
- Stabilisierung hoher Verfügbarkeiten im kommerziellen Betrieb
- Umschlag des zeitlich früher getätigten Forschungsaufwandes in die Produktion und Senkung des laufenden.

Die Konsequenzen dieser Entwicklung sind ja nicht unbedeutend.

Wenn man sich die Größenordnungen der Produktion ansieht und sie mit den in Tabelle 1 ausgewiesenen Kostenvorteilen in Bezug bringt, kommen für Unternehmen mit hohem Kernkraftwerksanteil beträchtliche Vorteile heraus.

Sehen wir uns deshalb den Stand in der Welt an.

Ende 1979 wurden in der Welt rund 240 Kernkraftwerksblöcke mit einer Leistung von mehr als 125 000 MW in 22 Ländern industriell betrieben. In diesen und weiteren 14 Ländern sind Kernkraftwerke in Bau oder bestellt. Die Zahl der insgesamt neu in Betrieb gehenden Kernkraftwerke beträgt nochmals 330, ihre geplante Leistung 315 000 MW. Der Anteil der Kernkraftwerkskapazitäten an der gesamten installierten Leistung der Länder beträgt bereits bis zu 30 % (siehe Tabelle 2).

Diese Kernkraftwerke haben insgesamt - wie das Energieprogramm der EG vom November 1979 für dieses Wirtschaftsgebiet ausweist - jetzt bereits Kostenvorteile gegenüber der Kohle von ca. 20 % und gegenüber Öl (ohne Berücksichtigung der Ereignisse im Irak/Iran) 30 ... 40 %. Die hier angedeutete Entwicklung läßt sich gut am Beispiel Großbritanniens demonstrieren (Bild 1).

Doch bevor wir zu einer endgültigen Aussage über die Wirtschaftlichkeit von Kernkraftwerken kommen, noch einige Analysen der wichtigsten Kostenkomponenten, v. a., der Investitionskosten und der Kernbrennstoffkosten.

2. Analyse der Investitionskosten

Eine wichtige Komponente der Selbstkosten der Elektroenergieerzeugung - die Abschreibungen - wird wesentlich von den Investitionskosten, oder häufig auch Anschaffungskosten genannt, bestimmt. Der Absolutwert der Abschreibungen pro Jahr ist dabei weitgehendst unabhängig von der jährlichen Energieproduktion.

Die Investitionskosten haben, wie die Tabellen 2 und 3 zeigen, gewaltige Veränderungen erfahren. Während in den "günstigen" Zeiten Kernkraftwerke nur

	KKW	Kohle- kraft- werke	Öl- kraft- werke	Währungs- einheit
USA (Ø 1978) ¹⁾	1,54	2,32	3,95	c/kWh
Großbritannien (Ø79)	1,02	1,29	1,31	p/kWh
BRD	3,97	7,55		Pf/kWh
Frankreich (78)	10,4	12,6	14,1	cts/kWh
Schweden (76)	7	9 ¹⁾ /10 ²⁾	11	Öre/kWh
Italien	3,83		5,51	c/kWh

1) ohne Rauchgasentschwefelung bei Kohlekraftwerken

2) mit Rauchgasentschwefelung bei Kohlekraftwerken

Tabelle 1: Stand der Selbstkosten einiger Kraftwerkstypen /1-7/

Land	Installierte KKW- Kapazitäten /MW _e /	Anteil der Kernenergie an der EEE insgesamt / % /
USA	50 846	12,5
Belgien	1 761	24,6
BRD	8 219	10,2
Frankreich	6 726	13,4
Großbritannien	7 168	12,9
Italien	1 160	2,5
Niederlande	526	6,6
Schweiz	2 531 ^{x)}	ca.30
Spanien	1 100	7
Japan	13 467	12
UdSSR	18 022	
DDR	1 830	11
VR Bulgarien	880	21

x) einschließlich Anteile aus französischen Kernkraftwerken

Tabelle 2: Leistungs- und Arbeitsanteile an den Gesamtkapazitäten

100 ... 120 \$/kW kosteten, muß man bei heutigen Bestellungen mit dem 14 ... 18-fachen Wert rechnen. Ähnlich, wenn auch auf Grund der höheren Ausgangsposition prozentual vielleicht nicht so beeindruckend, verändern sich aber auch die Kosten der Steinkohlenkraftwerke in den USA (Tabelle 4). Auch andere Länder zeigen ähnliche Entwicklungen (Tabelle 5).

Die genauere Analyse dieser Entwicklung zeigt folgendes:

Die im Rechnungswesen allgemein als Investitions- oder Anschaffungskosten ausgewiesene Komponente setzt sich aus zwei Faktoren zusammen:

- Vergabepreis (vertraglicher Aufschlußpreis des NAN)
- Bauherrnkosten (Anschaffungsnebenkosten)

Dabei beinhaltet der Vergabepreis nichts anderes als die direkt entstehenden Kosten plus eines zulässigen Gewinnanteils für die Ausrüstungen, berechnet von den NAN. Bei Kernkraftwerken sieht die typische Aufschlüsselung folgendermaßen aus:

Reaktoranlage	32 %
Turbogenerator	16 %
Wasser-Dampf-Kreislauf	14 %
elektrotechnische Einrichtung	12 %
Leittechnik	6 %
Bauteil	20 % Stand 1977/78

Für Steinkohlenkraftwerke gilt die nachfolgende Aufteilung:

Kesselanlage	31 %
Maschinenanlage	22 %
elektrotechnische Anlage	5 %
Leittechnik	3 %
Umweltschutz (einschließl. Rauchgasentschwefelung)	18 %
Nebenkosten	8 %
Bauteil	13 % /9/

Die Anschaffungskosten haben vor 10 ... 15 Jahren noch mehr als 3/4 der Gesamtkosten bestimmt. Heute sind sie auf weniger als 50 % gesunken, während die Bauherrnkosten stark zugenommen haben. Tabelle 6 verdeutlicht das. Anders ausgedrückt, es betrugen um das Jahr 1970 im günstigen Fall die Bauherrnkosten rund 25 ... 30 \$/kW, heute rechnet man bei Inbetriebnahmen um Mitte der 80er Jahre mit rund 500 ... 550 \$/kW, d. h. dem mehr als 20-fachen!

Während bisher die Summe der Einzelpreise der NAN die Investitionskosten bestimmten, machen heute Finanzierungskosten und Preiseskalation den größten Teil der Kosten für die Errichtung aus.

An dieser Stelle darf man nicht verschweigen, daß wesentliche Voraussetzungen für eine gesellschaftliche Akzeptanz - hier ist die weltweite Besinnung auf die Bedeutung des Umweltschutzes zu nennen - nicht nur in KKW zu qualitativen

Planungs- jahr	Inbetriebnahmejahr	Kosten /Mio US-\$/	% der Steigerung bezogen auf Position 1
1967	1972	105	100
1969	1975	187	178
1971	1978	276	263
1973	1981	448	427
1974	1983	623	593
1975	1985	750	714
1976	1986	922	878
1978	1990	1675	1595

Tabelle 3: Entwicklung der Investitionskosten eines 1000 MW-LWR-Blockes
in den USA

Planungs- jahr	Inbetrieb- nahmejahr	Kosten /Mio US-\$/	% der Steigerung bezogen auf Position 1
1967	1972	135	100
1969	1975	250	170
1971	1978	425	315
1973	1981	495	365
1974	1983	715	530
1975	1985	890	660
1976	1986	1120	830

Tabelle 4: Entwicklung der Investitionskosten eines vergleichbaren 1000-MW-
Steinkohlekraftwerkes in den USA

Kernkraftwerk	Aufnahme des kommerziellen Betriebes	spezifische Investi- tionskosten /Can. \$/kW/
Pickering A	1971	375
Pickering B	1973	1138
Bruce A	1977	634
Bruce B	1978	1229
Point Lepreau	1980	1409
Gentilly	1981	1343
Darlington	1986 - 1988	1474

Tabelle 5: Entwicklung der spezifischen Investitionskosten kanadischer
Kernkraftwerke

Veränderungen führt. Diese Problematik ist diesem Kreis sicher hinlänglich bekannt. Ihre ökonomischen Auswirkungen sind natürlich das absolute Ansteigen beider Investitionskomponenten.

Noch ein Wort zu den Errichtungszeiten. Ihre Verlängerung ist eine entscheidende Ursache für diese Entwicklung. Wie Tabelle 7 ausweist, traten innerhalb von 7 Jahren Verlängerungen der Errichtungszeiten von 40 % und mehr ein. Das bedeutet natürlich auch länger laufende Kredite. Die inzwischen ohnehin gestiegenen Zinsen erhöhen den Gesamtpreis somit beträchtlich, ganz abgesehen von den Auswirkungen möglicher Arbeitsproduktivitätseinbußen.

Sieht man sich allein die Veränderung der Genehmigungsfristen an, so erhält man folgendes Bild: /nach 2/

Projekt	Jahr des Bau- antrages	Genehmigungs- fristen (Monate)	Zahl der unter die Genehmigung fallenden Probleme
1	1966	12	128
2	1970	30	344
3	1972	36	696
.	1974	45	2189
5	1977	66	ca. 3000

Selbstverständlich ist es im Rahmen dieses Vortrages nicht möglich, alle Faktoren tiegründig zu analysieren. Ziel dieses Ausfluges in die Investitionsökonomie war es lediglich

- 1) verständlich zu machen, daß sich Struktur und Inhalt des Begriffes "Investitionskosten" wesentlich verändert haben und
- 2) die Hauptursachen und Konsequenzen dieser Entwicklung hier auszuweisen.

Diese sind zusammengefaßt

- Auswirkungen der inflationären Tendenzen und der Preisekalation auf allen Gebieten, besonders aber bei kommerziellen Operationen
- Verlängerung der Genehmigungs- und Bauzeiten
- Verschärfung der sicherheitstechnischen und Umweltschutzanforderungen und der sich daraus ergebenden qualitativen Veränderungen und Verzögerungen.

3. Analyse der Kernbrennstoffkosten

Die Kernbrennstoffkosten stellen die wesentliche, während des Betriebes der Kernkraftwerke auch in ihrer absoluten Höhe beeinflußbare Kostenkomponente dar. Sie bestimmen den überwiegenden Teil der variablen Betriebskosten im Jahr.

Auch wenn der Begriff Brennstoffkosten identisch mit dem konventionellen Kraftwerk ist, beinhaltet er nicht das gleiche. Der Hauptunterschied hat seine Ursachen in der hohen Energiekonzentration pro Volumeneinheit und seiner langen Verweilzeit im Reaktor (ca. 3 Jahre bei LWR). Das bringt insbesondere für

Pla- nungs- jahr	Inbe- trieb- nahme- jahr	spezif. Investi- tionsk. /\$/kW/	Vergabepreis insg.	Bauherrnkosten insg.					
				davon			Zinsen währ. des Baues	Preis- eska- lation	sonstiges Unvorher- ges.
				Sicherh.	indir.	+Umwelt- schutz			
				\$	\$	\$	%	%	%
1967	1972	105	76	- ¹⁾	5	24	5	13	6
1969	1975	187	65	- ¹⁾	6	36	10	20	6
1971	1978	276	62	- ¹⁾	8	38	8	25	5
1973	1981	448	59	12	9	41	11	26	4
1974	1983	623	48	9	8	52	14	34	4
1975	1984	750	44	8	9	56	15	37	4
1976	1986	922	44	9	8	56	14	38	4

1) nicht gesondert ausgewiesen

Tabelle 6: Struktur der Investitionskosten gegenwärtiger und zukünftiger Kernkraftwerke in den USA

Baubeginn	1967	1969	1972	1974
Dokumentation + Genehmigung	6	6	12-18	12-18
Prüfung und Untersuchung der Unterlagen	9 - 12	12 - 15	15-18	18-21
Bauzeit	42	46	54	60
Prüfung und Kontrolle der Ergebnisse	6	6	6	6
Summe	63-65	70-73	87-96	96-105

Tabelle 7: Errichtungszeiten von Kernkraftwerken in Monaten in den USA /2/

kurzfristige Aussagen über die Bewegung dieser Komponente und bei der Abrechnung Probleme. Für die hier anzustellenden Betrachtungen soll dieses Problem jedoch ausgeklammert werden.

Auch bei den Kernbrennstoffkosten haben sich in den 70er Jahren wesentliche Veränderungen vollzogen. In der Leitwährung für die Preise der meisten Komponenten des Kernbrennstoffzyklusses ausgedrückt, in US-\$ also, haben sich die reinen Kosten ca. verfünffacht. Nimmt man eine einfache Aufrechnung der Kostenkomponenten des Kernbrennstoffs vor, so erhält man folgendes Bild: (Tabelle 8)

gültiger Zeitraum	Kosten je kg Uran (3,2 % Anreicherung) / \$/kg U ²³⁵ (3,2 %)/	daraus resultierende Kernbrennstoffkosten / c/kWh /
1970	257	0,16
1974	667	0,3
1978	1360	0,69
1980 / Mai	1561	0,77

Tabelle 8: Entwicklung der typischen Kernbrennstoffkosten auf der Basis der Preise für die Komponenten auf den Hauptwarenmarkten

Jedoch gibt es in der Regel auf den westlichen Märkten keine Unternehmen, die alle Produktionsschritte des Kernbrennstoffzyklusses für den Betreiber des KKW ausführen. Vielmehr muß der Betreiber dafür bei verschiedenen Auftragnehmern selbst Sorge tragen. Deshalb zunächst eine Kurzanalyse der wichtigsten Komponenten im Kernbrennstoffzyklus.

1. Uranerz

Der Preis für Uranerz ist im Zeitraum 1973 - 1977 etwa auf das 5 ... 7-fache in US-\$ angestiegen. Verschiedene politische und wirtschaftliche Erwägungen sind die Ursache dafür, daß in den Jahren 1974 - 1978 ein typischer Verkäufermarkt entstand. Bei einem hohen Bedarf an Uran konnten die Lieferer weitgehendst die Preise in die Höhe treiben. So stiegen diese etwa im Zeitraum 1970 - 78 von ca. 6 \$/lb U₃O₈ auf bis zu 45 \$/lb U₃O₈.

In der Zwischenzeit sind einige Faktoren, die das Ansteigen bewirkte, zumindestens zeitweilig weggefallen. Dazu gehören das Sinken der Nachfrage und die Freigabe von Uran zu neuen Vertragsabschlüssen auf wichtigen Hauptwarenmarkten. Diese Phase zeigt Bild 2. Das Sinken in diesem Jahr bedeutet unter anderem, daß der Uranerzpreis in den Ländern, deren Gelentwertung wesentlich langsamer fortschreitet als beim US-\$, in die Größenordnungen von Anfang der 70er Jahre kommt.

2. Konversion von U₃O₈ in UF₆

Infolge der geringen Bedeutung dieser Komponente hier nur soviel, daß sie möglicherweise infolge Kapazitätsmangels bald ansteigen wird. Der Einfluß sollte aber weiterhin um 5 % der Kernbrennstoffkosten bleiben.

3. Anreicherung

Hier sind folgende Entwicklungen zu berücksichtigen:

Bis etwa 1975 beherrschten die USA den gesamten westlichen Markt. Gegenwärtig bieten verstärkt westeuropäische Firmen zu hohen Preisen ihre Dienstleistungen auf diesem Gebiet an. Die dem Department of Energy (DOE) der USA unterstehenden Anreicherungsanlagen erhöhen ihre Preise systematisch, wie Bild 3 ausweist. Der Stand vom August 1980 ist 105,54 \$/kg TAE für Requirements Contracts und 98,95 \$/kg TAE für Adjustable, Fixed Commitment Contracts.

4. Brennelementfertigung

Nachdem bis in die zweite Hälfte der 70er Jahre diese Kosten relativ konstant blieben – man sprach sogar von der Insel der Stabilität im Kernbrennstoffzyklus – beginnen nunmehr Einflüsse neuer Anforderungen an Qualität und Quantität der Fertigung, die Steigerungsraten über die allgemein bekannten Eskalationsraten anwachsen zu lassen. Ein genaueres Beobachten ist infolge der Dezentralisierung der Fertigung schwer möglich.

5. Wiederaufbereitung und Entsorgung

Diese Komponente hat bisher die höchsten Steigerungsraten erfahren. Da jedoch für die Wiederaufbereitung von Brennstoff aus Leichtwasserreaktoren noch keine kommerzielle Anlage in der Welt stabil arbeitet, sind diese Komponenten sehr spekulativ. Damit entfällt gegenwärtig auch jede echte Möglichkeit, in größerem Umfang einen Erlös für das im abgebrannten Brennstoff enthaltene Plutonium und Uran 235 zu erzielen. Aus diesen Gründen sollten die in den Tabellen ersichtlichen Schätzungen dieser Komponente mit größter Vorsicht betrachtet werden. Die Tabellen 10 – 12 geben eine Übersicht über diese Entwicklung. Gleichzeitig wird der Einfluß der Komponenten auf die spezifischen Stromerzeugungskosten deutlich.

Besonders interessant wird natürlich der Einfluß von Veränderungen einzelner Komponenten auf die Brennstoffkosten. Dieser ist in Bild 4 prinzipiell dargestellt.

Gestatten sie mir noch einige Worte zum Anteil der Brennstoffkosten an den Gesamtkosten der Elektroenergieerzeugung. Er betrug in der Regel bis 1973/74 weniger als 25 %. Er ist infolge der sofortigen Auswirkungen der Veränderungen auf die Brennstoffkosten und des verzögerten Einflusses vor allem auf die Abschreibungen in den meisten Ländern auf bis zu 50 % gestiegen. Wir dürfen dabei aber nicht vergessen, daß die Auswirkungen erhöhter Investitionskosten auf die Gesamtkosten eben wesentlich später deutlich werden.

	spezifische Basiswerte	Kosten je kg U (3,2%) /\$/	% der Brennstoffkosten	spez. Kostenkomponente /c/kWh/
Uran	78/lb U ₃ O ₈	85	33	0,052
Konversion	1,05 \$/kgU	15	6	0,009
Anreicherung	26 \$/kg TAE	111	43	0,068
Fertigung	82,5 \$/kgU	83	32	0,05
Wiederaufarbeitung	-37 \$/kgU	-37	-14	-0,021
Indirektes	0 %	-	-	-
Summe		237	100	0,158

Tabelle 9: Struktur der Kernbrennstoffkostenkomponente um 1970

	spezifische Basiswerte	Kosten je kg U (3,2%) /\$/	% der Brennstoffkosten	spez. Kostenkomponente /c/kWh/
Uran	13 \$/lb U ₃ O ₈	160	24	0,074
Konversion	1,5 \$/kgU	1,5	2	0,005
Anreicherung	75 \$/kg TAE	320	48	0,151
Fertigung	70 \$/kgU	70	11	0,033
Wiederaufarbeitung	0 \$/kgU	0	0	0
Indirektes	15 %	100	15	0,14*
Summe		667	100	0,302

Tabelle 10: Struktur der Kernbrennstoffkostenkomponente 1974

	spezifische Basiswerte	Kosten je kg U (3,2%) /\$/	% der Brennstoffkosten	spez. Kostenkomponente /c/kWh/
Uran	42 \$/lb U ₃ O ₈	512	36	0,25
Konversion	4,5 \$/kg U	29	1,5	0,01
Anreicherung	80 \$/kg TAE	342	21	0,14
Fertigung	130 \$/kg U	130	7,5	0,05
Wiederaufarbeitung	140 \$/kg U	140	8	0,06
Indirektes	18 %	207	26	0,18
Summe		1360	100	0,69

Tabelle 11: Struktur der Kernbrennstoffkostenkomponente 1978

	spezifische Basiswerte	Kosten je kg U (3,2%) /\$/	% der Brennstoffkosten	spez. Kostenkomponente /c/kWh/
Uran	31,25 \$/lb U ₃ O ₈	381	24	0,18
Konversion	2,85 \$/kg U	41	3	0,02
Anreicherung	101,6 \$/kg TAE	434	29	0,21
Fertigung	185 \$/ kg U	185	11	0,08
Wiederaufarbeitung	260 \$/kg U	260	17	0,14
Indirektes	20 \$	260	17	0,14
Summe		1561	100	0,77

Tabelle 12: Struktur der Kernbrennstoffkostenkomponente - Mai 1980

4. Zusammenfassung und Schlußfolgerungen

1. Trotz aller Probleme bei der Einschätzung der Wirtschaftlichkeit kann festgestellt werden, die Kernkraftwerke haben in den 70er Jahren ihren großen wirtschaftlichen Durchbruch erzielt. Die Kostenvorteile gegenüber konventionellen Kraftwerken betragen gegenwärtig zumindestens in den hochindustrialisierten Ländern mit durchschnittlichen Rohenergieträgereigenaufkommen 20 ... 40 %.
2. Die weitere Entwicklung der Ökonomie der Kernkraftwerke wird v. a. von folgenden Faktoren beeinflußt:
 - Die Preisentwicklung auf den imperialistischen Märkten läßt ein weiteres Ansteigen der Investitionskosten erwarten. Infolge eines entstandenen Defizits von Umweltschutzmaßnahmen in konventionellen Kraftwerken dürften jedoch deren Investitionskosten stärker betroffen werden.
 - Die Verknappung der billigen Uranvorräte und die Kommerzialisierung des Kernbrennstoffversorgungsprozesses läßt ein weiteres Ansteigen der Brennstoffpreise erwarten. Eine objektive Bremse hierfür stellt nur der geschlossene Kernbrennstoffzyklus dar.
 - Die Energiekrise der kapitalistischen Welt mit ihrer Preisentwicklung bei konventionellen Rohenergieträgern läßt erwarten, daß in stärkerem Maße die Preise im Kernbrennstoffzyklus sich an den hohen Preisen konventioneller Rohenergieträger orientieren, d. h., daß sich Äquivalenzpreise verstärkt herausbilden.
 - Die langfristigen Einschätzungen zur Wirtschaftlichkeit der Kernenergetik besagen, daß selbst bei ungünstigen Ausgangsbedingungen Kostenvorteile für die Kernkraftwerke auch in den 80er Jahren erhalten bleiben.
3. Bei allem Optimismus für die Kernenergie muß ich am Schluß noch auf folgendes aufmerksam machen:
Zur Entscheidung über den Bau zukünftiger Kernkraftwerke werden in zunehmendem Maße, neben denen in Zahlen ausdrückbaren wirtschaftlichen Faktoren, Einschätzungen zu

- langfristigen politischen Entwicklungstendenzen
- längerfristig zugänglichen Ressourcen und
- Industrie- und Baukapazitäten
herangezogen.

Das sind letztendlich auch die Gründe, daß die Bestellungen neuer Kernkraftwerke zwar optimistisch einzuschätzen sind, aber nicht unbedingt rasant vorwärtschreiten müssen.

Literatur:

- /1/ Jahrbuch der Atomwirtschaft 1980
- /2/ Atom 266 (1978) 12
- /3/ Atomtechnik im Ausland (1979) 3
- /4/ Kerntechnik 20 (1978) 11
- /5/ Michaelis, H.
Ist Kernenergie wirtschaftlich?
KAT-3-77
- /6/ Schmitt, D. u. a.
Parameterstudie zur Ermittlung der Kosten der Stromerzeugung
aus Steinkohle und Kernenergie
R. Oldenbourg Verlag München 1979
- /7/ Atom (1980)(2)
- /8/ Wirtschaftswissenschaft (1980) 6
- /9/ M. Peltzer
Wirtschaftlichkeitsvergleich von Stromerzeugungskosten
von EKW und Steinkohlenkraftwerken
GKSS 80/E/9
- /10/ Kernenergie 23 (1980) 2

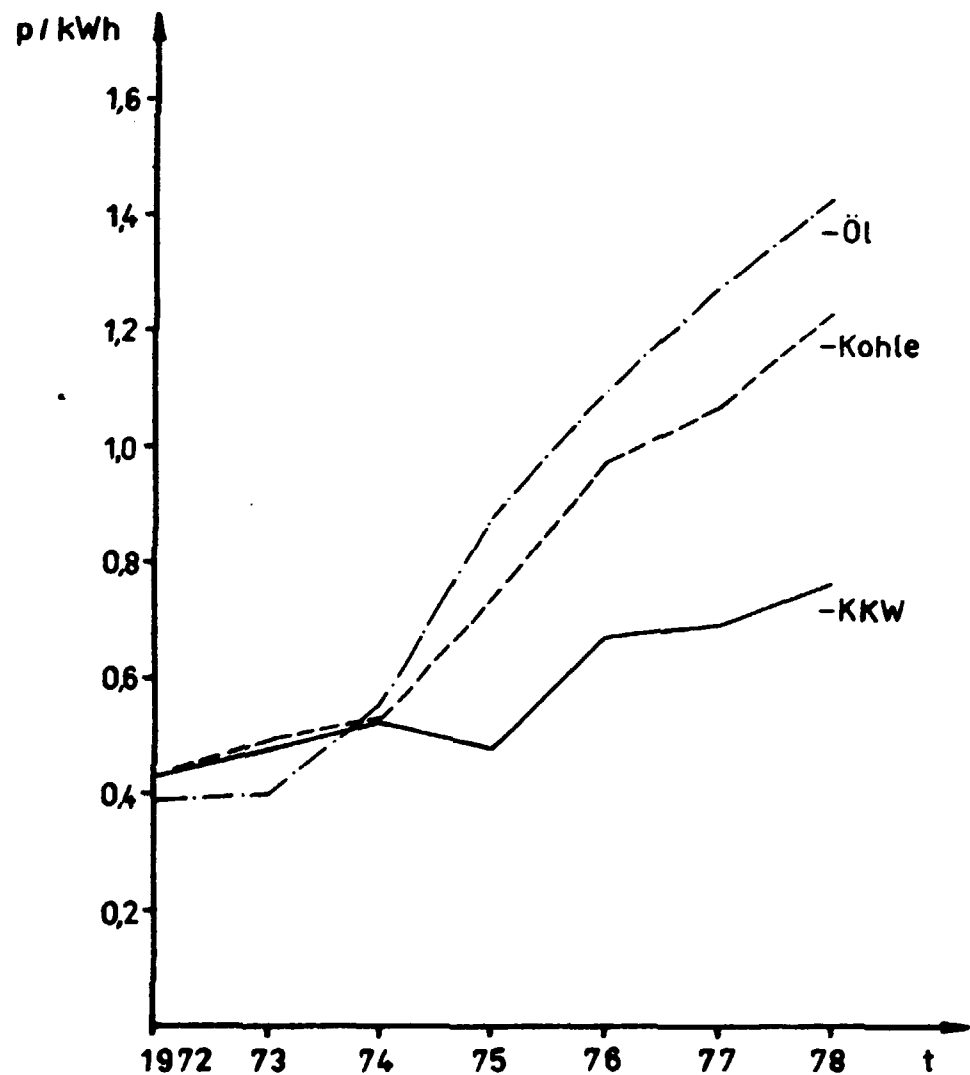
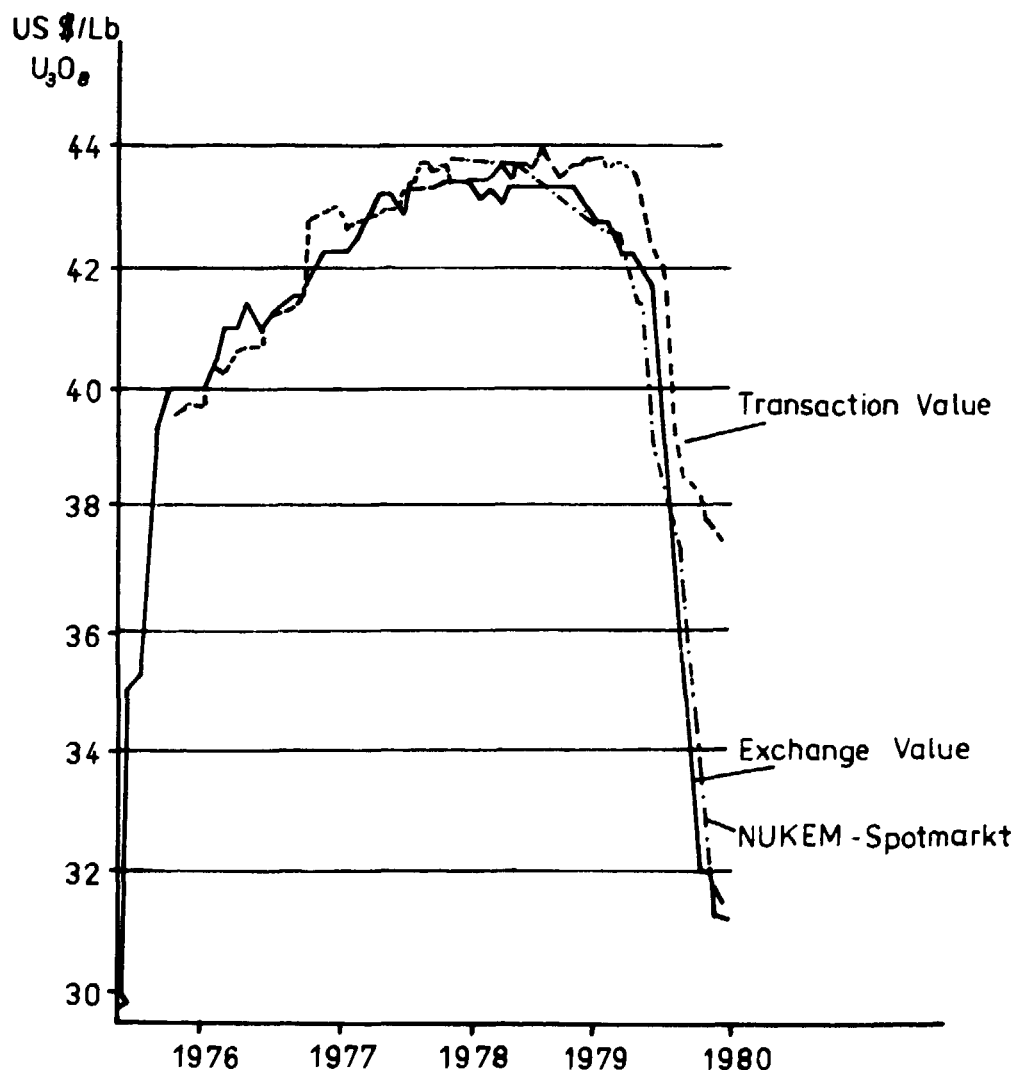


Bild 1: Selbstkostenentwicklung englischer Kraftwerke [2]

Bild 2: Entwicklung des Uranpreises

Transaction Value
Exchange Value } nach NUEXCO
Spotmarkt-NUKEM



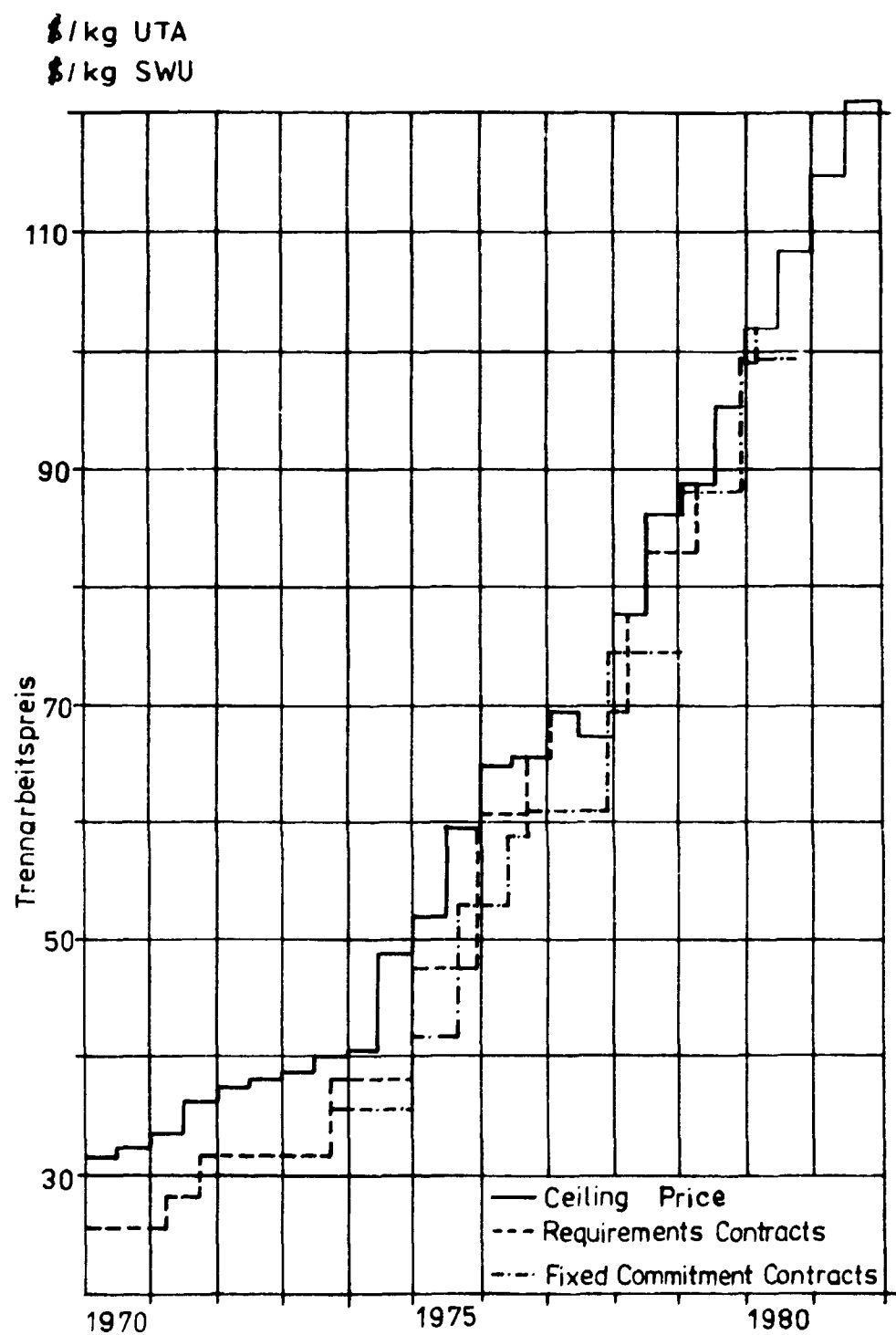


Bild 3 : Entwicklung des US-DOE - Anreicherungspreises

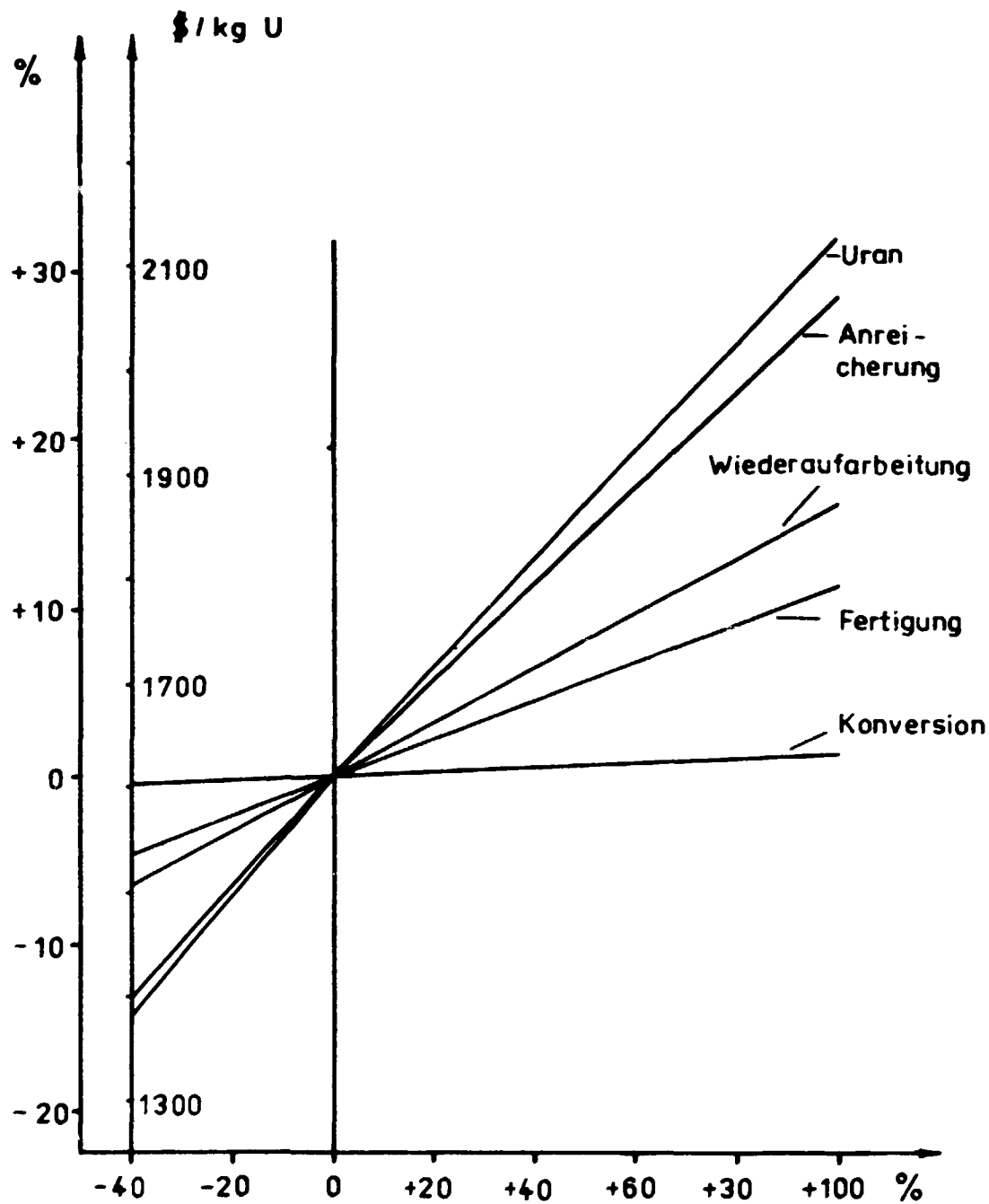


Bild 4: Entwicklung des Kilopreises bei Veränderung einzelner Komponenten
(Basis 1980, Mai)

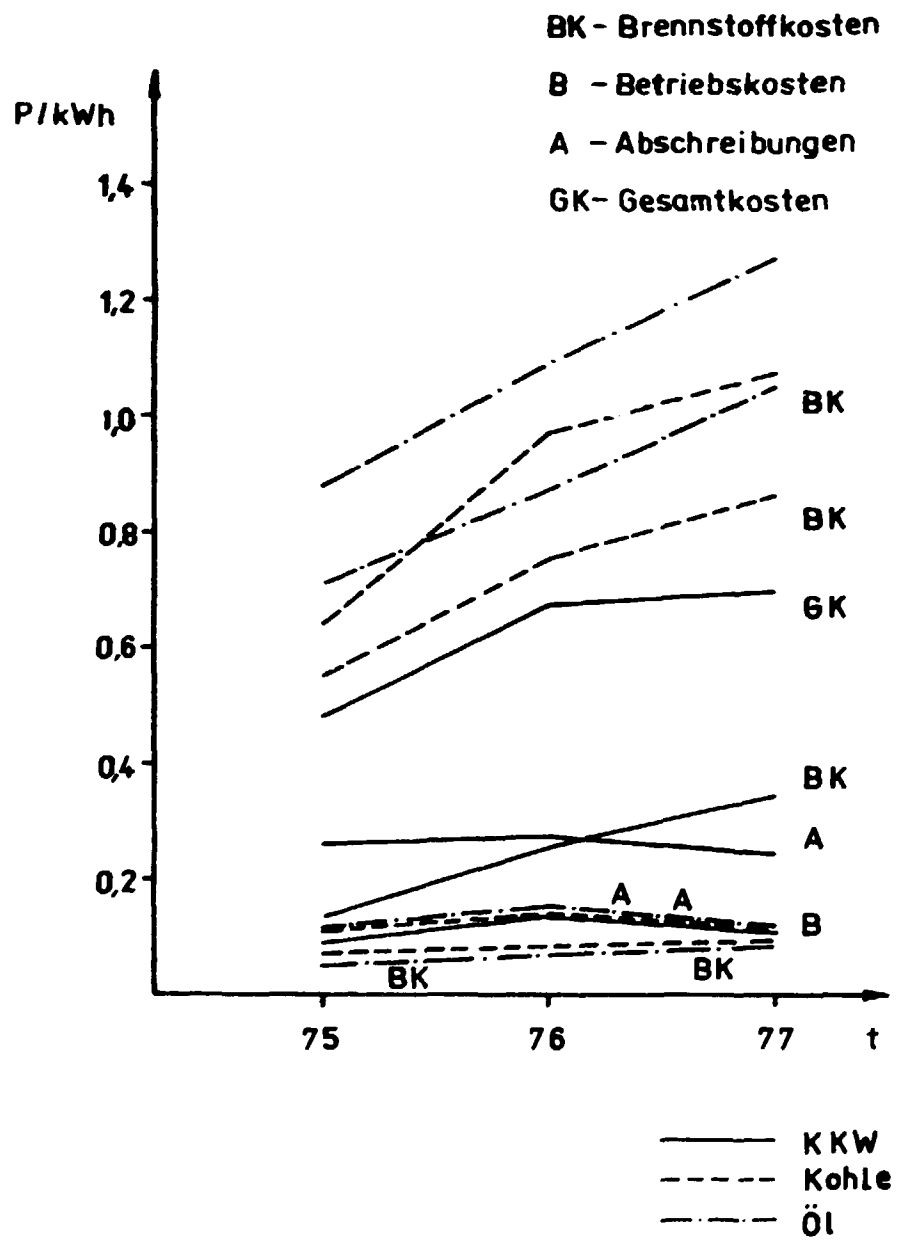


Abb: Entwicklung der Kostenkomponenten
in Großbritannien

HIGH-ENERGETIC NEUTRON EMISSION IN FISSION

H. Marten and D. Seeliger
Technical University Dresden, GDR

First experimental results of our investigations of the high-energetic part of fission neutron spectra indicate the existence of a spectrum component with an average energy of about 4 MeV (14.6 MeV neutron induced fission of ^{238}U analysed in the spectrum energy range 20 - 30 MeV). Some possible sources of high-energetic fission neutrons are discussed.

Introduction

Investigations of the high-energetic part of fission neutron spectra are important for two main reasons:

- i) Fission neutron spectra have been measured for many fissioning systems in the spontaneous as well as in the induced fission. Because of the very low neutron emission cross-sections at high energies the measured spectra extend to about (10 - 15) MeV usually. The experimental errors are relatively high in this energy range. Results of different authors are contradictory (for instance /1/).
- ii) The main physical reasons of high-energetic neutron emission in fission are investigated insufficiently. Many groups showed the existence of the central component of fission neutrons /2/. In spite of many further investigations our knowledge about the mechanism of their emission is slight. Different theoretical works were published /3/. Comparing measured spectra at relatively high emission energies (above 10 MeV) with calculated spectra of "normal" fission neutrons (evaporated neutrons from the fully accelerated fragments) we try to get informations about the spectrum of "abnormally" emitted neutrons and consequently about some questions of fission dynamics. Moreover, we consider the results of other groups (for instance /4/).

To expand the measurable energy range of fission neutron spectra we developed a high-sensitive spectrometer using the method of the two-dimensional measurement of neutron time-of-flight and the corresponding scintillator proton recoil energy /5/. FORTRAN programs for the calculation of "normal" neutron spectra up to high emission energies have been elaborated /6/.

Theoretical approximations

Firstly we make use of the relatively simple model of Madland and Nix /7/, which describes measured fission neutron spectra at high energies (up to 15 MeV) rather good (code BSSN).

Secondly the code NCMA was developed to calculate energy spectra of evaporated fission neutrons for eligible fragment masses. Assuming the Weißkopf formulae /8/ we consider the following aspects:

- initial distribution of excitation energy and nuclear spin of the fragments /9,10/;
- description of the nuclear level density by the semiempirical formalism of Ignatjuk et al. /11/, which takes into account the shell effects depending on excitation energy (shell correction from /12/),
- cascade character of neutron emission,
- determination of neutron binding energies from /13/>,
- transformation into the laboratory system using the average kinetic energy of the fragment.

Using the code NCMA we can calculate the c.m.s. and l.s. fission neutron spectra and their average energies, the multiplicity distribution and the average number of emitted neutrons.

First results showed a rather good correspondence with experimental data. The Weißkopf concept holds true only for emission energies which are not too high. However, the calculated spectrum is influenced by the Weißkopf formulae as well as by the special conditions like excitation energy distribution and emission from fragments of a relatively high velocity.

First experimental results

Fig. 1 represents the results of the measurement of the high-energetic neutron spectrum part from the 14.6 MeV neutron induced fission of ^{238}U . The experiment has been carried out at a 150 kV deuteron accelerator /14/ (pulsed ion beam of 5MHz repetition rate, 1 ns pulse width and 35 μA current). Locating the uranium sample of 2173 g weight straight besides the neutron-producing tritium target an average fission event rate of $5 \cdot 10^7$ per second was realized. Because of the relatively high path of flight (5 m) the energy resolution was sufficiently good up to 30 MeV neutron energy. The experimental method (two-dimensional measurement of neutron time-of-flight and scintillator proton recoil energy, background suppression - especially n/μ -discrimination -, on-line coupling of the spectrometer to a minicomputer) is described in /5/. For high neutron energies one has to consider the folding of the neutron spectrum by the time resolution function of the spectrometer. Fig. 1 illustrates this effect (measured spectrum - dotted line, unfolded spectrum - dashed-dotted line). Obviously the measured neutron yield in the energy range 20 - 30 MeV is higher than the expected one. We compared the measured spectrum with the Watt and Maxwellian spectrum, which describe the fission neutron spectrum in the energy region up to 10 MeV, and with the result of our calculation using the code BSSN. Fitting the experimental data to a Maxwellian distribution we obtained a "temperature" parameter of (2.5 ± 0.6) MeV, i.e. the average energy of this high-energetic spectrum component amounts to (3.7 ± 0.9) MeV.

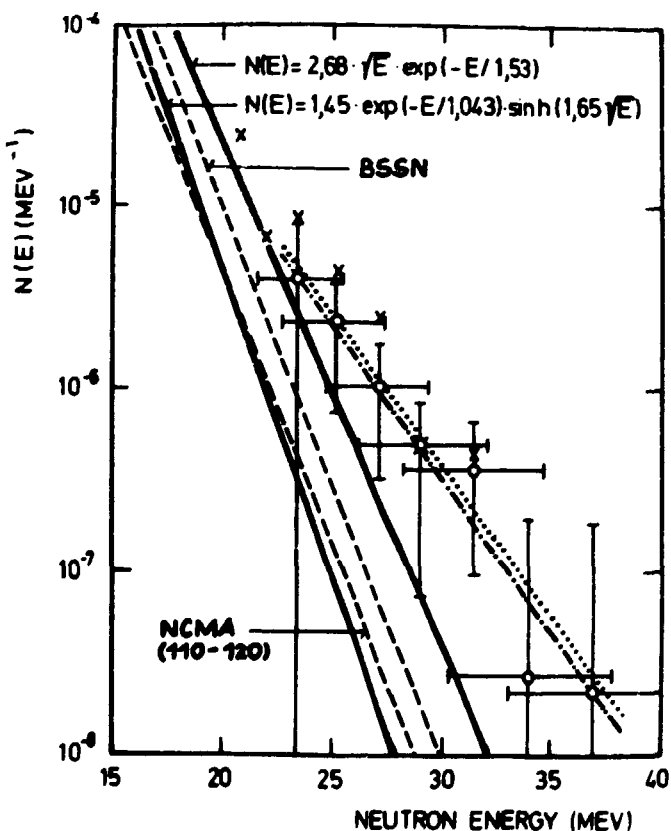


Fig. 1
Neutron emission spectrum in the 14.6 MeV neutron induced fission of ^{238}U .
x - 1st run (meas. time 73 h)
o - 2nd run (meas. time 10 h).
The scintillator proton recoil energy bias was (19.5 ± 1.0) MeV for the first spectrum (x) and (22.2 ± 1.0) MeV for the second one (o).
Further remarks in the text.

Discussion

The following sources of high-energetic neutron emission in fission are conceivable:

- i) Statistical equilibrium neutron emission by highly excited fragments (fragment mass 110 - 120, greater than 155);
- ii) Neutron emission caused by the change of strong fragment deformation (local heating in the former tail region) /3, Rubtchenja/;
- iii) Fast neutron emission due to the rapid change of the nuclear potential during scission /3, Fuller, Boneh/;
- iv) About 10 % of the fission alpha-particles are emitted as ${}^5\text{He}$ originally, which decay in a very short time ($T_{1/2} = 8 \cdot 10^{-22}$ s). The average energy of the neutrons from ${}^5\text{He}$ decay amounts to (4.0 ± 0.3) MeV /15/;
- v) Hypothetic neutron emission due to an extremely high energy release in an abnormal fission process which is characterized by the simultaneous formation of superdense fragments with a higher binding energy compared with normal nuclei /16/.

To calculate the spectrum of evaporated neutrons from highly excited fragments in the fragment mass number range 110 - 120 we made use of the program NCMA (average excitation energy 35 MeV, variance 64 MeV²). The calculated spectrum, which was weighted by the corresponding mass yield, does not explain the measured one (fig. 1).

The spectrum of the neutrons from ${}^5\text{He}$ decay was measured by Cheifetz et al. up to 10 MeV. Considering the spectrum of alpha-particles from ${}^5\text{He}$ decay and the relatively low yield of such events one has to exclude these neutrons as the reason of the measured high-energetic component.

It should be of interest to calculate the spectrum of "abnormally" emitted neutrons in the framework of the different emission models using a realistic potential. On the other hand, one can investigate the statistical equilibrium neutron emission in the fission by variation of the incident energy more exactly.

Up to now the theoretical as well as the experimental investigations are insufficient to characterize the full picture of neutron emission in fission.

Reference

- / 1/ Старостов, Б.И. и.гр., Ядерные Константы 2 (1980) 3
- / 2/ Bowman, H.R. et al., Phys. Rev. 126(1962)2120,
Kapoor, S.S. et al., Phys. Rev. 131(1963)283,
Skarsvag, K. et al., Nucl. Phys. 45(1963)92,
...
- / 3/ Fuller, R.W., Phys. Rev. 126(1962)684,
Pik-Pitchak, G.A., Jad. Fiz. 10(1969)321,
Boneh, Y. et al., Phys. Rev. C 10(1974)893,
Rubtchenja, V.A., RI-28 (Leningrad 1974)
- / 4/ Samjatnin, J.S. et al., Jad. Fiz. 29(1979)595
- / 5/ Grimm, W. et al., Conf. on Neutron Physics, Kiev 1980,
Symp. on Selected Topics of the Interaction of Fast Neutrons and
Heavy Ions with Atomic Nuclei, Gaußig (GDR) 1980
- / 6/ Märtens, H. et al., Gemeinsamer Jahresbericht 1980, ZfK(1981)
- / 7/ Madland, D.G. and J.R. Nix, LA-UR-79-147, 1979 Annual Meeting
of the American Nuclear Society, Atlanta, Georgia
- / 8/ Blatt, J.M. and V.F. Weißkopf, Theoretische Kernphysik, Leipzig 1959
- / 9/ Browne, J.C. et al., Phys. Rev. C 10(1974)2545
- /10/ Wilhelmy, J.B. et al., Phys. Rev. C 5(1972)2041

- /11/ Ignatjuk, A.B. et al., Conf. on Neutron Physics, Kiew 1977,
part I, 60
- /12/ Seeger, P.A. et al., Nucl. Phys. A 238(1975)411
- /13/ Garvey, G.T. et al., Rev. Mod. Phys. 41(1969)S1
- /14/ Seeliger, D. et al., Nucl. Instr. Meth. 66(1968)157
- /15/ Cheifetz, E. et al., Phys. Rev. Lett. 29(1972)305
- /16/ Märtens, H. et al., Proc. Int. Symp. on the Interaction of Fast
Neutrons with Nuclei, Gaußig (GDR) 1979, ZfK-410(1980)116

ON-LINE EXPERIMENT FOR THE DETERMINATION OF NEUTRON EMISSION SPECTRA BY
THE TWO-DIMENSIONAL MEASUREMENT OF THE NEUTRON TIME-OF-FLIGHT AND THE
SCINTILLATOR PROTON RECOIL ENERGY

W. Grimm, H. Märtens and D. Seeliger
Technical University Dresden, GDR

Abstract

Coupling a 4096 channel analyser to the minicomputer KRS 4200 via SI 1.2 and CAMAC an on-line experiment with open loop was developed to determine neutron emission cross-sections in a wide energy range (1-40 MeV) by the two-dimensional measurement of the neutron time-of-flight (TOF) and the corresponding proton recoil energy (PRE).

The suppression of the experiment-specific and the cosmic background is realized by the use of a heavy shielding and the n/ γ - resp. the n/u-discrimination method.

A FORTRAN 4000/4200 program system including CAMAC application (control and data processing) arranges the data transfer as well as the check, correction, concentration and analysis of the measured spectra.

1. Introduction

Neutron emission spectra from high-energetic nuclear reactions and nuclear fission extend for a wide energy range. The emission cross-section varies over many orders of magnitude. In particular, it reaches very small values at high emission energies.

The measurability of the high-energetic parts of such neutron emission spectra requires the application of a spectrometer with a sufficient high sensitivity. Therefore, it is necessary to suppress the background of all kinds intensively. The two-dimensional measurement of the neutron TOF and the PRE makes it possible to select the optimum PRE threshold for a given neutron TOP channel resp. channel range in the analysis process, i.e. to determine neutron emission cross-sections with a minimum-possible error for each neutron energy from one experiment.

The first time we used the described measuring arrangement in an experiment which was aimed at the search for high-energetic neutrons in the 14.6 MeV neutron induced fission of ^{238}U /1/.

2. The spectrometer. Background suppression

A schematic representation of the spectrometer and the on-line coupling to the minicomputer is given in fig. 1.

The high-efficient neutron detector (see fig. 1) is located in a heavy

collimating shielding to suppress the experiment-specific background.

The luminescence diode in front of the scintillator enables the continuous stability check of the time resolution of the neutron TOF spectrometer /2/.

An electronic system for particle discrimination by the charge comparison method /3/ is used to suppress the background counts of the detector caused by γ -rays and penetrating components of the cosmic rays.

Especially cosmic muons with energies around 1 GeV give rise to a background part with about 3.5 s^{-1} event rate and an average pulse height of about 20 MeV with reference to the PRE for the used detector.

The n/u-discrimination method makes it possible to suppress the background to less than 0.5 % in the region of the muon hump (fig. 2).

The separability of the particle discrimination unit is restricted to an adjustable dynamic range. One is able to expand it by the use of two (or more) of such devices. We present the following example:

1st unit: dynamic range from 1 to 15 MeV (mainly n/ γ -discrimination),
2nd unit: dynamic range from 10 to 45 MeV (mainly n/u-discrimination)

(data with reference to the PRE).

The both analogous-to-digital converter (ADC), which receive the time-to-analogous converter (TAC) output resp. the PRE spectroscopic pulse, work in coincidence with the neutron identifying output signal of the electronic particle discrimination system (fig. 1). Finally the obtained sum words are stored in the intermediate memory of 4 K capacity.

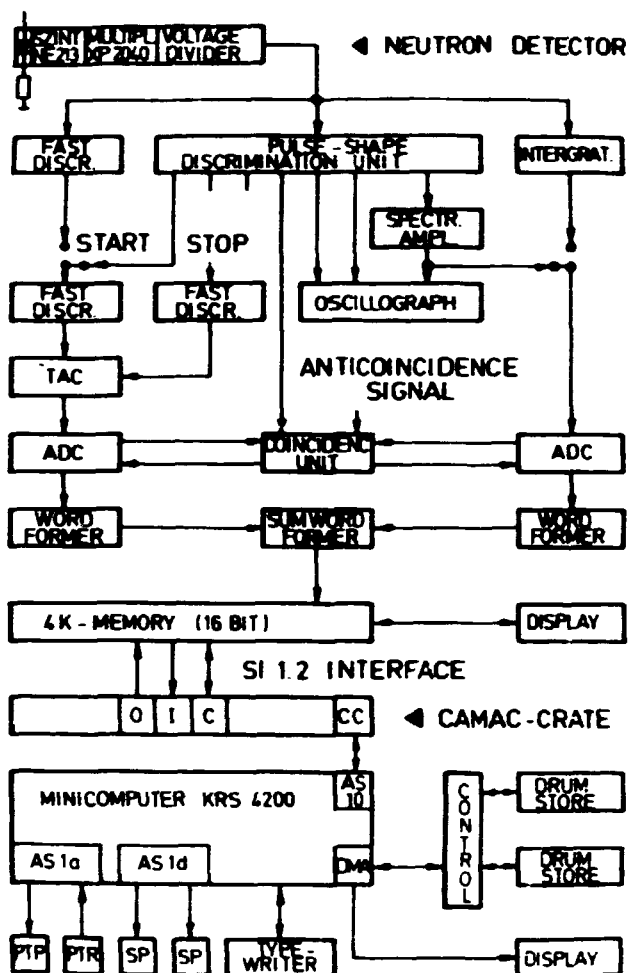


Fig. 1
Schematic representation of the spectrometer and the coupling to the mini-computer (see text).

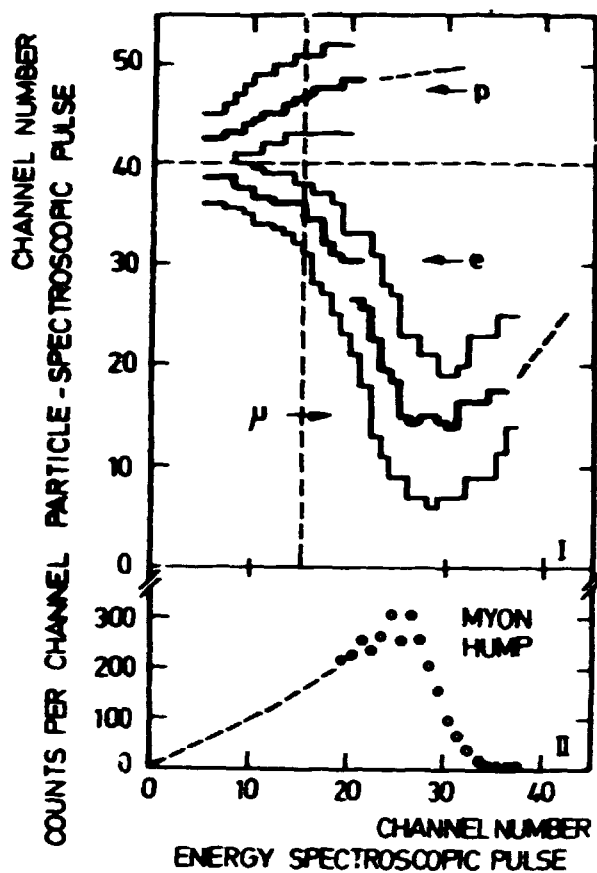
3. On-line coupling. Program system

The coupling of the 4096 channel analyser working two-dimensionally to the minicomputer is realized via the standard interface SI 1.2 and CAMAC. We apply a 24 bit data input device with a SI 1.2 input unit /4/ and a control module /5/ (fig. 1). In this way, we can carry out the data transfer and the control of the analyser.

The FORTRAN 4000/4200 programming language /6/ including CAMAC utilization enables a comfortable working out and modification of the computer programs. To realize an extensive flexibility of the program system application a complex was developed, whose parts may be connected according to the specific aim of the experiment (for instance calibration measurements, measurements with samples).

We worked out computer programs for

- control,
- input/output operations,
- data check and correction,
- addition and subtraction operations,
- calculation of one-dimensional spectra for adjustable channel ranges (for calibration, see fig. 3),
- display representation,
- analysis of the summarized two-dimensional spectra from measurements with resp. without sample (i.e. calculation of the neutron emission spectra).



Pig. 2/I

Particle branches in a two-dimensional representation illustrate the performance of the μ/π -discrimination. The radiation is from a Po-Be-neutron-source.

p - branch of neutron events,
e - branch of γ -events,
 μ - branch of cosmic muon events.

External limits of the branches (weak lines) indicate the 5 % level of the peak height for a given PRE spectroscopic pulse channel number.

Pig. 2/II

Background pulse height spectrum caused by muons (calculated from the results of the two-dimensional measurement represented in fig. 2/I).

4. Analysis of experimental data

To calibrate the TOP and the PRE coordinate of the two-dimensional spectrum we measure the scattered spectrum of 14 KeV neutrons on carbon and a 3 MeV neutron peak.

We make use of the relativistic dependence of the neutron energy E_n on the TOP t :

$$E_n = E_0 \left(\left(1 - \left(\frac{L}{t} \right)^2 \right)^{-1/2} - 1 \right)$$

(E_0 - rest energy of the neutron, L - flight path, c - velocity of light).

We assume a linear approximation of the dependence of the pulse height on the proton energy for PRE above (6-8) KeV. This is sufficiently accurate with reference to the error of calibration in this energy range.

The detector efficiency was calculated by the use of the Monte-Carlo-code NEUCEP /7/ accepting the light output data of Verbinski et al. /8/. We made up a (40,40) efficiency matrix as a function of neutron energy and PRE bias. In the analysis the topical detector efficiency for a given TOP channel and the selected PRE threshold is determined by double-linear interpolation.

The user has to put in the desired PRE range in the beginning of each analysis cycle. Obviously the resulting neutron energy spectrum for a given PRE threshold is characterized by two ranges with relatively high errors (in the near of the threshold energy because of the uncertainties of efficiency determination and at relatively high neutron energies for statistical reasons) and by a well determined intermediate region. Therefore, the user can get a neutron energy spectrum in a wide energy range with a minimum of uncertainty by variation of the PRE bias and the following concentration of the results of the analysis cycles.

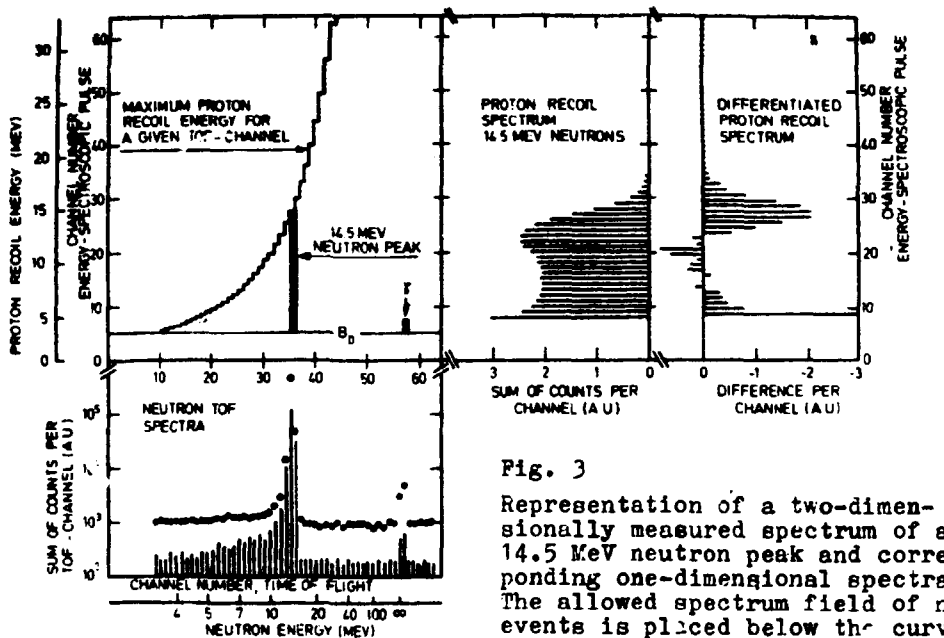


Fig. 3

Representation of a two-dimensionally measured spectrum of a 14.5 MeV neutron peak and corresponding one-dimensional spectra. The allowed spectrum field of neutron events is placed below the curve which represents the maximum proton recoil energy for a given TOF channel.

5. Conclusions

The described on-line experiment aimed at the determination of neutron emission spectra in a wide energy range - especially in the high-energetic part - represents a versatile-applicable system. It is easily enlargable with regard to storage dividing, storage capacity and CAMAC utilization.

The energy resolution is rather good for relatively high neutron energies, since we chose a large path of flight ($L = 5 \text{ m}$, (2-3) ns time resolution). The sensitivity of the experiment as a function of neutron energy depends on the reaction rate in the sample and the specific background conditions mainly.

Reference

- /1/ Märten, H. and D. Seeliger, Proc. Int. Symp. on the Interaction of Fast Neutrons with Nuclei, Gaußig (GDR) 1979, ZfK-410(1980)116
- /2/ Sassonov, S. and W. Seifert, Gemeinsamer Jahresbericht 1977, ZfK-350(1978)213
- /3/ Ortlepp, H.-G., Proc. Int. Symp. on Nuclear Electronics, Dresden (GDR) 1980
- /4/ Rahn, W. et al., Preprint TU 05-20-74
- /5/ Krause, R., unpublished
- /6/ MOS Programmierhandbuch FORTRAN 4000/4200, Systemunterlagen-dokumentation (1975), VEB Robotron
- /7/ Hermsdorf, D., Gemeinsamer Jahresbericht 1976, ZfK-315(1977)192
- /8/ Verbinski, V.V. et al., Nucl. Instr. Meth. 65(1968)8

Application of Wigner-transformations in Heavy Ion Reactions

Henning Esbensen
NORDITA, 17 Blegdamsvej, DK-2100 Copenhagen Ø, Denmark

1. Introduction

One of the main features of inelastic heavy ion reactions is the excitation of collective surface vibrations. In the following we shall discuss a model, based on Wigner transformations and classical dynamics, that gives a semiclassical description of the excitation of surface vibrations due to the Coulomb and nuclear interaction in heavy ion collisions.

The treatment will consist of three stages, viz. the preparation of classical initial conditions compatible with the quantal ground state of surface vibrations, the dynamical evolution of the system governed by Liouville's equation (i.e. classical mechanics) and finally the interpretation of final results after the interaction in terms of excitation probabilities, elastic and inelastic cross sections, etc. The precise meaning of these three stages of the treatment will become clear in the subsequent section.

The first and the last stage are exact and based on the Wigner transformations while the time evolution described by classical mechanics is an approximation. We shall later return to the question of the applicability of this approximation and give some illustrative examples.

2. The Wigner transformation

In quantum theory one cannot ask for the simultaneous probability of coordinate and momentum since this would lead to violation of the uncertainty principle. However, one can formally define a distribution $a(p,q)$ that looks like a phase space distribution using the following transformation of the density matrix ρ :

$$a(p,q) = \int \frac{dq'}{2\pi\hbar} e^{-ipq'/\hbar} \rho(q + q'/2, q - q'/2) \quad (2.1)$$

If one integrates this expression over all momenta, one just obtains the quantal coordinate distribution, and similarly if one instead integrates over all coordinates, one would obtain the quantal momentum distribution. Thus using eq. (1) the average value of quantities that depend only on either the coordinate or the momentum will be in exact agreement with the quantal results, while the average of quantities that depend on products of coordinate and momentum will not in general be the same as in a quantal treatment.

One can invert this transformation and for a given classical phase space distribution define a density matrix as follows:

$$\rho(q, q') = \int dp e^{ip(q-q')/\hbar} a(p, \frac{q+q'}{2}) \quad (2.2)$$

The transformations in eqs. 1 and 2 are the so-called Wigner transformations, originally introduced by E. Wigner¹⁾, and they provide the connection between classical and quantum mechanics in the semiclassical model described in the introduction.

In order to illustrate the application of this transformation, let us consider a one dimensional system characterized by a Hamiltonian that has a complete set of eigenfunctions $\psi_n(q) = \langle q | n \rangle$. From these eigenfunctions and eq. (1) we can construct a set of generalized "phase space" distributions

$$a_{nm}(p, q) = \int \frac{d\xi}{2\pi\hbar} e^{-i\xi p/\hbar} \psi_m(q + \xi/2) \psi_m^*(q - \xi/2) \quad (2.3)$$

They fulfil the relations:

$$\int dp dq a_{mm}(p, q) = \delta_{m,m} \quad (2.4)$$

$$\int dp dq a_{mm}(p, q) a_{m'm'}^*(p, q) = (2\pi\hbar)^{-1} \delta_{m'm'} \delta_{m'm'} \quad (2.5)$$

Since we assume that the eigenfunctions ψ_n constitute a complete set of wave functions, the Wigner transformation provides a complete set $a_{nm}(p, q)$ of functions in the space of phase space distributions. The diagonal distributions $a_{nn}(p, q)$ are normalized (cf. eq. (4)), but they do not in general have one of the basic properties of phase space distributions of being non-negative.

Let us now investigate the quantal probabilities that one can ascribe to a given phase space distribution $a(p, q)$. From eq. (2) we can determine a density matrix ρ and consequently, we can calculate the probability P_n that the system is in the state $|n\rangle$

$$P_n = \langle m | q | n \rangle = \int dp dq dq' \psi_m^*(q) e^{ip(q-q')/\hbar} a(p, \frac{q+q'}{2}) \psi_m(q') \quad (2.6)$$

Changing variables: $q = Q - \xi/2$ and $q' = Q + \xi/2$ we obtain using the definition in eq. (3)

$$P_n = 2\pi\hbar \int dp dQ a(p, Q) a_{nn}(p, Q) \quad (2.6)$$

Taking off-diagonal matrix elements of ρ one can of course get information about the quantal phases.

For a harmonic oscillator the distributions $a_n = a_{nn}(p, q)$ depend on p and q only through the oscillator energy $E = p^2/(2m) + 1/2 m\omega^2 q^2$ and are given by

$$a_n(p, q) = \frac{(-1)^n}{\pi\hbar} \exp\left(-\frac{2E}{\hbar\omega}\right) L_n\left(\frac{4E}{\hbar\omega}\right) \quad (2.7)$$

where $L_n(x)$ are the Laguerre polynomials. In particular, the distribution corresponding to the ground state is a Gaussian

$$a_0(p, q) = (\pi\hbar)^{-1} \exp\left(-\frac{p^2}{m\hbar\omega} - \frac{m\omega q^2}{\hbar}\right) \quad (2.8)$$

We can now give a more precise definition of the semiclassical model briefly described in the introduction. Thus consider a one dimensional harmonic oscillator initially in the ground state and perturbed by a time-dependent external potential $V(q, t)$, i.e. we have the Hamiltonian

$$H = \frac{p^2}{2m} + \frac{1}{2} m\omega^2 q^2 + V(q,t) \quad (2.9)$$

where we assume that the perturbation is constant in space and time for very early and very late times, say for $|t| > T$. From the Wigner transformed quantal ground state density one obtains the distribution given in eq. (8), which is used as initial condition for the classical phase space distribution: $a(p,q, -T) = a_0(p,q)$. In the second stage one calculates the time evolution of $a(p,q,t)$ using classical mechanics, i.e. one solves Liouville's equation:

$$\frac{\partial a}{\partial t} = -\frac{p}{m} \frac{\partial a}{\partial q} + m\omega^2 q \frac{\partial a}{\partial p} + \frac{\partial V}{\partial q} \frac{\partial a}{\partial p} \quad (2.10)$$

and end up with the final distribution $a(p,q,T)$. From this distribution one can then calculate the excitation probabilities using eq. (6).

It seems natural in our model, which is based on classical dynamics, to distinguish between a semiclassical and a semiquantal approximation, where semiclassical refers to results obtained directly from the final phase distribution, while semiquantal refers to results obtained after the quantization of the final phase space distribution has been performed by means of the inverse Wigner transformation.

3. Dynamical approximation

Again we shall illustrate the procedure by considering a harmonic oscillator perturbed by an external time-dependent potential. The time evolution of the wave function is determined by the Schrödinger equation

$$i\hbar \frac{\partial \psi}{\partial t} = H\psi \quad (3.1)$$

where H is given by eq. (2.9). From the density matrix $\rho = |\psi\rangle\langle\psi|$ and eq. (2.1) we get the generalized phase space distribution

$$a(p,q,t) = \int \frac{d\xi}{2\pi\hbar} \psi(q+\xi/2, t) \psi^*(q-\xi/2, t) e^{-i\xi p/\hbar} \quad (3.2)$$

The exact equation of motion for $a(p,q,t)$ can be obtained from the Schrödinger equation (1)

$$i\hbar \frac{\partial a}{\partial t} = \int \frac{d\xi}{2\pi\hbar} e^{-i\xi p/\hbar} \left\{ \psi^*(q-\xi/2) H \psi(q+\xi/2) - \psi(q+\xi/2) H \psi^*(q-\xi/2) \right\} \quad (3.3)$$

$$\begin{aligned} \text{Since } \psi^*(q-\xi/2) \frac{\partial^2 \psi(q+\xi/2)}{\partial q^2} - \psi(q+\xi/2) \frac{\partial^2 \psi^*(q-\xi/2)}{\partial q^2} \\ = 2 \frac{\partial^2}{\partial \xi^2} \left\{ \psi(q+\xi/2) \psi^*(q-\xi/2) \right\} \end{aligned}$$

we obtain from a partial integration in eq. (3) [i.e. we replace $\partial/\partial\xi$ by $i\hbar/\hbar$ and ξ by $i\hbar\partial/\partial p$], using the explicit form of H in eq. (2.9) and the

definition (2)

$$\frac{\partial \alpha}{\partial t} = - \frac{p}{m} \frac{\partial \alpha}{\partial q} + m\omega^2 q \frac{\partial \alpha}{\partial p} + \frac{i}{\hbar} \left\{ V(q + \frac{i\hbar}{2} \frac{\partial}{\partial p}) - V(q - \frac{i\hbar}{2} \frac{\partial}{\partial p}) \right\} \alpha. \quad (3.4)$$

In the classical limit, i.e. for $\hbar \rightarrow 0$, eq. (4) becomes identical to Liouville's equation (2.10). Moreover, eq. (4) is identical to Liouville's equation for all interactions of the form

$$V(q, t) = V_0(t) + q V_1(t) + \frac{1}{2} q^2 V_2(t), \quad (3.5)$$

so the semiclassical treatment depicted earlier will be in exact agreement with the quantal treatment for this type of interactions.

4. Forced linear harmonic oscillators

In order to illustrate some simple features of our model, let us consider the case of a forced linear harmonic oscillator, i.e. in section 2 and 3 we choose the interaction

$$V(q, t) = -q F(t) \quad (4.1)$$

Then the solution to Liouville's equation (2.10), with eq. (2.8) as initial condition, is

$$\alpha(p, q, t) = (\pi\hbar)^{-1} \exp \left(- \frac{(p - p_0(t))^2}{m\hbar\omega} - \frac{m\omega}{\hbar} (q - q_0(t))^2 \right) \quad (4.2)$$

where $(p_0(t), q_0(t))$ is the solution to the classical Hamiltonian equations of motion

$$\begin{aligned} \dot{q}_0(t) &= p_0(t)/m \\ \dot{p}_0(t) &= -m\omega^2 q + F(t) \end{aligned} \quad (4.3)$$

with initial condition $p_0(-\infty) = 0$ and $q_0(-\infty) = 0$. Eq. (2) follows simply from the fact that the general solution to the classical equations of motion is

$$\begin{aligned} p(t) &= p_0(t) + p_i(t) \\ q(t) &= q_0(t) + q_i(t) \end{aligned} \quad (4.4)$$

where (p_0, q_0) is the solution just mentioned, while (p_i, q_i) is the solution to the homogeneous equations $\dot{q}_i(t) = p_i(t)/m$ and $\dot{p}_i(t) = -m\omega^2 q_i(t)$ with initial condition $p(-\infty) = p_i(-\infty)$ and $q(-\infty) = q_i(-\infty)$.

From eqs. (2.6) and (2.7) we can now determine the excitation probabilities. However, since our model is in exact agreement with a quantal treatment in the example discussed here, cf. the previous section, we already know that the excitation probabilities are given by a Poisson distribution

$$P_n = \frac{x^n}{n!} \exp(-x), \quad x = E_0/\hbar\omega \quad (4.5)$$

where $E_0 = \frac{p_0^2}{2m} + \frac{1}{2} m\omega^2 a_0^2$. Instead of performing the quantization of the final energy distribution, one could also determine the classical distribution of energy transfers. One can show that this distribution is

$$g(\Delta E) = (2\pi\hbar\omega E_0)^{-1/2} \exp\left(-\frac{(\Delta E - E_0)^2}{2\hbar\omega E_0}\right) \quad (4.6)$$

The mean value and spread are given by

$$\langle \Delta E \rangle = E_0 \quad , \quad \sigma(\Delta E) = (\hbar\omega E_0)^{1/2} \quad (4.7)$$

which are identical to the quantal results obtained from the Poisson distribution eq. (5). Moreover, for $E_0 \gg \hbar\omega$ we have a correspondence between the semiclassical and the quantal distribution of energy transfer, since the Poisson distribution (5) tends towards the Gaussian (6) in this limit.

5. Applications in heavy ion reactions

In the coherent surface excitation model²⁾ the nuclear radius is parameterized in terms of the amplitudes $a_{n\lambda\mu}$ of collective surface vibrations

$$R(\theta, \varphi) = R_0 \left(1 + \sum_{n\lambda\mu} a_{n\lambda\mu} Y_{n\lambda\mu}^*(\theta, \varphi) \right) \quad (5.1)$$

The intrinsic Hamiltonian for these vibrations is assumed to be harmonic

$$H_{vib} = \sum_{n\lambda\mu} \left(\frac{1}{2} \frac{\pi_{n\lambda\mu}^2}{D_{n\lambda}} + \frac{1}{2} D_{n\lambda} \omega_{n\lambda}^2 / a_{n\lambda\mu}^2 \right) \quad (5.2)$$

where $\pi_{n\lambda\mu}$ are the momenta conjugate to the amplitudes $a_{n\lambda\mu}$. The mass parameters $D_{n\lambda}$ and the frequencies $\omega_{n\lambda}$ are extracted from experiments or from RPA calculations.²⁾

Let us shortly describe the application of the semiclassical model developed in the previous sections to heavy ion reactions. The time evolution of the relative motion of two nuclei as well as their surface vibrational degrees of freedom ($\pi_{n\lambda\mu}, a_{n\lambda\mu}$) is governed by classical dynamics, and all these degrees of freedom are coupled through the Coulomb and nuclear interaction. The initial conditions for the relative motion are purely classical, while the initial conditions for the vibrational degrees of freedom ($\pi_{n\lambda\mu}, a_{n\lambda\mu}$) are the gaussian phase space distributions obtained from a Wigner transformation of the ground state (cf. eq. (2.8)). In stead of solving Liouville's equation for the time evolution of these phase space distributions one can use the Monte Carlo method and repeatedly solve the classical Hamiltonian equations, choosing the initial conditions for ($\pi_{n\lambda\mu}, a_{n\lambda\mu}$) as random numbers distributed according to the initial gaussian phase space distributions³⁾.

The fluctuations in the shapes of two colliding nuclei due to the zero-point motion of surface vibrations (i.e. due to the fluctuations in the amplitudes $a_{n\lambda\mu}$ in the initial phase space distributions) will lead to substantial fluctuations in the scattering angle, the energy loss and angular momentum loss from the relative motion of the two nuclei (see refs. 2, 3 and 5).

One can also try to quantize the excitation of collective surface modes and determine inelastic cross sections $(d\sigma/d\Omega)_{n\lambda}$ for the excitation of a definite mode $(n\lambda)$. A direct application of the expression for inelastic cross sections obtained from the Wigner transformation formalism²⁾ is not feasible in practice, since a reasonable statistics demands a very expensive calculation. However, inelastic cross sections have been calculated⁴⁾ by assuming that the excitation of surface modes is governed by Poisson statistics. This assumption is probably quite reasonable, since the fluctuation in the nuclear radius due to zero-point motion of a definite mode is usually much smaller than the diffuseness of the nuclear interaction between heavy ions. For more details the reader should consult the references.

References

- 1) E. Wigner, Phys. Rev. 40 (1932) 749
- 2) Proceedings of the International School of Physics "Enrico Fermi", "Nuclear Structure and Heavy Ion Collisions" (LXXVII), Varenna 1979, see the articles by R. A. Broglia, C. H. Dasso and A. Winther, and by H. Esbensen
- 3) H. Esbensen et al., Phys. Rev. Lett. 41 (1978) 296
- 4) R. A. Broglia et al., Phys. Lett. 87B (1979) 15, 89B (1979) 22
Nucl. Phys. A345 (1980) 263
- 5) R. A. Broglia et al., Progress in Particle and Nuclear Physics, vol. 4
(1980) 345

MODELS AND THEORIES FOR HEAVY-ION COLLISIONS

Georg Wolschin
Institut für theoretische Physik der Universität Heidelberg

Abstract: Examples for the description of low-energy heavy-ion collisions in terms of phenomenological transport models are presented. The basis for a fully microscopic treatment of these reactions is provided by the time-dependent Hartree-Fock approximation (TDHF). A theory to extend TDHF in a random-matrix model for the residual force to account for nucleon-nucleon-collisions is given. The effect of the collision term is investigated numerically in a one-dimensional model.

1. Introduction: It appears that the most consistent description of the available experimental data on low-energy heavy-ion collisions can presently be achieved using phenomenological transport models. They are based on transport equations such as the master equation and the Fokker-Planck equation which are well-known from statistical mechanics. Several selected examples for such models are compared with the data in the next section. It is not intended to give a review of the available models and theories.

Microscopic theories for such reactions are transport theories, and the time-dependent Hartree-Fock treatment (TDHF). The former are based on the assumption that the collective variables governing the reaction are known. The coupling to the intrinsic degrees of freedoms is then treated as random. It causes the irreversible dissipation of collective energy. Within this approach transport equations can be derived (which may be compared to the ones used in the phenomenological models) and transport coefficients can be calculated. A review is available in ref. [1]. The time-dependent Hartree-Fock approximation [2] is a mean-field theory without stochastic features. Since the residual force is neglected in TDHF, two-body dissipation due to the nucleon-nucleon collisions can not be incorporated. As an example for a recent microscopic theory, section 4 of this talk contains a random-matrix model for the residual force in order to extend TDHF towards a more realistic yet fully microscopic description of heavy-ion collisions.

2. Phenomenological Transport Models Starting point for transport models in the choice of collective variables. The most prominent ones are the center-of-mass distance \vec{r} of the two fragments, mass (or charge) asymmetry A_1/A and deformation degrees of freedom ϵ_i . From the analysis of experimental data one can establish a hierarchy of relaxation times associated with these variables:

$$\begin{aligned} T_R &\approx 0.3 \cdot 10^{-21} \text{ s} & T_\epsilon &\approx 4 \cdot 10^{-21} \text{ s} \\ T_\epsilon &\approx 1.6 \cdot 10^{-21} \text{ s} & T_A &\approx 5 \dots 20 \cdot 10^{-21} \text{ s}. \end{aligned}$$

Typical interaction times are of the order of $1 \dots 5 \cdot 10^{-21}$ s. The radial kinetic energy is dissipated first, followed by the loss of relative angular momentum, the evolution of shape deformations, and the relaxation of the mass asymmetry. The equilibration of the N/Z ratio occurs very fast due to the strong driving force towards the potential valley in the N-Z plane. It may not be describable as a statistical relaxation process.

To treat energy and angular-momentum dissipation in a nonequilibrium-statistical model, the c.m. distance \vec{r} and its conjugate momentum \vec{p} are considered as classical collective variables. Their distribution function $f(\vec{r}, \vec{p}, t)$ obeys a Fokker-Planck equation

$$\frac{\partial f}{\partial t} + \frac{p}{\mu} \vec{\nabla}_r f - \vec{\nabla}_r U \vec{\nabla}_p f = - \sum_{i=1}^3 \frac{\partial}{\partial p_i} (v_i f) + \sum_{i,j=1}^3 \frac{\partial^2}{\partial p_i \partial p_j} (D_{ij} f). \quad (1)$$

The change of the probability distribution governed by the conservative force ($-\vec{\nabla}U$) and inertia is written on the left-hand side whereas the r.h.s. with drift coefficients and diffusion coefficients D_{ij} describe shift and spread of the probability distribution. They are connected via the Einstein relations. A solution of the equation requires specification of potential U , inertia parameter μ (mostly taken as the reduced mass), and the transport coefficients. In applications the distribution function is assumed to be Gaussian and the equations for the first and second moments of \vec{r} and \vec{p} are solved. The ones for the first moments correspond to the Newton equations which have been used in early analyses of heavy-ion collisions. Those for the second moments allow to account for the statistical fluctuations in the collective variables. An approximate analytical solution of the moment equations which is based on a parametrization of the deflection function rather than the potential results in the angular distributions of Fig. 1.

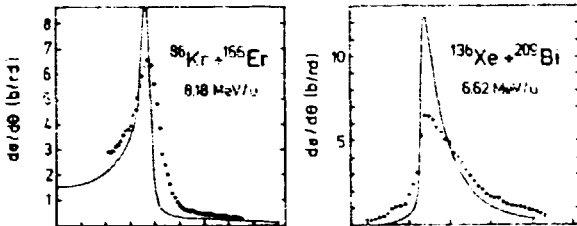


Fig. 1. Angular distributions for deeply inelastic reactions (ref. 5)

of freedom into the description. Treating a quadrupole deformation ϵ of both fragments on the basis of a transport equation^{3,7}, the results of Fig. 2 are obtained for the energy and angular-momentum distributions. The consideration of fragment deformations and statistical fluctuations in both energy and angular-momentum loss is essential to reproduce the data⁸.

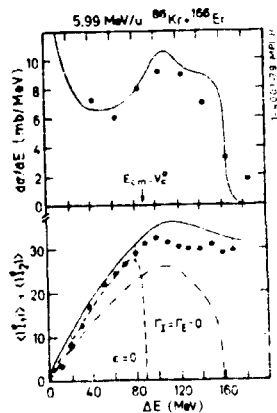


Fig. 2. Energy and angular momentum distribution (ref. 7)

They reproduce the anisotropic experimental results⁶, which are characteristic for deeply inelastic collisions quite well. Since quantal fluctuations are not included in a description based on equation (1) the calculated distributions are however, too narrow.

The most pronounced feature of DIC is the large energy loss. Fragment kinetic energies extend well below the Coulomb barrier for spheres and hence, indicate a large deformation of the composite system of scission. This can be accounted for by introducing deformation degrees

These results are obtained after integrating the solutions of the transport equation over impact parameter. The underlying impact-parameter dependence of the mean values and variances is shown in Fig. 3. The mean value for the dissipated angular momentum increases, and decreases as the sticking limit is reached, whereas the statistical fluctuations saturate at small impact parameters (large energy loss). This results in the rise and fall of the spin alignment P_{zz} as function of energy loss⁹, which has also been measured recently.

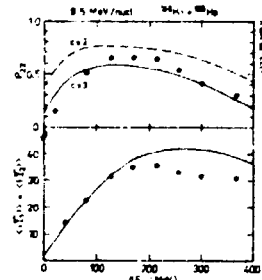


Fig. 4. Fragment spin alignment and transferred mean angular momentum

The mass or charge transfer occurring in DIC can be considered as a transport process^{11,3}. It has mostly been analysed on the basis of the equation

$$\frac{\partial P(A, t)}{\partial t} = - \frac{\partial}{\partial A} (v_A P) + \frac{\partial^2}{\partial A^2} (D_A P). \quad (2)$$

Its solutions are Gaussian for constant transport coefficients, or a linear dependence of v_A on A , as in case of a parabolic driving force. All other cases require numerical solutions or approximation schemes. A combination of eqs. (1) and (2) yields the results of Fig. 5 which show the broadening of the mass spread with increasing energy loss.

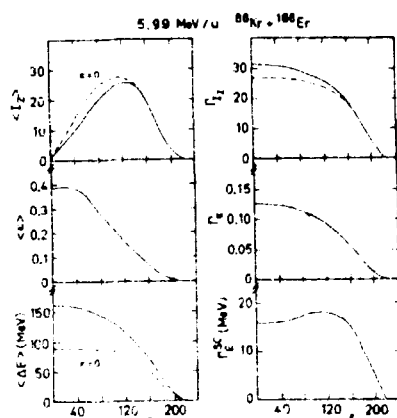


Fig. 3. Mean values and variances for dissipated angular momentum, deformation and energy loss (ref. 7)

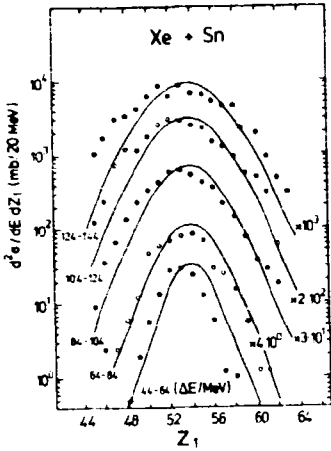


Fig. 5. Charge transport (ref. 12)

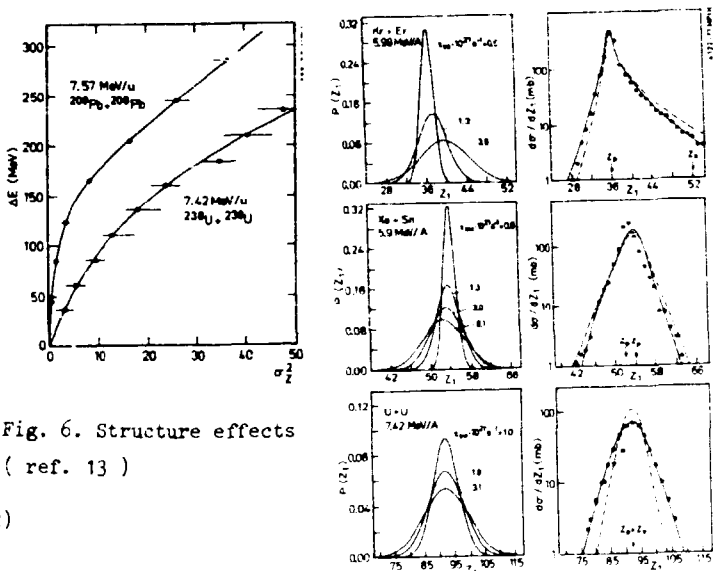


Fig. 6. Structure effects
(ref. 13)

Fig. 7. Element distributions

Of particular interest is the influence of nuclear shell structure on the mass diffusion process. It shows up clearly in the correlation between total kinetic energy loss and variance of the charge distribution for Pb+Pb and U+U, Fig. 6. It has been proposed to interpret the broad element distributions for U+U by means of the drift towards the closed Pt-shell.¹⁴⁾. Since the shell minima in the driving potential are washed out when the system is heated up they do not seem to give rise to a shoulder in the element distribution at the Pb-region, Fig. 7.

3. Microscopic Model: TDHF A fully microscopic model for heavy-ion collisions which differs drastically in its physical content from transport theories is provided by the time-dependent Hartree-Fock approximation.²⁾. It reduces the many-body problem to a set of A coupled nonlinear equations for the single-particle wavefunctions

$$i \dot{\Psi}_n = (T + U_{HF}) \Psi_n \equiv H_{HF} \Psi_n \quad (3).$$

The many-body wavefunction is at all times a single slater determinant of the Ψ_n . The mean single-particle potential U_{HF} is calculated selfconsistently from the nucleon-nucleon interaction and the one-body density

$$U_{HF} \Psi_n = \int d^3x' \psi(x-x') [g_1(x+t) \Psi_n(xt) - g_1(x-t) \Psi_n^*(x't)]$$

$$g_1(x-t) = \sum_{n \neq 1} \Psi_n(xt) \Psi_n^*(x't). \quad (4)$$

In terms of the one-body density the Hartree-Fock equations can be written as

$$i \dot{g}_1 = [H_{HF}(g_1), g_1]. \quad (5)$$

Numerical solutions of the TDHF-equations can be obtained in three dimensions under certain geometrical restrictions. They have been used extensively to simulate heavy-ion collisions.¹⁵⁾. The underlying physical assumption is a long mean free path of the nucleons such that nucleon-nucleon collisions due to the residual force can be neglected. The collective motion of the system can be calculated on a microscopic basis, the collective variables need not be specified as in a transport theory.

The theory contains, however, no stochastic features, so that the description of truly irreversible processes is beyond its scope. For example, it is not possible to treat the formation of a fully equilibrated compound nucleus. It is therefore desirable to combine the advantages of TDHF and transport theories. Steps in this direction will be indicated in the next section.

4. Microscopic Theory: TDHF plus Collision Term Different from most previous approaches designed to extend TDHF¹⁶⁾ we use a random-matrix model for the residual nucleon-nucleon interaction¹⁷⁾. The total Hamiltonian is written as

$$H = (T+U) + (U-U) = H_{HF}(t) + V(t) \quad (6)$$

where $U(t)$ is the time-dependent mean field and U the two-body interaction. The residual interaction $V(t)$ is neglected in TDHF. Here it is assumed to have statistical properties which cause the loss of phase memory in the system. We start from the Liouville equation for the A-body density $\rho_A(\vec{x}_1 \dots \vec{x}_A; \vec{x}'_1 \dots \vec{x}'_A; t)$

$$i\dot{\rho}_A = [H_{HF}, \rho_A] + [V, \rho_A], \quad (7)$$

transform to the interaction representation (ρ_A^I) and use a time-dependent Gaussian ensemble to evaluate the ensemble-average $\bar{\rho}_A^I$ of the A-body density matrix. By tracing over $(A-1)$ variables we obtain the equation of motion for the average one-body density which now contains the effect of the stochastic action of the residual force and is, therefore, time-irreversible. The collision term is still a function of two-and three-body densities. Upon factorization of $\bar{\rho}_2$ and $\bar{\rho}_3$ the result is in the weak-coupling limit and for vanishing memory effects

$$i\dot{\bar{\rho}}_{ss'}^{(0)} = [H_{HF}, \bar{\rho}_{ss'}^{(0)}]_{ss'} + iC \sum_{ijk} [\bar{V}_{skij}^2 + \bar{V}_{sjkj}^2] (1-\bar{\rho}_{kk}^{(0)}) \bar{\rho}_{jj'}^{(0)} + [(\delta_{ss'} - \bar{\rho}_{ss'}^{(0)}) \bar{\rho}_{ii'}^{(0)} - (1-\bar{\rho}_{ii}^{(0)}) \bar{\rho}_{ss'}^{(0)}]. \quad (8)$$

The mean-field term describes the coherent motion of the system. The collision term is reminiscent to the one in the Boltzmann equation¹⁸⁾ and accounts for the equilibration due to the nucleon-nucleon collisions.

5. One-Dimensional Numerical Model A one-dimensional numerical calculation¹⁹⁾ with a simple ansatz for the collision term²⁰⁾ serves to qualitatively illustrate its effect on the time evolution of the one-body density and its Wigner transform

$$\rho(xk; t) = (2\pi)^{-1} \int_{-\infty}^{+\infty} ds \exp(-ikx) \rho(x + \frac{1}{2}s, x - \frac{1}{2}s). \quad (9)$$

The TDHF equations (5) can be transformed into (xk) -space, and a collision term with equilibration time τ as a parameter is added to the r.h.s. of the TDHF-equation for $\rho(x, k, t)$:

$$T_{coll} = (2\pi)^{-1} [\rho(x, 2k - \tau; t) - \rho(xk; t)]. \quad (10)$$

It imposes an equilibration in momentum space towards the mean momentum k . The static Hartree-Fock equations are solved to obtain the initial density. Collisions of one-dimensional slabs containing 5 nucleons are shown in Fig. 8 at $E_{cm} = 7.53$ MeV / nucleon. The relaxation time is $\tau = 30$ fm/c so that the slabs still separate. For the short but still realistic relaxation time of $\tau = 5$ fm/c drastic effects of the collision term become apparent in the exit phase of the reaction, Fig. 9.: the system bounces back and eventually fuses. This is also illustrated in the contour plots of Fig. 10 for the Wigner function in the exit phase; the collision term drives the system towards the equilibrated compound nucleus. It seems provable that the low- k cut off for fusion observed in 3-dim.

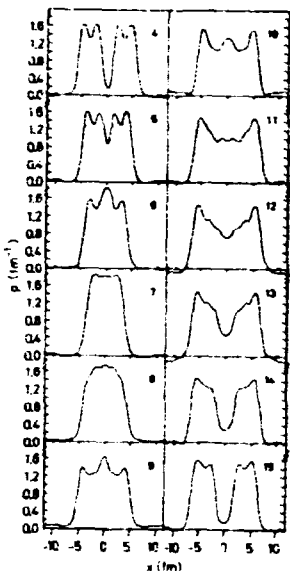


Fig. 8. Time evolution
of one-body density.
Times in 10 fm/c (ref.19)

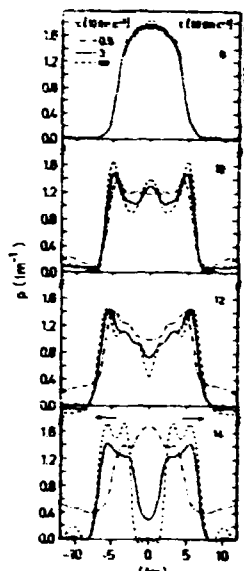


Fig. 9. As Fig. 7, but
different relaxation
times T (ref.19)

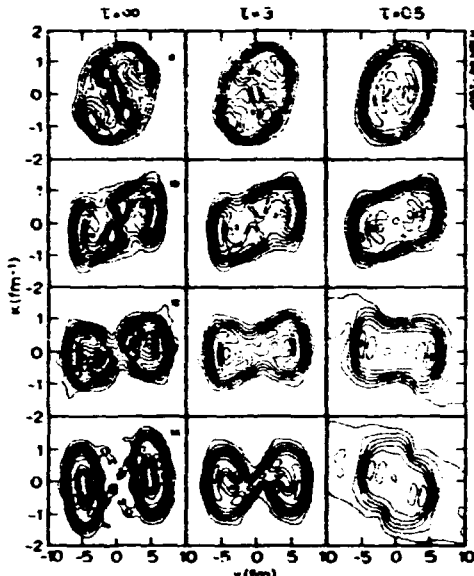


Fig. 10. Time evolution of Wigner function
 $f(x, k, t)$ (ref.19)

TDHF calculations²¹⁾, Fig. 11, is reduced or even eliminated when two-body dissipation is accounted for.

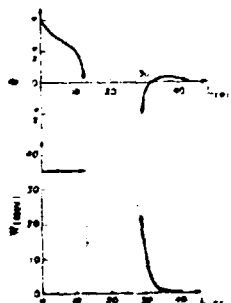


Fig. 11. Fusion window
as obtained in 3-dim.
TDHF (ref.21).

6. Conclusions Phenomenological transport models provided a simple and consistent method to understand most of the available data on low-energy heavy-ion collisions. A promising starting point for a fully microscopic theory of these reactions is the statistical treatment of residual nucleon-nucleon collisions on the basis of a mean-field approach. It provides the necessary features which are missing in present TDHF calculations, and allows to extend the theoretical description to higher bombarding energies.

References:

1. H. A. Weidenmüller, Prog. Part. and Nucl. Phys. Vol. 3, p. 49 (1980)
Pergamon Press and references therein.

2. J. W. Negele, in: *Theoretical Methods in Medium-Energy and Heavy-Ion Physics*, Plenum, New York, London, 1978 p. 235
3. G. Wolschin, Proc. Int. School of Physics "Enrico Fermi", Varenna, Italy 1979 (in press) and references therein
4. H. Hofmann, J. Grégoire, R. Lucas and C. Ngö, Z. Physik A 293 (1979) 229
5. C. Riedel and G. Wolschin, Z. Physik A 294 (1980) 17
6. G. Rudolf et al. Nucl. Phys. A, in press
W. W. Wilcke et al. Phys. Rev. C, in press
7. G. Wolschin, Phys. Lett. 88 B (1979) 35
8. A. Oimi et al. Phys. Rev. Lett. 41 (1978) 688
9. G. Wolschin, Fizika 9 (1977) 513; Nucl. Phys. A 316 (1979) 146
10. G. J. Wozniak et al. Phys. Rev. Lett. 45 (1980) 1081
11. W. Hörenberg, Phys. Lett. 52 B (1974) 289
J. de Phys. C5 (1976) 141
12. R. Schmidt, V.D. Toneev and G. Wolschin, Nucl. Phys. A 311 (1978) 247
13. A.D. Hildenbrand et al.: Phys. Rev. Lett. 39 (1977) 1065
T. Tanabe et al.: Nucl. Phys., A 342 (1980) 194
14. R. Schmidt and G. Wolschin, Z. Physik A 296 (1980) 215
15. S.E. Koonin, Proc. Int. School of Nuclear Physics, Erice, Italy 1979
16. G. Mantzouranis and H.C. Pauli, Z. Physik A 281 (1977) 165
C.Y. Wong and H.F. Tang, Phys. Rev. Lett. 40 (1978) 1070
E. Orland and R. Schaeffer, Z. Physik A 292 (1978) 191
S. Ayik, preprint GSI
17. P. Grangé, G. Wolschin and H.A. Weidenmüller, to be published
18. L.P. Kadanoff and G. Baym, *Quantum Statist. Mech.* Benjamin, N.Y. 1962
19. P. Grangé, J. Richert, G. Wolschin and H.A. Weidenmüller, to be published
20. J. Richert, D.M. Brink and H.A. Weidenmüller, Phys. Lett. 87 B (1979) 6
21. H. Flocard, S.E. Koonin and M. Weiss, Phys. Rev. C17 (1978) 1682

THE ROLE OF DEEP INELASTIC TRANSFERS IN PRODUCTION OF "DIRECT" ALPHA PARTICLES IN NUCLEAR REACTIONS INDUCED BY HEAVY IONS

L.Pomorski, M.Gruszecki, W.Karek, A.N.Mezentsev, A.Popescu, D.G.Popescu and L.I.Volkov
Laboratory of Nuclear Reactions, Joint Institute for Nuclear Research, Dubna, USSR

Abstract. The comparison of experimental data for α -particles and deep inelastic transfer reaction products obtained in inclusive measurements in the reactions $^{nat}\text{Ag} + ^{40}\text{Ar}$ (285 MeV) and $^{197}\text{Au} + ^{40}\text{Ar}$ (290 MeV) has revealed their great similarity which is considered to be evidence for a large contribution from deep inelastic transfer reactions (DIT) to the production of "direct" α -particles in the reactions induced by ^{40}Ar ions. The influence of the DNS potential energy and the high nuclear stability of ^4He on the large yield of α -particles as compared to other products is discussed.

1. INTRODUCTION

Since the work of Britt and Quinton /1/, it has been known that H₂ induced reactions involve the formation of "direct" α -particles and protons. Their angular distributions are forward peaked, their energy spectra are characterized by higher energies compared to the evaporation ones, and production cross sections amount to several hundreds of millibarns at bombarding energies well above the Coulomb barrier. Recently, the traditional studies based on simple inclusive experiments have been extended to correlation ones which involve coincidence measurements for α -particles and light fragments /2-7/, for α -particles, protons and γ -rays from a conjugate heavy fragment /8-12/, and for α -particles and fission fragments /13-15/.

In papers of our group /16-18/ we propose a new approach to this problem which is based on the comparison of the angular distributions, energy spectra and production cross sections for "direct" α -particles with the analogous characteristics of the typical products of deep inelastic transfers (DIT). In the present paper such comparison is made for the two reactions: $^{nat}\text{Ag} + ^{40}\text{Ar}$ (285 MeV) and $^{197}\text{Au} + ^{40}\text{Ar}$ (290 MeV). We also suggest to interpret the high yield of "direct" α -particles as compared to DIT products, on the basis of the form of the double nuclear system/DNS/ potential energy and the high nuclear stability of the α -particle.

2. EXPERIMENTAL TECHNIQUE

The experiments have been performed using an external ^{40}Ar ion beam (300 MeV) from the S-300 heavy ion cyclotron of the JINR Laboratory of Nuclear Reactions. The products of the reactions investigated were detected by using both the ($\Delta E-E$) technique and a combination of magnetic analysis and the ($\Delta E-E$) technique /19/. The second method was employed for measurements of the energy spectra and production cross sections for the isotopes of elements ranging from He to Cl, at an emission angle of 40°. An ionization chamber served here as a ΔE detector.

3. EXPERIMENTAL DATA

As well known, DIT products possess three main experimentally observable features which permit their reliable separation from the products of other nuclear reactions /20/. These features are: (i) Asymmetric centre-of-mass angular distributions,

(ii) Almost symmetric energy spectra with a maximum corresponding to the exit Coulomb barrier for a conjugate nucleus.

(iii) The obeyance of isotopic production cross sections to the Ω_{qq} -systematics.

3.1. Angular Distributions.

The c.m. angular distributions of the α -particles emitted in the bombardment of silver and gold targets with ^{40}Ar ions are shown in fig. 1. The solid curves are drawn through experimental points. The dashed curves characterize a contribution from the symmetric part of the angular distribution at forward angles. The angular distributions of ^4He and elements ranging from Li to C are presented in fig. 2. It is seen that as one goes from typical DIT products (C, B, Be) to light particles, the angular distributions change smoothly while the anisotropy decreases.

An interesting result is obtained if we compare the asymmetric parts of the angular distribution. These parts can be obtained by subtracting from the total angular distribution of the symmetric part which dominates at backward angles. The asymmetric parts of the angular distribution of the elements ranging from C to He are compared in fig. 3. One can see that the slopes of lines are identical for all the elements.

3.2. Energy Spectra.

The α -particle energy spectra for the reactions $^{197}\text{Au} + ^{40}\text{Ar}$ (290 MeV) and $^{nat}\text{Ag} + ^{40}\text{Ar}$ (285 MeV) are presented in fig. 4. The energies corresponding to the exit Coulomb barriers for nuclei conjugated with α -particles (^{233}Am , ^{191}Au and ^{193}Au) are indicated with arrows. It is seen that the maxima of the energy spectra at forward angles, where the main contributors are "direct" α -particles, correspond to the exit Coulomb barriers.

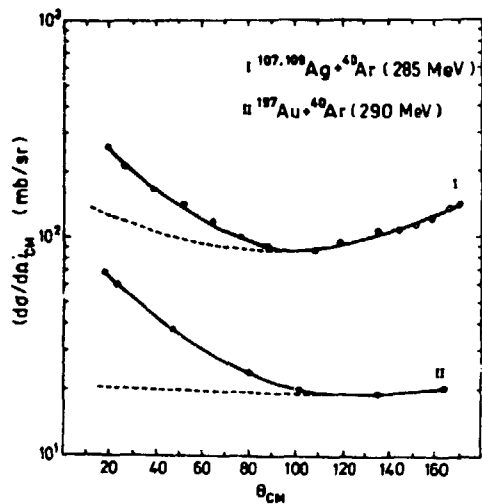


Fig. 1. The angular distributions of α -particles produced in the reactions $^{nat}\text{Ag} + ^{40}\text{Ar}$ (285 MeV) and $^{197}\text{Au} + ^{40}\text{Ar}$ (290 MeV).

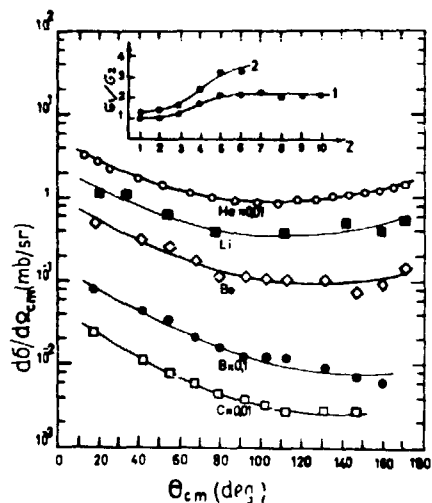


Fig. 2. The angular distributions of He to C produced in the reaction $^{nat}\text{Ag} + ^{40}\text{Ar}$ (285 MeV).

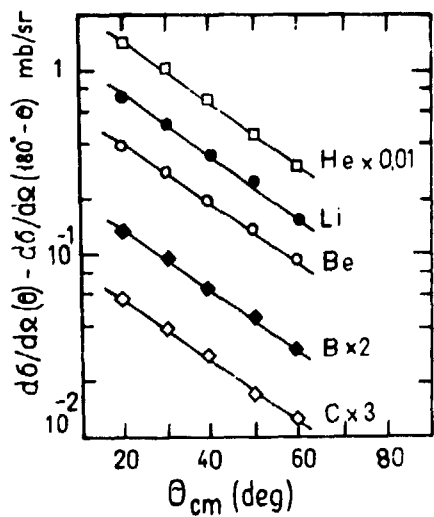


Fig. 3. The asymmetric parts of angular distributions for He to C produced in the reaction $^{nat}\text{Ag} + ^{40}\text{Ar}$ (285 MeV).

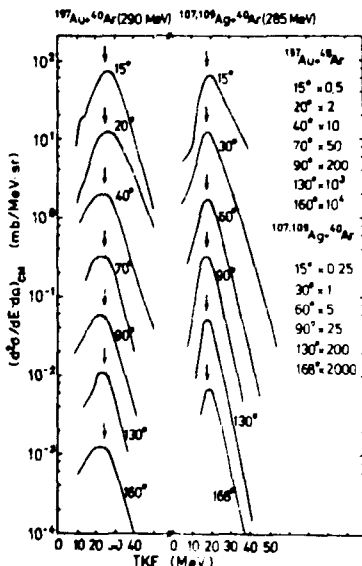


Fig. 4. The energy spectra of α -particles produced in the reactions $^{197}\text{Au} + ^{40}\text{Ar}$ (290 MeV) and $^{107,109}\text{Ag} + ^{40}\text{Ar}$ (285 MeV) for different detection angles.

In the reaction $^{nat}\text{Ag} + ^{40}\text{Ar}$ (285 MeV) the grazing collision angle is equal to 27° (lab.). Deep inelastic transfer reactions involving the turning of the DIT to the region of negative angles, and the emission of light fragments at an angle equal to -40° make the principal contribution to multinucleon transfer reaction cross sections at a measuring angle of 40° .

The energy spectra of the isotopes of elements from He to N, measured in this reaction at an emission angle of 40° are given in fig. 5. As one can see, the shape of the energy spectra of the helium isotopes ^3He , ^4He and ^6He is identical with that of the DIT products -- the isotopes of Li to N.

The Q_{gg} -systematics of cross sections for producing the isotopes of light elements in the reaction $^{nat}\text{Ag} + ^{40}\text{Ar}$ (285 MeV) at an emission angle of 40° is presented in fig. 6. A similar picture of the Q_{gg} -systematics is observed also for the isotopes of light elements produced in the reaction $^{197}\text{Au} + ^{40}\text{Ar}$ (290 MeV). In both reactions the cross sections for producing the isotopes ^3He , ^4He and ^6He obey the same Q_{gg} -systematics as do the isotopes of the heavier elements which could be produced only as a result of DIT reactions.

4. DISCUSSION OF THE MECHANISM OF PRODUCTION OF "DIRECT" ALPHA PARTICLES AS DIT PRODUCTS

The comparison of the experimental properties of "direct" α -particles and those of typical DIT products, made in the present paper shows that they are very similar. In our view, this

similarity cannot be an accidental one. It reflects the common mechanism of their production. However the strong predominance of the α -particle emission channel over the rest of DIT channels is a conspicuous fact. Fig. 7 shows the differential cross sections for producing the isotopes of elements ranging from He to Al in the reaction $^{197}\text{Au} + ^{40}\text{Ar}$ (290 MeV) at a measuring angle of 40° , plotted as functions of the neutron number N and proton number Z in the isotope. The cross section for producing ^4He is about two orders of magnitude as large as cross sections for production of other isotopes. This is all the more surprising since ^4He is the farthest element in Z and A from the initial nucleus ^{40}Ar . It is worth to note another interesting point in fig. 7. Starting from $Z=17$ (Al isotopes), the production cross sections for isotopes with maximum yields decreases with Z , but after fluorine the cross sections begin to increase. The maximum values correspond to nuclei with closed shells and subshells, such as ^{15}N , ^{12}C , and ^4He . An especially strong increase in cross section is observed for ^4He . A similar behaviour of differential cross sections is observed in the case of the reaction $^{nat}\text{Ag} + ^{40}\text{Ar}$ (285 MeV).

One can try to explain the predominance of the α -particle emission channel over other channels as being due to the features of the DNS potential energy and to the extraordinary nuclear stability of the α -particle. Fig. 8 shows the DNS potential energies as functions of Z and A of the light fragment, for the initial system $^{197}\text{Au} + ^{40}\text{Ar}$ (285 MeV). The calculations were performed using the ground-state nuclear masses, the energy of the Coulomb interaction for spherical nuclei, and the rotational energy corresponding to the middle of the range of the angular momenta contributing to DIT reactions. The DNS moment of inertia was taken to be a rigid-body one. The calculated DNS potential energies for the initial system $^{197}\text{Au} + ^{40}\text{Ar}$ (290 MeV) have a similar behaviour. In both reactions, the DNS potential energy has a minimum in the region of the lighter elements. This fact indicates that the initial DNS evolves in the direction of configurations with the largest mass asymmetry. The potential energy of the system with the α -cluster configuration has a deep minimum.

The second factor which facilitates the predominance of the α -cluster configuration in DIT reactions is the particular nuclear stability of ^4He . In order that the DNS - cluster configuration might evolve further toward the complete fusion of the nuclei, it is necessary to excite the ^4He nucleus thus providing the mobility of its nucleons. This however requires the transfer of a considerable part of excitation energy to

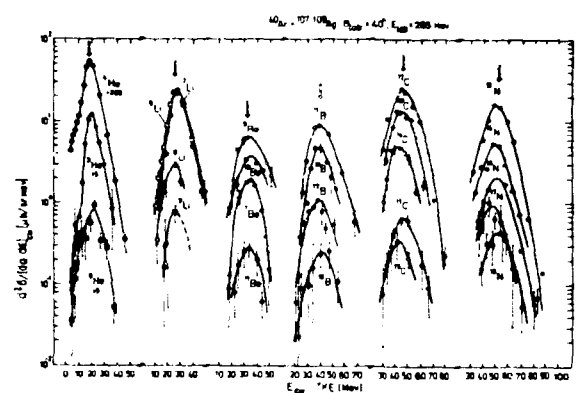


Fig. 5. The energy spectra of various isotopes of elements from He to N produced in the reaction $^{nat}\text{Ag} + ^{40}\text{Ar}$ (285 MeV) measured at an emission angle of 40° . The arrows indicate the exit Coulomb barriers.

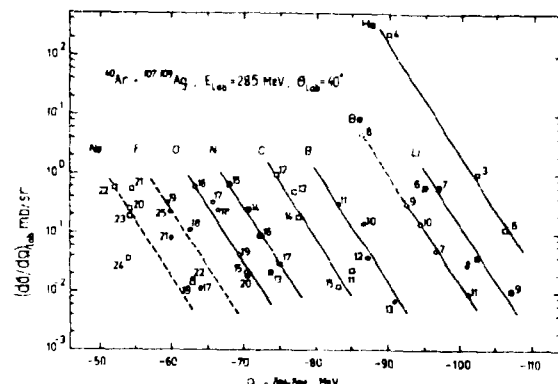


Fig. 6. The Q_α -systematics of differential cross sections for the isotopes of elements from He to Ne produced in the reaction $^{nat}\text{Ag} + ^{40}\text{Ar}$ (285 MeV) at an emission angle of 40° .

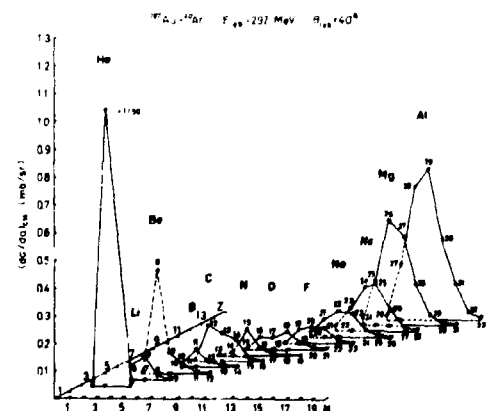


Fig. 7. Differential cross sections for producing the isotopes of elements from He to Al in the reaction $^{197}\text{Au} + ^{40}\text{Ar}$ (290 MeV), as functions of the number of neutrons N and protons Z .

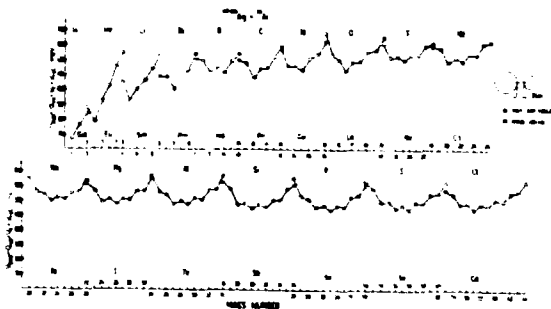


Fig. 8. The potential energy as a function of A and Z of the light fragment for the initial system $^{nat}_{Ag-40} + Ar$ (285 MeV). The calculations are made for "sticking" spherical nuclei with the distance of closest approach of 2 fermi, the initial angular momentum of 110 \hbar , and for ground-state nuclear masses. The value of $Q_{gg} = (m_1 + m_2) - (m_3 + m_4)$, where m_1 , m_2 , and m_3 , m_4 are the initial and final masses, respectively. The chemical symbols of the conjugate heavy fragments are also indicated.

REFERENCES

1. Britt H.C., Quinton A.R. Phys.Rev., 124(1961)877
2. Gelbke C.K. et al. Phys.Lett., 71B(1977)83
3. Ho H. et al. Z.Phys., A283(1977)235
4. Harris J.W. et al. Phys.Rev.Lett., 38(1977)1460
5. Miller J.M. et al. Phys. Rev.Lett., 40(1978)700
6. Camp A. et al. Phys.Lett., 74B(1978)215; Z.Phys., A291(1979)347
7. Bieler R. et al. Z.Phys., A292(1979)293
8. Inamura T. et al. Phys.Lett., 68B(1977)81
9. Zolnowski D.R. et al. Phys.Rev.Lett., 41(1978)92; Yamada H. et al. Phys.Rev.Lett., 43(1979)605
10. Westerberg L. et al. Phys. Rev., C18(1978)723
11. Siwick-Wilczynska K. et al. Phys.Rev.Lett., 42(1979)1599
12. Geoffrey K.A. et al. Phys.Rev.Lett., 43(1979)1303
13. Delagrange H. et al. Phys.Rev.Lett., 43(1979)1499; Logan D. et al. Phys.Rev., C22(1980)104
14. Dyer P. et al. Phys.Rev.Lett., 42(1979)560
15. Gierlik F. et al. Preprint JINR, P7-12839, Dubna, 1979
16. Volkov V.V. et al. Izvestia Ak. Nauk SSSR, seria fiz., 42(1978)2234;
Volkov V.V. In: Clustering Aspects of Nuclear Structure and Nuclear Reactions, Winnipeg, 1978, Eds. W.T.H. Vaeorts et al. Am.Inst. of Phys., New York, 1978, p.352;
Mikheev V.L. et al. Proc. of the EPS Topical Conf. on Large Amplitude Collective Nuclear Motion, Keszthely, Hungary, 10-16 June, 1979, Ed. by A.Kiss, J.Nemeth and J.Zimanyi, p.676
17. Volkov V.V. et al. Preprint JINR, E7-12411, Dubna, 1979
18. Volkov V.V. et al. Proc. of the Int. Workshop on Gross Properties of Nuclei and Nuclear Excitations. Hirschegg, Kleinwalsertal, Austria, January 14-19, 1980, p.138-141
19. Artukh A.G. et al. Nucl. Instr. and Meth., 83(1970)72
20. Volkov V.V. Phys.Rep., 44(1978)92.

the 4He nucleus, and this is unlikely to occur. As a result, the DNS evolution turns out to be blocked in the α -cluster configuration. The accumulation of the DNS α -cluster configuration and its subsequent decay lead to a high yield of "direct" α -particles.

In conclusion the authors express their deep gratitude to Academician G.N.Flerov for his stimulating interest in this work, A.G.Artukh, G.F.Gridnev and V.L.Mikheev for participating in the experiments and analysis of experimental data, and Mrs.L.V.Pashkevich for her help in preparing an English version of this paper.

RESONANCE PHENOMENA IN HEAVY ION REACTIONS

I. Rotter

Zentralinstitut für Kernforschung, Rossendorf, 8051 Dresden, GDR

Abstract

On the basis of the continuum shell model, it is shown that the shape resonances may have doorway properties. Together with the unitarity of the S-matrix these properties of the shape resonances may lead to an l-dependent transparency of the optical potential.

1. Introduction

The resonance phenomena in heavy ion reactions are discussed in the literature for about twenty years. Nevertheless, they are not understood up to now. The many results obtained experimentally did not solve the problem but gave contradictory results which can not be interpreted on the basis of the usual nuclear reaction theories (see e.g. [1-3]). Even reactions induced by protons raised new problems in that nonstatistical effects are observed in cases where they should not appear [4].

On the basis of the continuum shell model it has been shown [5] that external mixing of the resonance states via the continuum may cause nonstatistical effects. Further, it has been suggested [6] that shape resonances may play the role of doorway states.

It is the aim of this talk to investigate the properties of the shape resonances in detail on the basis of a theory in which nuclear structure and nuclear reaction aspects are treated in a unified manner (continuum shell model). Shape resonances are included together with the compound nucleus resonance states of complicated nuclear structure into the resonance dependent part of the S-matrix. The unitarity of the S-matrix is considered and shown to cause an l-dependent transparency of the system.

2. The basic equations of the continuum shell model

In the continuum shell model version formulated by Barz et al. [7] the Schrödinger equation

$$(H - E) \psi_E^{c(+)} = 0 \quad (1)$$

is solved with

$$\psi_E^{c(+)} = \sum_{i=1}^M b_E^c(i) \phi_i + \sum_{c'=1}^A \int_{E_c'}^{\infty} dE' \alpha_E^c(E; c') \chi_E^{c'} \quad (2)$$

where the ϕ_i are the basic wavefunctions (eigenfunctions of $H_0 = H - V$) of the system with all A nucleons in bound single-particle states while the χ_E^c are the basic wavefunctions with A-a nucleons in bound states and the group of a nucleons in a scattering state. The reaction channel c is characterized by the

set of quantum numbers of the target nucleus, of the particle as well as of their relative motion.

In solving the Schrödinger equation (1), a projection operator formalism is used. The following three functions are defined

$$(E_R^{SM} - H_{QQ}) \Phi_R = 0 \quad (3)$$

$$(E^+ - H_{PP}) \xi_E^c = 0 \quad (4)$$

$$(E^+ - H_{PP}) \omega_R^{(+)} = H_{PQ} \Phi_R \quad (5)$$

where H_{QQ} stands for QHQ and so on. The operator Q projects onto the subspace of discrete states while P projects onto the subspace of continuous states ($P + Q = 1$). The eqs. (3) to (5) can be solved by standard methods. Eq. (3) is the traditional shell model problem. The eigenfunctions Φ_R and the real eigenvalues E_R^{SM} of the shell model Hamiltonian H_{QQ} provide the wavefunctions and energies of the discrete states which are called QBSEC (quasi bound states embedded in the continuum). Eqs. (4) and (5) are solved by the coupled channels method. It is $P\Phi_R = 0$ and $Q\xi_E^c = 0$.

The function ψ_E^c can be expressed by means of the three functions Φ_R , ξ_E^c and ω_R . After diagonalisation of the operator

$$H_{QQ}^{\text{eff}} = H_{QQ} + H_{QP} G_P^{(+)} H_{PQ} \quad (6)$$

appearing in the expression for ψ_E^c one gets

$$\psi_E^c = \xi_E^c + \sum_R (\tilde{\Phi}_R^{(+)} + \tilde{\omega}_R^{(+)}) \frac{1}{E - \tilde{E}_R + \frac{i}{2} \tilde{\Gamma}_R} \langle \tilde{\Phi}_R^{(-)} | H_{QP} | \xi_E^c \rangle. \quad (7)$$

The operator (6) is an effective operator in the subspace of discrete states. It consists of the traditional shell model Hamiltonian H_{QQ} and an additional term which takes into account the coupling to the continuous states ($G_P^{(+)}$ is the Green operator in the P space). The eigenvalues $\tilde{E}_R - \frac{i}{2} \tilde{\Gamma}_R$ and eigenfunctions $\tilde{\Phi}_R$ of H_{QQ}^{eff} are complex and energy dependent.

The function ψ_E^c and the cross section do not depend on the manner by which the whole function space is divided into the two subspaces. If however the Q space contains all wavefunctions with large amplitude inside the nucleus then the eigenfunctions and eigenvalues of H_{QQ}^{eff} depend smoothly on energy (with the exception of threshold effects [11]) and determine the wavefunctions, energies and widths of the resonance states. Such a definition of the Q space is possible if a cut-off technique for the single-particle (shape) resonances is used [7]. The Q space obtained corresponds to the function space used in the traditional shell model calculations. The P space defined as $1 - Q$ contains wavefunctions with small amplitude inside the nucleus and the correct asymptotic behaviour. The coupling matrix elements between the wavefunctions of the two subspaces

$$\tilde{\gamma}_{Rc} = (2\pi)^{1/2} \langle \tilde{\phi}_R^{(-)} | H_{QP} | \xi_E^{(+)} \rangle \quad (8)$$

are also smoothly energy dependent. According to eq. (7) the so-called resonance parameters can be obtained unambiguously

$$\bar{E}_R = \tilde{E}_R (E = E_R) \quad (9)$$

$$\bar{\Gamma}_R = \tilde{\Gamma}_R (E = E_R) \quad (10)$$

$$\bar{\gamma}_{Rc} = \tilde{\gamma}_{Rc} (E = E_R) \quad (11)$$

If no cut-off technique for the single-particle resonances is used and they belong to the P space then the eqs. (9) to (11) cannot be solved unambiguously although the cross section can be calculated. This problem is discussed in detail by Lemmer and Shakin [8].

It has been proven [9] that for a complete set of resonance states R,

$$\tilde{\gamma}_c^2 = \sum_R \tilde{\gamma}_{Rc}^2 \quad (12)$$

$$\tilde{\Gamma} = \sum_c |\tilde{\gamma}_c^2| \leq \sum_R \tilde{\Gamma}_R \quad (13)$$

can be defined as for an isolated resonance state.

3. The S-matrix

In the framework of the continuum shell model an expression for the S-matrix can be derived [9].

$$S_{cc'} = S_{cc'}^{(1)} - S_{cc'}^{(2)} \quad (14)$$

where

$$S_{cc'}^{(1)} = \exp(2i\delta_c) \delta_{cc'} - 2i\pi \langle \chi_c^{(-)} | V | \xi_c^{(+)} \rangle \quad (15)$$

depends smoothly on energy while

$$S_{cc'}^{(2)} = i \sum_R \frac{\tilde{\gamma}_{Rc'} \tilde{\gamma}_{Rc}}{E - \tilde{E}_R + \frac{i}{2} \tilde{\Gamma}_R} \quad (16)$$

contains the contributions of all the resonance states R.

The S-matrix has the familiar form. However, there are some essential differences to the expression for the S-matrix used usually.

- (1) Eq. (16) is valid for all energies. The functions \tilde{E}_R and $\tilde{\Gamma}_R$ depend smoothly on energy with the exception of threshold effects [11].

- (ii) The so-called resonance parameters $\tilde{\gamma}_{Rc}$, E_R and $\tilde{\Gamma}_R$ are calculated within the model (eqs. (9) to (11)). They are not parameters.
- (iii) The external mixing [10] of the resonance states via the continuum as well as the configurational mixing and the channel coupling, which all are caused by the residual interaction V , are taken into account in calculating the $\tilde{\gamma}_{Rc}$, E_R and $\tilde{\Gamma}_R$. The resonances are therefore correlated more or less.
- (iv) The functions $\tilde{\gamma}_{Rc}$ are complex. It follows from the unitarity of the S-matrix that $\text{Im } \tilde{\gamma}_{Rc}$ is generally a complicated function of all the $(E - E_R)^2 + \frac{1}{4} \tilde{\Gamma}_R^2$. Therefore, the resonance behaviour of $S_{cc}^{(2)}$ is determined by $\sum_R A_R / (E - E_R + \frac{1}{2} \tilde{\Gamma}_R)$ with energy independent A_R only for isolated resonance states R . Generally, it is much more complicated.
- (v) The sum over R in eq. (16) includes also the main contribution of the single-particle or shape resonances due to the cut-off technique used for them.

Consequently, the concept of a resonance state R defined in the continuum shell model differs from that of the Feshbach theory by the different consideration of the shape resonances. It differs also from that of the shell model approach to nuclear reactions formulated by Mehaux and Weidenmüller [12]. The resonance parameters of the S-matrix of the Mehaux-Weidenmüller-theory are not determined by the functions $\tilde{\gamma}_{Rc}$, E_R and $\tilde{\Gamma}_R$ as has been shown by Lemmer and Shakin [8]. Only the introduction of the QBSEC by Berz et al. [7] instead of the BSEC by Mehaux and Weidenmüller and the consideration of the external mixing [10] instead of the statistical assumptions allows the unified description of nuclear structure and nuclear reaction aspects and the derivation of eq. (16) for the S-matrix with the definitions (9), (10) and (11). The concept of a resonance state R defined in the continuum shell model corresponds however to the concept formulated on the basis of the R-matrix theory (Robson and Lane [13]). Thus, it is in agreement with the numerous calculations performed successfully for many years in analysing different nuclear reactions to get conclusions on nuclear structure.

4. Doorway states and shape resonances

A doorway state is defined in the continuum shell model as a state with a simple nuclear structure, i.e. a large spectroscopic connection to one of the channels. Furthermore, its internal or configurational mixing with other resonance states in the neighbourhood is small. Therefore, external mixing dominates and leads to the typical picture of a gross structure at about the energy of the resonance state in the cross section. If the internal mixing would not be small, the "gross structure" would be smeared over a larger energy region due to internal mixing and could hardly be identified.

Doorway states are e.g. isobaric analogue resonance states. Another example of doorway states are the shape resonances although they are assumed usually to belong to the direct reaction part.

Shape resonances have a large width in relation to a certain reaction channel c_1 . They are connected with a certain value $l = l_1$. The extreme case is

$$|\tilde{\gamma}_{Rc_1}^2| \approx \tilde{r}_R \quad (17)$$

for the channel c_1 and

$$|\tilde{\gamma}_{Rc}^2| = 0 \quad (18)$$

for all other channels $c \neq c_1$. In such a case the S-matrix elements are

$$\begin{aligned} S_{cc} &\approx 1 \text{ for all } c \neq c_1 \\ S_{c_1 c_1} &\approx -1 \\ S_{cc'} &\approx 0 \text{ for all } c \neq c' . \end{aligned} \quad (19)$$

The transmission coefficient is

$$T_c = \sum_{c'(*c)} |S_{cc'}|^2 = 1 - |S_{cc}|^2 \approx 0 \quad (20)$$

for all channels c including $c = c_1$. Since the imaginary part of the optical potential for the elastic scattering takes into account the contributions of the channels $c' \neq c$ it vanishes also in the considered case.

In the case of resonance states the widths of which are distributed statistically the values $|S_{cc}|^2$ show fluctuations with energy. The energy averaged value differs from unity and the corresponding transmission coefficient as well as the imaginary part of the potential differ from zero.

In the realistic case of 1 shape resonance corresponding to a certain value $l = l_1$ and N resonance states of a more complicated nuclear structure with the same spin and parity, the S-matrix elements are similar to those of an isolated giant resonance with resonance parameters determined by the shape resonance (4, 12, 13). Consequently, a shape resonance in a certain channel c_1 becomes apparent not only in the excitation function but also, due to its doorway properties, in a minimum in the imaginary part of the potential at $l = l_1$ according to eq. (20).

Recently, Frawley et al. [14] have presented a comparison of elastic scattering and total reaction cross section data in the region of the 9^- , 14.7 MeV resonance in $^{16}\text{O} + ^{12}\text{C}$. The comparison provided evidence that the data can be reconciled only if the background absorption for $l = 9^-$ is quite small in comparison with the absorption for smaller as well as higher l -values. It would be interesting to compare the experimental results of the resonance phenomena more quantitatively with the conclusion on shape resonances and their doorway properties as discussed here in the framework of the continuum shell model.

Brink et al. [15] showed that the strength of the imaginary part of the optical potential can explain much of the anomalous back angle scattering of alpha particles from different elements. Such a result agrees with the results obtain-

ed on the basis of the continuum shell model: The dominance of a certain value $l = l_1$ induced by the shape resonance leads to a more symmetric angular distribution than in the case with many interfering l -values. Thus, large back angle scattering together with small absorption for a certain l value suggests a doorway mechanism via shape resonances.

5. Conclusions

In this talk, the properties of shape resonances are investigated. Their mixing with the well known resonances of complicated nuclear structure is taken into account in the resonant part of the S-matrix $S_{cc}^{(2)}$. Due to the unitarity of the S-matrix, the imaginary part of the optical potential may show some strong l dependence. Further, back angle scattering may be large at the energy of shape resonances which show doorway properties.

Shape resonances play surely an important role in heavy ion reactions and have doorway properties due to their strong clustering and, consequently, small internal mixing with the resonance states of complicated nuclear structure. While the resonance behaviour of the excitation function is determined by the ratio Γ/D , i.e. by the concrete nuclear structure, the shape resonances depend more weakly on the nuclear structure of the interacting nuclei. The strong l dependence of the imaginary part of the optical potential together with the large back angle scattering should therefore be similar for neighbouring nuclei in contrast to the resonance behaviour.

References

- [1] N. Cindro, editor, Nuclear Molecular Phenomena, Proc. Int. Conf. on Resonances in HI Reactions, Hvar, Yugoslavia (Amsterdam - North-Holland) 1978
- [2] K.A. Eberhard, in: Selected Topics in Nuclear Structure, Proc. XVI Winter School Bielsko-Biala, Poland, ed. by Styczen and Kulessa, vol. 1, p. 308, 1978
- [3] J. Barrette et al., Phys. Rev. C20 (1979) 1759
- [4] W.K. Wells et al., Phys. Letters 86B (1979) 18; B.H. Chou et al., Phys. Rev. Letters 45 (1980) 1235
- [5] I. Rotter, Annalen der Physik (Leipzig), in press
- [6] I. Rotter, Phys. Letters 67B (1977) 385; Journ. of Physics G5 (1979) 685
- [7] H.W. Barz et al., Nucl. Phys. A275 (1977) 111
- [8] R.H. Lemmer and C.M. Shakin, Annals of Physics 27 (1964) 13
- [9] I. Rotter, to be published
- [10] I. Rotter, Journ. of Physics G5 (1979) 251
- [11] I. Rotter et al., Nucl. Phys. A297 (1978) 237
- [12] C. Mahaux and H.A. Weidenmüller, Shell Model Approach to Nuclear Reactions (Amsterdam - North-Holland) 1969
- [13] D. Robson and A.M. Lane, Phys. Rev. 161 (1967) 982
- [14] A.D. Frawley et al., in press
- [15] D. Brink et al., Nucl. Phys. A309 (1978) 359

DYNAMICAL POTENTIALS AND CHARGE EQUILIBRATION IN DEEP-INELASTIC HI-COLLISIONS

E.F. Hefter[§] and K.A. Gridnev[&]

§ Institut für Theoretische Physik, Universität Hannover, 3 Hannover, F.R.G.
& NIIF, Leningrad State University, Leningrad, USSR

Abstract: In the search for a unified approach to nuclear physics and for dynamical equations for the nuclear potential we step back to consider one-dimensional relations. We discuss the applicability of the soliton concept to nuclear physics. Quantitative and even more preliminary qualitative results support the notion to view the Korteweg - de Vries equation (KdVE) with its extensions as the phenomenological counterpart to the equation of the mass operator, thus providing us with a tractable model for the dynamical nuclear potential.

1. Motivation

Our interest in a dynamical nuclear potential is largely stimulated by its importance and the impact which a better knowledge of this quantity is going to have on the various problems dealt with in nuclear physics; it is certainly of special concern to the physics of heavy ion reactions^[1,2].

In nuclear physics we have nowadays a terrific range of models all of which explain only part of the phenomena observed: Classical and quantal, microscopic and macroscopic approaches compete with each other and sometimes even act in peaceful cooperation to yield useful interpretations of the experimental data. But we do not yet have a truly unified approach to nuclear physics. In a crude way the present state of the art could be summarized by saying that the simple models are too simple and that the sophisticated ones are too hard for us to provide us with reasonable chances for a speedy progress towards such a unified approach to nuclear physics. - In here we go a few steps back to one-dimensional relations to consider the application of methods hitherto not yet applied to nuclear physics, i.e. the soliton concept.

But before indulging into more detailed discussions we would like to draw attention to the strong disparity in our knowledge and experience related to the wavefunction ψ (or the density $\rho = |\psi|^2$) and the potential U . Various approaches to nuclear and elementary particle physics treat ψ and U on a symmetric footing as solutions of coupled nonlinear differential equations^[1-5]. Hence, one would expect each equation for the ψ to have its counterpart for U . The obvious discrepancy noted in practice is possibly due to the fact that the wavefunction ψ and the (probability) density ρ lend themselves more easily to our perception than the more abstract potential or field concepts.

To give some examples for the equations for ψ we name the Dyson, Dirac, (time dependent) Hartree-Fock (TDHF), and linear Schrödinger equations (LISE). The most primitive time independent one-dimensional forms of the last two equations may be written as

$$-\delta \cdot \ddot{\psi}_{xx} - (E + V_{nn} |\psi|^2) \cdot \psi = 0; \quad \ddot{\psi}_{xx} =: \partial^2 \psi / \partial x^2, \text{ etc.}; \quad (1)$$

and

$$-\delta \cdot \ddot{\psi}_{xx} - (E - U) \cdot \psi = 0 \quad (2)$$

where the factor δ depends as usual on the reduced mass μ of the system,

$$\delta = M^2 / (2\mu_i(A_i)); \quad \mu_i = \frac{m_i}{M_i} \frac{m_i}{M_i}. \quad (3)$$

The more sophisticated TDHF equations provide us even with dynamical evolution equations that allow us to follow the time development of ψ or $\rho = |\psi|^2$.

But what about the potential? - Within the theory of Fermi systems a prominent equation for the nuclear potential (meson field) is given by the nonlinear equation for the mass operator (MOE), which is coupled with the Dyson equation^[5]. Under the appropriate assumptions the latter may be reduced to the HF equation, which we know to be the self-consistent equivalent of the linear Schrödinger equation (cf. e.g. Eqs.(1),(2) and make the substitution $U = -V_{nn} |\psi|^2$ in Eq.(1)). In the case of the MOE a similar reduction is in principle possible, however, attempts to this nonlinear equation are in general restricted to the use of the otherwise very successful perturbation method, which does not allow for a satisfactory exploration of the properties of the mass operator. This is not really surprising since the experience gathered in the last two decades in the fields of nonlinear mathematics and physics, shows that such methods are not quite adequate for nonlinear evolution equations (NLE). E.g. they do not yield the famous soliton solutions that are characteristic for a large number of NLE's. Hence, we infer that it might be more appropriate to attack the potential problem, i.e. equations like the MOE, by aid of nonlinear methods. Indeed, further considerations even indicate that it is sensible to view solitons as representatives for stable

nuclear particles and their potential bags. - It is possibly useful to recall that solitons are stationary wave solutions of NLE's that behave very much like particles; they are stable objects that do not change amplitude, shape or velocity in their time development and that emerge completely unchanged from collisions with each other, but for a phase-shift.

Taking the MOE as the specific example of interest we start from the following assumptions (which could be justified in a more detailed discussion):

- A.1 The solution of the equation for the mass operator corresponding to stable systems should be given in terms of solitons.
- A.2 If A.1 is true then the study of the simplest soliton supporting NLE should already provide us with some bits of useful information.

Below we start with the easier part and concentrate on A.2. The necessary requirements for realistic solutions of the respective test equation are seen in the conditions:

- C.1 The (one) soliton solution of the test equation should allow for a realistic parametrization of the static shell model potential, V_{sm} , (which is equivalent to the corresponding Hartree-Fock potential, V_{HF} , cf. Eqs.(1),2)).
- C.2 The test equation should yield a consistent description of the potential for elastic scattering events, e.g. the optical model potential, V_{om} .
- C.3 In analogy to the dynamical equations for the wavefunction or the density, e.g. TDHF, the test equation should facilitate a dynamical description of scattering events, reactions, etc. involving the potential bags, e.g. V_{sm} .
- C.4 Possibly via extensions of the original NLE there should also be a chance to cater for dissipative phenomena which are very important for the treatment of deep inelastic collisions of heavy ions (DIC).

2. The soliton solutions of the nonlinear Korteweg - de Vries equation (KdVE)

The one-dimensional KdVE as the simplest NLE may be written in the form

$$u_t(x,t) = 6 \cdot u \cdot u_x + \delta \cdot u_{xxx} = 0. \quad (4)$$

Historically, it could not be solved completely until it was discovered that it is via the inverse scattering problem related to the linear Schrödinger equation, Eq.(2); i.e. formally its solution $u(x,t)$ appears as the potential of a related Schrödinger problem with $U = u(x,t)$. This is by chance (?) the kind of interrelation that facilitates very much the intended use of the KdVE as a test equation or as a possible phenomenological counterpart to the equation of the mass operator. The choice of the dispersion constant δ in the KdVE is rather arbitrary and depends only on the medium considered. In the present context it is suggestive to use the connection LISE-KdVE to define δ via Eq.(2). This notion finds additional support by a further accidental (?) interrelation between the one-soliton solution, $u_1(x,t=0)$, of the KdVE and the bound-state (soliton) solution $\phi_b = \sqrt{V_{nn}}/8 \cdot \text{sech}[\sqrt{V_o}/2^{\frac{1}{2}} \cdot x]$ of the Hartree-Fock equation, Eq.(1),

$$u_1(x,0) = -V_o \cdot \text{sech}^2[\sqrt{V_o}/2^{\frac{1}{2}} \cdot x] = -V_{nn} \cdot |\phi_b|^2 \text{ with } V_{nn} \approx 2\sqrt{2V_o}. \quad (5)$$

In the framework of this study the time dependence of the solutions of the KdVE does not provide us with any additional information so that we follow Eq.(5) in suppressing it.

The knowledge of u , allows us to study the static properties of the soliton solutions of the KdVE. To get a feel for the dynamics of such systems we have to consider more-soliton expressions, e.g. - the two-soliton solution $u_2(x,t)$,

$$u_2(x,t) = - \frac{\alpha_1^2 f_1 + \alpha_2^2 f_2 + 2(\alpha_2 - \alpha_1)^2 f_1 f_2 + \left(\frac{\alpha_2 - \alpha_1}{\alpha_2 + \alpha_1}\right) \cdot (\alpha_2^2 f_1^2 f_2 + \alpha_1^2 f_1^2 f_2)}{(1 + f_1 + f_2 + \left(\frac{\alpha_2 - \alpha_1}{\alpha_2 + \alpha_1}\right)^2 f_1 f_2)^2} \xrightarrow{t \rightarrow \infty} u_2^{(1)} + u_2^{(2)} \quad (6)$$

with

$$f_i = \exp[-\alpha_i(x - x_o^{(i)} - \alpha_i^2 t)/\sqrt{\lambda^2/2m}] \quad \text{and} \quad \alpha_i^2 = 2 \cdot V_o^{(i)}. \quad (7)$$

The $x_o^{(i)}$ denote the displacements of the two asymptotic solitons $u_2^{(1)}$ and $u_2^{(2)}$ from the origin. Below we center one of them, say $u_2^{(2)}$, at the origin, i.e. $x_o^{(1)}=0$. If we now suppress again the explicit time dependence by using $t=0$, then we are only left with $x=x_o^{(2)}$ to describe the relative separation between the two solitons and to simulate the time development of the system. Its history for all x and t is completely determined by Eqs.(6) and (7)!

For not too large differences $\Delta V = |V^{(1)} - V^{(2)}|$ between the amplitudes of the two solitons fig.1 illustrates how the dynamics evolve with $x_o^{(2)}$ (or t). In contrast to our experience from linear physics, there is no direct (linear) superposition of the two solitons at the moment of interaction. We rather observe that the smaller soliton apparently "swallows up" the surplus which was initially contained in the larger one. In such a manner the two seemingly simply interchange their places and the incident projectile continues its voyage. The resulting phase-shifts experienced by soliton 1 and 2, resp., are given by

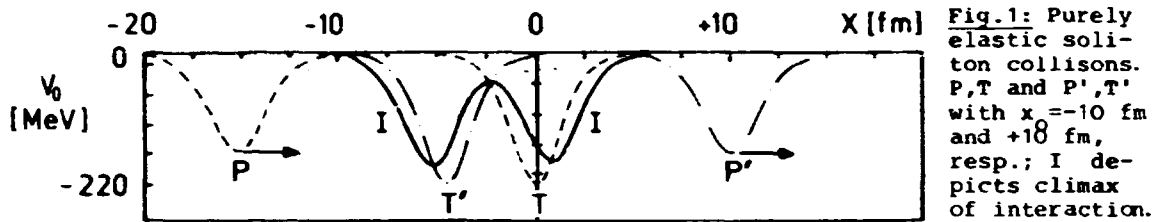


Fig. 1: Purely elastic soliton collisions. P, T and P', T' with $x = -10$ fm and $+10$ fm, resp.; I depicts climax of interaction.

$$c_i = (\sqrt{\delta}/\alpha_i) \cdot \ln[(\alpha_2 + \alpha_1)/(\alpha_2 - \alpha_1)]^2. \quad (8)$$

Returning to the one-soliton solution of the KdVE it is seen that the KdVE-conservation law $\int u(x,t) \cdot dx = \text{const}$ yields the following relationship for (adiabatic) transfers of the soliton $u_1(x,t)$ from a medium with the dispersion constant δ' to another one with δ :

$$C = \int_{-\infty}^{\infty} u_1(x,t) \cdot dx = 2\sqrt{2V_o' \delta'} = 2\sqrt{2V_o \delta} \longrightarrow V_o = V_o' \delta'/\delta. \quad (9)$$

In the original applications of the KdVE to water waves the dispersion constant δ contained also the depth h of the sea-bed, i.e. $\delta \sim h^3$. Assuming an adiabatic transfer of $u_1(x,t;h')$ from the depth h' to h , Eq.(9) yields

$$V_o(h) = V_o' (h'/h)^3 = V_o/(1+ah)^3 = V_o \cdot g_s^2(h) \quad (10)$$

with $a = \Delta h/h^2$. But in the present context such a functional form of the dispersion constant is certainly undesirable, cf. e.g. Eqs.(1) to (3). Hence, it is very fortunate to find out that the forced Korteweg - de Vries equation (FKdVE),

$$u_t(x,t) - 6 \cdot u \cdot u_x + \delta \cdot u_{xxx} = f(h) \cdot u, \quad (11)$$

with the "driving" term $f(h) \cdot u$ describes such a situation even more accurate. Ignoring higher order effects, which would introduce albeit small deviations, Eq. (10) is confirmed by solving Eq.(11) explicitly. However, a significant difference is that Eq.(11) does no longer require $u_1(\delta)$ and $u_1(\delta')$ to contain an explicit dependence on the depth, i.e. we have $\delta = \delta' = \delta/h^3$ and $u_1(\delta)$ and $u_1(\delta;h)$. The conservation law given above yields now

$$C = \int u_1(x,t;\delta;h') \cdot dx = \int u_1(x,t;\delta;h) \cdot dx + \int u_{ph}(x,t;\delta;h) \cdot dx \quad (12)$$

implying that the original soliton $u_1(h')$ is now reduced in its amplitude to lead to the soliton $u_1(h)$ and additional phonon contributions $u_{ph}(h)$. In some applications of the KdVE the phonons or oscillatory waves have been identified with damping and the like.

3. Application of the KdVE-solitons to nuclear physics

According to A.2 we would now like to test the applicability of the KdVE and its soliton solutions to nuclear physics; the 3.i below correspond to the C.i. **[3.1]** Square-well, harmonic oscillator and Saxon-Woods potential formfactors in the LISE are known to yield an appropriate shell model description for nuclei which is confirmed by self-consistent Hartree-Fock calculations. Putting these geometries in relation to the functional form of $u_1(x,0)$, cf. Eq.(5), we see without explicit calculations that $u_1(x,0)$ fulfills at least qualitatively condition C.1.

[3.2] In the conventional notation the elastic scattering interaction is given in terms of the optical model potential,

$$V_{om} = V_{Cl} + V + i(W_v + W_s) + V_{so} + V_1. \quad (13)$$

At least for $A_p \ll A_T$ and smaller projectile energies, E_p , the real central part of the nuclear interaction, V , is to a good approximation represented by the static potentials $V \approx V_{HF}$. Besides its x - (or r -) dependence, V is known to be a function of A_p , A_T and E_p , e.g.

$$V = -53 \cdot A_p \cdot \exp(-0.0066 \cdot E_p) =: -53 \cdot A_p \cdot g_{om}^2(E_p) \quad (14)$$

We added the coefficient A_p to account roughly for the predictions of the simple (deep) folding model. Restricting ourselves to the interaction of two particles, i.e. $i=2$ in Eq.(3), and exploiting Eqs.(5), (9) and (10) we obtain

$$V \approx u_1(x,0;A_1, A_2, E_p) = -V_o \operatorname{sech}^2[\sqrt{V_o/2\delta}x] \text{ with } V_o = \hat{V}_o [A_1 A_2 / (A_1 + A_2)] g_s^2(E_p) \quad (15)$$

and with $g_s^2(E_p) := (1 + \alpha' E_p)^{-3}$, cf. Eq.(10). In Eq.(15) we normalized the soliton amplitude via $\hat{V}_o = V_o A_1 A_2 / (A_1 + A_2) \rightarrow V_o = 53 \text{ MeV}$ to nucleon-nucleus scattering. The constant α' is for an arbitrary value of E_p , e.g. $E_p = 0$, adjusted to the $g_{om}^2(E_p)$ of Eq.(14). The u_1 of Eq.(15) compares surprisingly well

with relation (14), which is based on numerical material and formal considerations ^{6,7)}.

At this point it appears appropriate to stress that \hat{V}_o and a' are the only constants taken from nuclear physics, but for A_o and A_T !

The conservation law (12) tells us that we can not neglect the phonon-part u_{ph} which arises for $E_p > 0$. Attributing for simplicity a sech²-formfactor to u_{ph} (which in reality is closer to a Saxon-Woods shape) Eqs.(5),(10) and (12) lead to

$$W_v = u_{ph} = -W_o \operatorname{sech}^2[\sqrt{W_o/28}x] \text{ with } W_o(E_p) = V_o(E_p=0) \cdot (1-g_i(E_p))^{-2} \quad (16)$$

where $g_i(E_p) = g_s \approx g_{ow}$, cf. Eqs.(14) and (15), contains the explicit energy dependence P of W_v . Again, a surprisingly close correspondence to the W_v as based on nuclear physics is noted ⁸⁾.

The potentials u_1 and u_2 may be referred to as "dressed" effective nucleon-nucleon interactions depicting the interaction of the A_o -th fraction of the projectile with the A_T -th part of the target. The consequent extension to composite nuclei requires the transition from one-soliton solutions to N-soliton expressions ($N=A_o+A_T$). In a phenomenological manner we may try to simulate the results of such a hard work by aid of the substitution

$$x \longrightarrow x/R \text{ with } R = r_o(A_o^{1/3} + A_T^{1/3}) \quad (17)$$

in Eqs. (15) and (16). However, in that case we have to treat the amplitude V_o as an adjustable parameter (and to exchange the sech² in Eq.(16) by a Saxon-Woods formfactor) ⁹⁾.

The missing surface term W_s is to be associated with shell effects, resonances and the like which will only be accounted for in a more complete treatment with N-soliton expressions. It is claimed that spin-orbit and centrifugal potentials may - at least qualitatively - also be catered for within the soliton approach (but requiring $t \neq 0$ and the transition to generalized versions of the KdVE, resp.) ¹⁰⁾.

Before finishing this sub-section it should be mentioned that it is quite comforting - but not yet understood why that happens - to note that in spite of $A_o = A_T$, application of the u_1 of Eq.(15) yields quite an encouraging correspondence to the measured α - α phase-shifts ¹¹⁾.

Summarizing, we may state that the KdVE (in liaison with its generalized versions) does apparently fulfill condition C.2.

[3.3] As mentioned in section 2., the two-soliton solution of the KdVE contains with no free parameters the complete time evolution of the interaction of the two solitons. To get a feel of the applicability of u_2 to nuclear physics we proceed in a similar way as in the TDHF: We first prepare the two α -particles which we are going to consider ($R=1.91$ fm; $\mu_{1-3}=1/4$; $V=4\sqrt{R}=212$ MeV) separately and insert them then into the relevant dynamical equation; i.e. in the present case we have to apply Eqs.(6),(7) with the respective parameters. Because of the energy dependence of u_1 , cf. Eq.(15), the amplitude of the incident projectile is to be multiplied by $\exp(-0.0066 \cdot E_p)$. Fig.1 corresponds to 20 MeV and resembles very much one-dimensional TDHF calculations with solitons ¹¹⁾. Insertion of the respective parameters into Eq.(8) yields phase-shifts that are surprisingly close to the experimental ones ⁹⁾.

Such nice results and the similarity of fig.1 with TDHF calculations suggest strongly to exploit these features, e.g. in two-center shell model calculations. In the case of low energy collisions of identical particles (e.g. $\alpha + \alpha$) the two potential bags remain even at the distance of closest approach still "closed", but with increasing projectile energy they "open" more and more. For objects with a microstructure the "opening" of the potential bags corresponds to an increased probability for inelastic transitions and exchange processes ^{9, 12)}. Such a behaviour and the given interpretation are fully in line with the single-particle model employed for the explicit evaluation of the transport coefficients in DIC of heavy ions, cf. e.g. fig.10 of ref. ¹³⁾.

We conclude that the question posed by C.3 may be answered affirmative.

[3.4] A consistent extension of the original KdVE that accounts for dissipative processes is given by the Korteweg - de Vries - Burgers equation (KdVBE),

$$u_t(x,t) - 6 \cdot u \cdot u_x + 5 \cdot u_{xxx} = D \cdot u_{xx}, \quad (18)$$

where D is the diffusion coefficient. Two arguments which are not directly related to the proceeding, but which do advocate such an extension of the KdVE, are

(i) The Burgers equation (BE), i.e. Eq.(18) with $D=0$, has the same dispersion relation as the Fokker-Planck equation (FPE) which is usually applied to the "diffusion phase" of DIC. According to the theory of dispersive media this insinuates that the nonlinear version of the FPE, i.e. the BE, should be applicable to the same problem.

(ii) Treating DIC in a gas kinetic model in a fashion corresponding to the damping of sound in a gas (accounting for recombinations, etc. of the molecules) one arrives also of the KdVBE of Eq.(18).

To save time and space further suggestive arguments in favour of the use of Eq. (18) in nuclear physics are suppressed⁹⁾.

The following discussion of the KdVBE is unfortunately going to be a rather qualitative one. Yet, before going over to the physics of the KdVBE, we would like to draw attention to the prominent features of its solutions.

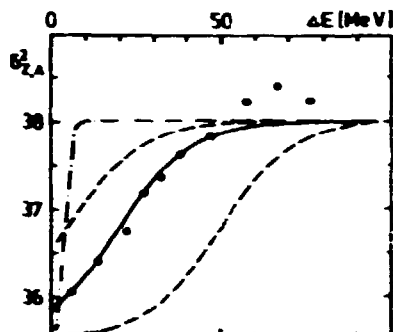


Fig. 2: The magnitude of $u(x,t) = u_{KdVBE}$ (denoted by $\beta_{A,z}^1$) is plotted as a function of $x = \Delta E$. The parameters $(P_0/2, x_0, D) = (V_0/2, x_0, D)$ for the dotted, broken, full and lower broken curves are $(1.25, 5, 1)$, $(1.25, 5, 13)$, $(1.25, 20, 13)$ and $(1.25, 50, 13)$, resp.. The points and the scaling are discussed in the text.

3.4.1 For $D=0$ the KdVBE is reduced to the KdVE with analytical stationary wave (soliton) solutions like the one given in Eq.(5). For $\beta=0$ we arrive at the BE which has analytical stationary wave solutions of the type

$$u_{BE}(x,t) = -V_0(1+\tanh[V_0(x-x_0-V_0 t/2)/2D])/2. \quad (19)$$

The amplitude $V_0=P_0$ gives the "height" of the "ramp" produced by the tanh; for the sake of simplicity we used $u_{BE}(-\infty)=0$, the extension to arbitrary $u_{BE}(-\infty)$ being straightforward. In fig. 2 the response of u_{BE} to different parametrizations $(V_0/2, x_0, D)$ is illustrated.

In the case of the KdVBE there are no known analytical solutions, however, in various contexts this equation has been solved numerically. For $D \gg 1$ its solutions resemble very much the analytical solutions of the BE, cf. fig. 2. But at a certain critical value

$$D_{crit} = \sqrt{2-\beta \cdot (u(-\infty)-u(+\infty))} \quad (20)$$

the behaviour of the u_{KdVBE} changes qualitatively from a monotonous shock-wave, cf. fig. 2, to a shock-wave with some oscillatory structure on top of it. Fig. 3 contains a qualitative representation of such a solution of Eq. (18).

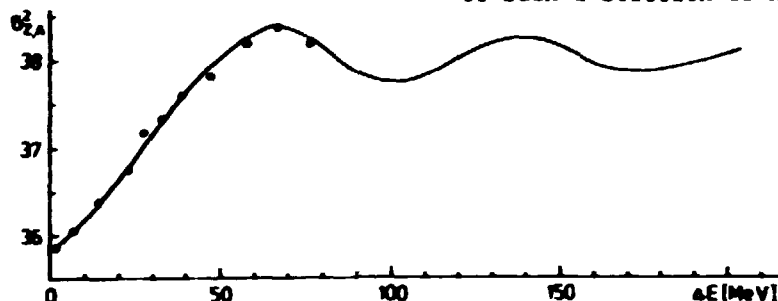


Fig. 3: The same as fig. 2 but with the full curve depicting the qualitative behaviour of the solution of Eq. (18) for $D < D_{crit}$.

3.4.2 As far as the physical interpretation of the constants β and D is concerned, they describe the effects of dispersion and dissipation, respectively. Taking it for granted that we have to apply Eq. (18) to dissipative processes in nuclear physics, e.g. to inelastic scattering processes and to DIC of heavy ions, the predictions of the KdVBE are as follows:

(i) For (high energy) collisions in which a lot of energy is dissipated in a very short time $\delta \ll D$ holds, cf. fig. 2. In reactions that involve only a few degrees of freedom, e.g. inelastic nucleon-nucleus scattering, the dotted curve in fig. 2 with a relatively small dissipation constant, $D=1$, should be adequate. Indeed, such an interpretation is consistent with the (microscopic) treatment of inelastic nucleon scattering, where the optical potentials in the entrance and exit channels are usually chosen to correspond to the kinetic energy of the incident projectile, E_p , and to $E'_p = E_p - Q$ (Q = Q -value, energy loss), resp..

In DIC of heavy ions at higher projectile energies we note a rapid dissipation of energy in the initial phase which is very soon followed by a decay of the di-nuclear system into the exit channel. The KdVBE suggests for this case a time development of the potential ($\propto \delta/P$) similar to the full curve in fig. 2.

(ii) Low energy processes proceed on a larger time scale, insinuating that the dissipation in the last part of the diffusion phase is relatively small, hence, we are very likely to encounter situations with $D < D_{crit}$. As illustrated in fig. 3, we are to get an additional oscillatory structure on the plateau of the solution of the $u_{KdVBE}(\Delta E)$.

But how do these predictions compare to other models and/or experiment?

Considering Eq. (18) as it stands, i.e. as a dynamical evolution equation for the nuclear potential, it has to be recalled that the discussions of Münchow et al. and of Pedotov et al.¹⁰⁾ lead to similar predictions. But if we want to go over to quantities that are directly measured then we have to recollect that mass and potential are intimately connected with each other; together with more de-

tained considerations this confirms the notion that the KdVBE should also be applied to the discussion of the mass distributions. Since the mass is a positive quantity, this necessitates the transition from Eq.(18) to its counterpart with a positive sign for the nonlinearity and hence also for its solution Eq.(19) (cf. also Eq.(5) with $\rho=|\phi|^2$). The final reaction products in DIC of heavy ions may be discussed in terms of the measured variances $\sigma_{A,z}^2$ of the mass and charge distributions as functions of the energy loss ΔE . The experimental points displayed in figs. 2 and 3 were copied from ref.¹⁴⁾ and correspond to $^{86}\text{Kr} + ^{92}\text{Mo}$ at $E_{\text{lab}}=430$ MeV. Obviously there are no problems in parametrizing these data by aid of the solutions of the BE and/or the KdVBE. - The overshooting in the data is observed in different reactions, but what about the oscillations? With a wishful eye they too may be discovered in the data of ref.¹⁵⁾, however, to establish their existence firmly further precision measurements would be required.

Recently Schmidt and Woschin¹⁶⁾ and Grossmann and Krappe¹⁷⁾ discussed the significance of anharmonic potentials and of inertia effects, resp., for the treatment of the mass transport in DIC of heavy ions. In its spirit and in terms of pure parametrizations the former is relatively close to the present interpretation.

Seemingly the latter may also be explained by aid of the stationary wave solutions of the KdVBE: Such an interpretation would have to exploit the funny property of the solutions of the (KdV)BE that the smaller solitary wave is swallowed up by the larger one when the two "collide". However, the time is not yet ripe for discussions of the details of such processes, since the qualitative correspondence of our results with other models and experiment does only give the impression of quantitative agreements because we simply parametrized the solutions of the (KdV)BE to obtain the correspondences shown above. In spite of the preliminary positive findings a final verdict on the physical content of the KdVBE will have to await the results of more elaborate investigations.

Nevertheless, we may conclude that the soliton approach fulfills at least qualitatively also the last condition, C.4.

4. Summary and outlook

We regret very much that the 'boundary conditions' did not allow us to provide you with a more detailed picture. As far as DIC of heavy ions are concerned the other contributions to this Symposium contain certainly more useful and elaborate material than we could have provided; but as far as nonlinear evolution equations and solitons are concerned we feel that more detailed discussions would certainly have been very helpful.

However, we hope that we managed to convince you that - with an input from nuclear physics consisting of only two numbers - the KdV(B)E yields with comparative ease an amazingly large amount of information and that the KdV(B)E constitutes the basis for a highly interesting one-dimensional approach to nuclear physics. Only further qualitative and esp. quantitative investigations can tell us whether we may proceed on such a basis towards three-dimensions and possibly even towards a truly unified theory of the atomic nucleus.

5. Acknowledgements: We are grateful to S. Krewald for helpful discussions related to the nature of the mass operator.

6. References

1. H.A. Weidenmüller in 'Progress in Particle and Nuclear Physics' (D.Wilkinson ed., Pergamon Press, 1980)
2. L. Münchow, A. Pfitzner and H. Schulz, Proc. of the ESINS Conf. Dresden, DDR, 1980, ZFK-Report 404 (1979) 29
3. S. Kubo, M. Namiki and I. Ohba, Prog. Theor. Phys. 55 (1976) 860
D.K. Campbell, Les Houches 1977 Vol.2 (North-Holland, 1978) pp.673
4. J.F. Schonfeld et al., Ann. Phys. (N.Y.) 128 (1980) 1 and refs.
5. A.L. Fetter and J.D. Walecka, 'Quantum Theory of Many-Particle Systems' (McGraw Hill, N.Y., 1971)
A.B. Migdal, 'Theory of Finite Fermi Systems' (Intersc., Wiley&Sons, 1967)
6. G. Eder et al., J.Phys.G:Nucl.Phys. 3 (1977) L127
7. C.A. Engelbrecht and H. Fiedeldey, Ann. Phys. (N.Y.) 42 (1967) 262
8. K.A. Gridnev and E.F. Hefter, Phys. Lett. 77A (1980) 490; preprint (SOL803)
9. K.A. Gridnev and E.F. Hefter, in prep. for Физ.Элем.Част.и Ат.Яд.
10. R. Ceuleneer and F. Michel, Mons, Belgium, priv. communication
11. Y. Nogami and C.S. Warke, Phys. Rev. C17 (1978) 1905
12. E.F. Hefter, Il Nuovo Cimento A (in press)
13. W. Nörenberg, GSI-Report 79-5
14. E.S. Hernandez et al., Proc. of Hirschegg (VIII), Austria, 1980, p.87
15. A. Mignerey et al., Proc. of Hirschegg (VIII), Austria, 1980, p.104
16. R. Schmidt and G. Woschin, Z. Physik 296A (1980) 215
S. Grossmann, Z. Physik 296A (1980) 251
17. S. Grossmann and H.J. Krappe, Marburg-HMI Berlin, preprint

ANGULAR MOMENTUM DISSIPATION IN DEEP-INELASTIC HEAVY ION COLLISIONS

G. Saupe

Technische Universität Dresden, Sektion Physik, DDR - 8027 Dresden

Deep-inelastic heavy ion reactions with a bombarding energy of 5 ... 10 MeV per nucleon in the centre mass system have been described in a simple classical model, which takes into account the following collective degrees of freedom: the distance R between the centres of the nuclei, the rotation angle Θ of the composite system about its centre of gravity and the rotation angles Θ_1 and Θ_2 of both ions. The corresponding momenta are the radial momentum P_R of the relative motion, the relative angular momentum L and the nuclear spins I_1 and $I_2/1$. The interaction between the ions contains the conservative Coulomb and nuclear potential (proximity /2/) and a dissipative part, which consists of the radial and tangential component of a friction force according to the two components of the relative velocity. In addition the transfer of kinetic energy into deformation energy of the system has been simulated by a simple modification of the interaction potential in the exit channel /3/.

The tangential component of the friction force has been constructed from considering the extension of the overlapping region during the reaction process.

Then a so called effective radius of gyration /3/

$$g^2 = \frac{\ln 1/2}{g} s_0 R \left(1 - \left(\frac{R_1 - R_2}{R}\right)^2\right) \quad (1)$$

can be introduced, where s_0 is the surface diffuseness parameter, R_1 and R_2 are the sharp nuclear radii. In this way one gets two terms of the tangential friction

$$F_{\tan}^{(i)} = f_t(R) \left(R\omega - \tilde{R}_1 \omega_1 - \tilde{R}_2 \omega_2 \right) \pm F_{\tan}^{(i)''}. \quad (2)$$

The first term

$$F_{\tan}^{(i)'} = f_t(R) \left(R\omega - \tilde{R}_1 \omega_1 - \tilde{R}_2 \omega_2 \right) \quad (3)$$

with $\tilde{R}_1 = 0.5 (R + R_1 - R_2)$ and $\tilde{R}_2 = 0.5 (R - R_1 + R_2)$ vanishes if the rolling condition $R\omega - \tilde{R}_1 \omega_1 - \tilde{R}_2 \omega_2 = 0$ is valid. The second part

$$F_{\tan}^{(i)''} = f_t(R) \frac{R^2}{\tilde{R}_1} (\omega_1 - \omega_2) \quad (4)$$

goes to zero if the classical sticking limit $\omega = \omega_1 = \omega_2$ is reached. So the differential equations for the mean values of the fragment spins take the form

$$\dot{L}_i = f_t(R) \left(\tilde{R}_1 (R\omega - \tilde{R}_1 \omega_1 - \tilde{R}_2 \omega_2) \mp g^2 (\omega_1 - \omega_2) \right) \text{ with } \begin{cases} - \text{ for } i = 1 \\ + \text{ for } i = 2. \end{cases} \quad (5)$$

The formfactor $f_t(R)$ has been used in the form given by Gross and Kalinowski /4/. These equations ensure the validity of the angular momentum conservation law

$$\dot{L} = -(\dot{L}_1 + \dot{L}_2) = -f_t(R) R (R\omega - \tilde{R}_1 \omega_1 - \tilde{R}_2 \omega_2). \quad (6)$$

The statistical fluctuations and correlations in the distribution function for the macroscopic degrees of freedom and their conjugate momenta are treated according to the linear response theory given by Hofmann and Siemens /5/. On the base of this formalism the mean value of the dissipated kinetic energy

$$\Delta E = \Delta E_{\text{rad}} + \Delta E_{\text{tan}} + \Delta E_{\text{def}} = E_{\text{CM}} - E_f \quad (7)$$

and the z-component of the transferred angular momentum

$$\Delta I_z = L_0 - L_{zf} = I_{1z} + I_{2z} \quad (8)$$

have been calculated and compared with experiment.

The square mean values of the nuclear spins are computed under the assumptions $\langle I_i \rangle = (0, 0, I_{iz})$ and $\langle \sigma_{ix}^2 \rangle = \langle \sigma_{iy}^2 \rangle = \langle \sigma_{iz}^2 \rangle / 6$. Then one gets the relation

$$\langle I_i^2 \rangle = \langle I_{iz}^2 \rangle + 3 \langle \sigma_{iz}^2 \rangle. \quad (9)$$

The alignment of the spin of the fragment i is given by

$$P_{zz1} = 1.5 \frac{\langle I_{iz}^2 \rangle}{\langle I_i^2 \rangle} - 0.5 = 1.5 \left(\frac{\langle I_{iz}^2 \rangle^2 + \langle \sigma_{iz}^2 \rangle^2}{\langle I_{iz}^2 \rangle^2 + 3 \langle \sigma_{iz}^2 \rangle^2} \right) - 0.5 \quad (10)$$

The calculated quantities $\Delta I_z(L_0)$, $\sigma_{2z}(L_0)$, $\langle I_2(Q) \rangle$ and $P_{zz2}(Q)$ have been compared with results of a model, which contains only the variables R and Θ [7], as well as with experimental data on the reaction $^{86}\text{Kr} + ^{238}\text{U}$ with an incident energy of $E_{\text{Lab}} = 750$ MeV [8].

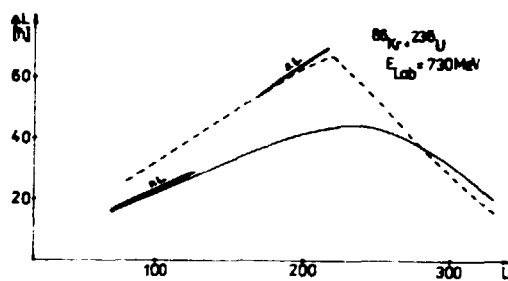


Figure 1: The transferred angular momentum $\Delta I_z(L_0)$. Solid line: four-dimensional model. Dashed line: two-dimensional model.

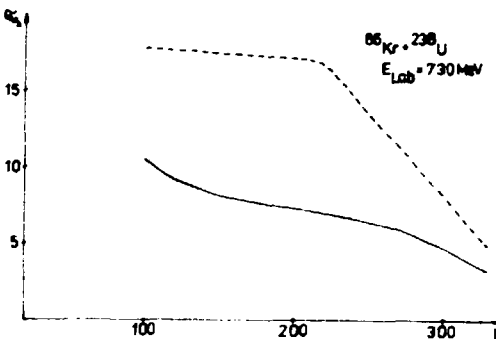


Figure 2: Statistical variance $\sigma_{2z}(L_0)$. Solid line: four-dimensional model. Dashed line: two-dimensional model.

One can state that only the rolling limit is reached, if the spins of the fragments are taken into account. In this case the assumption of the sticking limit leads to an overestimating of the transferred angular momentum for small values of the initial angular momentum L_0 . It is interesting that the statistical variance σ_{2z} for rotating fragments increases permanently for decreasing values of L_0 , whereas the curve $\sigma_{2z}(L_0)$ in the two-dimensional model remains constant after reaching the equilibrium.

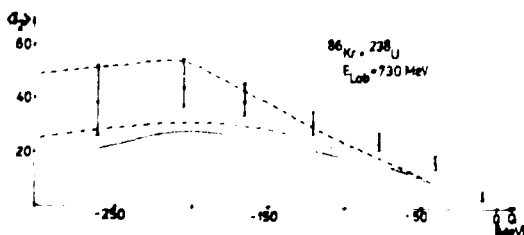


Figure 3: Mean value of the angular momentum, transferred to the heavier ion, on the Q -value.

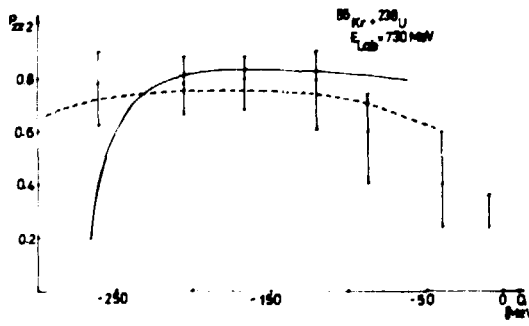


Figure 4: Alignment of the spin of the fragment 2 on the Q -value. Solid line: four-dimensional

Solid line: four-dimensional model. Dashed line: two-dimensional model. Dashed-dotted line: One-body-dissipation /8/.

model. Dashed line: two-dimensional model.

For the mean value of the angular momentum, transferred to the heavier ion, the result of a one-body dissipation model /8/ can be compared with those of the models mentioned above. It is seen that all theoretical approaches considered lead to data, which are in a good qualitative agreement with the experiment, but the absolute values are too small or too large. The alignment of this spin can be reproduced in the DI-region, but it is more and more difficult to describe the experimental data for approaching the QE-region.

From these comparisons one can conclude that further studies should treat the time development of the double nuclear system more carefully. So, the dynamical transition from two spherical nuclei to the deformed double nuclear system and further degrees of freedom of the internal rotations of the fragments should be taken into account in order to achieve a quantitative agreement between measured and calculated data on orientation effects in DIC.

References:

- 1.F. Becker, J. Blocki, M. Dworzecka, G. Wolschin, Phys. Lett. 76 B (1978), 35
- 2.J. Randrup, W.J. Swiatecki, F.C. Tsang, Preprint LBL-3603, Berkeley 1974
J. Blocki, J. Randrup, W.J. Swiatecki, F.C. Tsang, Ann. of Phys. 105(1977) #27
- 3.K. Siwek-Wilczynska, J.W. Wilczynski, Nucl. Phys. A264 (1976), 115
- 4.J.N. De, D.H.E. Gross, H. Kalinowski, Zeitschr. für Phys. A277 (1976), 585
- 5.H. Hofmann, P.J. Siemens, Nucl. Phys. A275 (1977), 464
- 6.G. Wolschin, Preprint MPI H - 1977 - V 29, Heidelberg 1977
- 7.R. Schmidt, R. Reif, Journ. of Phys. G5 (1979), L181 and to be published
- 8.P. Dyer et. al., Ann. Report, Seattle 1979, 102

SHELL EFFECTS IN THE ELEMENT DISTRIBUTION OF THE
 $^{238}_{\text{U}}$ + $^{238}_{\text{U}}$ REACTION

P. Mädler, R. Schmidt, J. Teichert

Technische Universität Dresden, Sektion Physik, DDR - 8027 Dresden

For the investigation of the U+U element distribution a Fokker-Planck equation has been used where the mass drift coefficient is calculated from a shell-corrected liquid drop potential. The discussion leads to the result that the experimental element distribution may be influenced by the shell structure of the nuclei.

Recently, experimental data of bombardments of thick $^{238}_{\text{U}}$ targets with $^{238}_{\text{U}}$ at three beam energies ($E = 8.3, 7.5$ and 6.5 MeV/u) have been reported by Kratz et al. /1/. Thereby an unexpected decrease of the production cross section $d\sigma/dZ_1$ for elements $Z_1 \leq 85$ for the lowest beam energy of 6.5 MeV/u compared to that of higher incident energies has been found (cf. fig. 1). Within the diffusion model of Riedel and Nörenberg /2/ this large decrease of the cross section $d\sigma/dZ_1$ at the lowest incident energy cannot be understood. However, it has been stressed by many authors /3,4,5,6/ that the nuclear shell structure may influence the mass transport. Therefore it seems possible that this discrepancy between the experimental data and the diffusion model results is caused by shell effects. According to that suggestion an analysis has been performed where the shell structure is taken into account for the description of the mass transport.

In accordance with ref.2 the mass transport is determined by a Fokker-Planck equation. The mass diffusion coefficient D_1 used is taken to be proportional to the nuclear temperature T_1 of the system ($D_1 = 75T_1/T_0$ in $\text{amu}^2 10^{21} \text{ s}^{-1}$; $T_0 = 1.364 \text{ MeV}$) and the mass drift coefficient v_1 is calculated according to the Einstein relation /6/ but using a shell-corrected liquid drop potential /7/. The interaction times and nuclear temperatures being functions of the initial angular momentum and of the incident energy are taken from classical trajectory calculations /8/.

In order to demonstrate the shell effects qualitatively and to avoid a rather cumbersome treatment of the thick target we have performed calculations for the initial incident energies. If some influence of the shell effects is observed it should be appear at the smaller effective incident energies too. Furthermore, we only compare the probability distributions $P(Z_1, T_1)$ of the mean initial angular momentum $\bar{l} = 2/3 l_{\text{gr}}$

exhibiting a similar shape as the element distribution. The results of our calculations are presented on the right hand side of fig.1. Due to the deep potential minimum at $Z_1 = 82$ (Pb-shell) there is a strong mass drift towards this direction and finally we shall find a maximum in the distribution at this point in the case of the two higher energies. At the lowest incident energy, however, this is not the case.

The probability distribution is determined by the incident energy via the different interaction times T_1 and the diffusion coefficients defined by the temperature T_1 on the one hand and the driving potential used /7/ entering the drift coefficient according to the Einstein relation on the other hand. A measure of the broadening of the distribution is the quantity $T_1 D_1$ which is shown for the three considered energies in fig.2 (The points correspond to the mean 1 in each case.). The dashed line denotes that value of the product $T_1 D_1$ for which a clear maximum is formed in the corresponding element distribution after the reaction time T_1 . From fig.2 we can see that such a maximum cannot be produced in the case of the lowest incident energy (lowest point) but well can be established in the other cases (upper points).

Summarizing one can conclude that the calculated probability distributions reproduce the qualitative behaviour of the experimental data. The performed investigation has shown that for incident energies smaller than a given value the shape of the probability distribution is different to that for higher incident energies due to the potential minimum at $Z_1 = 92$. This result leads to the suggestion that the referred experimental behaviour may be caused by shell effects.

It should be emphasized that in a more involved consideration the damping of the shell effects due to the temperature has to be taken into account. The results probably turn out in a more smooth behaviour of the probability distributions leading to a behaviour somewhat similar to the liquid drop calculations for the higher incident energies. However, at the smallest energy a smoothing out due to the (rather small) temperature cannot enhance the probabilities as well as the corresponding cross sections in the Pb-region, because the same value of $T_1 D_1$ has to be used and the reaction time is not enough for reaching this region with a large probability. Therefore the qualitative result established in this paper should be conserved.

Such investigations are in progress and will be published together with a more detailed study of the problem discussed above.

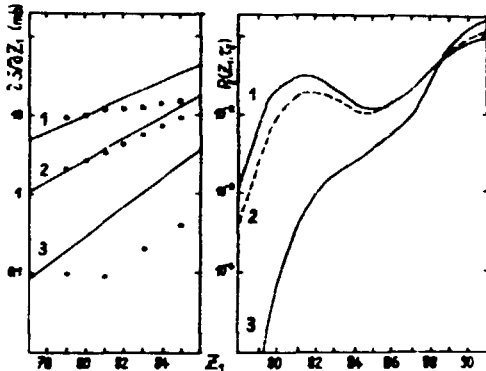


Fig. 1

left side: Experimental element distribution $d\sigma/dZ$, within the thick target reaction $^{238}\text{U} + ^{238}\text{U}$ for three different beam energies
7.65 MeV/u $\leq E \leq$ 8.30 MeV/u (1), 6.06 MeV/u $\leq E \leq$ 7.50 MeV/u (2) and
6.06 MeV/u $\leq E \leq$ 6.49 MeV/u (3). The theoretical curves are calculations based on the model presented in ref.2.

right side: Calculated distribution function $P_1(Z_1, \bar{T}_1)$ for the mean value of the participating initial angular momenta \bar{l} at given incident energies of 8.3 MeV/u (1), 7.5 MeV/u (2) and 6.49 MeV/u (3).

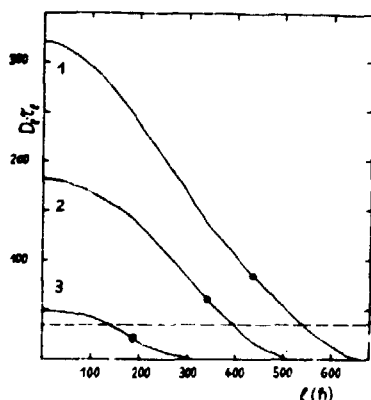


Fig. 2

The product of the diffusion coefficient D_1 and the interaction time \bar{T}_1 as function of the initial orbital angular momentum l for the same reaction and the corresponding incident energies of fig.1. For details see text.

References

1. J. V. Kratz et al. GSI Scientific Report 1979, GSI 80-3, p. 27
and M. Schädel et al. Phys. Rev. Lett. 41(1978)469
2. C. Riedel and W. Nörenberg Z. Phys. A290(1979)385
3. R. Schmidt and G. Wolschin, Z. Phys. A296(1980)215
4. S. Grossmann, Z. Phys. A296(1980)251
5. L.G. Moretto and R. Schmitt, J. de Phys. C5(1976)109
and L.G. Sobotta, G.J. Mathews and L.G. Moretto, Z. Phys. A292(1979)191
6. S. Ayik et al. Z. Phys. A279(1976)145
7. H. Freiesleben et al. Z. Phys. A292(1979)171
8. R. Schmidt et al. Nucl. Phys. A311(1978)247
and R. Schmidt and R. Reif, J. Phys. G 5(1979)L181

CONTRIBUTIONS OF VARIOUS REACTION MECHANISMS IN THE HEAVY-ION
MASS DISTRIBUTION

R. Schmidt and J. Teichert

Technische Universität Dresden, Sektion Physik, DDR - 8027 Dresden

A two-dimensional friction model has been extended to the mass asymmetry degree of freedom introducing a dynamical coupling between mass transport and relative motion. As an example the 515 MeV Kr + Kr reaction is analyzed. Consequences for the interpretation of the experimental element distribution are discussed.

The mass transport between two nuclei during a deep inelastic heavy-ion collision (DIC) has been successfully described in terms of Fokker-Planck equations /1/ or Master equations /2/. Thereby the assumption was made that after a short approach phase the two nuclei become highly excited and a relatively long lived (10^{-21} - 10^{-20} s) double nuclear system is formed. The nucleon exchange between projectile and target happens during the contact time of the double nuclear system and has been treated independently from the relative motion of the two nuclei.

In the present work we introduce a dynamical coupling between the relative motion described by means of a classical friction model /3/

$$\mu \ddot{\vec{R}} = - \frac{\partial U}{\partial \vec{R}} + \vec{\gamma} \dot{\vec{R}} \quad (1)$$

and the mass transport described by the Fokker-Planck equation /1/

$$\frac{\partial}{\partial t} P(A_1, t) = - \frac{\partial}{\partial A_1} (v_A P) + D_A \frac{\partial^2}{\partial A_1^2} P \quad (2)$$

for the probability density $P(A_1, t)$ as function of time t and the mass asymmetry A_1 , measured by the mass number of the projectile-like fragment. The quantities v_A and D_A are the mass drift and the mass diffusion coefficient, respectively.

We consider the coupling between the relative motion and the mass transfer via the time dependence of the mean value of the mass asymmetry $\langle A_1 \rangle(t)$, which induces an additional time dependence of the moments of inertia, the interaction potential and the friction tensor $\vec{\gamma}$ in eq.(1). The mass transport according to eq.(2) is influenced by the relative motion via the time variable and the calculated critical angular momentum.

In the case of the $^{86}\text{Kr}(515 \text{ MeV}) + ^{166}\text{Er}$ reaction the dynamical coupling increases the interaction times up to 15% for small l-values, whereas the deflection angles are decreased. This behaviour should be

typically for systems where the drift is directed to the symmetric configuration and thus induces a stronger attraction between the fragments during the collision. The longer contact time due to the dynamical coupling increases the mean values of the transferred mass towards the mass symmetry and gives larger variances σ_A^2 . At the same time the critical angular momentum is decreased by 5 .

In fig. 1 we compare the experimental element distribution with the calculated one within our dynamical approach. Good agreement is obtained for elements with charge numbers less than $Z_1 = 43$. The reason for the discrepancy for $Z_1 > 43$ in $d\sigma/dZ_1$, is that in our dynamical approach partial waves with $l_1 < 45$ are trapped into a potential pocket of the sudden interaction potential and thus are not scattered. It seems to be reasonable to assume that these trapped partial waves have available time to reach the mass equilibrium. If we further assume that this symmetric configuration decays through an adiabatic change of the interaction potential into two equal fragments rather than forms a compound nucleus an excellent agreement between the experimental and the theoretical element distribution

$$\frac{d\sigma}{dZ_1} = \left(\frac{d\sigma}{dZ_1} \right)_{DIC} + \left(\frac{d\sigma}{dZ_1} \right)_{eq} \quad (3)$$

is achieved. The upper assumption is supported by the fact that for this relatively heavy system the symmetric fragmentation is energetically preferred to that of the compound nucleus. Thus the second part in eq.(3) is practically identical with the equilibrium distribution for the whole phase space $P_{eq} \sim \exp(-U_1/T)$ with the driving potential U_1 and the nuclear temperature T of the system and a transition from the symmetric configuration to the compound nucleus became unlikely. The equilibrium contribution $(d\sigma/dZ_1)_{eq}$ looks like a "fast fission" process /4/, which have been assumed to appear if the fission barrier of the compound nucleus vanishes due to the high angular momenta transferred. Our analysis of the $^{86}\text{Kr}(515 \text{ MeV}) + ^{166}\text{Er}$ data indicate that a long lived component in the element distribution may occur even for non-vanishing fission barrier due to energetical reasons. In any case the dynamical coupling between relative motion and mass transfer suggests such a interpretation of the element distribution for the $^{86}\text{Kr} + ^{166}\text{Er}$ system although a more detailed investigation of this question is needed.

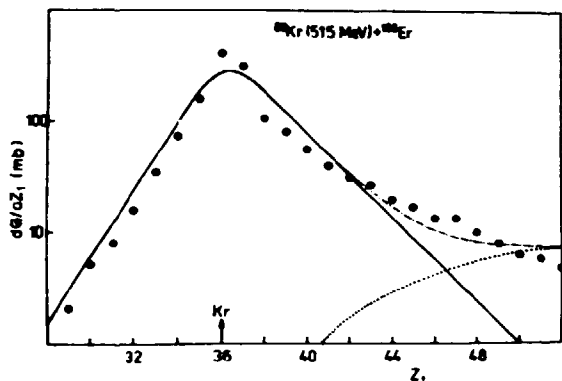


Fig. 1

Element distribution $d\sigma/dZ_1$, in the $^{86}\text{Kr}(515 \text{ MeV}) + ^{166}\text{Er}$ reaction. The experimental points are the data of Olmi et al. /5/. The solid curve corresponds to the (non-equilibrium) distribution for the deep inelastic fragments calculated within the dynamical model. The dotted line represents the equilibrium distribution for the trapped waves and the dash-dotted line is the sum of the solid and dotted curves.

References

1. W. Nörenberg, Phys. Lett. 52B(1974)289
2. L.G. Moretto and J.S. Sventek, Phys. Lett. 58B(1975)26
3. R. Schmidt and R. Reif, J. Phys. G 5(1979)L181
4. G. Gregoire et al., preprint DPh-N/MF/79/33 Saclay(1979)
and C. Ngo, ESINS-Conference Dresden(1980)
5. A. Olmi et al., Phys. Rev. Lett. 41(1978)688

MODEL CALCULATIONS OF FAST-NEUTRON INDUCED REACTION CROSS SECTIONS

M.Herman, An Jong Do, A.Marcinkowski
Institute of Nuclear Research, 00-681 Warsaw, Hoża 69

Abstract

Statistical model of multistep nuclear reactions with the inclusion of compound nucleus and preequilibrium emission is presented. Full gamma cascade and angular momentum conservation are incorporated in both mechanisms. The results are compared with some experimental cross sections for (n, xn) reactions. Suggestions on spin distribution of intermediate states are drawn.

1. Introduction

It is well known that a major part of the neutron absorption cross section is governed by the decay of compound nucleus. This was investigated for a long time with Hauser-Feshbach theory with a considerable success. However in last years a significance of preequilibrium emission has been undoubtfully pointed out. Thus it turns out necessary to include both mechanisms in theoretical calculations. Furthermore a detailed reaction analysis /e.g. isomeric cross sections interpretation/ requires theoretical estimates for the populations of discrete levels with defined spin and parity. This can be achieved solely if full gamma cascade is taken into account and angular momentum conservation is incorporated in both mechanisms. Unfortunately no theoretically founded preequilibrium model involving angular momentum effects exists. Some approximations were made in the frame of exciton model by Uhl et al.¹⁾ and Fu²⁾. Hereafter we propose a different approach to meet requirements mentioned above.

2. Formulation of the model

The preequilibrium emission is supposed to compete with compound nucleus decay only at first stage of the reaction while subsequent particles are emitted from the nucleus which has already equilibrated. It is further assumed that both mechanism contributions add up incoherently.

The compound nucleus decay is followed according to Hofmann, Richert, Tepel and Weidenmüller theory^{3,4)} accounting for the width fluctuation correction. The theory was recently improved⁵⁾ with the new formula for elastic enhancement factor which allows for more accurate treatment of the radiation channels. In the present model E1, E2 and M1 transitions are considered. They form a full gamma cascade within unbound as well as bound states and provide an occupation for the residual nuclei discrete levels. The radiative strength function is evaluated on the basis of Brink-Axel model⁶⁾ with allowance for Weisskopf estimate admixture. Highly excited states are approximated by the continuum calculated according to Gilbert-Cameron⁷⁾ or parameter free superconductivity model⁸⁾.

The preequilibrium emission is followed in the frame of geometry dependent hybrid model⁹⁾. In this model the emission probability is dependent on the incoming particle impact parameter through approximated reaction geometry considerations. This feature allows to treat each partial wave separately and to perform an angular momentum coupling of incoming particle spin S_a and orbital momentum l_a through target spin S_T and composite nucleus spin I to total angular

momentum of outgoing particle j_b and residual nucleus I_b . This can be written in the following form

$$\frac{d\sigma(E, I_b)}{dE} dE = \pi \lambda^2 \sum_I \sum_{J_b} \sum_{S_b} \sum_{I_a} g_I T_{I_a} \sum_n S_l(E, n) \cdot \frac{\sum_{I_b} \sum_{J_b} T_{I_b}^{j_b} \omega_{n,I_b}(U, I_b)}{\sum_{I_b} \sum_{J_b} \sum_{I_b} T_{I_b}^{j_b} \omega_{n,I_b}(U, I_b)} dE$$

where $S_l(E, n)$ is usual emission probability of hybrid model and g_I is statistical spin factor. All the sums satisfy the selection rules. The first term in this expression provides the energy dependence of the population of the residual nucleus levels while the second one describes the spin distribution of the preequilibrium component. The latter one is assumed to be proportional to the transmission coefficients $T_{I_b}^{j_b}$ and n -exciton states densities $\omega_{n,I_b}(U, I_b)$. At the moment the spin distribution of these states is an open problem. However the assumption of the spin dependence factorization is very likely to be valid and can be written in the form:

$$\omega(U, I) = \omega(U) \cdot \frac{2 I + 1}{2(2\pi)^{1/2} \Delta_n} \exp \left[- \frac{(I - I_0)^2}{2\Delta_n^2} \right]$$

It is assumed that energy behaviour of the spin cut-off parameter Δ_n for the exciton states is the same as the one for compound nucleus providing a simple relation

$$\Delta_n = a \Delta_{comp}$$

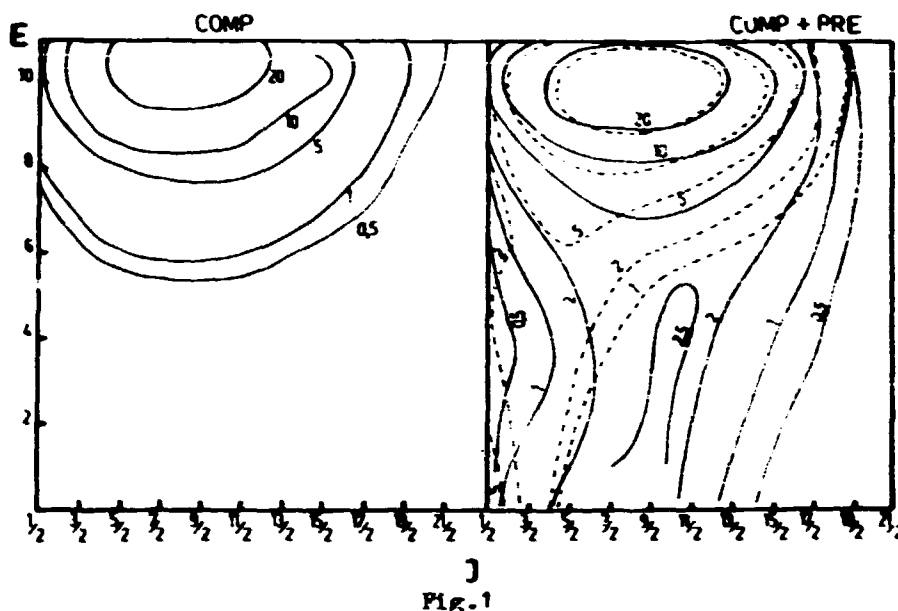
where 'a' is a free parameter. It is taken to be independent of the exciton number to keep the calculation time within a reasonable limit. This simplification seems to be justified because the dominant part of the preequilibrium emission comes from the very early stages of equilibration process. Thus "a" parameter can be treated as an average weighted with the contribution of a given exciton configuration.

3. Results

All the calculations were performed with the EMPIRE code ¹⁰⁾ on CYBER 73 computer. Brink-Axel model was used to evaluate the strength of E1 transitions while E2 and M1 transitions were calculated according to Weisskopf estimates retarded by the factor of 10. The level density parameters were those of Reffo ²¹⁾ and were tested against capture cross sections in the previous paper ¹¹⁾.

The preequilibrium emission modifies the population of the first residual nucleus continuum as compared to pure compound nucleus predictions. In Fig.1 this comparison is shown for the $^{111}\text{Cd}(n, n')$ reaction. The influence of the exciton states cut-off parameter on the calculations is also indicated with full and dashed lines which correspond to $a=1$ and $a=0.3$, respectively. It is evident from Fig.1 that the decrease of the spin cut-off parameter results in the concentration of the preequilibrium contribution at low spin states.

In Fig.2 the predictions of the model are compared with the experimental cross sections for inelastic scattering. The pure compound nucleus predictions are also presented in the figure /dashed line/ to indicate the relative contribution of both mechanisms. For Cd and Ag isotopes "a" parameter was taken equal



one in order to reproduce the data, while for heavy ^{190}Os nucleus a value of 0.4 seemed to be more suitable. These results suggest that spin cut-off parameters for exciton states and compound nucleus states are rather close each other.

Once "a" values have been extracted from the analysis of inelastic scattering an attempt was made to interpret the multistep reaction excitation functions. No parameter adjustment was employed in these calculations. Their results are shown together with the experimental data in Fig.3. It should be noticed that most of them concern the population of a discrete level with defined spin and parity thus sensitive to the gamma cascade and angular momentum coupling effects. The overall agreement is remarkable. Some deviations for Ir and Os isomeric cross sections can be probably ascribed to a insufficient information on the level scheme.

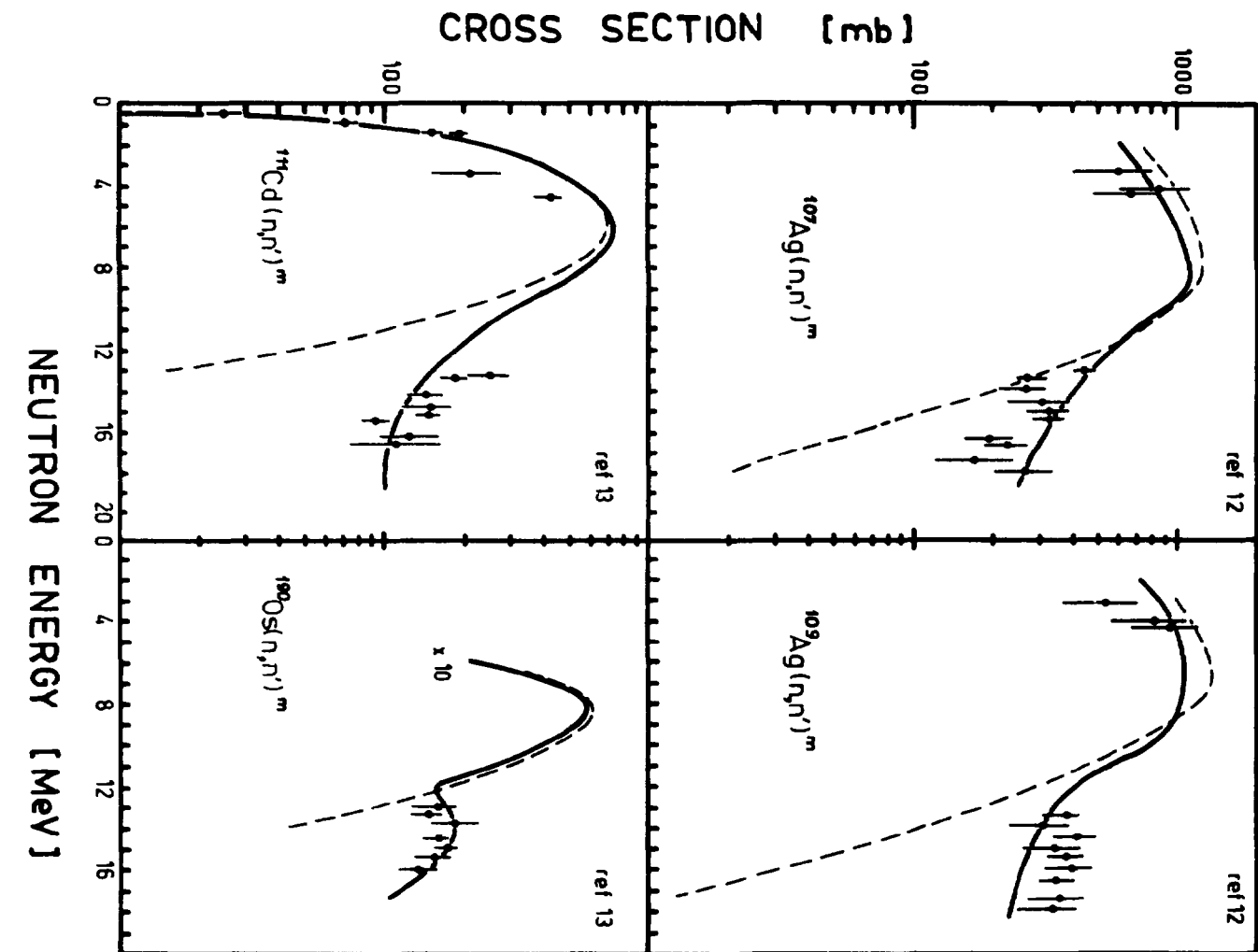


FIG. 2

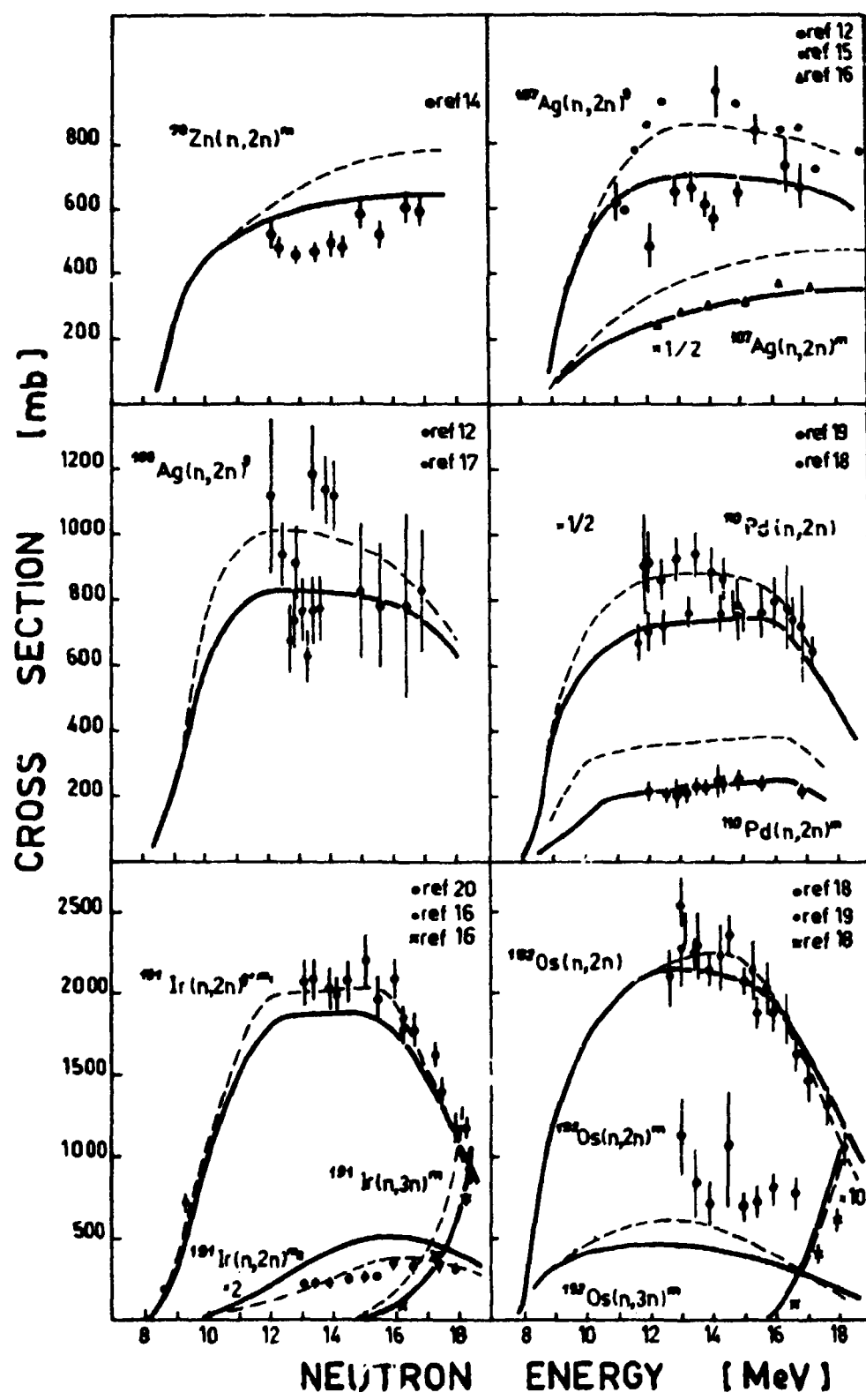


Fig. 3

References

1. M.Uhl, B.Strohmier, Course on Nuclear Theory for Applications, Trieste, 17 January - 10 February, 1978.
2. C.Y.Fu, BAPS 24/1979/884.
3. J.W.Tepel, H.M.Hofmann, H.A.Weidenmüller, Phys.Lett. B49/1974/1.
4. H.M.Hofmann, J.Richert, J.W.Tepel, H.A.Weidenmüller, Ann.of Phys. 90/1975/ 403.
5. H.M.Hofmann, T.Mertelmeier, M.Herman, J.W.Tepel, Z.Physik A297/1980/153.
6. P.Axel, Phys.Eev. 126/1962, '71.
D.M.Brink, Ph.D.Thesis, Oxford University, Oxford, England 1955.
7. A.G.W.Cameron, G.Gilbert, Can.J. of Phys.43/1965/1446.
8. W.Augustyniak, M.Herman, A. Marcinkowski, INDC /SEC/-61/LN p.266.
9. M.Blann, Nucl.Phys. A213/1973/570.
10. M.Herman, A.Marcinkowski, to be published
11. M.Herman, A.Marcinkowski, Nucl.Phys. in press
12. W.Augustyniak, M.Herman, A.Marcinkowski, Nucl.Phys. A247/1975/231.
13. M.Herman, A.Marcinkowski, J.Bielewicz, P.Oblozinsky, Nucl.Phys.A297/1978/335.
14. J.Dresler, U.Garuska, M.Herman, A.Marcinkowski, unpublished
15. L.A.Rayburn, Phys.Rev. 130/1963/731.
16. B.P.Bayhurst, J.S.Gilmore, R.J.Prestwood, J.B.Wilhelmy, N.Jarmie, E.H. Erkkila, R.A.Hardekopf, Phys.Rev. C12/1975/451.
17. P.Cuzzocrea, E.Perillo, S.Notarrigo, Nuovo Cim. 54B/1968/53.
18. W.Augustyniak, M.Herman, A.Marcinkowski, B.Zwięgliński, Nucl.Phys., A285/1977/145.
19. H.H.Bissegem, M.Borman, E.Magiera, R.Warnemünde, Nucl.Phys.A157/1970/481.
20. F.Iabri, G.Reffo, M.Herman, A.Marcinkowski, Proc. of the Sec. Int. Symp. on Neutron Induced Reactions, Smolenice, June 25-29, 1979, p.317.
21. G.Reffo, CNEN, Bologna, report RT/FI 78 11.

ОПРЕДЕЛЕНИЕ СЕЧЕНИЙ (n,α) -РЕАКЦИЙ НА ЯДРАХ СРЕДНЕГО ВЕСА В ОБЛАСТИ ЭНЕРГИИ НЕЙТРОНОВ 3 МЭВ МЕТОДОМ АКТИВАЦИОННОГО АНАЛИЗА

Г. Гельфер, У. Ян

Technische Universität Dresden, Sektion Physik; DDR - 8027 Dresden

М. Флорек, Я. Оравец, И. Сарка

Comenius University, Department of Nuclear Physics; CSSR - 81631 Bratislava

Аннотация

Методом активационного анализа проведены измерения сечений реакций (n,α) , вызываемых нейтронами с энергией ~ 3 Мэв в области ядер среднего веса. Для измерения наведённой активности использовался высокочувствительный детектор, работающий в режиме β - γ -совпадений. Определить $\sigma(n,\alpha)$ для ядра ^{55}Mn при $E_n \sim 3$ Мэв удалось впервые.

I. Введение

Вследствие (n,α) -реакций образуется гелий и возникает энергетический спектр ядер отдачи, что может вызывать изменения качеств облученного нейтронами вещества. Поэтому возможность возникновения дефектов в конструкционных материалах внутри быстрых реакторов имеет важное значение для вопросов безопасности, и знание об этом взаимодействии представляет большой интерес.

В области ядер среднего веса ($A = 20\dots 90$) главным механизмом протекания (n,α) -реакций является образование компаунд-ядра. Многочисленные исследования проводились нейtronами с энергией 14 Мэв. При энергии падающих нейтронов около 3 Мэв сечения (n,α) -реакций сравнительно низкие (по величине мбарн), так как α -частицы должны преодолевать кулоновский барьер составного ядра туннельным переходом. В настоящее время существуют лишь немногочисленные данные о (n,α) -реакциях в указанной области энергий нейтронов [1, 2]. Это связано и с тем, что плотность потока нейтронов, получаемых в нейтронных генераторах на основе реакции $D(d, n)^3\text{He}$ примерно на два порядка ниже плотности потока нейтронов из реакции $T(d, n)^4\text{He}$, являющейся источником нейтронов с энергией 14 - 15 Мэв.

II. Экспериментальная техника

В данной работе измерены экспериментально сечения (n,α) -реакций при $\bar{E}_n = (2,96 \pm 0,2)$ Мэв для ядер ^{69}Ga , ^{55}Mn и ^{51}V активационным методом. Источником нейтронов служил 500 кв-каскадный генератор Технического Университета Дрездена, Секция физики, с общим выходом нейтронов порядка $5 \cdot 10^8$ н/сек на 4π стер. (средний ток дейтонов - $250/\mu\text{A}$, ускоряющее напряжение - 400 кв, "толстые" D-Ti-мишени). При облучении исследуемые образцы находились под углом 0° отн. направления дейтонов, на расстоянии 1 см от мишени. Усреднённую по всей площади образца энергию \bar{E}_n нейтронов при выбранной нами геометрии эксперимента можно было определить только из расчёта.

Плотность потока нейтронов измерили 3 независимыми экспериментальными методами:

- активацией индия $^{115}\text{In}(n, n'\gamma)^{115m}\text{In}[\beta]$
- активацией серы $^{32}\text{S}(n, p)^{32}\text{P}$
- регистрацией протонов из сопутствующей реакции $\text{D}(\text{d}, \text{p})\text{T}$ при помощи полупроводникового детектора под углом 165° к направлению дейтонов в телесном угле $4 \cdot 10^{-5}$ стер. [4].

Сцинтиляционный счётчик и всеволновый счётчик служили как контрольные мониторы. В пределах ошибок все 3 метода давали согласующиеся величины для плотности потока нейтронов.

Использованные Ga-, Mn- и V-образцы имели форму

- круглого диска $\varnothing 5$ см толщины 1 мм сверхчистого галлия природного изотопного состава,
- кусочков одинаковой толщины марганца (100 % ^{55}Mn), полученных методом электролиза,
- порошкообразного ванадия (99,75 % ^{51}V).

Спектрометр для измерения наведённой активности, являющейся высокочувствительной и низко-фоновой детектирующей аппаратурой с телесным углом между образцом и счётчиками близким к 4π стер. [2], сконструирован на кафедре ядерной физики Университета им. Коменского, Братислава. Этот спектрометр работает в режиме β - γ -совпадений и состоит из двух сцинтиляционных счетчиков (75×75 мм NaJ с ФЭУ - 82), между которыми находятся два проточных счётчика (99 % Ag + 1 % пропан/бутан газ). В блок-схеме электронной системы есть один линейный сумматор в "г-части" спектрометра и один дискриминатор в " β -части", а также схема пропускания перед многоканальным анализатором, регистрирующим γ -спектры.

Проверка всей измерительной системы, включая определение самопоглощения γ -излучения и β -частиц в образцах, эффективного телесного угла регистрации и качества счётчиков и схемы совпадения проводилась при помощи известных нейтронно-индуктированных реакций $^{27}\text{Al}(\text{n}, \text{p})^{27}\text{Mg}$ и $^{27}\text{Al}(\text{n}, \gamma)^{28}\text{Al}$ при $E_n \sim 3$ Мэв. Эти реакции приводят к удобным временам полураспада дочерних ядер, в спектрах видны только изолированные γ -линии. Включение схемы β - γ -совпадений существенно улучшало фоновые условия.

III. Результаты

В данной работе получены следующие результаты при определении сечений реакций (n, α) при $E_n \sim 3$ Мэв [5]:

- $^{69}\text{Ga}(\text{n}, \alpha)^{66}\text{Cu} : \sigma < (17 \pm 13) / \mu\text{барн}$.
- $^{55}\text{Mn}(\text{n}, \alpha)^{52}\text{V} : \sigma = (10,4 \pm 2,8) / \mu\text{барн}$.
- $^{51}\text{V}(\text{n}, \alpha)^{48}\text{Sc} : \sigma \sim 1 / \mu\text{барн}$.

Несмотря на попытки сделать условия при облучении и измерении активности оптимальными, в случае ядра ^{69}Ga удалось получить только верхнюю границу сечения $\sigma(n, \alpha)$. Причиной является сопутствующие (n, γ)-реакции на обоих изотопах Ga.

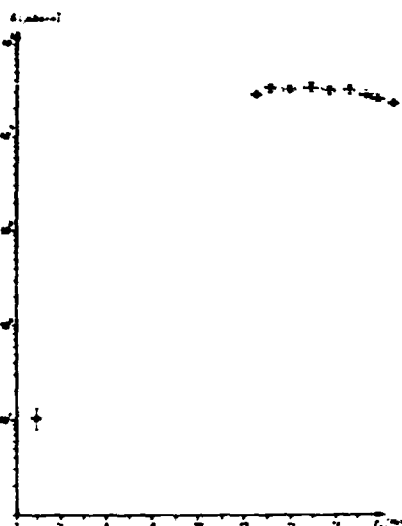


Рис. I Энергетическая зависимость сечения $\sigma_{\text{in}}(n, \alpha)$ в S_{2V}
 x - данная работа ($E_n \sim 3$ МэВ)
 • - данные из литературы
 ($E_n \sim 14$ МэВ)

не дает заметного вклада в результат, хотя сечение $\sigma(n,\alpha)$ при $E_n \sim 14$ МэВ много больше сечения $\sigma(n,\alpha)$ при $E_n \sim 3$ МэВ (рис. I). Влиянием медленных нейтронов также можно было пренебречь, что проверялось таким образом, что образец был обернут слоем кадмия.

Величина ~ 1 барн сечения $b(n,\alpha)$ для ядра $^{51}_{\Lambda}V$ не является верхней границей, а дает только порядок величины этого сечения. Лучшие результаты получить нам не удалось в связи с тем, что образец ванадия оказался у нас только два дня.

Особо следует подчеркнуть, что определить сечение $\sigma(n,\alpha)$ при $E_n \sim 3$ Мэв для ядра ^{55}Mn удалось впервые в этой работе (рис. I). Результаты других авторов а также теоретические оценки не опубликованы.

IV. Заключение

Проводилось тщательное экспериментальное исследование источников ошибок и других препятствующих факторов. В качестве примера указываем на то, что влияние образования $I4$ Нэв нейтронов в реакции $T(d, n)^4\text{He}$ на ядрах T из сопутствующей реакции $D(d, p)T$

Литература

- [1] J. Turkiewicz, Physics and Applications, Vol. 6 (1980) 13
 - [2] M. Florek et al., Physics and Applications, Vol. 6 (1980) 103
 - [3] J. Weber, M. Guillaume, Radiochem. Radioanal. Letters 1970
 - [4] A. Meister, Dissertation TU Dresden 1977
 - [5] U. Jahn, Diplomarbeit TU Dresden 1980

GAMMA - RAY MULTIPICITIES FROM $^{56}\text{Fe}(n,x\gamma)$ REACTIONS AT 14.6 MeV

R. Antalík, S. Hlaváč and P. Obložinský

Institute of Physics, Slovak Academy of Sciences
899 30 Bratislava, Czechoslovakia

γ multiplicities following emitted neutrons with energies 1 - 11 MeV as well as γ multiplicities of cascades passing through 3 specific transitions were measured. Special attention was paid to the effect of angular correlations. The data provide insight into decay modes of ^{56}Fe in a rather broad region of excitation energies. The discrepancies with the results of the advanced statistical model should be resolved in a specific experiment. The total γ spectrum measured in the continuous region up to 19 MeV provides an evidence about nonstatistical character of fast neutron capture.

1. Introduction

The present study is a continuation of our previous works^{1,2} on decay modes of highly excited levels populated in $^{56}\text{Fe}(n,x\gamma)$, $x=0,1,2$ reactions with 14.6 MeV neutrons. Here we deal mainly with the γ multiplicities obtained for various decay paths in the (n,γ) channel.

Decay path can be specified by a choice of gating condition. First, we choose the strongest γ -ray transitions which determined final steps of a cascade. Another choice was represented by the energy of scattered neutron thus locating a starting point of a cascade. As specific task for this type of measurement we deal in an approximate way with the problem of angular correlation.

Coincidence experiments, often requiring a great deal of patience, bring other rare fruits in a form of information about weak processes. We demonstrate it on (n,γ) spectra in the gamma energy region practically not studied so far.

2. Experimental arrangement and procedure

The arrangement is shown in fig.1. It essentially benefits from the idea of timing by means of associated α particles. Cylindrically shaped sample consisted of 400 g of pure natural Fe (91.7% ^{56}Fe). Pulse shape discrimination was applied for the NE 213 neutron time-of-flight spectrometer. The following spectra were recorded simultaneously. The Ge(Li) γ spectra in the mode singles and in the mode coincidences with the NaI(Tl) as well as the neutron spectra in both modes. The pulse height spectra from NaI(Tl) were stored in two-parametric pattern, time uncorrelated background was subtracted. The resulting spectrum was unfolded using the response functions.

The average multiplicities M were obtained from the relation

$$\frac{N_c}{N_s} = \sum_i \Omega_{E_i} = \sqrt{\frac{(\bar{M}-1)\Omega_{\bar{E}}}{\bar{M}\Omega_{\bar{E}}}} \quad \begin{array}{l} \text{when gated with } \gamma \text{ rays,} \\ \text{when gated with scattered neutrons.} \end{array} \quad (1)$$

Here, N_c and N_s stand for the coincidence and single counts observed in the gating detector. The total detection efficiency for the NaI(Tl) was determined experimentally and it was found to be nearly independent on the γ ray ener-

gy E. The average of the latter \bar{E} was extracted from the experimentaly observed spectrum.

Eq. (1) should be modified to account for the angular correlation between any of the γ rays emitted and the gating event. The general formalism for triple correlations³⁾ can, in principle, be applied here. In practice, however, the full formalism become extremly tedious to handle when several γ rays are emitted in a cascade and various decay paths are possible. Rather, we use physically transparent straightforward prescription where necessary simplifications are easier to apply.

Eq. (1) with angular correlation included can be written in the form

$$\frac{N_c}{N_s} = \sum_i \Omega_i \int 4\pi \sum_{\lambda_i \mu_i} (\vec{r}; \vec{\alpha}_i) P(\vec{r}; \vec{\alpha}_i) d\vec{\alpha}_i, \quad (2)$$

where $Z_{\lambda \mu}$ is intensity of the Poynting vector of the radiation field and $P(\vec{r}_0; \vec{\alpha}_i)$ is the normalized probability to find a spin of the state i oriented in the direction $\vec{\alpha}_i$ provided that the gating transition was emitted in the direction \vec{r}_0 . As the first approximation, the integral was evaluated under somewhat crude assumptions (i) the cascade is stretched and (ii) the orientation of spins in a course of a decay changes weakly. The explicit relations can be found in ref.⁴⁾.

To get feeling about the approximation made, we show in the lower part of fig. 2 the angular distributions of γ rays emitted in the $(n, n\gamma)$ channel. Calculated distribution for $2^+ \rightarrow 0^+$, 847 keV, transition is compared with the experimental data⁵⁾. The sum of the stretched cascade along the spin trajectory $5 \rightarrow 4 \rightarrow 3 \rightarrow 2 \rightarrow 0$ is compared with the exact result of ref.⁶⁾. The triple angular correlations demonstrated in the upper part of fig. 2 suggest that our geometry (note the heavy triangle) is rather advantageous for the γ gating, the correction to be applied is a few percent only. The multiplicities gated with neutrons should be increased by more than 10%. Additional measurement with the NaI(Tl) detector in the geometry "below" the plane ($\theta_{NaI} = 90^\circ$) is proposed to find the real amount of the effect discussed. For the time being we report the average γ multiplicities obtained from eq. (1) only.

3. Discussion

Theoretical analysis was performed in a frame of the advanced statistical model. The code STAPRE⁷⁾ modified to calculate γ multiplicities was used. The code incorporates preequilibrium emission of the first nucleon and realistic decay schemes when available. Statistically emitted γ supposed the strength function of the giant dipole type. The Γ_γ width was normalised to 2 eV at the neutron binding energy $B_n = 11.2$ MeV. For more details see refs.^{1, 2)}.

The average γ multiplicities gated with one of 3 strongest low lying transitions in ^{56}Fe are summarised in tab. 1. Accord with theoretical values is rather good. We note that contribution from direct particle feeding of low lying levels should decrease theoretical values. The experimental values of \bar{M} combined with the observed feedings of discrete levels reported earlier¹⁾ can be used to estimate the direct feedings. For 2_1^+ level it gives 120±70 mb.

The experimental average γ ray transition energy in $(n, n\gamma)$ channel was

Tab. 1.

Gate	M		
transition	keV	exper.	theor.
$2_1^+ + 0_1^+$	847	3.7(.3)	4.1
$4_1^+ + 2_1^+$	1238	4.5(.5)	4.5
$6_1^+ + 4_1^+$	1303	5.7(1.2)	5.4

found to be 2.8 MeV. More than 90% of the intensity of the inelastic γ ray cascades has its termination at the 847 keV level⁸⁾. This means that the effective excitation energy where from the γ decay starts is $E_{\text{exc}}^{(n,n\gamma)} = 10.4(.9)$ MeV.

The average γ multiplicities gated with scattered neutrons are shown in fig. 3. At the neutron energies below 3.5 MeV the multiplicities are influenced by the $(n,2n\gamma)$ channel. The theoretical curve refers to the ^{56}Fe target nucleus only. It is systematically above the experimental values in the pure $(n,n\gamma)$ region. As we have already shown, the angular correlations may well increase the data by more than 10%. The actual amount of this effect, however, remains to be solved.

The γ multiplicities related to the low neutron energies bring information on the region above the neutron binding energy. Preliminary analysis shows that at $E_{\text{exc}} = B_n + 1$ MeV it is $\langle r_\gamma / r_{\text{tot}} \rangle \approx 0.5$ giving thus more γ competition than reported earlier⁹⁾.

The total γ ray spectrum is shown in fig. 4. Rather broad region of γ ray energies from 11 to 15 MeV was not studied so far. The result show that the statistical description of γ emission fails here rather completely. Multistep direct processes in fast neutron capture should partly account for the observed discrepancies.

The authors are indebted to Prof. M. Blažek for his support of this work.

References

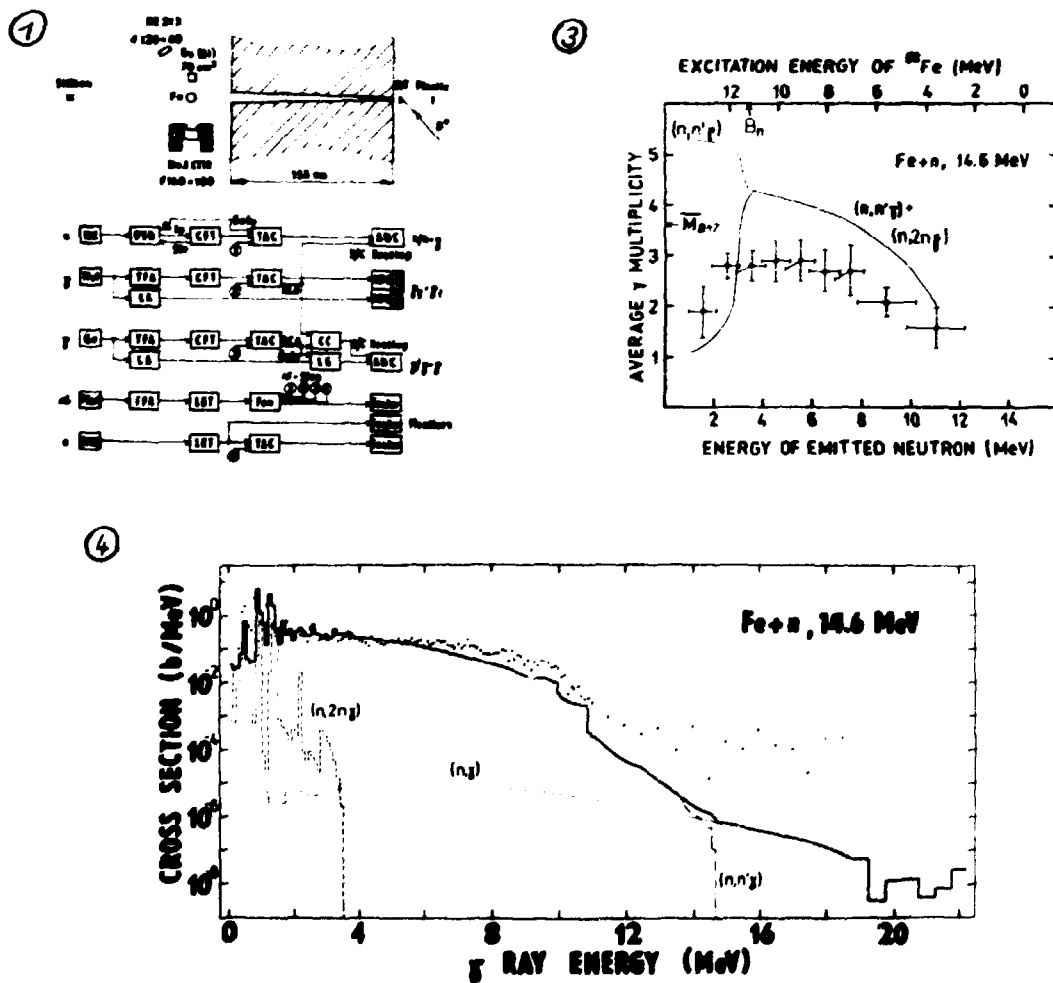
- 1) R. Antalík, S. Hlaváč and P. Obložinský, in Neutron Induced Reactions (ed. I. Ribanský and E. Běták, VEDA, Bratislava 1980) p. 277
- 2) R. Antalík, S. Hlaváč and P. Obložinský, contributed paper to the 5th All-Union Soviet Conference on Neutron Physics, September 15-19, 1980, Kiev (in Russian)
- 3) A. J. Ferguson, Angular Correlation Methods in Gamma-Ray Spectroscopy, (North-Holland, Amsterdam 1965) p.60
- 4) S. Y. van der Werf, Nucl. Instr. Meth. 153(1978)221
- 5) A. P. Degtjarev, Ju. E. Kozyr and G. A. Prokopets, Ukr. J. Phys. 22(1977)1464 (in Ukrainian)
- 6) H. Morinaga and T. Yamazaki, In-Beam Gamma-Ray Spectroscopy (North-Holland, Amsterdam 1976)p.59
- 7) M. Uhl and B. Strohmayer, code STAPRE, Report IRK 76/1, Vienna 1976
- 8) V. Corcalciuc, B. Holmqvist, A. Marcinkowski and G. A. Prokopets, Nucl. Phys. A307(1978)445
- 9) G. Stengl, M. Uhl and H. Vonach, Nucl. Phys. A290(1977)109

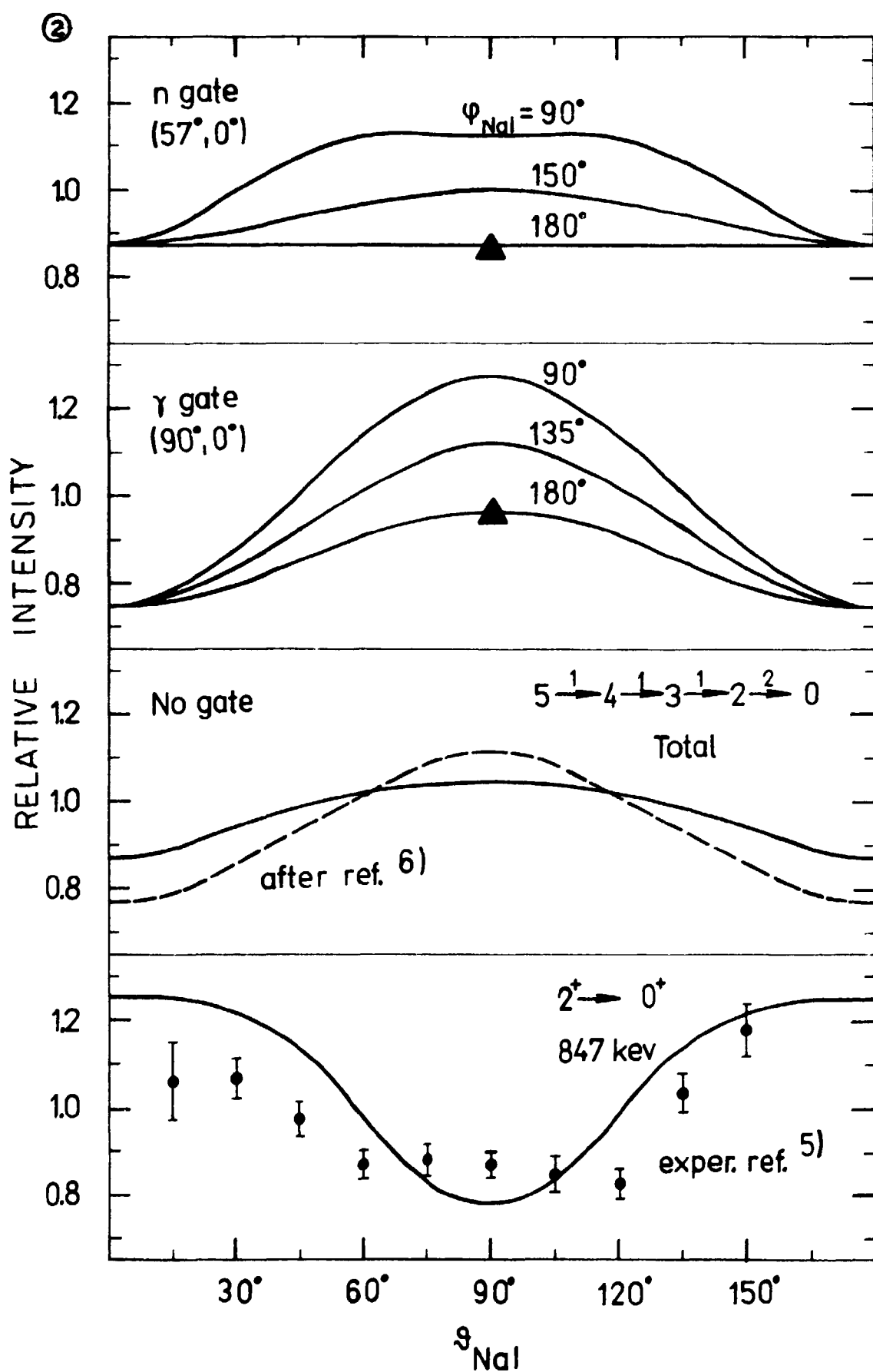
Fig. 1. The experimental setup and the simplified block diagram of electronics.

Fig. 2. The angular distributions calculated for various experimental situations. Simple distributions are shown for $2^+_1 \rightarrow 0^+$ transition and for the sum of all transitions. The upper curves include gating detector. The heavy triangles mark our experimental situation.

Fig. 3. The average γ multiplicity versus the energy of emitted neutron. The theoretical curves refer to the ^{56}Fe target nucleus only.

Fig. 4. The γ -ray production cross sections. The theoretical curves refer to the ^{56}Fe target nucleus only.





INVESTIGATION OF $^{28}\text{Si}(n,\alpha)$ ^{25}Mg IN TERMS OF STATISTICAL AND DIRECT REACTION MECHANISMS

D. Hermsdorf

Technische Universität Dresden, Sektion Physik
8027 Dresden, DDR

A reasonable and consistent interpretation of the experimental data available for neutron-induced α -particle-emission can only be achieved by taking into account direct reaction contributions. Using a direct ^3He -pick-up mode, spectroscopic factors for the lowest lying discrete levels of ^{25}Mg could be deduced.

1. Introduction

As has been shown formerly /1/ evaluated data for $^{28}\text{Si}(n,\alpha)$ available at present exhibits essential deviations. Furthermore, the data files are restricted to total excitation function mainly. Only the file MAT 1194 of the ENDF/B-general purpose library contains informations on partial excitation functions and angular distributions.

In contrast to this requests for angular and energy differential α -particle-emission data has been compiled in WRENDA for radiation damage calculations in fusion reactor design studies and for solid state physics applications.

The present work has been devoted to clarify discrepancies in experimental and evaluated data by use of a critical review of measurements and a consistent interpretation of the data in terms of nuclear reaction model calculations. The results will be incorporated in the file 2015 of the SOKRATOR library maintained by the CJD Obninsk.

2. Review of the experimental data base

Considering all measurements for $^{28}\text{Si}(n,\alpha)$ compiled in EXFOR and CINDA and the most recently published works the data base may be characterized as follows

- (i) a fairly good knowledge of excitation functions (n,α_i) ($i=0, 1, 2, 3, 4$) for the population of the lowest 5 discrete states in ^{25}Mg from threshold to about 20 MeV (see figs. 1 and 2);
- (ii) rare informations on total (n,α) excitation function above 7 MeV because of unknown contributions from α -transitions to highly excited states in ^{25}Mg (see fig. 3);
- (iii) scarce and contradictory measurements of angular distributions of the first few α -particle groups at 14 and 21 MeV /2, 3, 4, 5/ (see figs. 7, 8 and 9);
- (iv) no reliable α -particle-spectrum with an exception of an experiment at 14 MeV /6/ (see fig. 4).

Summarizing the situation the need for more precise angular distribution and total α -particle-emission spectra measurements should be emphasized.

Up to now $^{28}\text{Si}(n,\alpha)$ cross sections including angular distributions, spectra and excitation functions have not been subject of a systematical analysis in terms of different nuclear reaction models and data systematics. Therefore the present work was aimed to do this.

3. Reaction model calculations

3.1. Hauser-Feshbach-model

Preliminary results of the use of the Hauser-Feshbach-formalism to predict (n,α) -cross sections have been reported already /1/. Further improvements could be achieved by proper adjustment of level density parameters resulting in a reasonable description of the excitation functions from threshold up to about 10 MeV as can be seen from figs. 1, 2 and 3. Remaining differences between these results and the experimental material concerning mainly high energy tails of excitation functions and the asymmetry of angular distributions should be thought of due to other reaction mechanisms.

3.2. Exciton-model

The Exciton-model implemented in the code STAPRE /7/ was used to calculate contributions from pre-equilibrium emission of α -particles to excitation functions and spectra.

In order to compensate the reduction of compound-nucleus formation probability the strength of pre-equilibrium fraction parameterized in terms of the well-known relation for the matrix element $|M|^2 = FM \cdot A^{-3} E^{-1}$ yields a value $FM = 1\ 000$ MeV³ in accordance to a systematics found by Ribansky /8/. From fig. 4 it can be seen that pre-equilibrium α -particle emission doesn't influence the excitation functions of the first α -groups but only contributes to the more soft part of the particle spectrum to a very small extent.

However, the discrepancies mentioned above remain unexplained by this model.

3.3. Direct reaction model

Previous studies of direct reaction contributions to (n,α) start from knock-on processes /9/ or heavy-particle-stripping /6/ to explain the backward peaked angular distributions at 14 MeV /2, 3/ (see figs. 5 and 6).

In contradiction to those measurements more recent experimental results give strong evidence for forward peaked angular distributions /4, 5/ (see figs. 7, 8 and 9).

Following a systematics reviewed by Turkiewicz /10, 11/ the medium weight nucleus Si should exhibit direct reaction modes explicable by direct pick-up of 3 He-clusters. To investigate such a direct reaction mechanism calculations have been done using the coupled-channel-code CHUCK-II /12/.

The most problematic point in application of this code is the choice of optical potentials in the entrance (neutron) and exit (α 's) channel influencing strongly the structure and normalization of angular distributions. Well established potentials, which reproduce neutron and α -particle elastic scattering respectively, have been used /13, 14/. The bound state wave functions were calculated as eigenfunctions of a Woods-Saxon potential with a well depth adjusted to fit the separation-energy of a 3 He-particle whereas the interaction strength was assumed to be 487.2 MeV in a zero-range-approximation /12/.

In this picture excitation functions and angular distributions of the first 5 α -groups have been obtained.

4. Discussion of results

To compare the calculated data with experimental ones results of statistical and direct reaction model calculations have been superposed incoherently after a normalization of the direct contribution. This procedure has been performed independently in two ways

- the adjustment of direct contributions to the excitation functions (n_{α_i})
($i=0, 1, \dots, 4$) at about 20 MeV;
- the adjustment of this contribution to angular distributions at 14 and 21 MeV.

From this spectroscopic factors could be derived for the first 5 levels in ^{25}Mg which are compiled in table 1.

From this superposition following conclusions can be drawn in agreement with the general understanding

- (i) the direct contributions decrease with increasing excitation energy.
This can be illustrated using examples of angular distributions of the α_0 - and α_1 -group at 14 MeV (figs. 7 and 8)
- (ii) the direct contribution increase with increasing incident neutron energy.
This should be demonstrated using the α_0 -group angular distribution at 14 and 21 MeV (figs. 7 and 9)
- (iii) a consistent description of the available data including excitation functions and angular distributions can be achieved.

5. Conclusions

The attempt to interpret the experimental data base in an unique manner yields remarks on the reliability of experiments, evaluations and methods as follows

- (i) the experimental data by Leroux /2/ should be excluded from several aspects (experimental technique and form of angular distribution);
- (ii) Porti's results /3/ may be wrong due to a false assignment of α -groups-energies seen in the α -particle-spectrum (fig. 4);
- (iii) the normalization of Bohne's results /5/ for the excitation function of the α_0 -group should be improved using the slope derived from other experiments (fig. 1);
- (iv) in this model used here a backward peaked angular distribution is impossible but also a sharp peaked forward scattering of α -particles seen in Morgenstern's data /4/ at 14 MeV may not be explicable (see figs. 7 and 8);
- (v) the evaluation of ENDF/B-IV library may be improved in angular distributions mainly and should be extended to α -particle spectra;
- (vi) the success of this methods presented here should be tried to transfer to reactions like $^{29}\text{Si}(n,\alpha)$ and $^{29}\text{Si}(n,d)$ for which also only sparse informations can be found. Such work is in progress.

References

- /1/ D. Hermendorf, L. Neumann, Proc. IXth Symp. on Interaction of Fast Neutrons with Nuclei, Gaußig, 1979, ZfK-410, 1980, p. 147
/2/ B. Leroux, J. Dalmas, Ph. Th. Doan, Ph. Le Thanh, R. Chastel, Nucl. Phys. 67 (1965) 333
/3/ P. Forti, E. Gadioli, A. Marini, Nuov. Cim. 41 A (1966) 52
/4/ H. Morgenstern, D. Hilscher, J. R. Scheer, Nucl. Phys. 83 (1966) 369
/5/ W. Bohne, D. Hilscher, H. Homeyer, H. Morgenstern, J. R. Scheer, Nucl. Phys. A111 (1968) 417
/6/ P. Forti, E. Gadioli, A. Marini, Nuov. Cim. B1 (1966) 244
/7/ M. Uhl, B. Strohmaier, IRK.01/76, 1976
/8/ I. Ribanský, Š. Gmuca, Proc. 2nd Int. Symp., Smolenice, 1979, Physics and Applications, Vol. 6, 1980, p. 221
/9/ J. N. Massot, E. El-Baz, J. Lafoncrière, J. de Physique 26 (1965) 527
/10/ J. Turkiewicz, Proc. 2nd Int. Symp., Smolenice, 1979, Physics and Applications, Vol. 6, 1980, p. 13
/11/ W. Trzaska, S. Burzyński, K. Rusek, A. Trciński, I. M. Turkiewicz, J. Turkiewicz, P. Zupranski, Proc. IXth Symp., Gaußig, 1979, ZfK-410, 1980, p. 22
/12/ P. D. Kunz, private communication, 1978
/13/ W. Pilz, D. Schmidt, D. Seeliger, T. Streil, Proc. 2nd Int. Symp., Smolenice, 1979, Physics and Applications, Vol. 6, 1980, p. 127
/14/ C. M. Perey, F. G. Perey, At. and Nucl. Data Tables, 17 (1976) 82

Table 1: Spectroscopic data relevant to and deduced from $^{28}\text{Si}(n,\gamma)^{25}\text{Mg}$ reaction

Level no.	E _x /MeV	I ^T	Transf. L	spectroscopic factor g
0	0.0	5/2 ⁺	2	0.040 \pm 0.010
1	0.5251	1/2 ⁺	0	0.007 \pm 0.003
2	0.9748	3/2 ⁺	2	0.005 \pm 0.002
3	1.611	7/2 ⁺	4	0.007 \pm 0.003
4	1.965	5/2 ⁺	2	0.010 \pm 0.003

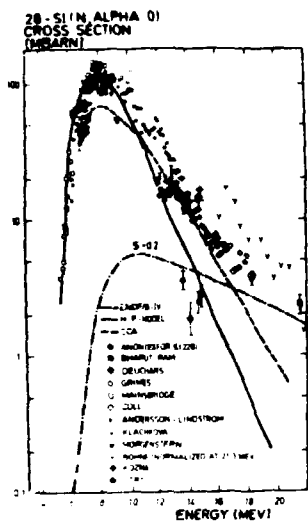


Fig. 1
Excitation function for $^{28}\text{Si}(n, \alpha)$.
The curves represent contributions
from statistical and direct reaction
calculations and the evaluation ENDF/B-IV

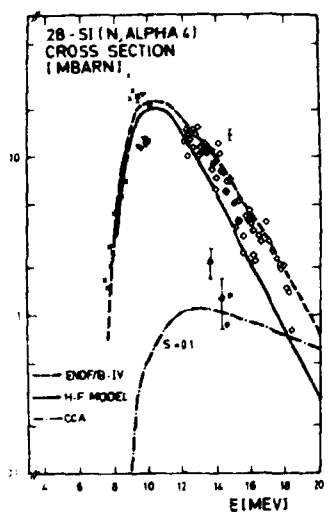


Fig. 2 Same as fig. 1 for
 $^{28}\text{Si}(n, d_4)$

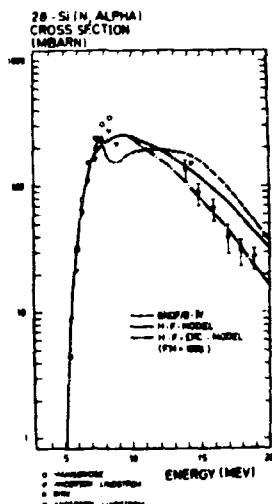


Fig. 3 Same as fig. 1 for
 $^{28}\text{Si}(n, d_2)$

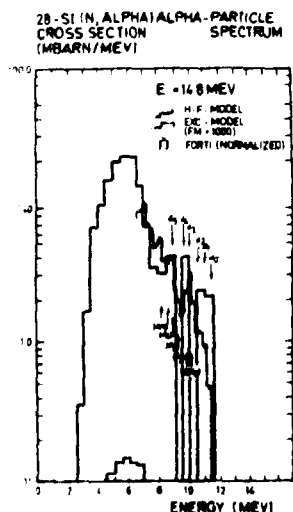


Fig. 4
Spectrum of α -particles emitted from
 $^{28}\text{Si}+n$ at 14.8 MeV neutron incidence
energy.
Calculations in the statistical model
are compared to experiments. α -transitions
to isolated states in ^{25}Mg are denoted
by arrows. Arrows in brackets corres-
ponds to Forti's energy calibration

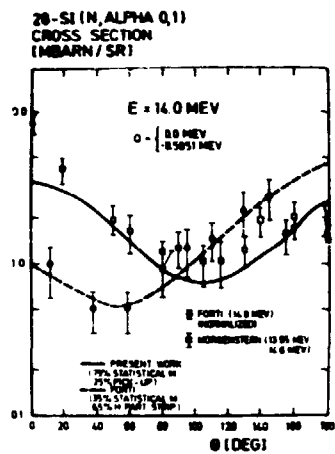


Fig. 5

Angular distribution of the $\alpha_0 + \alpha_1 -$
groups at 14 MeV.

The experimental data can be explained by a superposition of statistical and direct mechanism contributions.

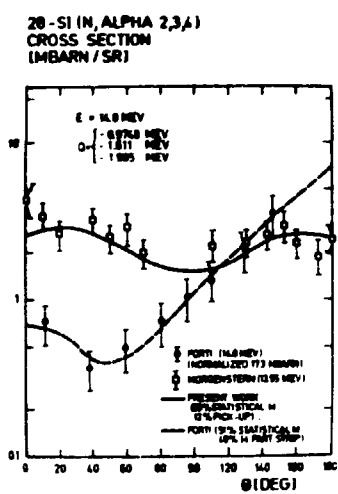


Fig. 6 Same as fig. 5 for the $d_2 + d_2 + d_2$ -groups at 14 MeV.

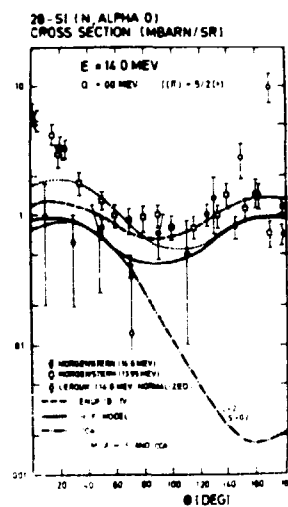


Fig. 7 Same as fig. 5 for the α -group at 14 MeV.

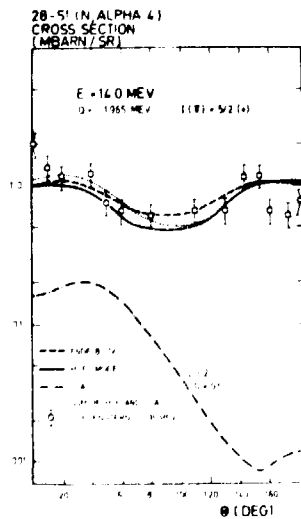


Fig. 8 Same as fig. 5 for the Δ_4 -group at 14 MeV:

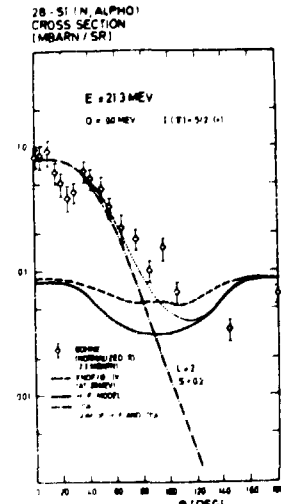


Fig. 9 Same as fig. 5 for the Δ -group at 21.3 MeV.

EXCITATION OF THE GROUND STATE BAND AND THE 3^+ NON-NORMAL PARITY STATE IN
28-SI BY NEUTRON INELASTIC SCATTERING AT INCIDENT ENERGIES BETWEEN 6.8 AND
14.8 MEV

D. Schmidt, D. Seeliger and T. Streil
Technische Universität Dresden, Sektion Physik, Dresden, GDR

Angular distributions to the 2_1^+ , 4_1^+ and 3_1^+ levels in the $^{28}\text{Si}(n,n')$ reaction had been measured at incident energies 6.8, 7, 8, 9, 10, 11, 12 and 14.8 MeV and have been analyzed. The best description of the ground state band in the frame of the collective model is obtained using a prolate quadrupole deformation with a negative hexadecapole component. The coupling between the 2_1^+ and 4_1^+ level can be neglected. The excitation of the 3_1^+ state can be understood as a spin-flip process by coupling to the ground state band.

1. Introduction

The direct excitation is known to give an essential contribution to the reaction mechanism in neutron scattering on low-lying states in the target nucleus. Especially for light nuclei the convenient model is the incoherent superposition of contributions calculated in the Hauser-Feshbach formalism and the collective model, respectively.

The topic of the present paper is restricted to the measurement and theoretical interpretation of excitation mechanism of the ground state band as well as the 3^+ state with non-normal parity coupled with this band in 28-Si. In the energy range from 6.8 to 14.8 MeV, different excitation modes are compared.

2. Experimental Procedure

The differential cross sections were measured with the tandem facility in the ZfK Rossendorf. A deuterium gas target using the $\text{D}(\text{d},\text{n})$ reaction was employed. The measurements were carried out with a computer-coupled multi-angle TOF-detector system consisting of eight detectors. The complete system and the monitoring method to obtain absolute cross sections are described in detail in ref. /3/.

At energies above 9 MeV the deuteron break-up will be remarkable and its neutron continuum is scattered also elastically. Therefore, the background increases for the neutron groups corresponding to higher excited levels.

3. Analysis of the Experimental Data

The aim of the theoretical interpretation is to show, that the incoherent superposition of compound and direct reaction contributions including multi-step processes describes sufficiently well the experimental data in the energy range called above.

For calculation of the compound reaction contribution in the Hauser-Feshbach model the computer codes ELIESE and STAPRE /5,6/ were used including proton and alpha channels, respectively, and the level continuum.

Two parameter sets were tested, firstly the spherical optical model parameters of OBST and coworker /7/. As pointed out in ref. /11/ and seen in fig.3, this potential gives too high Hauser-Feshbach contributions. Secondly, the potential

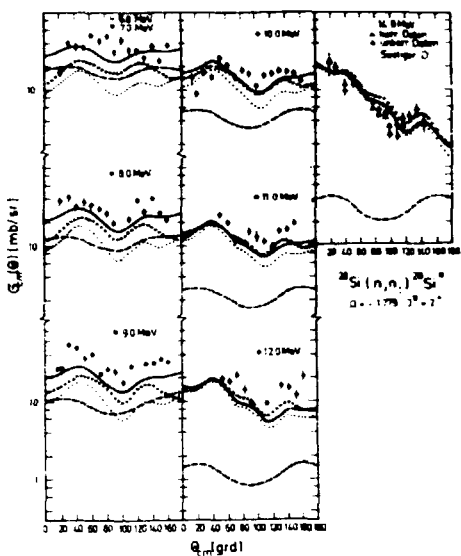


Fig.1

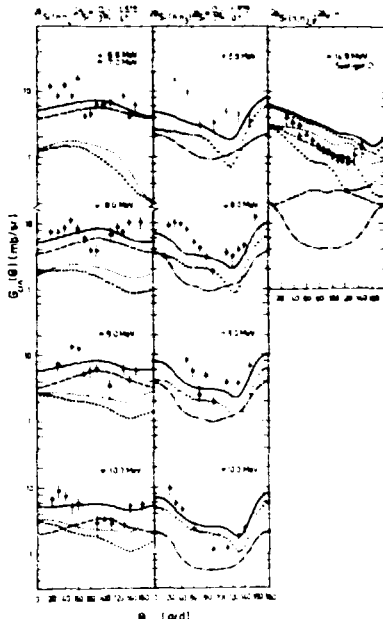


Fig.2

Fig.1 : Angular distributions to the 2_1^+ level.

The experimental cross sections (\downarrow , \uparrow) are shown with their absolute errors (- - - Hauser-Feshbach contribution, parameter set HF2; collective model in the coupled channels representation, parameter set CC2; $\times \times \times$ as curve , but only coupling $2_1^+-0_1^+$ and $3_1^+-0_1^+$ gs — sum of - - - and ; for parameters see table 1)

Fig.2 : Angular distributions to the 4_1^+ level.

(for notation see fig.1; the analysis of the 0^+ state will be reported later)

used in the coupled channels method with reduced imaginary part is chosen also for the Hauser-Feshbach calculation. The coupled channels method includes explicitly the inelastic channels, therefore the imaginary part of the optical model must be reduced. This energy-dependent potential was extracted by variation of the direct contribution to the first 2^+ state angular distributions. As seen, this reduction of the imaginary part gives a sufficiently good description /11/ (see figs. 1 and 4).

The direct reaction contributions were calculated with the coupled channels method using the code CHUCK /8/. For excitation of the ground state rotational band different deformation modes of the ground state have been taken into account.

Starting from the deformation parameters proposed by REIF /9/ the results in ref. /10/ show at 10 MeV incident energy a no sufficient description of the 2_1^+ and 4_1^+ level excitation.

An essentially better description gives a prolate (positive) quadrupole de-

formation with negative hexadecapole component, as shown in fig.1. The sum curve from Hauser-Feshbach part and coupled channels calculation including coupling of the 2_1^+ and 4_1^+ states, don't describe the experimental data sufficiently well in the backward-angle region. A quite better description can be obtained without coupling between the 2_1^+ and 4_1^+ states. Additionally, by using the energy-dependent imaginary part of the optical potential in the Hauser-Feshbach calculations the interpretation also at 7 and 8 MeV bombarding energy is sufficiently good.

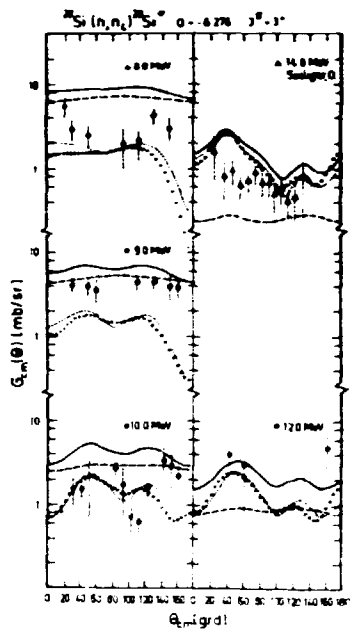


Fig.3

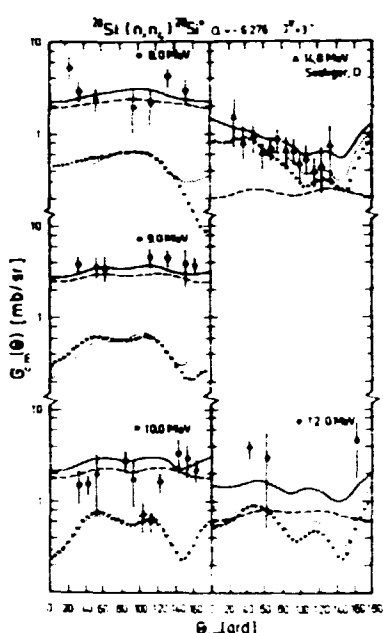


Fig.4

Fig.3 : Angular distributions to the 3^+ level.

(--- Hauser-Feshbach contribution, parameter set HF1; o o o collective model in the coupled channels representation, parameter set CC1; as curve o o o, but $V_{LS} = 0.0$; —— sum of curves --- and ; for parameters see table 1)

Fig.4 : Angular distributions to the 3^+ level.

(for notation see fig.1)

Fig.2 shows the analysis of the 4_1^+ state excitation using the parameter set CC2. Shape and magnitude of the angular distributions are caused mainly by the hexadecapole component. The best description is obtained also as for the 2_1^+ state without coupling between 2_1^+ and 4_1^+ states. The value of the hexadecapole component have been chosen with $B_4 = -0.30$ for the best description at 10 MeV bombarding energy. If the $2_1^+-4_1^+$ coupling is included, the angular distribution is more smoothed and the description will be wrong. Furthermore, the energy-dependent potential gives the right order of magnitude in the Hauser-

Feshbach part.

Table 1 : Optical Parameters

	$v_V/\text{MeV}/$	$r_V/\text{fm}/$	$a_V/\text{fm}/$	$w_S/\text{MeV}/$	$r_S/\text{fm}/$	$a_S/\text{fm}/$	$v_{SO}/\text{MeV}/$
SOM/7/ } HF1	52.0	1.15	0.78	12.1	1.25	0.47	4.9
CC1	52.0	1.15	0.78	$0.67 \cdot E - 0.8$	1.25	0.47	4.9(0.0)
HF2 } CC2 }	52.0	1.15	0.78	$0.57 \cdot E + 0.26$	1.25	0.47	4.9

The 3^+ state can be understood as quadrupole vibrational one excited from the ground state by a spin-flip process. Fig.3 shows the calculation with the parameter set CC1. But it can be seen that the angular distribution calculated at 14.8 MeV is not in good agreement with the experimental points. The influence of the spin-orbit coupling is very small.

An essentially better description is obtained using the CC2 parameter set for 14.8 MeV bombarding energy as shown in fig.4. The exclusion of the $2_1^+-4_1^+$, $2_1^+-3^+$ and $4_1^+-3^+$ coupling, respectively, influences weakly on magnitude and shape of the angular distributions. The main contribution of the spin-flip process comes in from the $l=2$ transition.

Using an energy-dependent imaginary part in the optical potential the description of the Hauser-Feshbach contribution will be better in a wide energy region, seen by comparison of figures 3 and 4.

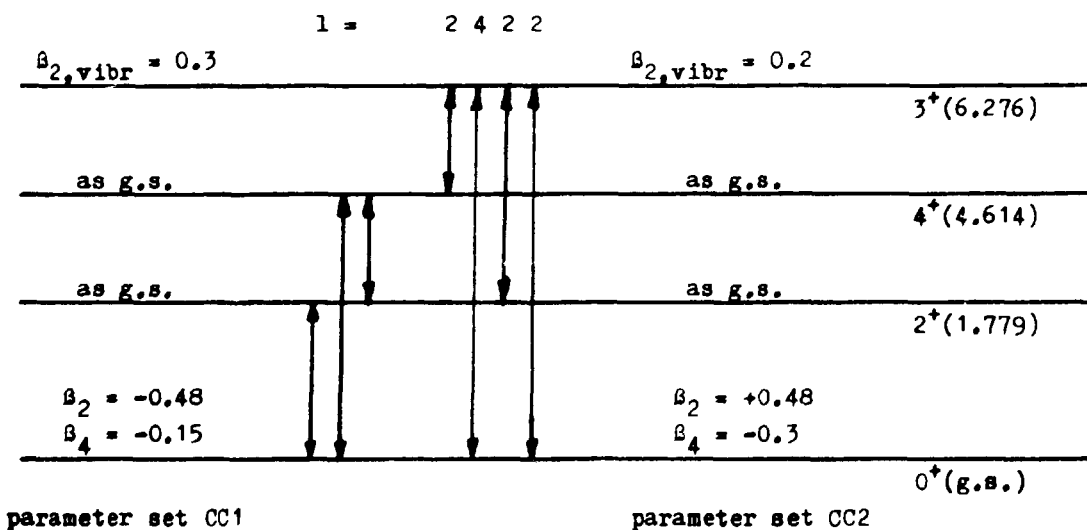


Fig.5 : Coupling Scheme

4. Conclusions

The analysis of the experimental data from the $^{28}\text{Si}(n,n')$ reaction in the energy range from 6.8 to 14.8 MeV shows the possibility to describe the ground state deformation in the frame of the collective model using coupled channels method with a prolate quadrupole deformation $B_2 = +0.48$ and a negative hexadecapole component $B_4 = -0.30$. For coupling of the ground state rotational band dominates the coupling to the ground state. The 3^+ non-normal parity state excitation can be understood as spin-flip process with the main contribution $l=2$.

An incoherent superposition of Hauser-Feshbach and direct reaction contributions can be applied using an energy-dependent imaginary part in a wide energy region.

5. References

- /1/ W.Pilz, D.Schmidt, D.Seeliger, T.Streil, Proc. of Conf. on Neutron Induced Reactions, Smolenice (1979) 127
- /2/ S.Mittag, W.Pilz, D.Schmidt, D.Seeliger, T.Streil, Kernenergie 22 (1979) 237
- /3/ P.Eckstein, H.Helfer, D.Kätzmer, J.Kayser, R.Krause, D.Lehmann, W.Pilz, J.Rumpf, D.Schmidt, D.Seeliger, T.Streil, Nucl.Instr.Meth. 169 (1980) 533
- /4/ D.Seeliger, thesis, Technische Universität Dresden (1961)
- /5/ G.Kießig, thesis, Technische Universität Dresden (1974)
- /6/ M.Uhl, B.Strohmaier, report IRK 76/01, Vienna (1976)
- /7/ A.W.Obst, J.L.Weil, Phys.Rev. C 7 (1973) 1076
- /8/ P.D.Kunz, University of Colorado, code CHUCK, unpublished
- /9/ H.-W.Barz, report ZfK-185, Rossendorf (1969)
- /10/ W.Pilz, D.Schmidt, D.Seeliger, T.Streil, report ZfK-410, Rossendorf (1980) 57
- /11/ D.Schmidt, D.Seeliger, T.Streil, Proc. of IV. Conf. on Neutron Physics, Kiev (1980), in print

EVALUATION OF γ -PRODUCTION CROSS SECTIONS OF NEUTRON - INDUCED REACTIONS IN Si

D. Hermsdorf, E. Paffrath

Technical University Dresden, Department of Physics
8027 Dresden, GDR

The paper reports on the calculation of γ -ray emission spectra and production cross sections resulting from neutron-induced reactions on all stable isotopes of Si by use of different theoretical methods of the γ -de-excitation of highly-excited nuclei. The intercomparison of theoretical and experimental data confirms the reliability of the γ -cascade-formalism included in the code STAPRE to predict unknown cross sections.

1. Introduction

At recent times requests for γ -ray spectra and γ -production cross sections resulting from neutron-induced nuclear reactions in Si has been strengthened and confirmed. The data need arise mainly from the radiation shielding aspects in fast breeder and thermonuclear reactor concepts /1/.

In contrast to the requirements the user will find scarce and inaccurate experimental data or strongly deviating sets of evaluated data included in ENDL-2 (MAT 7820) and ENDF/B-IV (MAT 1194).

Therefore, this work was aimed at a scanning of latest experimental results and an interpretation of the total data base in terms of theoretical models of nuclear reaction mechanisms including the γ -de-excitation mode of highly excited nuclei. For this, γ -ray spectra, excitation functions for discrete γ -transitions and γ -production cross sections for (n,γ) , $(n,n\gamma)$, $(n,\alpha\gamma)$, $(n,p\gamma)$, $(n,2n\gamma)$ and other one have been calculated for all stable isotopes of Si using relevant computer codes.

2. Theoretical methods

Recently a systematical investigation was carried out to prove the reliability of the γ -cascade-formalism included in the Statistical-Model code STAPRE /2/ for the prediction of γ -production cross sections. An excellent agreement between experimental data and the calculated one could be achieved by a proper adjustment of parameters necessary for description of particle transitions (transmission coefficients and nuclear level densities) and the γ -de-excitation (multipole-strength functions and γ widths)/3/.

Starting from a well-established parameter set, which fits the particle channels simultaneously /4/ radiation widths and the E1-strength have been varied to yield a reasonable interpretation of the experimental data base. Using these parameters γ -ray spectra and cross sections for (n,γ) , $(n,n\gamma)$, $(n,\alpha\gamma)$, $(n,p\gamma)$ and $(n,2n\gamma)$ have been calculated in the neutron incidence energy range from 1 MeV to 20 MeV.

Difficulties arise only in description of the neutron capture channel at low energies (below 100 keV) and above 10 MeV. The capture mechanism is known to

proceed via more direct processes above 10 MeV neutron energy.

To complete the calculations the code FISPRO /5/ has been applied to obtain contributions from the Direct-Semidirect-Model to the capture cross section. Furthermore, the direct contribution to the spectra of capture- γ -rays have been estimated in the frame of an Exciton Model for γ -ray emission developed by Prokopets /6/.

3. Results and Conclusions

All calculated data have been confronted with experimental one either in the natural abundance or in the natural composition in dependence on the experimental conditions.

Fig. 1 shows the neutron capture cross section for natural Si. Because of the poor experimental material any conclusions cannot be drawn concerning the reliability of the theoretical approach.

On the other hand the γ -transitions between low-lying levels in ^{28}Si excited by neutron inelastic scattering are reasonably well studied. Therefore the comparison between model predictions and experimental results yield information on the quality of parameters inherent in the theory used. An example is given in fig. 2.

No measurements exist on the continuous γ -ray spectra emitted by (n,γ) , $(n,p\gamma)$ and $(n,2n\gamma)$ reactions. Scarce data can be found for the effective $(n,x\gamma)$ reaction only, but this may be due to $(n,n'\gamma)$ and $(n,2n\gamma)$ reactions mainly. For this, differential as well as integral data are available at different neutron incidence energies from 2 to 20 MeV.

A typical spectrum for γ -rays emitted after nuclear reactions in natural Si induced by 13.8 MeV neutrons is shown in fig. 3 together with a calculation done by STAPRE. Finally fig. 4 presents the excitation function of the total γ -production cross section in Si.

Of course, the situation cannot be reviewed totally because of unknown or strongly discrepant data. But in the cases shown here the agreement between experimental and theoretical data is surprisingly good and confirms the reliability of the theoretical methods applied in the code STAPRE.

All data obtained in the present work will be part of the file 2015 of the so-viet nuclear data library SOKRATOR.

References

- /1/ WRENDA-Catalogue, INDC(SEC)-73/URSF, 1979
Nuclear Data for Fusion Reactor Technology, IAEA-TECDOC-223, 1979
- /2/ M. Uhl, B. Strohmaier, IRK-76/01, 1976
- /3/ B. Bassaragtscha, D. Hermsdorf, D. Seeliger, 2nd Int. Symp., Smolenice, 1979; Physics and Applications, Vol. 6, 381, 1980
- /4/ D. Hermsdorf, L. Neumann, 9th Int. Symp., Gaußig, 1979; ZfK-410, 147, 1980
- /5/ V. Benzi et al., RT/FI(69) 44, CNEN Bologna, 1969

/6/ V. A. Pluyko, G. A. Prokopets, 7th Int. Symp., GauBig, 1977; ZfK-376, 15, 1978

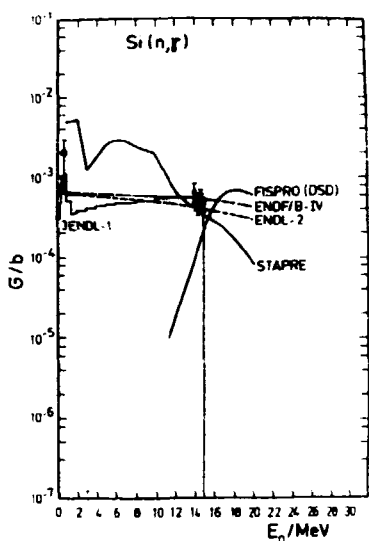


Fig. 1 Neutron capture cross section for natural Si. Experimental data will be compared with former evaluations and present calculations carried out by STAPRE and FISPRO.

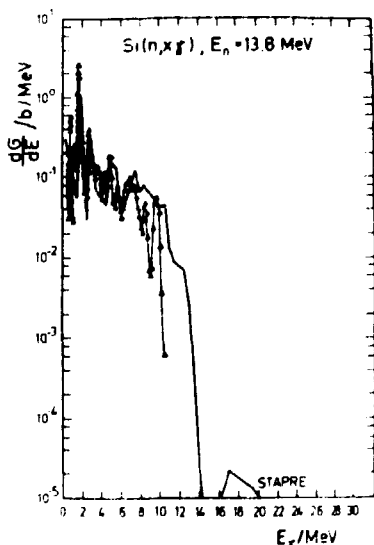


Fig. 3 Spectrum of γ -quanta emitted by natural Si following nuclear reactions induced by 13.8 MeV neutrons. Experimental data will be compared with calculated data.

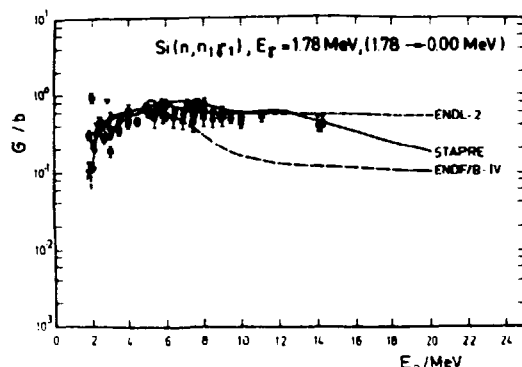


Fig. 2 Excitation for the emission of the 1.78 MeV γ -quanta resulting from the $2_1^+ \rightarrow 0_1^+$ transition in ^{28}Si . Experimental data will be compared with former evaluations and present results obtained by STAPRE.

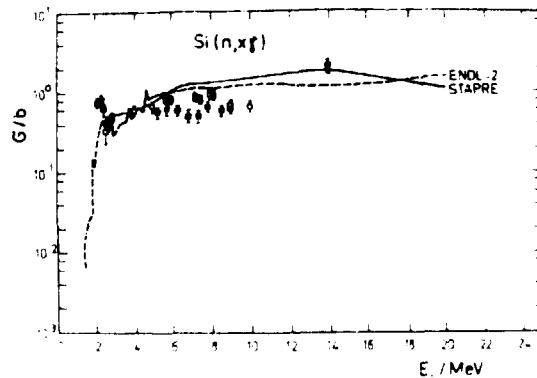


Fig. 4 Excitation function of the γ -production cross section of natural Si. Experimental data will be compared with former evaluations and present calculation.

СЕЧЕНИЕ РЕЗОНАНСНОГО ПОГЛОЩЕНИЯ НЕЙТРОНОВ ДЛЯ ГАЗООБРАЗНОГО UF_6 И ХИМИЧЕСКИЙ СДВИГ НЕЙТРОННЫХ РЕЗОНАНСОВ

К. Зайдель, А. Майстер
Технический Университет Дрезден, ГДР
Д. Пабст, Л.Б. Пикельнер, В. Пильц
ОИЯИ Дубна, СССР

I. Химический сдвиг нейтронных резонансов

Исследование химических сдвигов нейтронных резонансов было впервые проведено в ОИЯИ /I - 4/ на ядрах ^{238}U . Значение сдвига ΔE_0 описывается приближенно выражением

$$\Delta E_0 = \frac{Z_e^3}{6\epsilon_0} \Delta \rho(0) \cdot \Delta \langle r_p^3 \rangle \quad (1)$$

где $\Delta \rho(0)$ - разность электронных плотностей на месте ядра для пары химических соединений,

$\Delta \langle r_p^3 \rangle$ - изменение среднеквадратичного радиуса заряда ядра Z_e при переходе от основного к возбужденному состоянию ядра.

В реальном измерении величина ΔE_0 маскируется эффектом изменения формы резонанса при переходе от одного химического соединения к другому, что связано главным образом с различием в спектре колебаний кристаллических решеток. Можно экспериментальное значение сдвига записать в виде

$$\Delta E_0^{\text{эксп}} = \Delta E_0 + \Delta E_0^{\text{попр}} \quad (2)$$

где $\Delta E_0^{\text{попр}}$ - поправка, отмеченная выше. Ее вычисление было подробно рассмотрено в работе /2/ и основывалось на подходе Бенксаона и Линна /5/. Для точного описания формы резонанса была использована модель Нернга-Линдеманна, которая аналогична модели Энштейна, но распространена на два атомов U и X . Зависимый частотный спектр, т.е. спектр колебаний, связанных с атомами урана, имеет вид

$$g(hv) = a_1 \delta(hv - hv_1) + a_2 \delta(hv - hv_2); \quad a_1 + a_2 = 1; \quad (3)$$
$$hv_1 / hv_2 = \sqrt{m_X / m_U}$$

С помощью такой модели удалось хорошо описать различие в форме спектров для нескольких пар химических соединений урана. Однако при этом оставалось неясным, не является ли модель слишком грубой для точного описания резонанса, а в разностном спектре происходит компенсация систематических ошибок модели. Для проверки было предпринято измерение, в котором сравнивались спектры пропускания нейтронов для кристаллического образца UO_3 и молекулярного газа UF_6 .

2. Эксперимент

Измерение спектров пропускания по времени пролета для поликристаллического UO_3 и газообразного UF_6 при температуре $T = 373$ К проходилося на пучке импульсного реактора ИБР-3С, работавшем в бустерном режиме с линейным электронным ускорителем ЛУЭ-40. Чтобы обеспечить одинаковые экспериментальные условия, измерение велось с двумя мишенями, вводимыми в пучок поочередно на 5 минут. Каждый пятиминутный спектр контролировался по показаниям пучкового монитора с счетчика стар-

товых импульсов и при выполнении заданных условий постоянства добавлялся к хранящемуся в памяти ЭВМ ТРД-1 спектру данного образца. После этого в пучок автоматически вводился следующий образец. Весь тракт регистрации нейтронов обеспечивал возможность работы при мгновенных загрузках до $3 \cdot 10^5$ имп/сек, что было необходимо для получения достаточно высокой статистической точности спектров. Спектр для $^{238}\text{UF}_6$ в области 6,67 эВ-резонанс представлена в верхней части рис. I.

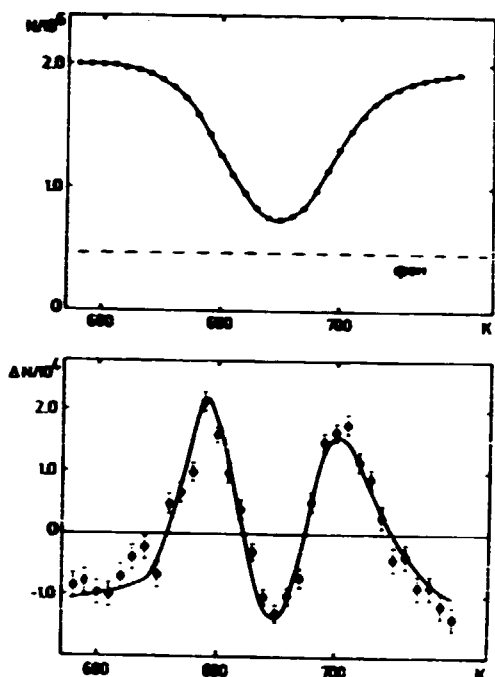


Рис. I
Вверху: экспериментальный спектр пропускания по времени пролета для 6,67 эВ-резонанса в $^{238}\text{UF}_6$ (точки) и результат расчета (сплошная кривая).
Внизу: разность экспериментальных спектров для $^{238}\text{UO}_3$ и $^{238}\text{UF}_6$ после подгонки (точки) и результат расчета (сплошная кривая).

3. Сечение резонансного поглощения нейтронов для молекулярного газа

Для вычисления сечения резонансного поглощения нейтронов в молекулярном газе необходимо учитывать движение молекул в целом и внутреннее возбуждение. Это сечение в зависимости от энергии E_n можно представить в виде

$$\sigma(E_n) = \sum_{\{n_i^0\}} W_{\{n_i^0\}} \sum_{\{n_i^1\}} \langle P_{\{n_i^0\}} \rangle \cdot \sigma_c(E_n, \Delta E_n) \quad (4)$$

$\{n_i^0\}, \{n_i^1\}$ - совокупности квантовых чисел молекулы до и после взаимодействия,

$W_{\{n_i^0\}}$ - вероятность состояния $\{n_i^0\}$

$P_{\{n_i^0\}}$ - вероятность перехода $\{n_i^0\} \rightarrow \{n_i^1\}$ при захвате нейтрона.
 $\langle \rangle$ означает усреднение по ориентациям молекулы,

$\sigma_c(E_n, \Delta E_n)$ - сечение для молекул, которые поглощают или испускают энергию

$$\Delta E_n = E_{n^1} - E_{n^0}$$

Для симметричных молекул типа X_n ($n = 2, 3, 4, 5, 6$), у которых ядро X поглощает нейтроны и находится в центре масс, оказывается возможным рассмотрение только колебательных переходов молекул и пренебрежение вращательными переходами /6/. Те нормальные колебания ω молекулы, которые связаны с движением ядра X , описываются с помощью совокупности квантовых чисел $\{n_{\omega}\}$. Вероятность перехода $\{n_{\omega}^0\} \rightarrow \{n_{\omega}^1\}$ при захвате нейтрона ядром X можно вычислить по формулам /6/:

$$\begin{aligned}
 P_{\text{abs}}^{(k)} = & \prod_{\{n_k\}} |K \Phi_{n_k}(Q_{n_k}) |^2 \exp[i k_x b_{n_k} Q_{n_k} m_x^{-1}] \Phi_{n_k}(Q_{n_k})|^4, \\
 K \Phi_{n_k}(Q_{n_k}) | \exp[i k_x b_{n_k} Q_{n_k} m_x^{-1}] \Phi_{n_k}(Q_{n_k})|^2 = \\
 = & Z_{n_k}^{(k-n_k)} \cdot \exp[-Z_{n_k} \cos \beta_{n_k}] \cos^{(k-n_k)} \beta_{n_k} \cdot \left(\frac{E_n}{h v_k} \right)^{\frac{1}{2}} (Z_{n_k} \cos \beta_{n_k})^2, \\
 Z_{n_k} = & \frac{E_n}{h v_k} \frac{m_k}{m_X + m_k} \cdot b_{n_k}^2
 \end{aligned} \tag{6}$$

Q_{n_k} - нормальная координата α -составляющей k -го нормального колебания,
 Φ_{n_k} - волновые функции линейного гармонического осциллятора,
 b_{n_k} - нормированное смещение ядра X из положения равновесия,
 k_x - волновой вектор нейтрона,
 L_{n_k} - присоединенные полиномы Лагенра,
 β_{n_k} - угол между направлением падающего нейтрона и направлением смещения ядра за счет α -составляющей k -го нормального колебания,
 $h v_k$ - энергия кванта k -го нормального колебания.

Молекула UF_6 имеет шесть нормальных колебаний. Однако в смещение ядра урана дают вклад только трижды вырожденные нормальные колебания ν_3 и ν_4 с энергией квантов $h v_3 = 0,0776$ эВ и $h v_4 = 0,0231$ эВ /7/.

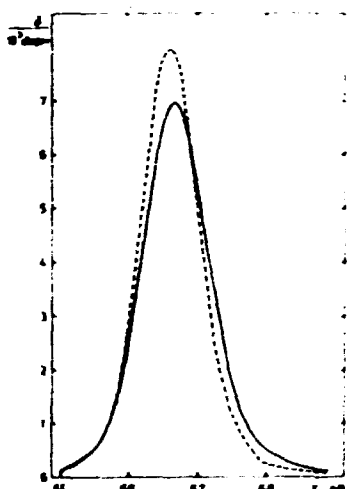


Рис. 2. Сечение резонансного поглощения для 6,67 эВ резонанса в $^{238}UF_6$ при температуре $T = 373$ К с учетом (сплошная кривая) и без учета (пунктирная кривая) возбуждения молекул.

На рис. 2 представлены рассчитанные сечения резонансного поглощения нейтронов для 6,67 эВ-резонанса в $^{238}UF_6$ с учетом и без учета внутреннего возбуждения молекул. Самое важное преимущество в случае UF_6 состоит в том, что расчет не содержит свободных параметров и что частоты колебаний хорошо известны.

Подобные расчеты для UF_6 выполнили Боуман и Брок /7/. Для их цели было достаточно относительно грубое приближение, а именно существенное ограничение числа яонов в начальном состоянии и пренебрежение процессами, которые связаны с поглощением нескольких яонов. Таких приближений нет в наших расчетах.

4. Результаты

Совмещение экспериментальных нейтронных спектров для UO_3 и UF_6 по методу наименьших квадратов /1/ дало $\Delta E_0^{\text{эксп}} = (118 \pm 66)$ мкэВ. Для определения $\Delta E_0^{\text{теор}}$ были рассчитаны теоретические спектры пропускания для кристаллической и газовой мишеней, которые хорошо описывают экспериментальные спектры (рис. I). Совмещение теоретических спектров тем же способом, что и экспериментальных дало

$\Delta E_0^{\text{теор}} = 139$ мкэВ. Разность теоретических спектров хорошо согласуется с разностью экспериментальных (те и другие после подгонки), как это видно из рис. I. Окончательный результат для химического сдвига $\Delta E_0 = (21 \pm 21)$ мкэВ. Ошибка включает статистическую ошибку эксперимента, а также все ошибки расчета, связанные с неточностью силовых постоянных и частот молекулы UF_6 и ошибок параметров колебаний UO_3 . Для перехода к $\Delta \langle r_p^2 \rangle$ согласно (I) нужно знать $\Delta g_e(0)$ для рассматриваемых UF_6 и UO_3 . Сейчас таких данных нет, но из одинаковой валентности этих соединений можно ожидать, что плотности электронов мало отличаются, а следовательно и ΔE_0 близко к нулю, что согласуется с полученным результатом.

Более существенным для нас является тот факт, что получено подтверждение достаточной точности описания сечения в области резонанса с помощью кристаллической решетки, применяемой в наших расчетах.

Литература

- /1/ Акопян Г.Г. и др. ОИЯИ, Р3-II740, Дубна, 1978.
- /2/ Зайдель К. и др. ОИЯИ, Р3-II741, Дубна, 1978.
- /3/ Зайдель К. и др. ОИЯИ, Р3-II742, Дубна, 1978
- /4/ Зайдель К. и др. ОИЯИ, Р3-80-135, Дубна, 1980.
- /5/ Jackson, H. J., Murr, S. J., Phys. Rev., 127(1962)491.
- /6/ Летохов В.С., Милогин В.Г. ЖЭТФ, 1976, 70/3, с. 794.
- /7/ Бондарев, С.А., Смирнов, А.А., Phys. Rev., 221(1969)50.
- /8/ Белянин В.С., Термофизические свойства гексафторидов урана и вольфрама, АН СССР, Москва, 1976.

ROTATING TARGET INTENSE NEUTRON GENERATORS

T. Sztericskai

Institute of Experimental Physics, Kossuth University
H-4001 Debrecen, P.O.Box 105, Hungary

Intense 14 MeV neutron generators with a yield of 10^{12} n/s are required not only in the fast neutron physics but by the CTR material program, neutron therapy, neutron radiography etc. The constructions of intense neutron generators were studied on the basis of published data. The paper gives a short survey on the technical problems and solutions of intense neutron generators are suited for the use in fast neutron physics.

1. Introduction

There is a growing interest over the world on 10^{12} n/s or higher yield fast neutron sources. These sources are mostly used in the applied nuclear physics, CTR material research and in the radiotherapy. There were published several reviews on this subject [1,2] excluding or including the plasma devices as 14 MeV neutron sources. The papers, describing the Cockcroft-Walton type accelerators based 14 MeV neutron source are in [3,4] and their technical solutions in [5]. The neutron sources needed in the CTR surface and material program are well described in [6]. A summary on the facilities used in the radiotherapy are in reference [7]. The technical evolution of intense sealed tube neutron generators is shown in [8]. Typical applications of intense 14 MeV neutron generators are shown on Fig. 1.

INTENSE 14 MeV NEUTRON GENERATORS IN		
CTR MATERIAL PROGRAM	RADIOTHERAPY	ACTIVATION ANALYSIS RADIOGRAPHY NUCLEAR PHYSICS
REQ.: 14 MeV peaked E_n , 10^{14} n/s flux	REQ.: E_n 10 MeV 15 rad/min /SSD of 1m/	REQ.: E_n =14 MeVx
Rotating solid targets, gas jet targets	Sealed tubes isocentric facilities	Solid tritium Rotating targets, d^+ or t^+ handled beam
Users: LLL, CEA, LASL Chalk River	Users: UK, USA, Germany, Saudi arabia, Switzerland	Users: LLL, AWRE, JAERI NRPB, Chalk River

Fig.1. Typical applications for intense 14 MeV neutron generators

A neutron source is called intense neutron source [3] if its neutron yield is about of higher than 10^{12} n/s. These monoenergetic, 14 MeV neutron sources are required by the neutron physical laboratories working on the nuclear data measurements needed for the fusion and fast reactor technology [9].

2. The setting up of intense neutron generators

The block diagram representation of an intense neutron generator shows in Fig. 2. not too much difference compared to an usual one. It involves d^+ ion source, an accelerating tube, beam handling facilities, tritium target and as serving facilities high voltage power supplies, vacuum and cooling systems as well as shielding and health physics facilities.

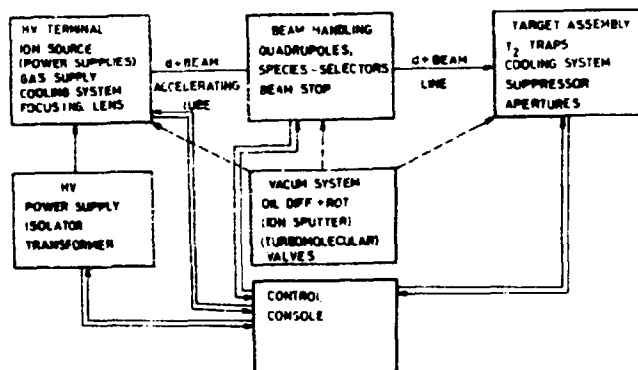


Fig. 2. Typical set-up of a 14 MeV neutron generator

The main technical problem related to the intense neutron generators is the tritium target. To get an intense 14 MeV neutron source, the target should be dissipate on the some millimeter diameter spot several kW beam power as it is required on the basis of specific neutron yield vs dissipation function in the Fig. 3. [10]. The figure shows the best efficiency for d^+ beam. The demands on monoenergetic 14 MeV neutron source should be reduced because the solid occluded tritium targets are strongly decaying with increasing temperature. The equilibrium hydrogen pressure vs temperature for Ti, Sc and Er hydrides are shown in Fig. 3. [10]. The use of thick tritium target with water cooling and thick target backing makes it evident, that every intensive neutron generator gives more broad 14 MeV energy line than a small thin ones with air cooling.

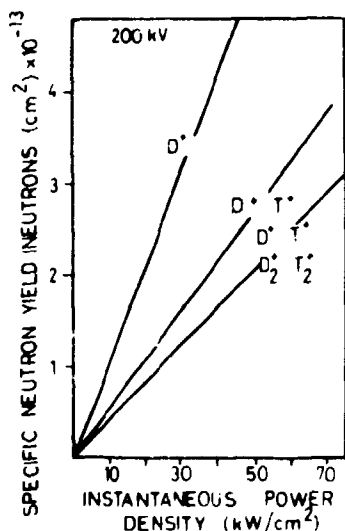


Fig. 3. The specific neutron yield vs dissipation for solid target

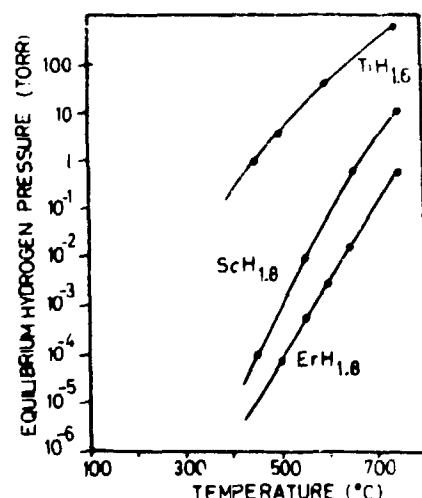


Fig. 4. The equilibrium hydrogen pressure vs temperature for Ti, Sc, Er

3. Ion sources and accelerating tubes

The typically applied ion source in an intense neutron generators is the duoplasmatron. The duoplasmatron and the some times used duopigatron [11] are giving suitable high ion current with proper beam shapes after extraction. The monoatomic ion ratio is a bit lower at the duoplasmatron, but a necessary ion species selection uses to be used on the beam line to the target. The duoplasmatron [12] has a good gas efficiency, gives about 75 % monoatomic ions and

there are many commercially available types. These commercial types are very similar in construction, there are breakable and domountable types too. The most significant difference is in their cooling, there are forced air, freon, water and oil cooled versions. A typical 30-100 mA beam current duoplasmatron dissipates 2-3 kW power and its cooling is technically problem on the high voltage terminal. A good cooling method is the closed circuit, heat exchanging, deionized water cooling with permanent pH monitoring and regulating. The duopigatrons deliver more monoatomic ions and their application is optimal over 100 mA beam current. The RTNS-II generator uses a modified version plasma source [13]. The large volume plasma source gives excellent uniformity [14] for large surface neutron sources for the CTR material program.

A small beam spot is available only by suitable focusing and beam handling facilities. The most commonly used focus system is the einzel-lens after the extraction of ions from the source. There are magnetic, static quadrupole lenses, magnetic long lenses etc. to get the available smallest beam profile at the target. The main problem is that the used 15-200 mA, 10-50 mm diameter beams are in the intermediate region of both space charge and space charge free ion optics. The most of calculations are made by non-space charge optical methods and the technical solutions are reflecting the space charge optics solutions. The reason for such designs is the insufficient knowledge of space charges and their effects on the accelerated beams.

ION SOURCE .

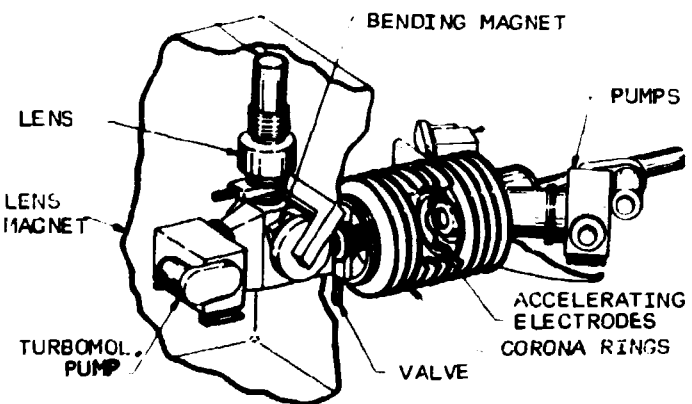


Fig.5. The ion species selection on the high voltage terminal of RTNS-II

The after extraction ion species selection on the HV terminal reduces the load of accelerating tube, but increases the power needed on the terminal. Ion selection is used before acceleration in the RTNS-II generator [16] and it is planned in Bratislava [17]. A magnetic ion selection after acceleration is in use at the commercially available, SAMES produced intense neutron generator in Harwell at NRPB [18]. A magnetic-electrostatic separator /Wien-filter/ is designed in Debrecen [19]. The lay-out of a part of RTNS-II beam line at the end of ion source is shown on Fig.5.

There are four companies producing intense pumped neutron generators. All of them; the SAMES, the HIGH VOLTAGE ENG., the GENERAL IONEX and the RADIATION

DYNAMICS are selling 10^{12} n/s yield generators with 10-40 mA target currents. All of these manufacturers adopted their homogenous field, multigap accelerating tubes from other own generators. All of in research institutes developed tubes are single gap accelerating tubes with field dividing, the isolator rings shielding electrodes. The typical field in the accelerating gap is between 15-25 kV/cm. These structures are used at the LANCELOT [20], in CHALK RIVER [21], at the INTTF in the SANDIA Lab. and is under construction in Debrecen [5,19]. Designed a strong focusing, space charge effects regarding one gap accelerating tube at Debrecen is shown on Fig. 6 on the basis of [19]. A Pierce-geometry accelerating tube is in use at a differentially pumped tritium gas target neutron generator in Madison [22].

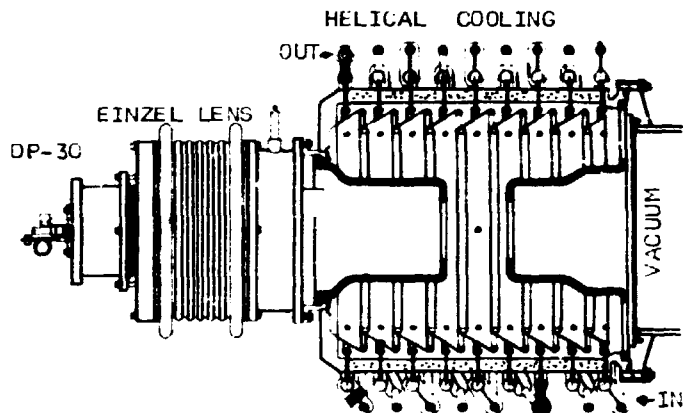


Fig.6. A typical single gap accelerating tube for intense neutron generator

4. Beam handling

The accelerated 10-200 mA d^+ beams show some space charge effects, so the enlargement of them should be prevented. The simplest solution is the use of a long solenoid lens along the beam as it is at the LANCELOT [20]. In the case of longer beam lines there are applied several magnetic or static quadrupoles. The RTNS-II generator has three quadrupole triplets on a several meter long beam line as it is shown on Fig.7 by the artist's representation of the generator.

The Debrecen generator shall use electrostatic quadrupole quartet [19] after acceleration. The NRPB's SAMEs manufactured generator has two magnetic quadrupole doublets on a six meter long beam line [18]. Although the water cooled diaphragmas are reducing the target current, they are utilized in every case if a small diameter beam spot is needed.

5. The rotating targets

Rotating disc target assemblies are manufactured for intense neutron generators by MULTIVOLT LTD of Crawley [23] or by NUKEM GmbH [24]. A NUKEM target assembly consists of several usual 1.10^{12} - 2.10^{12} Bq activity 30-50 mm diameter TiT targets, the MULTIVOLT targets are 200 mm outer diameter 1.10^{13} Bq annular TiT targets on a thick oxygen free copper target backing. The NUKEM targets are directly cooled by water, the MULTIVOLT targets are cooled indirectly

through the target backing. The direction of heat transfers is radial at the RTM series MULTIVOLT targets. The half life of MULTIVOLT targets are about 200 h at 3.8 kW/cm^2 target load [25]. These targets are utilized in Hamburg, and each target can be used for a week in cancer treatments [26]. The target disc is rotating by 700-1100 rpm speed.

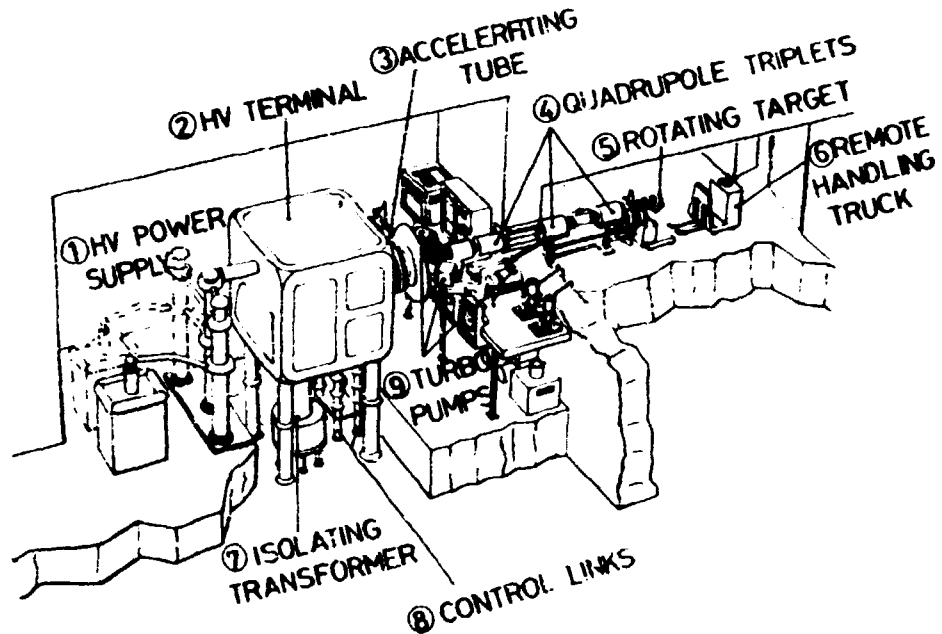


Fig.7. The artists representation of RTNS-II neutron generator

Large surface rotating TiT targets are on the beam at the LANCELOT, the RTNS-I [27], and in the RTNS-II [28] neutron generators. These targets are shaped on a part of a sphere and their thickness are about one millimeter. They are directly water cooled from the back side of the target. A special air bearing has been developed for the RTNS-II target assembly [29] for use at 5000 rpm speed. A MULTIVOLT rotating disc target assembly is shown on Fig.8. The thin,

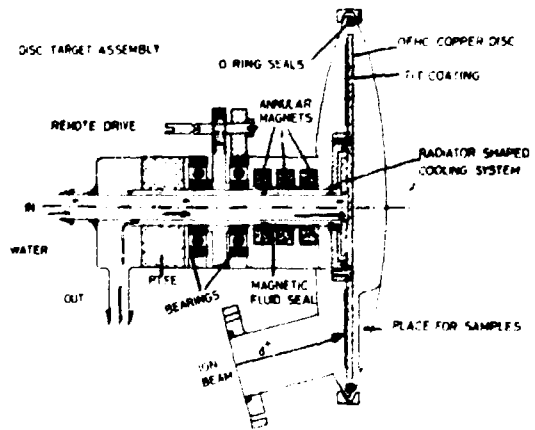


Fig.8. A rotating disc target assembly with magnetic fluid vacuum seals

part of a sphere target assembly of the RTNS-II is shown on Fig.9. The target backing of this one has a sandwich structure that contained convoluted channels

to produce a turbulent cooling water flow. The water flows through the target backing at a rate of 10 l/min.

The targets in an intensive DT neutron generator have usually short life time. The neutron output drops to half its initial value in the RTNS-I [30] with 16 mA/400 kV d⁺beam within a 50 hours time interval. The RTNS-II generators target life time has been reported [3] 70 hours at 40 mA/350 kV beam. The MULTIVOLT targets - tritiated in Saclay - drop to half of their initial yield on an unanalyzed beam of 12 mA/500 kV in about 10 hours continuous operation, but at 8 mA/600 kV analyzed beam with 1100 rpm speed shows about 200 hours time delivering more than 10^{12} n/s. The original yield was $2.7 \cdot 10^{12}$ n/s. These measurements were made at the NRPB in Harwell [31].

6. Power supplies, HV terminals

The type of high voltage power supply used in an intense neutron generator depends on the actual needs and the structure of the generator. The usual mains frequency operated power supplies are capable of delivering up to 50-60 mA currents at 200-300 kV [32,33]. A good review on the properties of high voltage, high current power supplies is given in [34]. The insulated Core Transformer generators are available with voltages up to 500 kV and 200 mA currents. The Dynamitron type of power supplies are available for intense neutron generator purposes with ratings of 500 kV and 100 mA. A motor generator

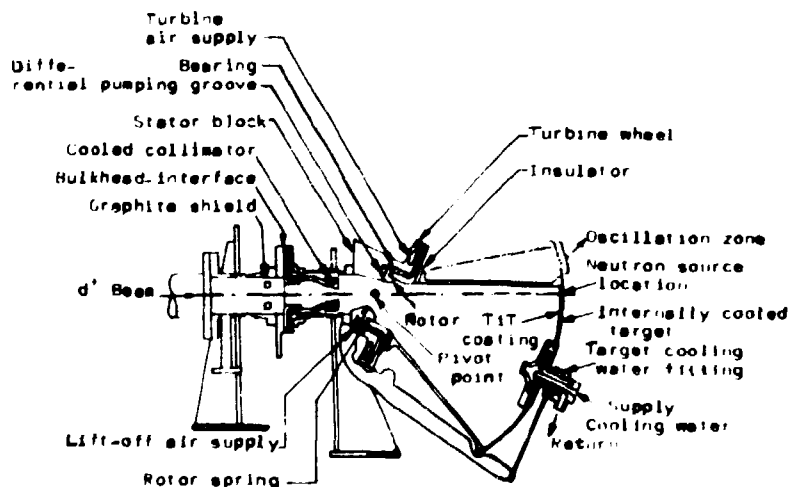


Fig.9. The internally cooled sandwich formed on a part of a sphere target with its air bearing in the RTNS-II neutron generator

converts the line frequency to 2 kHz in the HAEFEI Co. manufactured air insulated cascade rectifier of RTNS-II [16]. This power supply can be regulated with a coefficient of 0.1 % and delivers less than 0.5 % ripple. Special care has to be taken to protect the silicon rectifier diodes to avoid their radiation damage.

The HV terminals of intense neutron generators are powered usually by isolating transformer. The power needed on the HV terminal is between 2-8 kW. This power is needed by the ion source, focusing or analysing systems and the ion source control. Some care has to be taken at the cooling of the ion source

if the cooling media is water. The deionized cooling water has to be maintained to keep its original pH value.

7. Cooling and vacuum systems

The target with a dissipation of several kW and the ion source with similar one need a closed circuit heat exchanger cooling system, where the waste heat are removed by ordinary tap water. The cooling water resistivity should be permanently controlled and maintained above 1 Mohm cm by an ion exchanger used for target cooling can be simple deionized water circulated in the closed circuit to decrease the radiation hazard connected to the cooling water. Industrial cooling machines are used in the 250 kV/30M MARCONI-ELLIOTT neutron therapy system and will be applied in Debrecen as well.

In the vacuum systems of these generators are practically every types of usual nor ultra high vacuum components. The vacuum pumps are mostly mechanical and diffusion pumps but the one of the most sophisticated system, the RTNS-II uses more turbomolecular pumps and one of them is placed on the HV terminal. The application of cryo and getter pumps is very useful because they are decreasing the tritium hazard. The 20-100 cm³/h gas consumption ion sources need 3000-5000 l/min pumping speed oil diffusion pumps; these pumps are available commercial goods.

The several 10 mA charged particle beams passed through the ion optical system may have a shape far from a good uniformity circular one. There are in use water cooled collimators and diaphragms on the beam line but beam profile monitors have not been reported in use an intense neutron generator. An oscillating wire beam monitor would intercept too much power in a several 10 mA beam. The target current monitors mostly are calibrated by calorimeter method because the rotating targets are far from an ideal Faraday cup.

8. Radiation protection

The activity of the tritium targets used in an intense neutron generator is in the range of $3 \cdot 10^{12}$ - $4 \cdot 10^{13}$ Bq/ 100-1000 Ci /. The first radiation hazard is connected to the tritium target handling and use. A 10^{13} Bq activity target used in an intense neutron generator could pollute the vacuum system and exhausting in the air, the environment. Most of the generators have tritium traps in the exhausting system of the vacuum pumps. The primary radiation hazard of a working neutron generator is the 10^{12} - 10^{13} n/s source strength neutron field. A careful measurement was for the 10^{12} yield MARCONI-ELLIOTT sealed tube generator shielding for usual silicone and lime-stone concrete as well as for plaster [35]. The lime-stone concrete shows lower residual gamma activity after use of the neutron source. An ordinary shielding thickness of 2 m can be used for a 10^{12} n/s yield neutron generator if the target room an area of 6x6 .

A radiation problem is related to the target assembly activated by the fast neutrons. The application of a pneumatic rabbit system is fundamental in the use of intense neutron generators. There are special target assembly changing trucks for fast target and sample changing at the LANCELOT and the RTNS-II. The artist's drawing of the RTNS-II generators shows his truck on Fig. 7. A "cooling time" of 50 hours is enough before the changing of the neutronQ type tube in the Hillertron therapy units steel collimator head [36].

A not well known radiation problem is that every charged particle accelerators are producing X rays due to the bremsstrahlung of charge particles in the target and due to the secondary electrons. Similarly there is not calculable exactly the effects of the prompt gammas induced in the target hall by the neutrons. The influence of gammas induced by the slow neutrons gives similar effects. These give photons, a high photon background around the intense neutron generators.

NAME	STATE	VIELD MV	HIGH VOLTAGE/ TARGET CURRENT MV/A	ION SOURCE	ACCEL. TUBE	BEAM #	TARGET	VACUUM	APPLICATIONS	REFERENCES IN [2]
PTNS-1	IN USE	2×10^{-12}	400kV/2mA	DOPPLASATION (d^2)	MULTI GAP	6 mm	TIT, PART OF A SPHERE	OIL DIFF.	CTR, THERAPY, ACTIVATIONS	[1], [2], [4], [6], [7], [8], [10], [11], [12]
PT-AS-1	IN USE	10^{-13}	400kV/15mA	MULTIAPPETURE PLASMA (d^2)	FOUR GAPS	10 mm	TIT, PART OF A SPHERE	TIT, DISC,	CTR, THERAPY, ACTIVATIONS	[1], [2], [3], [10]
LANCELOT	IN USE	0.1×10^{-12}	100kV/30mA	DOPPLASATION ($d^2 + l^2$)	ONE CAP	50 mm	TIT, PART OF A SPHERE	LEO PUMPS	CTR	[3], [5], [6], [12]
CHALK RIVER IN USE	4×10^{-12}	300kV/2.5mA	DOPPLASATION (d^2)	OHT GAP	10 mm	TIT, DISC	OIL DIFF.	CTR, ACTIVATI-	[3]	
NASA-LAUREL PLAN	10^{-12}	300kV/3.0mA	DOPPLASATION (d^2)	"	"	54 mm	TIT, DISC	OIL DIFF.	THERAPY	[4]
SANDIA CONCEPT	4×10^{-12}	300kV/40A	MAGNETIC MULTI- POLE (d^2)	ONE GAP	300 cm^3	WT, DISC	"	CTR	"	[3]
SI-XD+	CONCEPT	10^{-13}	3.50kV/2.5mA	DOPPLASATION	ONE GAP	3400 cm^3	TIT, PART OF A SPHERE/PLX/	OIL DIFF.	BIOLOGY	[4, 5]
NEPS	IN USE	10^{-12}	0.00kV/1.0mA	DOPPLASATION (d^2)	MULTI GAP	6 mm	TIT, DISC	OIL DIFF.	RADIOLOGY, NUCL. DATA	[2]
ANERI	IN USE	2×10^{-12}	300kV/1.0mA	DOPPLASATION (d^2)	MULTI GAP	10 mm	TIT, DISC	"	"	[2]
DTNAGEN	IN USE	3×10^{-12}	300kV/1.0mA	DOPPLASATION (d^2)	MULTI GAP	20 mm	TIT, DISC	OIL DIFF.	THERAPY	[4, 5], [6], [10], [11]
JAERI	IN USE	10^{-12}	400kV/3.0mA	DOPPLASATION (d^2)	MULTI GAP	"	TIT, DISC	TUB BOMBOL.	CTR, ACTIVATI-	[20, 21]
INSTIPP	IN USE	10^{-13}	1.80kV/400A	MOPPLICATION (d^2)	ONE CAP	16 mm	TIT, set, ET	OIL DIFF.	TARGET TEST	[12], [42]
IGCA	PLAN	10^{-12}	3.50kV/1.0mA	DOPPLASATION (d^2)	TWO GAPS	10 mm	TIT DISC	OIL DIFF.	ACTIVATIONS, NUCL. DATA	[6], [12]
PUSA-V	PLAN	10^{-12}	3.00kV/1.0mA	DOPPLASATION (d^2)	MULTI CAP	10 mm	TIT, DISC	OIL DIFF.	ACTIVATIONS, NUCL. DATA	[22], [124]
TAD	PLAN	10^{-12}	3.00kV/1.0mA	DOPPLASATION (d^2)	ONE GAP	10 mm	TIT, DISC	OIL DIFF.	ACTIVATIONS, NUCL. DATA	"
IRTE	PLAN	10^{-12}	2.00kV/3.0mA	DOPPLASATION (d^2)	ONE GAP	10 mm	TIT, DISC	OIL DIFF.	ACTIVATIONS, NUCL. DATA	"

Table I. Solid Target Intense 14 Mev Neutron Generators

9. Summary

The construction of an intense neutron generator is a technically solvable but not too simple problem. The most complicated, expensive parts in a

generator are the ion source, accelerating tube, target assembly, HV power supply and the radiation shielding. An institute with an appropriate technical background and economical basis can develop an intensive 14 MeV neutron generator for their needs. A short survey on the existing and planned solid target intense neutron generators and their main parameters are given in Table 1. The references are in ref. [5]. The past two generators are under construction in TU Dresden and in KLTE Debrecen.

References

- 1./ H.H. Barschall: An.Rev.Nucl. and Particle Sci. 28 /1978/. UWFD^M-231 /1978/
- 2./ Special issue of Nucl. Instr. Meth 145 /1977/
- 3./ H.H.Barschall: UWFD^M-331 /1979/
- 4./ J. Csikai: INDC /NDS/-114/65, 265
- 5./ T.Sztaricskai: ATOMKI Közl. 22 /1980/ 47 /in Hungarian/
- 6./ Int.Conf.Rad.Test.Fac. for CTR Surf. and Mat.Progr. ANL-CTR-75-4
- 7./ Special issue of Int.J.Rad.Oncology, Biol.Phys. 3 /1977/ 361-406
- 8./ T.Sztaricskai: ATOMKI Közl. to be published
- 9./ Proc. IAEA Adv Group Meeting on Nucl. Data for Fus.Reactor Techn., Vienna, 1978.
- 10./ J.C. Crawford, W Bauer: ANL-CTR-75-4 /1975/ 227
- 11./ M.D.Gabovich: Physics and technology of plasma ion sources, Atomizdat, Moscow, 1972 /in Russian/
- 12./ M.von Ardenne: der Elektronenphysik, Verlag der Wissenschaften, Berlin 1956
- 13./ J.E. Osher, G.W. Hamilton: 1974 LBL-3399
- 14./ A.P.H. Goede et al: in Proc. Int. Symp. on Heating in Toroidal Plasmas, Grenoble, 1978.
- 15./ J.C.Crawford: ANL-CTR-4, 227
- 16./ R.Booth e al: Nucl. Instr. Meth. 145 /1977/ 25
- 17./ J.Pivarc et al: INDC /CSR/-2/L, May 1980
- 18./ C.L. Harvey: Personal communication
- 19./ E. Koltai et al: ATOMKI Közl. 22 /1980/ 155
- 20./ J.B. Hourst, M. Roche: ANL-CTR-75-4, 208
- 21./ F.M. Bacon et al: IEEE Trans. Nucl. Sci. NS-26, No-1/1979/ 1505
- 22./ P. M. Deluca: Phys. Med. Biol. 23/1978/ 876
- 23./ Multivolt Ltd. of Crawley, Great Britain, RTH target assably data sheets
- 24./ NUKEM GmbH, Hanau, GFR, Accelerator target catalog N-753-4-5.
- 25./ M.R.Cleeland: RDI, New York, Technical Inf. Ser. TIS-74-2
- 26./ D.D.Cossuta: personal communication
- 27./ R.Booth et al: IEEE Trans. Nucl. Sci NS-20 No-1, /1973 / 472
- 28./ J.C. Davis: in Proc. Sec. Top. Meeting on Techn. of Contr. Nucl. Fusion, Richland, USA, Sept. 21-23, 1976
- 29./ R.Booth, C.M.Logan: Nucl. Instr. Meth 142 /1977/ 471
- 30./ R.Booth et al: Brit. J. Radiol.: 47/1974/ 737
- 31./ C.L. Harvey: personal communication
- 32./ Haefely Co.: Manual of High Voltage Rectifier 200 kV/40 mA
- 33./ Transformator und Röntgenwerke Dresden: High Voltage Power Supply Data
- 34./ G. Pető: Izotópteknike 16 /1973/ 861 /in Hungarian/
- 35./ D.Greene et al: Brit. J. Radiol 44 /1971/ 116
- 36./ D. Major: Personal communication

ROTATING TARGET FOR A 300 keV NEUTRON SOURCE: DESIGN

J. Pivarč, J. Král

Institute of Physics, Slovak Academy of Sciences,
899 30 Bratislava, Czechoslovakia

A b s t r a c t : A rotating target whose disk will be able to rotate up to 1100 rpm has been designed. The target consists of the MoTiT subtargets of a 4.5 cm diameter. A neutron yield of $10^{12} \text{ n. s}^{-1}$ and a useful target lifetime of around 100 mA h.cm^{-2} are expected. The rotating target is proposed with respect to heat dissipation and the removal of 3 kW.cm^{-2} in continuous operation. One stage of the differential pumping is used between the air and the target chamber so that the leak rate into the vacuum is less than $10^{-5} \text{ Pa m}^3.\text{s}^{-1}$. The target will be used for the production of 14 MeV neutrons in a 300 keV air-isolated electrostatic accelerator.

1. Introduction

For the development of a high current neutron source it is very important to find the most suitable target. Unrotating solid tritium targets are extensively reported in the papers /1-2/. In many cases these targets are not suitable as monoenergetic neutron sources, particularly with increasing source strength. The reason is a high heat load which corresponds to a high tritium desorption rate /3/. In such cases rotating targets become important. Various types of such targets have been constructed /3-7/. Their technical performance is different. Many of them have an annular section a small part of which only is bombarded by D⁺ or (DT)⁺ ions. The target heat load must not exceed a fixed safe limit. It is about 192 °C for the TiT target, ZrT-313 °C, ScT-325 °C, ErT-405 °C and YT-426 °C.

In the present paper the rotating target is reported. It has been developed for an intense section of a multipurpose 14 MeV neutron source /3-10/. Because of the health hazard connected with radioactive tritium gas, the whole target system is closed. Special attention has been paid to the safety aspects of the target and heat dissipation and removal of 3 kW. cm^{-2} . Possibilities are also shown of increasing the target lifetime.

2. Rotating target design

The scheme of the rotating target is shown in Fig.1. The subtargets are located on a rotation disk. It has been designed to use the 16 MoTiT subtargets manufactured in the USSR /11/. These targets are standardly most available. The diameter of the subtargets is 4.5 cm and the effective diameter is 4 cm. The atomic ratio is 1.5. The thickness of the subtarget backing and the TiT layer is 0.03 cm and 2-5 μm, respectively. The concentration of the tritium is 60 GBq.cm⁻². The "ring" shaped target /D_{int}= 19 cm, D_{ext}= 28 cm/ contains totally 15 TBq tritium. The layout of the subtargets on the disk periphery is seen in Fig.2.

During the operation the target is cooled by water which is driven through the centre of the rotating target assembly to a cavity from where it is further

delivered to eight 0.5 cm diameter channels. Two subtargets are connected to one channel. To cool the target to a suitable temperature with respect to the tritium desorption rate it is necessary to supply the channels by a sufficient amount of cooling water. Our design assumes that water consumption would not be higher than $70 \text{ l} \cdot \text{min}^{-1}$, which corresponds to the minimum water velocity in channels of $1.5 \text{ m} \cdot \text{s}^{-1}$.

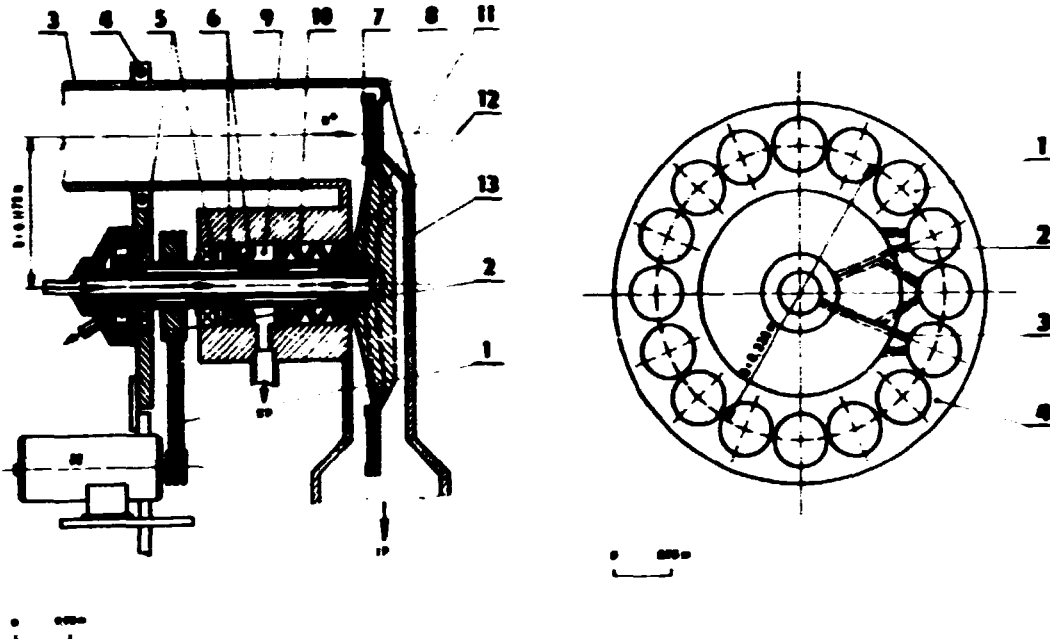


Fig.1. The scheme of the rotating target system. 1-V belt, 2-pulley, 3-beam tube, 4-isolation support, 5-bearings, 6-simmerings, 7-ring, 8-target, 9-support, 10-sealing "rings", 11-rotor, 12-water channels, 13-stator, IP-ion pump, DP-differential pump and M-electric motor.

Fig.2. The layout of the 4.5 cm subtargets through the rotation disk periphery. 1-subtarget, 2-water outlet, 3-water inlet and 4-clamping ring.

The rotor of the rotating target is moved in a vacuum of 10^{-3} - 10^{-4} Pa. It is separated from the high vacuum by three special O rings sealing which are fixed by a support. Two simmerings separate the vacuum chamber from the outside environment. The cavity placed between the rings and the simmerings is pumped by a differential pumping system. It involves a mechanical rotary pump and a foreline trap. The target chamber is pumped by the EGZ 100 ion pump. The pumping speed of the pump is $100 \text{ l} \cdot \text{s}^{-1}$ for air at a pressure of 10^{-3} Pa. The rotor is further carried in two high precision ball bearings which allow only a small free vibration. We expect that the bearings will be suitable for target operations at any speed up to 1100 rpm, although the necessary target revolution rate for the heat dissipation of $1.5 \text{ kW} \cdot \text{cm}^{-2}$ is about 35 rpm /12/.

The detailed scheme of layout of the neutron source target chamber with the rotating target is shown in Fig.3. The main data of the rotating target device are summarized in Tab.1.

3. Target lifetime

The lifetime T of the rotating target is a function of the beam intensity I , the half-lifetime $T_{1/2}$ and the bombarded target surface S . There holds

$$T = I \text{ (mA)} T_{1/2} \text{ (h)} / S \text{ (cm}^2\text{)} /13/.$$

The half-lifetime $T_{1/2}$ can be calculated by the formula

$$T_{1/2} = \alpha \beta T_{1/2} \text{ }_s \cdot I_s U_s S / I U S_s,$$

where α and β are factors which determine the increase of $T_{1/2}$ due to the use of the separated ion beam and the rotation of the target, $(T_{1/2})_s$ is the half-lifetime of the subtarget, I_s , U_s , S_s and I , U , S are the beam currents, accelerating voltages, target spot sizes given in paper /14/ and Tab.1, respectively.

The neutron yield dropped to half its initial value in about $(T_{1/2})_s = 90$ min at a beam current of about 0.4 mA of a 400 keV ion beam on a 1.27 cm spot size /14/. These values were used in our calculations.

The lifetime of the rotating target increases about the factor 2 /15/, through the use of the separated ion beam. We can also assume that the lifetime increases about 75 ($0.5/6.7 \times 10^{-3}$) times if the action time of the ion beam during the revolution and the revolution time are 6.7×10^{-3} s and 0.5 s (100 rpm), respectively. Then, the rotating target half-lifetime is about 10 h. For the beam intensity $I = 10$ mA, the half-lifetime $T_{1/2} = 10$ h and the subtarget spot size $S = 1 \text{ cm}^2$ the lifetime is about $T = 100 \text{ mA h/cm}^2$.

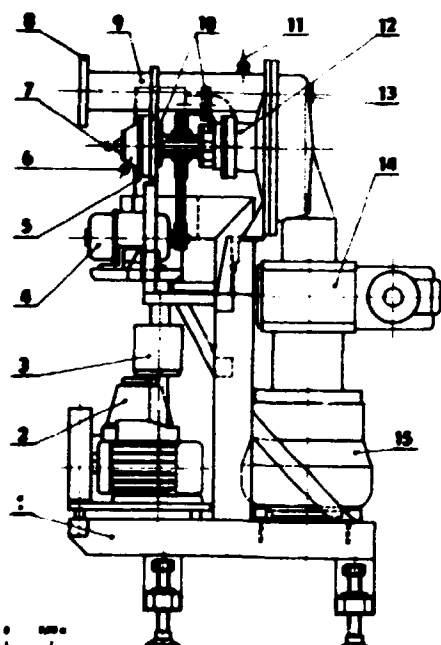


Fig.3. The detailed scheme of the layout of the neutron source target chamber with the rotating target. 1-holder, 2-rotary pump, 3-solenoid valve, 4-electric motor, 5-foreline trap, 6-water out, 7-water in, 8-flange in, 9-beam tube, 10-bearings, 11-feed-through, 12-stator, 13-sample, 14-solenoid valve and 15-ion pump.

The lifetime of the rotating target can also be increased by:

1. the vapour of a 0.2 μm thin protective Al layer on the subtarget surface about the factor 2-3 /16/ and
2. the increase of the target disk diameter.

The calculated rate T determines only the estimated minimum value of the lifetime.

4. Conclusions

In the production of neutrons by means of a high power neutron source it is necessary to use a large surface rotating target. Such a target has been designed in our lab. We realize that the technical performance of the rotating target is not easy. But we expect that there will not be problems with its production and testing in our simulated conditions. We cannot eliminate, of course,

that certain difficulties can arise in the subtargets and disk vacuum sealings and the water inlet and outlet channel production.

Table 1. The main data of the rotating target device

Neutron source strength ($n.s^{-1}$)	$5 \times 10^{11} - 3 \times 10^{12}$
Maximum flux ($n.cm^{-2}.s^{-1}$)	$4 \times 10^{10} - 2 \times 10^{11}$
Beam energy (keV)	300
Beam source strength before acceleration (kW)	0.25 - 1.5
Target current (mA)	5 - 30
Spot size (cm^2)	1
Target diameter (cm)	28
Target heat dissipation ($kW.cm^{-2}$)	1.5 - 9
Target speed (rpm)	35 - 1100
Sample-target distance (cm)	0.7
Target lifetime ($mA.h.cm^{-2}$)	100

The authors wish to thank Dr. M. Blažek, DrSc. the director of the IPSAS for his support and kind interest in this work and Dr. P. Obložinský for helpful discussions.

References

1. Mostafa A.B.M.G., Nucl. Instr. and Meth. 125 (1975) 493
2. Pivarč J., Ph.D. Thesis, Bratislava (1975), unpublished
3. Pivarč J., Atomki Közlemények 13 (1976) 463
4. Booth R. et al., Nucl. Instr. and Meth. 129 (1974) 353
5. Hourst J. B. et al., Nucl. Instr. and Meth. 145 (1977) 19
6. Cloth P. et al., Atomki Közlemények 18 (1976) 439
7. Sztaricskai T., private communication (1980)
8. Pivarč J. et al., INDC (CSR) - 2/L⁺ Special, IAEA Nuclear Data Section Report, Vienna, May (1980)
9. Pivarč J. et al., Acta Phys. Slovaca 30 (1980) 119
10. Pivarč J. et al., Rotating target for a 300 keV neutron generator: Design, IPSAS Report, Bratislava (1979), in Slovak
11. Mišení tritievje /deuterievje/, Techničeskije uslovja, TU.I. 173-71 Report, IJUAN, Kiev (1971)
12. Pivarč J., Heat diagnostic of a rotating target for a 300 keV neutron generator, IPSAS Report, Bratislava (1979), in Slovak
13. Smith D.L.E., Proc.Int.Conf. on Accelerator Targets Designed for the Production of Neutrons, EUR 3895 d-f-e, Liege (1985), 5
14. Sikkema C.P. et al., Nucl. Instr. and Meth. 124 (1975) 161
15. Stengl G. et al., Nucl. Instr. and Meth. 140 (1977) 197
16. Fabian H., Proc.Int.Conf. on Accelerator Targets Design for the Production of Neutrons, EUR 2641.e, Grenoble (1966) 134

О НЕКОТОРЫХ БИОМЕДИЦИНСКИХ ИССЛЕДОВАНИЯХ В ОИЯИ С ПОМОЩЬЮ МЮОННЫХ АТОМОВ.

Сабиров Б.М.

Объединённый Институт Ядерных исследований, Лаборатория Ядерных проблем.

ВВЕДЕНИЕ.

Одним из аспектов использования достижений ядерно-физических методов элементного анализа является использование их в биологии и медицине. Исследование химического состава живого организма без нарушения его жизнедеятельности очень важно для научной и практической биологии и медицины. Для элементного *in vitro* или *in vivo* анализа применяются различные методы: метод радиоактивных изотопов, метод денситометрии рентгенограмм/⁴/, метод фотонной абсорциометрии/^{5,26}/, метод активационного анализа/^{1,3,15}/ и флуоресцентного анализа/^{2,15}/ . Наиболее распространённым и хорошо изученным методом является нейтроноактивационный. В некоторых случаях нейтроноактивационным методом содержание каких-либо элементов определялось с точностью до 1.5-2.0%. Но этот метод имеет свои недостатки: доза облучения составляла несколько десятков, а иногда и сотен и даже тысяч рад/³. Поэтому такие исследования, где нужны хорошие точности, проводят или *in vitro*, или на людях, которые должны быть подвергнуты лучевой терапии. Для всех видов активационных и флуоресцентных *in vivo* исследований с применением тяжёлых частиц характерной трудностью является невозможность локализации их в исследуемом участке тела.

Новый метод прижизненного неразрушающего элементного анализа родился на стыке физики элементарных частиц и атомной физики после открытия стрицательного мюонозона и после многочисленных экспериментальных и теоретических исследований процесса их атомного захвата при остановке в веществе/⁶. В основе метода лежит способность мюона, замедляясь в веществе до малых скоростей, переходить в связанное состояние атома, заменяя на одной из атомных орбит электрон и образуя при этом возбуждённый мезоатом. При девоизлужении мезоатом излучает присущее ему характеристическое электромагнитное излучение, энергия которого примерно в 200 раз больше энергии обычного электронного рентгеновского излучения этого же элемента/⁷. Суммарная интенсивность линий К-серии какого-либо элемента пропорциональна вероятности атомного захвата мюона всеми атомами данного элемента.

ЭКСПЕРИМЕНТЫ С ЖИВОТНЫМИ.

Впервые идею использования мюонов для элементного анализа живого организма выдвинули независимо друг от друга Х.Даниэль(ФРГ)/⁸/ и группа советских физиков (Зинов В.Г., Конин А.Д., Мухин А.И.)/⁹/ . Вскоре были сделаны расчёты на фантоме человека и получен синтетический спектр мезорентгеновского излучения/¹⁰/ . Затем были проведены *in vitro* измерения мезорентгеновских спектров на отдельных органах и частях тела животных и людей/¹¹⁻¹⁴/ . Во всех работах/⁸⁻¹⁴/ были продемонстрированы уникальные и широкие возможности нового метода, получившего название метода мюонной диагностики. Но главный шаг не был сделан - не было поставлено ни одного эксперимента с живым организмом *in vivo*.

Первые такие эксперименты были начаты в Лаборатории Ядерных проблем Объединённого Института Ядерных исследований в 1973г. в рамках специального биологического эксперимента совместно с Институтом Медико-Биологических проблем на белых крысах линии *Wistar* /²⁰/ . Вес каждой крысы был 180-200 гр.

Методика измерения спектров мезорентгеновского излучения довольно хорошо отработана: стрицательные мюоны высокой энергии, получаемые от синхроциклотрона на 680 МэВ, останавливались в организме животного. Момент остановки мюона выделялся

системой сцинтилляционных счётчиков (рис.1). Блок-схема электронной аппаратуры подробно описана в /17/. Крыса помещалась в специально изготовленный пенал из пенополистирола с отверстиями для доступа воздуха. Размеры пучка мезонов обеспечивали равномерное облучение всего тела животного. Кванты мо-мезорентгеновского

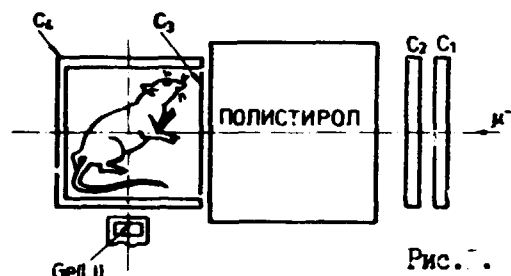


Рис. 1.

излучения из мишени регистрировались $\text{Ge}(\text{Li})$ детектором 41 cm^3 . Электронные блоки для временного канала детектора позволяли получить временное разрешение (ПШМ) быстрых совпадений $T_g - T_{\mu-\text{раст}} = 12 - 15 \text{ нсек}$, что дало возможность надёжно выделять мезорентгеновское излучение на фоне рассеянного излучения от ускорителя в месте расположения экспериментальной установки.

Сигналы X_μ сортировались в зависимости от времени их прихода в гамма-детектор с помощью малой ЭВМ НР-2116С в режиме "on-line" и накапливались на магнитных дисках и лентах. При этом была возможность постоянно вести визуальный контроль за ходом эксперимента на графическом дисплее. Один из первых рабочих X_μ спектров, полученный при облучении крысы, показан на рис.2. Вычисле-

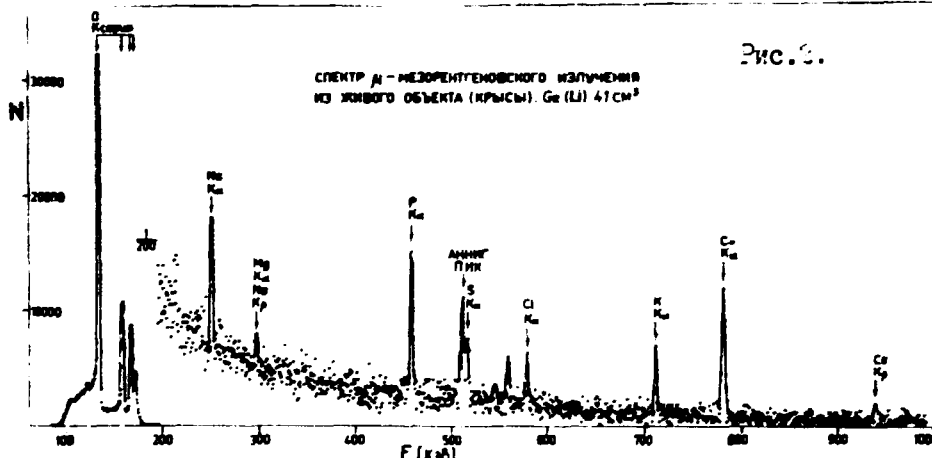


Рис.2.

нное число импульсов под каждым пиком соответствовало относительному вкладу данного элемента в исследуемый объект. Вводилась поправка на зависимость эффективности детектора от энергии

и на вклад более высоких переходов в K-серии каждого элемента.

Закономерности атомного захвата мюонов в различных химических соединениях ещё только устанавливаются /18,19/ и нельзя утверждать, что интенсивность X_μ однозначно и достаточно просто связана с количеством атомов разного сорта, содержащихся в исследуемом объекте. В качестве первого приближения, которое видимо более справедливо для механической смеси атомов (или для биологических объектов) можно использовать с точностью несколько процентов выражение $\frac{w_i}{\sum w_i} \approx \frac{p_i}{\sum p_i}$, т.е. относительная интенсивность мезорентгеновского спектра i -го элемента в механической смеси $\frac{w_i}{\sum w_i}$ равна относительному весовому содержанию данного элемента $\frac{p_i}{\sum p_i}$. Это простое соотношение подлежит экспериментальной проверке для различных тканей организма. В частности, минеральная и органическая компоненты кости представляют собой в некотором смысле механическую смесь кристаллов гидрооксиапатита и коллагена /21/. В связи с освоением человеком космического пространства исследование минеральной насыщенности кости приобрело особую актуальность /5,22/.

Поэтому следующим шагом было исследование влияния фактора космического полёта (гипокинезии) на элементное содержание живого организма и в особенности на содержание кальция в скелете животного. Для этого были измерены спектры X_μ на 3 крысах линии W^{183} , испытавших трёхнедельный орбитальный полёт на искусственных

спутниках Земли "Космос-605" и "Космос-690". Крысы экспонировались на пучке μ^- -мезонов до полёта, сразу после полёта и спустя месяц после приземления/20/, измерения X_{μ} спектров проводились с помощью $Ge(Li)$ детектора 55 см³. Результаты измерений приведены в Табл. I. В последней колонке в качестве иллюстрации приведены относительные вклады (в %) элементов в организм крысы.

Таблица I.

Элемент	Отношение содержания элементов после полёта к содержанию их до полёта.			Относительное содержание элементов (в %) в крысе №I через месяц после полёта
	"Космос-605"		"Космос-690"	
	крыса №1	крыса №2	крыса №3	
C	1.26 ± 0.05	1.11 ± 0.03	1.13 ± 0.03	19.7 ± 0.5
N	1.11 ± 0.29	1.03 ± 0.02	1.02 ± 0.02	3.0 ± 0.6
O	0.95 ± 0.03	0.98 ± 0.03	0.98 ± 0.02	75.0 ± 1.8
Na	0.70 ± 0.07	1.06 ± 0.08	1.10 ± 0.35	0.123 ± 0.011
Mg	0.90 ± 0.52	1.2 ± 0.6	-	0.032 ± 0.014
P	1.02 ± 0.04	1.02 ± 0.05	0.98 ± 0.08	0.492 ± 0.015
S	0.97 ± 0.05	1.14 ± 0.09	1.18 ± 0.14	0.031 ± 0.013
Ca	0.69 ± 0.17	0.94 ± 0.13	1.0 ± 0.3	0.110 ± 0.012
K	0.86 ± 0.10	0.97 ± 0.12	1.07 ± 0.17	0.250 ± 0.014
Ca	0.89 ± 0.06	1.08 ± 0.10	0.95 ± 0.07	0.954 ± 0.028

Полученные данные показывают, что в результате действия факторов космического полёта не происходит заметного выноса тяжёлых элементов из организма животных, а наступает вероятно перераспределение их между тканями или органами тела. Поэтому изменение минеральной насыщенности костной ткани следует наблюдать на отдельных частях скелета. Кроме этого, в связи с дальнейшим увеличением сроков пребывания человека в орбитальном полёте и обнаружением при этом существенных отклонений в жизнедеятельности всего организма и отдельных его органов/22,25/ требуется выработать наиболее реалистическую оценку мер по профилактике и терапии нарушений водно-солевого обмена.

ИССЛЕДОВАНИЯ С ЛЮДЬМИ.

В рамках сотрудничества между ОИЯИ и ИМЕЛ МЗ СССР был осуществлён эксперимент по анализу минерального состава костной ткани человека после пребывания его в экстремальных условиях/24/. Исследование проведено с 18 здоровыми мужчинами в возрасте 32-37 лет. Все они в течение 182 суток находились в условиях строгого постельного режима (антиортостатической гипокинезии). Для полной имитации условий невесомости создавался небольшой (~4°) наклон кровати в сторону головы. Все испытуемые были разделены на три группы: первая была контрольной; вторая выполняла комплекс профилактических мероприятий (физическая тренировка, миоэлектростимуляция, приложение отрицательного давления на нижнюю часть тела, водно-солевые добавки к рациону) и третья испытывала 35% от физической нагрузки второй группы. Измерения X_{μ} спектров проводились на пятонной кости за 4 суток до начала режима гипокинезии и спустя 4 суток после его окончания в специальном металлическом домике. Фон от ускорителя в месте расположения испытуемого по оценкам дозиметрической службы за 3 часа измерения составил ~7.0 мбэр, т.е. ~0.03 от предельно допустимой квартальной дозы на весь организм для непрофессионалов. Специальный пучок мюонов/23/ с энергией 30 МэВ через отверстие в стене бокса поступал на устройство для обеспечения остановок мюонов в центральной части пятонной кости. Оце-

нка поглощённой дозы в пятчной кости, обусловленной суммарным количеством остановившихся μ^- -мезонов при скорости реальных остановок $\sim 10^3 \text{ сек}^{-1}$, за 3 часа измерений оказалась не более 0.25 бэр, что составляет ~ 0.07 от предельно допустимой квартальной локальной дозы на пятчную кость для непрофессионалов. На рис.3 показан типичный спектр мезорентгеновского излучения из пятчной кости человека при 3-часовой экспозиции на мюонном пучке. Для отработки методики проводились измерения X_μ -спектров из пятчной кости четырёх экспериментаторов, которые показали на отсутствие систематических ошибок, превышающих статошибку.

В результате показано, что величина относительного содержания атомов С, Н и О имеет разброс относительно средних значений ненамного превышающий статошибку. Отношение содержания кальция и фосфора для каждого индивидуума остается постоянным, а распределение для суммарного вклада фосфора и кальция (и каждого из Ca^{+2} отдельности) примерно на порядок шире статистической погрешности и отражает индивидуальные различия в степени минеральной насыщенности губчатой кости. Изменение суммарного содержания фосфора и кальция в результате гипокинезии достигает фактора 2 для I группы. Средние значения изменений ($P+Ca$) по трём группам (соответственно: -12%, 0% и +12%) демонстрируют некоторую тенденцию к реакции на профилактические мероприятия. Не исключено, что изменения в содержании минеральной компоненты больше зависят от индивидуальной реакции организма на состояние гипокинезии. Такое предположение подтверждается наличием корреляции между степенью изменения минеральной насыщенности и её исходным уровнем (рис.4): максимальное уменьшение

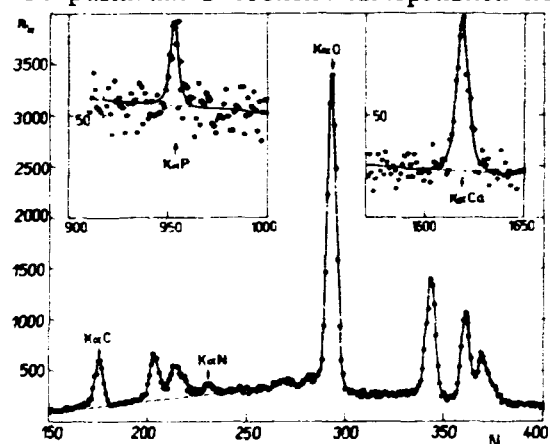


Рис.3.

($P+Ca$) наблюдается для испытуемых с максимальной начальной минеральной массой кости, и наоборот. В подобной работе американских учёных/26/, проведённой методом фотонной абсорбциометрии, обнаружена слабая, но противоположная тенденция: у лиц с высокой минеральной массой наблюдается меньшая потеря её. Причина видимо кроется в различии методов: во втором методе исследуется состав всей кости, включая кортикальный слой и частично мягкую ткань. Поэтому оба этих метода следует рассматривать как взаимно дополняющие друг друга.

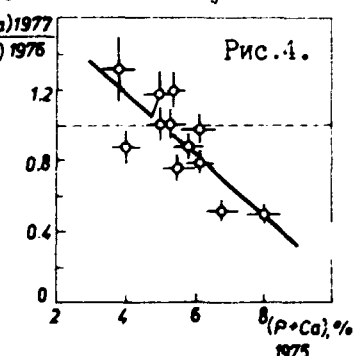


Рис.4.

АБСОЛЮТНАЯ КАЛИБРОВКА МЕТОДА МЮОННОЙ ДИАГНОСТИКИ.

Чтобы знать о фактическом вкладе какого-либо элемента в содержание объекта, было проведено исследование образца губчатой кости двумя методами: мюонной диагностики и физико-химическими методами/27/. Вес образца был около 150 гр. В физико-химическом анализе, кот. проводился на кафедре патологической физиологии Московского медицинского стоматологического института им. Н.А. Семашко, определялось весовое содержание Ca^{+2} элементов на 100 гр сырой ткани, для кот. получены данные мезорентгеновской методикой. Коэффициент α есть поправочный коэффициент, на кот. надо умножать относительную интенсивность X_μ спектра данного элемента, чтобы получить его весовое содержание. Данные для костной ткани, так же, как и для лёгких элементов/14/, свидетельствуют о том, что с точностью $\sim 7\%$ минеральную и органическую компоненты кости, а также окружающую её мягкую ткань можно с точки зрения атомно-

го захвата мюонов рассматривать как компоненты механической смеси.

ЗАКЛЮЧЕНИЕ.

Исследования с помощью мюонных атомов демонстрируют несомненные преимущества мюонного прижизненного неразрушающего анализа по сравнению с другими: возможность осуществления трёхмерной локализации пучка мюонов на исследуемом участке; возможность определять содержание элемента независимо от того, в какое химическое соединение он входит; чувствительность при малой дозе облучения. Ограничения метода: слабые интенсивности мезонных пучков и невозможность регистрировать водород. Поэтому метод мюонных атомов должен дополняться другими ядерно-физическими методами.

ЛИТЕРАТУРА.

1. Труды II Совещания по использованию новых яд.-физич. методов для научно-технич. и нар.-хоз. задач, Дубна, 1975г.
2. Van Rinsvelt H.A.e.a., Nucl.Instr.&Meth. 142, 171(1977); 149, 429(1978).
3. In VIVO Neutron Activation Analyses, Proc.of a Panel, Vienna, 17-21 April, 1972.
4. Аккерман Ю., Биофизика, "Мир", М., 1964.
5. Rambaut P. et al., Aerospace Med. 43, №.6, 646(1973); Smith D. et al., J.Lab.Cl.Med. 87, 5, (1976)
6. Мезоны в веществе, ОИЯИ, Д.1, 2, 14-10908, Дубна, 1977.
7. Вайсенберг А.О., Мю-мезон, "Наука", М., 1964.
8. Daniel H., Nucl.Med., 8, 311(1969).
9. Зинов В.Г. и др., Авт.Свид.-во СССР №333452 от 12.5.1970. Бюлл.ОИПОТЗ, 1972, №II; ОИЯИ, Р14-6407, Дубна, 1972.
10. Роузен Л., Труды ІУ Межд.конф.по физике выс.энергий и структуре ядра, Д.1-6349, Дубна, 1972, стр.589.
11. Taylor M.L. et al., Rad.Res., 54, 335(1973).
12. Daniel H. et al., Biomed.Tech., 13, 222(1973).
13. Daniel H. et al., Phys.Med.Biol., 20, 1035(1975).
14. Hutson R.L. et al., Rad.Phys., 120, 193(1976).
15. Труды III Сов.по использ. новых яд.-физич. методов для научно-технич. и народно-хоз. задач, Дубна, 1978.
16. Akimov Yu.K. et al., Nucl.Instr.&Meth., 104, 581(1972).
17. Андерт К. и др., ОИЯИ, Р15-10373, Дубна, 1977.
18. Герштейн С.С. и др., УФН, 97, 1969, с.3.
19. Петрухин В.И. и др., ЖЭТФ, 70, 1976, с.1145; ссылка 6, стр.88; P.Vogel et al., Phys. Lett., 70B, 39(1977); Schneuwly H. et al., Phys.Lett., 66A, 188(1978); Schneuwly H. et al., Nucl.Phys., A312, 419(1978).
20. Арльт Р. и др., ОИЯИ, И-11844, Дубна, 1978.
21. Глимчер М., в сб.: Современные проблемы биофизики, ИЛ, М., 1961, с.94.
22. Красных И.Г., Космическая биология и авиакосмич.медицина, 8, №I, 1974, с.68.
- Wheelon G. et al., The Proc. of the Skylab Life Sciences Symp., 1, 353(1974).
23. Демьянин А.В., Роганов В.С., ОИЯИ, И-4026, Дубна, 1968.
24. Евсеев В.С. и др., ОИЯИ, И-12286, Дубна, 1979.
25. Schneider V., VIII-th Meeting of the Joint USA-USSR working group on Space Biology and Medicine, Washington, D.C., USA, 1977.
26. Vogel J.D., Whittle M.W., Proc.Skylab Life Sciences Symp., 1, 387(1974).
27. Воложин А.И. и др., ОИЯИ, Р15-80-210, Дубна, 1980.

МЕТОДИЧЕСКИЕ АСПЕКТЫ ИЗМЕРЕНИЯ МЮ-МЕЗОРЕНТГЕНОВСКОГО ИЗЛУЧЕНИЯ НА СИНХРОЦИКЛОТРОНЕ ЛИП ОИЯИ (ОБЗОР).

Сабиров Б.М., Экштейн П. - Лаборатория Ядерных проблем ОИЯИ, Дубна.
Ортлепп Х.-Г. - Технический Университет г.Дрездена.

Введение.

В данном обзоре описываются некоторые особенности применения традиционных ядерно-физических методов/1,2/ в экспериментах с мезонами, в частности с остановившимися мю-мезонами. Особенности эти обусловлены спецификой остановки мюона в веществе и физикой захвата отрицательного мюона атомом и ядром. Мезоны получают на ускорителях с энергией протонов $E_p \leq 1$ Гэв и транспортируют к экспериментальной установке, причём время жизни свободного мю-мезона τ_0 равно $2.2 \cdot 10^{-6}$ сек. Затем мезоны замедляются в слое вещества до тепловых энергий и захватываются атомом и ядром. Этот процесс можно разделить на следующие этапы:

1. Замедление от энергий ~ 100 Мэв до $E_{\mu} \sim 1 \div 10$ Мэв за время $\tau_{\text{торм}} \sim 10^{-9} \div 10^{-10}$ сек. (в газах в 10^3 раз больше).

2. Мезон достигает энергии, при которой скорость мюона становится сравнимой со скоростью внешних электронов атомных оболочек, $v \sim c$, а энергия определяется условием: $1/2 m_{\mu} \alpha^2 c^2 \geq E_{\mu} \approx 2$ кэв, за время $\sim 10^{-13} \div 10^{-14}$ сек/3.

3. После достижения энергии ~ 2 кэв мезон, масса которого более чем в 200 раз превышает массу электрона, заменяет один из электронов атома и образует возбуждённый мезоатом. Время этого перехода составляет $10^{-11} \div 10^{-12}$ сек.

4. После захвата атомом мюона на уровне с высокими значениями главного квантового числа n начинается каскадный процесс переходов на уровень с более низкой энергией (или с меньшими значениями n) благодаря электромагнитному взаимодействию за счёт двух механизмов: а) Оже-процесса; б) радиационных переходов, причём энергия мезорентгеновского излучения примерно в 200 раз больше энергии обычного электронного рентгеновского излучения. В лёгких элементах время, требуемое для достижения мюоном основного состояния не превышает $10^{-12} \div 10^{-13}$ сек, а в тяжёлых оказывается ещё меньше/4/.

5. Мюон, достигнув К-орбиты атома, с некоторой вероятностью W_e - распадается по схеме $\mu^- \rightarrow e^- + \bar{\nu}_e + \gamma$ и с вероятностью $1-W_e$ - захватывается ядром, при этом ядро возбуждается и испускает с различной вероятностью γ -кванты, нейтроны, протоны и др. вплоть до ядерных осколков/5,6/. Оба этих процесса имеют характеристическое время, обусловленное временем жизни мюона в электромагнитном поле ядра с зарядом Z , и которое уменьшается от τ_0 для самых лёгких элементов до 70-80нсек для урана и тория.

Энергетический спектр мезорентгеновского излучения, находящийся в области чувствительности $Ge(Li)$ детекторов, простирается от $E_x = 18.64$ кэв (K_{μ} для $^{7}_{3}Li$) до E_x более чем 10 Мэв для тяжёлых элементов/7/. Энергетический спектр электронов (позитронов) при распаде $\mu^- (\mu^+)$ определяется двухкомпонентной теорией нейтрино и простирается от 0 до ~ 60 Мэв /7/.

Физическая основа измерений мезорентгеновского излучения.

Для исследования физико-химических свойств вещества с помощью отрицательных мю-мезонов изучается их поведение при проходе ими 3-го и 4-го этапов, измеряя при этом интенсивность мезорентгеновского излучения элементов, входящих в химические соединения. Этап 5 характеризуется испусканием или электрона после распада μ^- или продуктов ядерного захвата мюона. Кезоны попадают в мишень поляризо-

ванными вдоль импульса. При прохождении этапов 1,2,3 и мезатомного каскада 4 мюон деполяризуется за счёт столкновения с электронами, фазы атомного захвата и спин-орбитальных взаимодействий для различных атомов и соединений с различной степенью^{9/}. Изучение степени остаточной поляризации (P_μ) на К-орбите даёт информацию о каскаде мюона в мезоатоме, молекулярной структуре вещества, кинетике химических реакций. Исследование γ -квантов, вылетающих из ядра после захвата мезона, даёт сведения об особенностях возбуждения ядра при мю-захвате, дополнительные сведения о структуре ядра.

Более информативными, хотя и более сложными, являются совпадательные эксперименты. Измерение остаточной поляризации P_μ в совпадении с различными линиями К-серии X_μ даёт информацию о деталях мезоатомного каскада, механизме деполяризации^{8/}. Регистрация ядерных γ -квантов в совпадении с электроном распада может дать уникальную информацию о монопольном электрическом возбуждении ядра при распаде мезона на К-орбите. Много сведений даёт точное измерение энергии X_μ . Мы рассмотрим вопросы спектрометрии мезорентгеновского излучения при атомном и γ -квантов при ядерном захвате мюонов, измерения $P_\mu + X_\mu$ и обработки спектрометрической информации.

Регистрация остановок мезонов в мишени.

Эксперименты проводились на мезонном каньле синхроциклостра на 680 МэВ в Лаборатории Ядерных проблем ОИЯИ. Использовался сепарированный мюонный пучок с импульсом частиц 158 МэВ/с(83 МэВ)/10/. Интенсивность мезонов в пучке $55+7 \cdot 10^4$ сек⁻¹, мюонных остановок в максимуме составляло $\sim 10+13 \cdot 10^3$ сек⁻¹ в мишени толщиной $\sim 3\text{гр}/\text{см}^2$ и площадью $80 \times 80 \text{ mm}^2$, причём примесь пионов была 0.002, полуширина импульсного распределения $\Delta p/p = \pm 5\%$. При выводе пучка "с растяжкой" частицы относительно равномерно распределены в интервале 6мсек при частоте следования циклов ускорения синхроциклостра 110сек^{-1} . На рис.1 показана схема расположения телескопа из сцинтилляционных счётчиков на мюонном пучке.

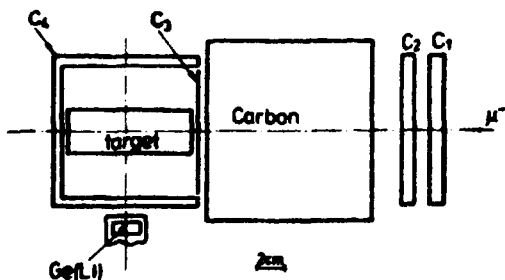


Рис.1. Расположение телескопа на пучке мезонов. Размеры: С1 и С2 - $10 \times 10 \times 1 \text{ см}^3$; С3 - $80 \times 80 \times 1 \text{ см}^3$; С4 - $80 \times 110 \times 8 \text{ см}^3$.

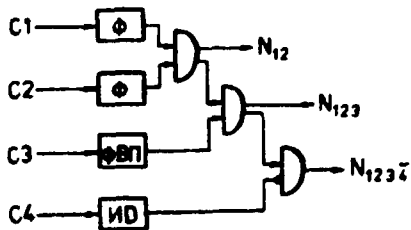


Рис.2. Упрощённая блок-схема выделения остановок N_{1234} .

Подбором толщины углерода мезоны замедляются до такой энергии, чтобы большинство из них останавливались в мишени (для 158МэВ/с - 13см или $30\text{гр}/\text{см}^2$). Упрощённая блок-схема логики выделения остановок изображена на рис.2. Счёт N_{123} обычно составляет 60-70% от N_{12} . Число остановок в мишени регистрируется счётом N_{1234} , при этом важно, чтобы число "пустых" остановок, т.е. число срабатываний счётчиков 1234 без мишени, было минимальным, т.к. это обуславливает паразитный фон. Как правило это число не превышало 0.5-0.7% от N_{12} или $\sim 1\%$ от N_{123} .

Детекторы и спектрометрическая электроника.

В наших экспериментах применялись различные $\text{Ge}(\text{Li})$ - детекторы: плоско-параллельный с чувствительным объемом 2.4 см^3 и с энергетическим разрешением 650 эВ при $E_{\gamma}=100 \text{ кэВ}$ и коаксиальные с чувствительными объемами 27 см^3 , 41 см^3 и 55 см^3 и с энергетическим разрешением около 2.5 кэВ при $E_{\gamma}=1,3 \text{ МэВ}$. Детекторы располагались под углом 90° к пучку мюонов и были окружены разными защитами для уменьшения фона.

На рис.3 изображена блок-схема электроники для регистрации мезорентгенового излучения. Все блоки изготовлены в ОИЯИ. Верхняя часть вырабатывает сигналы "монитор", "остановка мюона" (старт), "Т_γ" (стоп) и Е_γ.

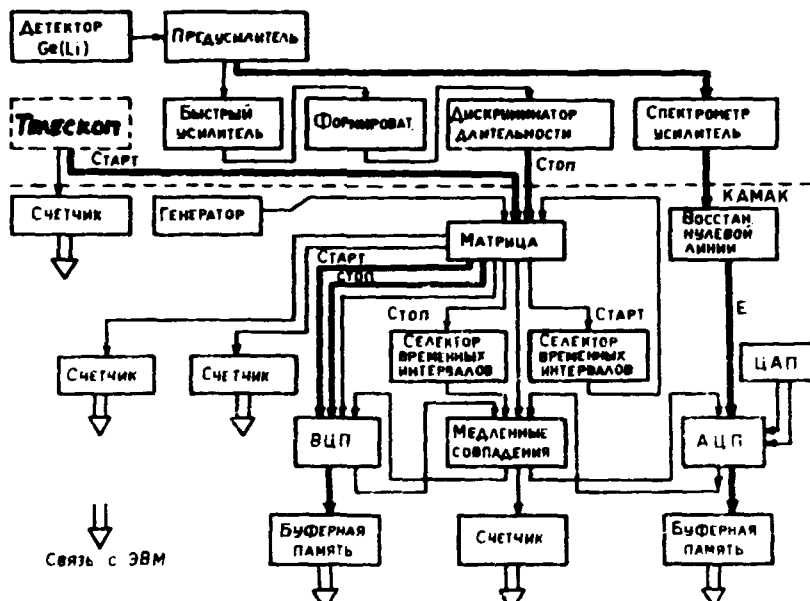


Рис.3. Блок-схема электроники для регистрации мезорентгенового излучения

Ниже пунктирной линии выделена часть, выполненная в стандарте КАМАК, в которую входят: амплитудно-цифровой преобразователь (АЦП), имеющий число каналов, изменяемое командами из ЭВМ в пределах $N=256 \div 8192$; восстановитель нулевой линии (ВЧЛ), предотвращающий ухудшение разрешения с повышением загрузки и служащий буферным блоком между спектрометрическим усилителем и АЦП; времязадающий преобразователь (ВЗП); две буферные памяти (БП), рассчитанные на прием 4 16-разрядных слов и имеющие мертвое время 100 нсек; схема медленных совпадений (СМС); матрица; селектор временных интервалов (СВИ); цифро-аналоговый преобразователь (ЦАП); счетчики и контроллер //.

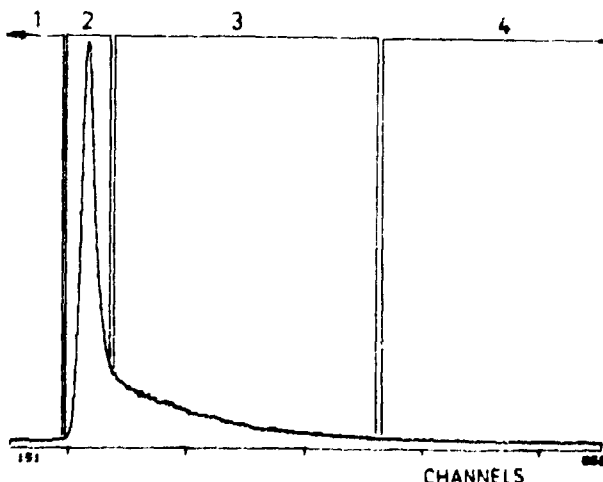


Рис.4. Временное распределение квантов при остановке мюонов в CH_2Cl_2 .

Конфигурация системы КАМАК – однокаркасная и двухсторонняя связь с ЭВМ типа НР-2116С осуществляется специальным контроллером. Для организации и установки режимов работы блоков КАМАК и дальнейшего накопления и сортировки двухмерных спектров были составлены программы **SETKA** и **STOKA** /1/. Основной целью программы **SETKA** является оптимизация режима работы схемы медленных совпадений т.е. задержек и разрешающего времени. Кроме того набираются временные спектры и энергетические спектры с совпадениями и без, что позволяет оценить уменьшение эффективности регистрации низкоэнергетических квантов вблизи порога системы временной привязки.

В качестве примера на рис.4 приводится временное распределение квантов при остановке мюонов в мишени CH_2Cl_2 . Основная задача программы **STOKA** состоит в разбиении временного спектра на ряд отдельных участков – "окон" и в сортировке кодов от АИЛ соответственно этим окнам и последующей записи на магнитный диск в виде энергетических спектров длиной в 4006 каналов. Окно 1 на рис.4 соответствует событиям, зарегистрированным детектором в "отрицательное время" относительно мю-стопа, т.е. это фоновый спектр. Окно 2 соответствует мгновенным событиям, т.е. мезорентгеновскому излучению. Окно 3 соответствует "задержанным" квантам, т.е. квантам, вылетающим из ядра после захвата мюона. Окно 4 использовалось для регистрации случайно совпадающих квантов из размещенных вблизи детектора калибровочных источников.

Перенос данных на ЭВМ СЕС-2500 и обработка спектров.

Обработка полученных спектров производилась с помощью программы **SAMFC** /12/, полученной нами из США и адаптированной на ЭВМ СЕС-2500. Длина слова ЭВМ НР-2116С имеет 16 разрядов. Поэтому была написана программа для чтения ленты с магнитофоне НР-2116 на магнитофоне СЕС и включена в АИЛ в качестве подпрограммы. Основные функции этой программы заключались в "распаковке" 16-разрядных слов и записи их в виде 60-разрядных слов, поиске требуемых идентификаторов спектра и занесение содержания его в отведененный массив. Обработка спектров подробно описана в /12/.

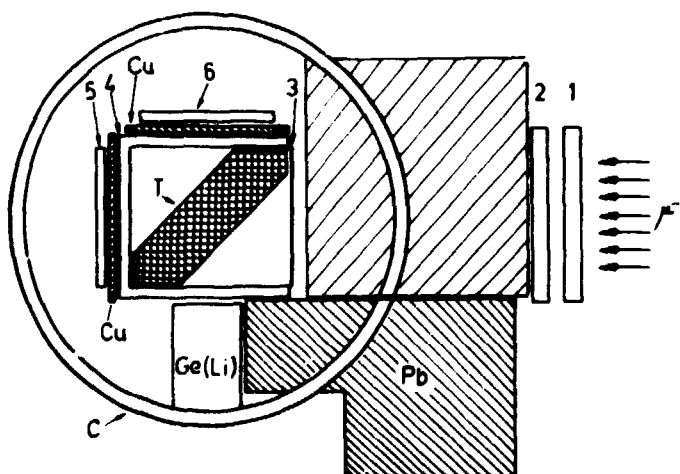


Рис.5. Схема расположения аппаратуры в совпадательном эксперименте $\bar{\mu} + X_{\mu}$.

Измерение остаточной поляризации в совпадении с линиями мезорентгеновского излучения.

Деполяризация измерялась методом прецессии спина мюона в слабом поперечном магнитном поле $H=50$ гс, которое создавалось катушками Гельмгольца (рис.5). Электроны распада регистрировались совпадениями двух счетчиков 5 и 6 с 4-м. Для регистрации X_μ применялся Ge (L_i) - детектор 27 см³. Исследуется временное распределение сигналов от электронных телескопов относительно мю-стопа, сопровождающееся регистрацией кванта X_μ . Детектор позволяет выделить в спектре участки, соответствующие переходам: 2p→1s, 3p→1s, 4p→1s и 5p→1s.

Литература:

1. Алты-, бета- и гамма-спектроскопия под ред. К.Зигбана Атомиздат, М.1969.
2. Абрамов А.И. и др. Основы эксперим. методов яд. физики, Атомиздат, М.1970.
3. Fermi E., Teller E., Phys. Rev. 72, 399, 1947
4. Кириллов-Угрюмов В.Г. и др. Атомы и мезоны Атомиздат, М.1980.
5. Mudhopadhyay N. C., Phys. Rep. 30C, п. 1, 1977
6. Балашов В.В. и др. Поглощение мезонов атомными ядрами, Атомиздат, М.1978.
7. Вайсенберг А.С. Мю-мезон, Наука, М.1964.
8. Армът Р. и др. ОИЯИ, ФИ5-7202, Дубна, 1973.
9. Akylas V. R., Vogel P., Hyperfine Inter. 3, 77, 1977
10. Фоганов В.С., ОИЯИ ЛЯП, Б1-9-4707, Дубна, 1969.
- II. Акимов Ю.К. и др. ОИЯИ, ИЗ-1202I, ИЗ-12022, Дубна, 1978.
12. Routti J. T., UCRL-19452, 1969; Routti J. T., Prussin S. G., Nucl. Instr. a. Meth. 72, 125, 1969

ИЗМЕРЕНИЕ ХАРАКТЕРИСТИЧЕСКОГО РЕНТГЕНОВСКОГО ИЗЛУЧЕНИЯ ЭЛЕКТРОННО- КОМПЬЮТЕРНЫХ КОЛЛЕДЖЕЙ НА КОЛЛЕКТИВНОМ УСКОРИТЕЛЕ ТЯЖЕЛЫХ ИОНОВ ОИИМ

Г. Морнак⁺, Г. Миллер⁺, Г. Музоль⁺⁺

⁺ Объединенный институт ядерных исследований, Дубна СССР

†† Технический Университет, Дрезден ГДР

Для диагностики лучка на коллективном ускорителе тяжелых ионов ОИМ разработан диагностический метод для анализа электронно-ионных коверц на основе измерения характеристического рентгеновского излучения этих коверц. Представлены первые результаты измерений характеристического рентгеновского излучения ионов ксенона, наполненного в электронном коверце.

В рамках создания уникальной системы диагностики пучка на коллектическом ускорителе тяжелых ионов (КУТИ) СИБИИ стоит задача – исследовать процесс ионизации атомов, находящихся в электронном кольце КУТИ и определить их число. При этом желательно ориентироваться на такое решение проблемы, которое позволит получать нужную информацию без замедления в процессе работы ускорителя.

Атомы, находящиеся в электронном кольце, испускают кванты характеристического рентгеновского излучения при заполнении вакансий из внутренних атомных оболочках. Эти вакансы возникают вследствие ионизации электронным ударом и в соответствующих процессах перестройки атомной оболочки при заполнении первичных вакансий. Возникающее рентгеновское излучение несет информацию о степени ионизации атомов и об их числе в электронном кольце, так как энергия рентгеновских линий характерным образом изменяется при повышении степени ионизации атома^{1,2/}, а из числа рентгеновских событий можно сделать выводы о числе ионов в электронном кольце^{3/}.

С целью измерения характеристического рентгеновского излучения построен спектрометрический комплекс, работающий на линии с ЭВМ. Блок-схема дана на рис. I.

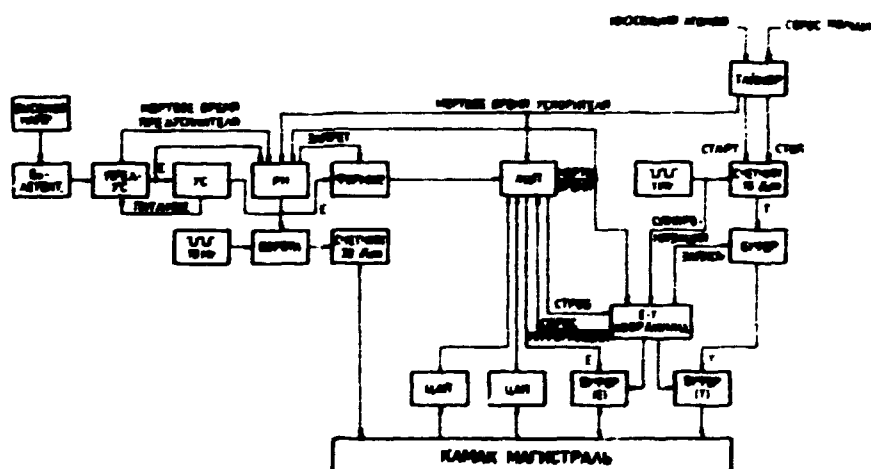


Рис. I Схема измерительного комплекса для спектроскопии характеристического рентгеновского излучения электронно-ионизирующего кольца.

Для измерения используется сверхчистый Ge - детектор в связи с предусилителем, находящимся в пульсирующем режиме фотооптической обратной связи. Детектор находится в свинцовом экранировании, которое защищает его от импульсов тормозного излучения, возникающих во время работы КУТИ.

Работа отдельных узлов электроники спектрометрического комплекса подробно описана в ^{4/}.

Проведены первые эксперименты с целью измерить характеристическое рентгеновское излучение из электронно-ионных колец Дубненского КУТИ ^{4/}.

На рис.2 показано спектр характеристического рентгеновского излучения ионов ксенона, накопленные в электронном кольце. Для сравнения на нижней части рис.2 изображен калибровочный спектр K - линии элементов теллура и лантана и L - группы свинца. Рентгеновское L - излучение свинца тоже можно наблюдать во время измерения на ускорителе, потому что кванты тормозного излучения электронов возбуждают в свинце экранирования характеристическое рентгеновское излучение. Это также происходит в материале титаново переходного окна, т.е. появляется пик рентгеновского излучения титана на верхнем спектре в рис.2. L - линии от ксенона не были измерены, потому что переходное титановое окно и воздух между переходным окном и детектором ослабляют их интенсивности на несколько порядков. Настоящее время измерения составляло 0,84 сек., т.е. 700 циклов ускорения с временем измерения 1,2 мсек. в одном цикле.

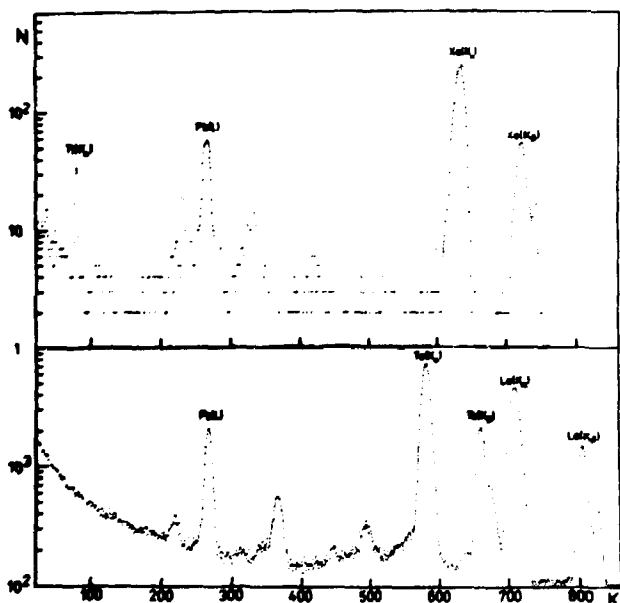


Рис. 2. Рентгеновский спектр атомов ксенона, накопленные в электронном кольце. На нижнем участке показан калибровочный спектр, полученный флуоресцентным возбуждением атомов теллура и лантана. Из калибровки следует 47 эВ в канале, что соответствует 170 эВ на полу值得一сте пика K - линии титана.

На основе получаемых спектров мы рассчитали произведение из числа электронов и ионов $(2 \pm 0,8) \cdot 10^{23}$ частиц в одном кольце.

Во время эксперимента в адгезаторе КУТИ измеренное давление остаточного газа составлялось $(5,5 \pm 0,8) \cdot 10^{-8}$ торр и максимальное парциальное давление в импульсе ксенона было $3 \cdot 10^{-6}$ торр. Однако надо заметить, что первичная цель наших исследований было измерение характеристического рентгеновского излучения накопленного в электронном кольце ксенона, но не получить количественные данные о числе частиц в кольце. Чтобы получить точные количественные результаты, необходимо надо проверить совпадение между временем инъекции импульса атомов ксенона и

электронным кольцом, который должен в это время пересекаться траектория газового импульса.

Проведенные эксперименты показали возможность проведения рентгеновских измерений на КУТИ. Более того, получаемое хорошее энергетическое разрешение и полезное отношение эффект-фон подтвердили, что наряду с измерением характеристического рентгеновского излучения с целью исследования характеристик электронно-ионных колец возникает возможность проведения ряда физических экспериментов по исследованию структуры атомных оболочек высокомонизованных атомов и взаимодействий в них.

Литература

1. Зиберт Х.-У. и др. ОИЯИ, Р9-9657, Дубна, 1976.
2. Шорнак Г. и др. ОИЯИ, Р7-11876, Дубна, 1978.
3. Шорнак Г. и др. ОИЯИ, Р13-12540, Дубна, 1979.
4. Zschermann G. et al. JINR, E9-12539, Dubna 1979

ГЕОМЕТРИЧЕСКИЕ ЭФФЕКТЫ В РЕНТГЕНОВСКИХ КРИСТАЛЛ-ДИФРАКЦИОННЫХ СПЕКТРОМЕТРАХ С ИЗОГНУТЫМИ КРИСТАЛЛАМИ

Г.Шорнак[†], Г.Мюллер[†], Г.Музиоль⁺⁺

+ Объединенный институт ядерных исследований, Дубна СССР

++ Технический Университет, Дрезден ГДР

Представлены аналитические и численные исследования влияния конечных размеров источника и кристалла на форму и позиции дифракционных линий в рентгеновских кристалл-дифракционных спектрометрах с изогнутыми кристаллами.

I. Введение.

Технический и методический прогресс в различных областях науки является основой повышения точности кристалл-дифракционных спектрометров и исключает типичные для работы таких спектрометров ошибки. Однако, необходимо знать типы ошибок, которые могут возникнуть и их относительные величины. Некоторые эффекты приводят к сдвигам дифракционных рефлексов, а другие - к изменениям только в форме дифракционной линии. Сдвиги рефлексов могут привести к систематическим ошибкам при измерении длин волн или энергий.

В настоящей работе мы исследуем сдвиги и изменения форм дифракционных линий отражающих спектрометров из-за конечных размеров источника и кристалла, т.е. из-за геометрических причин. Для трансмиссионных спектрометров эта проблема разработана в /1/ и изображена в /2,3/.

Исследование влияния геометрии на дифракционные линии проводится без учета структуры кристалла, поглощения и снижения энергии излучения и эффектов связанных с изгибом кристалла.

2. Геометрия измерения и эффективный угол дифракции.

На рис. I показана схема измерения. Принимается, что дифракция на всех решетках определенной плоскости происходит с равномерной вероятностью. Чтобы рассмотреть те случаи, где поверхность кристалла не совпадает с кругом Роуланда, мы в дальнейшем принимаем для толщины кристалла определенные пределы и считаем, что отражение квантов происходит от каждой плоскости решетки с равномерной вероятностью. Координаты произвольной точки выпуска рентгеновских квантов

$Q(x, y, z)$ радиационного источника определены от точки T круга Роуланда. Аналогично определены координаты каждой дифракционной точки $B(r, t, h)$ кристалла от точки S того же круга.

Из рис. I можно вывести следующие формулы:

$$a = R \cdot \sin \vartheta \quad (1)$$

$$b = R \cdot \cos \vartheta \quad (2)$$

$$v = e \cdot \sin \sigma' \quad (3)$$

$$w = e \cdot \cos \sigma' \quad (4)$$

$$\tau = t/R \quad (5)$$

$$\sin \sigma' = \frac{1}{R} [(b-y) \sin(\vartheta-\tau) - x \cos(\vartheta-\tau)] \quad (6)$$

$$\cos \sigma' = \frac{1}{R} [(b-y) \cos(\vartheta-\tau) + x \sin(\vartheta-\tau)] \quad (7)$$

Используя формулы (6) и (7) в (3) и (4) получим

$$v = (b-y) \sin(\vartheta+\tau) - x \cos(\vartheta+\tau) \quad (8) \quad w = (b-y) \cos(\vartheta+\tau) + x \sin(\vartheta+\tau) \quad (9)$$

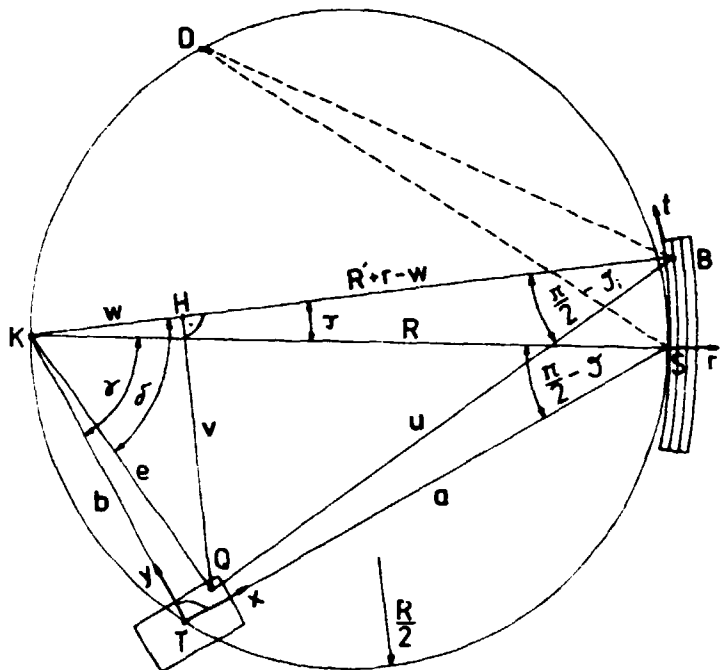


Рис. I Схема геометрии кристалло-дифракционного спектрометра

T - происхождение координат источника;
S - происхождение координат детектора;
Q - произвольная точка испускания квантов источником;
B - произвольная точка дифракции квантов кристаллом;
R - диаметр круга Рууланда;
R' - равно R в случае спектрометра типа Иоганна, равно $R \cos \gamma$ в случае спектрометра типа Иоганнесена

Пространственное расстояние между произвольными точками эмиссии и дифракции квантов имеет вид

$$u = [(R+r-w)^2 + v^2 + (h-z)^2]^{1/2} \quad (10)$$

Обратив внимание на треугольник QBH, $\sin \gamma$, можно определить к

$$\sin \gamma = \frac{R+r-w}{u} = \frac{R+r-w}{(R+r-w)^2 + v^2 + (h-z)^2}^{1/2} \quad (II)$$

Уравнение (II) является основой для аналитического исследования зависимости позиции дифракционных линий от геометрических размеров кристалла.

Полученные результаты показаны в таблице I.

Таблица I. Влияние конечных размеров кристалла и источника на позиции дифракционной линии для спектрометра типа Иоганна ($\Delta\lambda/\lambda$ - сдвиг длины волны из-за изменения дифракционной линии)

кристалл	$\Delta\lambda/\lambda$	источник	$\Delta\lambda/\lambda$
высота h_0	$\frac{1}{24} \frac{h_0^2}{R^2 \sin^2 \gamma}$	высота z_0	$\frac{1}{24} \frac{z_0^2}{R^2 \sin^2 \gamma}$
ширина t_0	$-\frac{1}{24} \frac{t_0^2}{R^2} \cot^2 \gamma$	ширина y_0	$\frac{1}{24} \frac{y_0^2}{R^2 \sin^2 \gamma}$
толщина r_0	$\frac{1}{8} \frac{r_0^2}{R^2} \cot^2 \gamma$	толщина x_0	0

Чтобы изучить влияние геометрии на форму и позиции дифракционных линий, рассчитываем при помощи Монте-Карло - программы БЕОМС функцию распределения $D(\gamma_B - \gamma)$, где γ - произвольный дифракционный угол и γ_B - угол Брэгга. Эта функция имеет форму: $D(\gamma_B - \gamma) = \frac{1}{V} \int_V [\sin(\gamma_B - \gamma) - \sin \gamma] dV \quad (12)$

где V - 6-размерный объем кристалл-источник.

Определенный дифракционный рефлекс можно получить через

$$F(\vartheta) = \int_0^{\infty} D(\vartheta_0 - \vartheta) f(\vartheta) d\vartheta \quad (13)$$

$f(\vartheta)$ означает неискаженный гауссовский профиль дифракционной линии.

На рис.2 показаны результаты расчета функции $D(\vartheta_0 - \vartheta)$ для высоты источника $z_0 = 10$ мм. Все остальные размеры принимаются равными нулю.

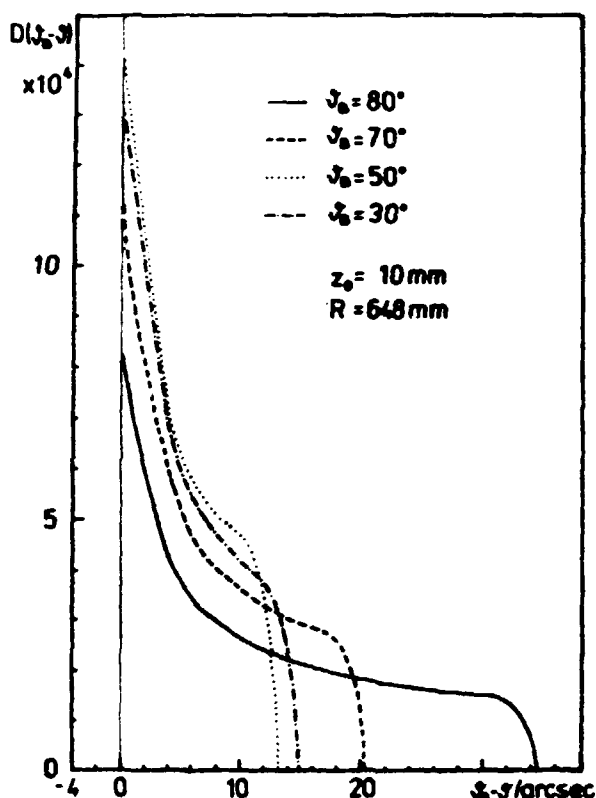


Рис. 2 Функция $D(\vartheta_0 - \vartheta)$ для различных углов дифракции ϑ_0 . При конечном размере высоты z_0 источники.

Представленный способ расчета дает возможность исследовать влияние различных геометрических конфигураций на дифракционные линии и получить представления о корреляции между геометрией кристалла и источником, диаметром круга Роуланда и углом измерения.

Литература

- /1/ J.Schwartz et. al, Nucl.Instr. methods 154 (1978) 105
- /2/ C.van Huffel, Z.Phys. 150 (1966) 444
- /3/ J.J.Reidy, in "The Electromagnetic Interaction in Nuclear Spectroscopy", North Holland, Amsterdam 1975, p. 839

О ПРАВИЛАХ СУММ ДЛЯ НЕУПРУГОГО РАССЕЯНИЯ ЭЛЕКТРОНОВ И НУКЛОНОВ

А.И.Блохин, А.В.Игнатик, В.П.Лунев
Физико-энергетический институт, Обнинск, СССР

Аннотация

Проанализированы различия формфакторов прямых переходов в реакциях неупротого рассеяния электронов и нуклонов, и определены соответствующие этим реакциям интегральные интенсивности мультипольных возбуждений ядер.

При анализе экспериментальных данных по возбуждению гигантских мультипольных резонансов в реакциях неупротого рассеяния электронов широко используется энергетически изваженное правило сумм [1]

$$\tilde{S}_\lambda^{\text{эл}} = \sum_i \omega_i B_i(E\lambda; 0 \rightarrow \lambda) = \lambda(2\lambda+1) \frac{3\hbar^2}{8\pi m} \frac{Z^2}{A} R_0^{2\lambda-2} \quad (1)$$

где ω_i - энергия и $B_i(E\lambda; 0 \rightarrow \lambda)$ - приведенная вероятность электрических мультипольных возбуждений ядер. Вклад в правило сумм служит обычно одним из главных критериев коллективности возбуждений, а также их локализованности в гигантских резонансах. Если для приведенной вероятности переходов воспользоваться формулами обобщенной модели ядра, то соотношение (1) можно представить в виде правила сумм для параметров динамической деформации $\beta_\lambda(\omega_i)$ соответствующих мультипольных возбуждений

$$S_\lambda^{\text{эл}} = \sum_i \omega_i \beta_\lambda^2(\omega_i) = \lambda(2\lambda+1) \frac{4\pi}{3A} \frac{\hbar^2}{2mR_0^2} \quad (2)$$

Полученная таким способом оценка интегральной интенсивности мультипольных возбуждений весьма часто применяется не только при анализе рассеяния электронов, но и распространяется на динамические параметры мультипольных возбуждений ядер в реакциях неупротого рассеяния протонов, α -частиц и даже тяжелых ионов [2]. Хорошо известно, однако, что для реакции с нуклонами формфакторы прямых переходов существенно отличаются от формфакторов электронного рассеяния, и в этих условиях универсальный вид правила сумм для различных частиц вряд ли может быть оправдан. В рамках микроскопического подхода формфакторы прямых переходов в реакциях неупротого рассеяния нуклонов можно записать как

$$F_\lambda(r, \omega) = \int_0^\infty V_\lambda(r, r') \rho_\lambda^{tr}(r', \omega) r'^2 dr' \quad (3)$$

где $V(r, r')$ - мультипольная компонента эффективного взаимодействия налетающей частицы с ядром и $\rho_\lambda^{tr}(r, \omega)$ - переходная плотность рассматриваемого возбуждения ядра. Для общего вида эффективных сил анализ интегральной интенсивности мультипольных возбуждений, соответствующих данному формфактору (3), является весьма сложной и трудоемкой задачей. В то же время решение задачи существенно упрощается, если воспользоваться сепарабельным представлением эффективных сил

$$V_\lambda(r, r') = \chi_\lambda f_\lambda(r) f_\lambda(r') \quad (4)$$

которое успешно применяется при микроскопическом описании низкомеханических колективных возбуждений ядер [1]. Для такой параметризации эффективных сил формфакторы интересующих нас переходов будут иметь вид

$$F_\lambda(r) = \frac{\rho_\lambda}{\sqrt{2\lambda+1}} f_\lambda(r) \quad (5)$$

а параметры динамической деформации будут определяться соотношениями

$$\beta_\lambda(\omega_i) = \sqrt{2\lambda+1} \chi_\lambda \int_0^\infty f_\lambda(r) \rho_\lambda^{tr}(r, \omega_i) r^2 dr \quad (6)$$

В соответствии с таким определением параметров для интегральной интенсивности мультипольных возбуждений в реакциях неупругого рассеяния нуклонов получим правило сумм

$$S_\lambda^{\text{яд}} = \frac{\hbar^2 A}{8\pi m} \chi^2 \left\{ \lambda(\lambda+1) \left\langle \left(\frac{f_\lambda(r)}{r} \right)^2 \right\rangle + \left\langle \left(\frac{df_\lambda(r)}{dr} \right)^2 \right\rangle \right\} \quad (7)$$

где угловыми скобками обозначено усреднение по волновым функциям основного состояния ядра. Если привлечь к построению эффективных сил (4) условия согласования [1, 3], то для формфактора $f_\lambda(r)$ получим соотношение

$$f_\lambda(r) = R_o \frac{dV_o(r)}{dr} \quad (8)$$

где $V_o(r)$ – потенциал модели оболочек. С точностью до различий оптического и оболочечного потенциалов формфакторы $F_\lambda(r)$ при согласованном выборе эффективных сил имеют тот же вид, что и при феноменологическом описании прямых переходов в коллективной модели [1]. Предполагая, что распределение плотности для основного состояния ядра определяется тем же формфактором, что и оболочечный потенциал, и используя для вычисления соответствующих этому распределению интегралов метод перевала, получим квазиклассическую оценку правила сумм (7)

$$S_\lambda^{\text{яд}} = \frac{\hbar^2 (2\lambda+1)}{2m A a R_o} \cdot 12 \cdot 10^3 \left(\frac{2}{7} \right)^6 \sqrt{\frac{\pi}{35}} \left\{ 1 + \lambda(\lambda+1) \frac{3}{5} \left(\frac{7}{5} \right)^6 \sqrt{\frac{35}{15}} \frac{a^2}{R_o^2} \right\} \quad (9)$$

где a – диффузность оболочечного потенциала. На рис. I показано сравнение данной оценки с правилом сумм (2) для электрических переходов, а также с результатами численных расчетов правила сумм (7) для волновых функций потенциала Будса–Саксона. Можно видеть, что отличия правил сумм для электрического и ядерного формфакторов оказываются весьма значительными при всех мультипольностях как в сравнительно легком ядре ^{48}Ca , так и в тяжелом ядре ^{208}Pb . Следует отметить, что при использовании более сложной, чем (4), параметризации эффективных сил, в частности, при выделении в таких силах изоскалярной и изовекторной компонент, в рамках сформулированного выше подхода мы можем исследовать не только различия формфакторов ядерных и электрических переходов, но и отличие параметров динамической деформации в реакциях рассеяния протонов, нейтронов и α -частиц [4]. Интегральной характеристикой ожидаемых в этом случае отличий в интенсивности мультипольных возбуждений могут служить представленные на рис. I правила

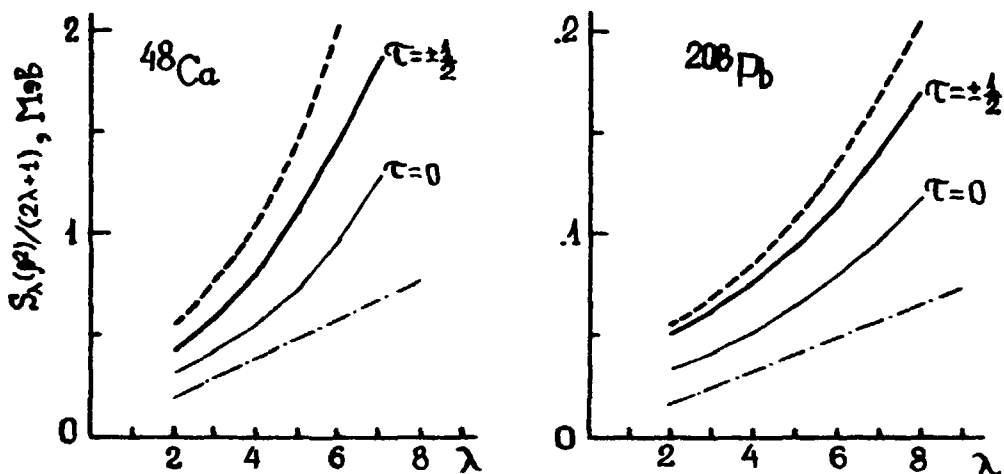


Рис.1. Величина энергетически взвешенного правила сумм для электромагнитного (штрих-пунктир) и ядерного (сплошные кривые) оператора мультипольных переходов. Пунктиром показана квазиклассическая оценка правила сумм (9).

вила суммы для параметров деформации, соответствующих рассеянию α -частиц ($T=0$) и нуклонов ($T = \pm 1/2$). В связи с обсуждаемыми различиями в правилах сумм для различных ядерных реакций возникает естественный вопрос о спектральном распределении таких различий. На основе проводившихся расчетов спектральной интенсивности мультипольных возбуждений ядер в прямых ядерных реакциях [5] можно сделать вывод, что отличия в правилах сумм для ядерного и электрического формфакторов возникают главным образом за счет высокогенеретических переходов, расположенных сравнительно равномерно в широкой области энергии возбуждений от 20 + 30 МэВ до порога рождения мезонов. Такие переходы играют, по-видимому, определяющую роль в формировании жесткой компоненты спектров неупругого рассеяния нуклонов [5], а возможно и жесткой компоненты спектров реакций нуклонного обмена.

Литература

1. Бор О., Структура атомного ядра. Мир, М., 1977, т.2.
2. Satchler G. Phys. Rep., 14C, 97, 1974
Bertrand P. Ann. Rev. Nucl. Sci., 26, 457, 1976.
3. Rowe D.J. Phys. Rev., 162, 866, 1967,
Пятов Н.И. СИЯИ, Р4-8208, Р4-8380, Дубна, 1974;
Лунев В.П. Изв. АН СССР, сер. физ., 41, 199, 1977.
4. Блохин А.И., Игнатик А.В., Лунев В.П. Нейтронная физика. ЦНИИатоминформ, М., 1980, ч. I.
5. Блохин А.И., Пронин В.Г. ЯФ, 30, 1258, 1979.

ОЦЕНКА СЕЧЕНИЙ РЕАКЦИЙ ($n,2n$), ($n,3n$) НА ДЕЛЕНИХ ЯДРАХ

В.М.Бычков, В.И.Пляскин

Физико - энергетический институт, Обнинск, СССР

Ранее в ряде работ, например [1,2], было показано, что спектры нейтронов и сечения реакции ($n,2n$) для неделяющихся ядер с хорошей точностью описывается в рамках статистической теории ядерных реакций и экспоненциальной модели предравновесного распада. Включение в рассмотрение деления приводит к усложнению расчетов и к трудностям, связанным с выбором параметров для описания ширмы делительного канала. Эту задачу можно существенно упростить, сделав некоторые приближения. На тяжелых ядрах, где вероятностью испускания заряженных частиц можно пренебречь, доминирующими каналами распада составного ядра являются испускание нейтронов и деление. Поэтому, в расчетах по статистической теории фактически достаточно определять величину Γ_n/Γ_s – отношение нейтронной и делительной ширмы распада составного ядра. В данной работе для определения Γ_n/Γ_s использована систематика этой величины из экспериментов по делению ядер. Сечение реакции ($n,2n$) записывается, как сумма равновесной и предравновесной компонент:

$$\sigma_{n2n}(E_n) = \sigma_{n2n}^{eq}(E_n) + \sigma_{n2n}^{pre}(E_n) \quad (1)$$

Предравновесная компонента оценивается следующим образом

$$\sigma_{n2n}^{pre}(E_n) = \sigma_a(E_n) \int_0^{E_n + Q_{2n}} P^{pre}(\epsilon) F_1 d\epsilon \quad (2)$$

здесь: $\sigma_a(E_n)$ – сечение поглощения нейтрана с энергией E ;
 Q_{2n} – энергия реакции ($n,2n$) ;
 $P^{pre}(\epsilon)d\epsilon$ – вероятность предравновесной эмиссии нейтрана с энергиями от E до $E + dE$;
 F_1 – коэффициент, учитывающий вероятность деления остаточного ядра (A): $F_1 = \frac{\beta_1}{1 + \beta_1}$; $\beta_1 = \left(\frac{\Gamma_n}{\Gamma_s} \right)_A$

Равновесная компонента сечения вычисляется в рамках испарительной модели Вайскопфа с учетом эффективного уменьшения вероятности образования компаунд-ядра из-за предравновесной эмиссии:

$$\sigma_{n2n}^{eq}(E_n) = [\sigma_a(E_n) - \sigma_{n3n}^{pre}(E_n) - \sigma_{n2n3}(E_n)] \frac{1}{T_1^2} \int_0^{E_n + Q_{2n}} E e^{-E/T_1} F_1 d\epsilon \quad (3)$$

здесь: T_1 – термодинамическая температура, связанная с параметром плотности уровней в модели Ферми-газа соотношением:

$$T_1^2 = E - 2T_1$$

F_1 – имеет тот же смысл, что и в формуле (2).

В области начальных энергий нейтрана выше порога реакций ($n,3n$), ($n,2n$), формула (1) записывается, как

$$\sigma_{n2n}(E_n) = \sigma_{n2n}^{eq}(E_n) + \sigma_{n2n}^{pre}(E_n) - \sigma_{n2n3}(E_n) - \sigma_{n3n}(E_n) \quad (1')$$

Равновесная и предравновесная компоненты сечения реакции ($n,3n$) записываются следующим образом

$$\begin{aligned} \bar{\sigma}_{n3n}^{(n)}(E_n) &= [\bar{\sigma}_n(E_n) - \bar{\sigma}_{n2n}^{pre}(E_n) - \bar{\sigma}_{n3n}(E_n) - \bar{\sigma}_{n4n}(E_n)] \times \\ &\times \frac{1}{T_1^2} \int_0^{E_n + Q_{3n}} E_1 e^{-E_1/T_1} \frac{\int_{E_1 + Q_{3n}}^{E_1 + Q_{3n}} E_2 e^{-E_2/T_1} F_2 dE_2}{\int_{E_1 + Q_{3n}}^{E_1 + Q_{3n}} E_2 e^{-E_2/T_1} dE_2} dE_1 \quad (4) \end{aligned}$$

где: Q_{3n} - энергия реакции ($n,3n$).

$$\begin{aligned} F_2 &= \frac{\beta_2}{1+\beta_2}; \quad \beta_2 = \left(\frac{\Gamma_n}{\Gamma_f}\right)_{A-1}; \quad T_1 = T_1 \sqrt{1 + Q_{2n}/E_n} \\ \bar{\sigma}_{n3n}^{pre}(E_n) &= \bar{\sigma}_n(E_n) \int_0^{E_n + Q_{3n}} P^{pre}(E_1) F_1 dE_1 \frac{\int_{E_1 + Q_{3n}}^{E_1 + Q_{3n}} E_2 e^{-E_2/T_1} F_2 dE_2}{\int_{E_1 + Q_{3n}}^{E_1 + Q_{3n}} E_2 e^{-E_2/T_1} dE_2} \quad (5) \end{aligned}$$

Формулы (4,5) справедливы при энергии падающего нейтрона ниже порога реакций ($n,4n$) и ($n,3nf$). Расчеты сечений реакций ($n,2n$) и ($n,3n$) по приведенным выше соотношениям выполнены для ядер U^{238} , Pu^{239} , Np^{237} . Для этого было необходимо знание только трех параметров: сечения поглощения $\bar{\sigma}_n(E_n)$, параметра плотности уровней a и отношения Γ_n/Γ_f . Сечение поглощения взято из расчетов по оптической модели со сферическим потенциалом. Параметр плотности уровней выбран из условия наилучшего описания функций возбуждения реакций ($n,2n$) и ($n,3n$) в широком диапазоне массовых чисел ядер $100 < A < 200$ и определялся из соотношения $a = A/12$. Значения Γ_n/Γ_f , как указывалось выше, взяты из экспериментов по делению ядер. Результаты расчета приведены в таблице.

Таблица

Сечения реакций ($n,2n$) и ($n,3n$) на ядрах Np^{237} , Pu^{239} , U^{238}

E_n	Np^{237}		Pu^{239}		U^{238}	
	$\bar{\sigma}_{n2n}$, мб	$\bar{\sigma}_{n3n}$, мб	$\bar{\sigma}_{n2n}$, мб	$\bar{\sigma}_{n3n}$, мб	$\bar{\sigma}_{n2n}$, мб	$\bar{\sigma}_{n3n}$, мб
6	-	-	50	-	-	-
7	25	-	224	-	500	-
8	295	-	307	-	1070	-
9	442	-	341	-	1305	-
10	500	-	356	-	1405	-
11	531	-	355	-	1420	-
12	549	-	349	-	1390	40
13	541	9	284	-	1240	240
14	490	50	212	27	920	460
15	366	103	143	71	620	660
16	279	158	117	102	460	800
18	197	230	95	163	290	935
20	165	261	76	180	210	990

Литература

1. Бычков В.М., Пашенко А.Б., Пляскин В.И. Вопросы атомной науки и техники. Серия: Ядерные константы. 1978, № 29, с. 7.
2. Meister A., Seeliger D., Seidel K. Kernenergie, 1977, v.20, p.395.